Mitigation of Abrasion Damage of Offshore Structural Concrete

By

© Ali Eed Abdel-Hafez, B.Sc.

A thesis submitted to the

School of Graduate Studies

in partial fulfillment of the requirements for the degree of

Doctor of Philosophy (Civil Engineering)

Faculty of Engineering and Applied Science

Memorial University of Newfoundland

September 2022

St. John's, Newfoundland, Canada

Abstract

The usage of concrete is wide and covers many construction applications. However, each application requires concrete with specific requirements as it is subjected to different types of loading actions. In a harsh environment, offshore structural concrete is subjected to abrasion action resulting from interacting with moving ice sheets. That interaction could cause considerable wear leading to possible damage, higher maintenance cost, and decreased life cycle.

In this thesis, two approaches are introduced to limit this abrasion damage. The first one is through enhancing the ability of the concrete, used in such an environment, to resist such abrasion damage. This can be achieved by optimizing the concrete main composition (coarse to fine aggregate ratio (C/F), maximum aggregate size (Am)) and by adding different types of additions (supplementary cementitious materials (SCMs), fibers, and nano particles). The second approach is through using a high abrasion-resistant external layer as a shield against ice-abrasion damage.

It is believed that this study could lead to more effective usage of offshore concrete. This could lead to a far more cost-effective offshore structure, huge maintenance cost savings, and providing an incentive to extend construction for new offshore structures in harsher environmental regions which is highly demanded.

Keywords: Concrete, offshore, abrasion action.

Acknowledgments

After expressing gratitude to Almighty "ALLAH" for his innumerable bounties and for providing me with the strength to face life, I would like to gratefully thank Dr. Amgad Hussein associate professor of civil engineering at Memorial University of Newfoundland, for his endless fatherly guidance. I would also like to express my gratitude to, Dr. Stephen Bruneau associate professor of civil engineering at Memorial University of Newfoundland, and Dr. Sam Nakhla associate professor of civil engineering at Memorial University of Newfoundland. I owe them a hearty thank you for their invaluable advice, unwavering support, and lengthy constructive debates and remarks. Without them, this work would not have been possible. I'd also like to express my gratitude to them for providing me with this fantastic opportunity, which has had a huge impact on my career and personal development.

The funding provided by Kvaerner oil and gas Ltd., School of Graduate Studies, is greatly acknowledged.

Furthermore, I would like to thank Mr. Dennis Cramm Mechanical division manager of Engineering technical services at Memorial University of Newfoundland. In addition, I would like to thank both Mr. Shawn Organ and Mr. Jason Murphy the laboratory staff at Memorial University of Newfoundland for their help that made this work happen. I also would like to thank Lidan Tao, the environmental lab instructor at Memorial University of Newfoundland for her help.

Moreover, I would have to thank Mahmoud Said for his help and advice. I would like also to thank all my colleagues who helped me through this investigation, Mohamed Said, Mohamed Zurgani, Titli Pramanik, Sarah Khalil, Mohamed Sadek, and Moftah Elwehashy. A special thanks to the rest of the graduate students whom I worked with.

Finally, I want to express my heartfelt gratitude to my mother and father for their unconditional support, encouragement, and belief in me at all times. I'd like to express my gratitude to my wife for her motivation and assistance. I also would like to thank my brothers for being always there for me.

Table of Contents

List of tables

List of figures

List of Symbols

d_c	Damage parameters in compression
d_g	Deviated depth
d_t	Damage parameters in tension
r_g	Distance from the origin
V_t	Total abraded volume
M_t	Total abraded mass loss
ρ	Density of the tested concrete
$d_{avg.}$	Average abrasion depth
A_t	Total abraded surface area
R_a	Un-abraded surface roughness
y_i	Difference between the height at each point and the mean value.
w_g	Abraded groove width
r_{go}	Outer radius of the groove
r_{gi}	Inner radius of the abraded groove
t	Dressing wheel thickness
L	Chord length at a specific depth d_g
r_w	Dressing wheel radius
Θ	Angle of partial rotation around axis (2).
n	Number of abraded grooves

List of Nomenclature or Abbreviations

AEA	Air-entraining agent
Am	Maximum aggregate size
BBFs	Bundled basalt fibers
BFs	Basalt fibers
C/F	Coarse to fine aggregate ratio by volume
CCSFs	Copper coated steel fiber
CDP	Concrete damaged plasticity
CFRP	Carbon fiber reinforced polymer
DME	Dynamic modulus of elasticity
ESLWA	Stalite expanded slate lightweight aggregate
FA	Fly ash
FBFs	Filament basalt fiber
FEM	Finite element modeling
FRP	Fiber reinforced polymers
FRP	Fiber reinforced polymers
FS	Flexural strength
GU	General sse Portland cement
HPC	High performance concrete
HPLWAC	High performance lightweight aggregate concrete
HPNWC	High performance normal weight concrete

HPSDC	High performance specified density concrete
ITZ	Interfacial transition zone
K	Shape factor of the yielding surface in the deviatoric plane
LVDTs	Linear variable differential transducers
LWA	Lightweight aggregate
MK	Metakaolin
NCS	Nano colloidal silica
NPs	Nano particles
NSC	Normal strength concrete
NTD	Nano titanium dioxide
NWA	Normal weight aggregates
PPFs	Polypropylene fibers
RFT	Reinforcement
RPM	Revolutions per minute
SCMs	Supplementary cementitious materials
SF	Silica fume
SME	Static modulus of elasticity
SP	Polycarboxylate-based superplasticizer
SSD	Saturated surface dry state
STS	Splitting tensile strength
UHPC	Ultra-high performance concrete

Co-authorship statement

I, Ali E. Abdel-Hafez, hold a principal author status for all the manuscript chapters (Chapters 2 - 6) in this dissertation. However, each manuscript is co-authored by my supervisor and co-researchers, whose contributions have facilitated the development of this work as described below.

- Paper 1 in Chapter 2: Ali E. Abdel-Hafez, Amgad Hussein, and Stephen Bruneau, "Evaluating the ASTM C944 Rotating Cutters Method for Determining the Abrasion Resistance of Concrete" published in the ASTM journal of testing and evaluation, April 2021 (Published).

I was the primary author, with authors 2 - 3 contributing to the idea, its formulation and development, and refinement of the presentation.

- Paper 2 in Chapter 3: Ali E. Abdel-Hafez, Amgad Hussein, and Stephen Bruneau, "Abrasion resistance of the high performance specified density concrete for offshore structural application"

I was the primary author, with authors 2 - 3 contributing to the idea, its formulation and development, and refinement of the presentation.

- Paper 3 in Chapter 4: Ali E. Abdel-Hafez, Amgad Hussein, and Stephen Bruneau, "Impact of fibers inclusion on the abrasion resistance of the high performance specified density concrete"

I was the primary author, with authors 2 - 3 contributing to the idea, its formulation and development, and refinement of the presentation.

- Paper 4 in Chapter 5: Ali E. Abdel-Hafez, Amgad Hussein, and Stephen Bruneau, "Influence of nano particles addition on the abrasion resistance of the high performance specified density concrete"

I was the primary author, with authors 2 - 3 contributing to the idea, its formulation and development, and refinement of the presentation.

- Paper 5 in Chapter 6: Ali E. Abdel-Hafez, Amgad Hussein, Stephen Bruneau, and Sam Nakhla "Finite element analysis for the flexural behavior of two layers concrete beam"

I was the primary author, with authors 2 - 4 contributing to the idea, its formulation and development, and refinement of the presentation.

Chapter 1 Introduction and overview

1.1. Research motivation

Concrete particles are removed when concrete interacts with moving objects. Concrete's abrasion resistance is described as its ability to endure mechanical action as well as its proclivity to protect its surface. Abrasion activity on concrete buildings occurs in a variety of ways and through various mechanisms. The dynamic motion of automobiles, for example, affects the concrete in pavements (Nader, Meysam, and Aqel 2014). The depth of the resulting surface texture is determined by the ongoing movement of the wheels and is influenced by road noise. Concrete buildings in marine conditions are also susceptible to mechanical wear. The abrasion of the concrete surface caused by ice grinding, crushing, and sliding poses a serious threat to the structural integrity of the concrete structure. Worn surfaces also increase friction, increasing local and global strains on the structure, as well as accelerating reinforcement corrosion through loss of cover and crack development.

This contact could result in significant wear, resulting in potential damage, increased maintenance costs, and a shorter life cycle. The 1.3 billion-dollar (CAN) Confederation Bridge in Canada, which connects Prince Edward Island to the mainland at New Brunswick, is an example of a construction in an ice-infested sea. The bridge's monitoring revealed some wear damage to the concrete pillars at the water's edge as a result of contact with floating ice sheets (see Fig. 1-1). On its concrete pillars, some repair and restoration work has been proposed and is now being carried out.

Fig. 1-1 Effect of interacting with moving ice on the concrete of pier 23 of the Confederation Bridge, from Newhook and McGinn (Newhook and McGinn 2007).

1.2. Background and literature review

A specific kind of concrete is used for offshore constructions. To endure such extreme weather conditions, it must be of high performance ("ACI 318-14" 2014). It must also, in some circumstances, be of a lighter weight. Offshore platforms, for example, are built on land and then towed to their final destination. Concrete with a specified unit weight is required for the towing phase. As a result, using lightweight aggregate became an appealing option (Fernandes, Bittencourt, and Helene 2008). However, replacing all of the coarse aggregate in concrete with lightweight aggregate results in concrete with inferior mechanical characteristics and abrasion resistance. As a result, for offshore structural applications, it is preferable to partially replace coarse aggregate with lightweight aggregate, and the produced concrete is known as specified density concrete or modified normal density concrete.

For offshore structural applications, high-performance specified density concrete (HPSDC) has been frequently employed. In 1991, 450,000 tonnes of concrete, primarily HPSDC with 50% coarse aggregate substitution by the lightweight aggregate, were used in the building of the Hibernia platform, a massive gravity-based structure (Hoff and Elimov 1995). It was also utilized in the building of the Troll A GBS platform (Sandvik, Hovda, and Smeplass 1994), which at the time was the world's biggest moving structure. In 1996, the HPSDC enabled such a massive construction to be towed in the sea. Furthermore, HPSDC is now being employed in the construction of West White Rose's new gravity-based structure. There is, however, a desire for a more advanced HPSDC to be utilized in harsher environments, such as the Arctic. The Arctic has 13% of the world's undiscovered oil and 30% of the world's undiscovered gas (Gautier et al. 2009), making it a key resource for the future of oil and gas. However, the investigation is still limited because of the severe hostile environmental conditions that the concrete is subjected to there.

Despite the HPSDC's significance and cost invested in it, there are just a few studies on it. (Bogas and Gomes 2014) investigated the impact of nano-silica addition on specified density concrete produced with various cement contents, beginning wetting conditions, coarse lightweight aggregate types, and volumes. The use of LWA resulted in a decrease in elastic modules. The nano silica addition had a limit effect on the concrete’s strength and deformability. Although abrasion resistance is one of the primary concerns of HPSDC in the marine environment, it is not yet explored.

The abrasion resistance of concrete is directly related to its composition. The kind of aggregates (Kılıç et al. 2008), the concrete's C/F aggregate ratio, and the maximum aggregate size (Nikbin et al. 2014) all have an impact. The incorporation of various types of supplementary cementitious materials (SCMs) can also impact the abrasion resistance of concrete. (Rashad 2013) investigated the impact of metakaolin (MK) on concrete and discovered a 46.24% increase in the abrasion resistance, as well as increased compressive strength and splitting tensile strength. (Sujjavanich et al. 2017) discovered that including MK coupled with fly ash (FA) at various blending ratios improved concrete abrasion resistance.

Basalt fibers (BFs) have recently gained popularity as a viable option in concrete reinforcement. BFs are inorganic materials that are made by melting and extruding basalt rocks. This technique is environmentally friendly and uses little energy, making BFs quite inexpensive (Deák and Czigány 2009). BFs have a significantly better tensile strength, a lower specific gravity, and are corrosion resistant as compared to steel fibers (Fibers Unlimited 2007). BFs also demonstrated strong chemical stability in high alkaline conditions, allowing for good adherence to the surrounding matrix (Basalt Fibers LTD. 2013). Because of these properties, BFs are a great choice for offshore structural applications.

A survey of the literature revealed studies on the use of continuous basalt fibers as a concrete structure reinforcing material (Sim, Park, and Moon 2005). However, just a few studies on the influence of adding chopped basalt fibers on concrete characteristics have been found. (Dias and Thaumaturgo 2005) investigated the connection between the number

of fibers in basalt fibers including geopolymer cement concrete mixes and fracture toughness. The basalt fiber-incorporated beams had greater ultimate loads, lower fracture sensitivity, and more displacement before failure. (Zhao et al. 2010) examined the impact strength of concrete reinforced with basalt fibers and discovered that the inclusion of basalt fibers improved the impact strength significantly. Incorporation of basalt fibers into concrete has been shown to increase tensile strength (Borhan 2013), impact resistance (Fu et al. 2018), and compressive strength (Jiang et al. 2014) in previous studies.

The effect of nano silica on the mechanical properties of concrete was reported to be superior. (Zhao, Kong, and Yang 2012) experimented to investigate the influence of nano silica addition and discovered that the concrete's compressive strength and freeze/thaw resistance improved. Furthermore, (Sobolev et al. 2009) found that adding 0.25 percent (by mass of cement) of nano silica improved compressive strength by 10%. The addition of 10% increased the compressive strength of the concrete by 166%. Furthermore, (Shih, Chang, and Hsiao 2006) found that adding 0.6 percent nano silica to cement pastes increased compressive strength by about 46 percent after 56 days. Furthermore, as (Lin et al. 2008) showed, the effect of nano silica inclusion on the compressive and flexural strength of concrete was apparent and much more effective than that of silica fume addition.

Regardless, the influence of nano titanium dioxide (NTD) on the mechanical characteristics of concrete was studied. (Zhang and Li 2011) used NTD at 1%, 3%, and 5% by mass of cement and found improvements of 18.03%, 12.76%, and 1.55%, respectively, as compared to a control mixture. (Nazari 2011) showed that curing in saturated limewater

enhanced compressive strength by 36.58%, 48.78%, 56.1%, and 65.85%, respectively, when NTD was added at 0.5%, 1%, 1.5%, and 2% by mass of cement.

Another option, on the other hand, maybe adopted. To preserve the concrete's surface, an exterior coating is applied. Various research that studied the behavior of two layers reinforced concrete beams experimentally were found through a review of the literature. (Saiidi, Vrontinos, and Douglas 1990) studied the behavior of a reinforced concrete beam enhanced with a concrete layer in the compression and tension zones experimentally in 1990. (Iskhakov et al. 2014) carried out experimental research for a two-layer beam with a high-strength concrete layer atop a normal-strength concrete layer in 2013. In 2016, (Iakov Iskhakov, Ribakov, and Holschemacher 2017) investigated the compression zone behavior of two-span composite beams made of high-strength concrete. (Hamed 2018) proposed utilizing ultra-high-performance concrete (UHPC) as the top layer and high-performance fibers reinforced concrete as the bottom layer for composite beams in 2018. (Lam and Do 2019) studied the appropriate position (upper layer or lower layer) of the fibers reinforced concrete layer in relation to the normal strength concrete layer such that sliding between them is minimized under loading in June 2019. This study was carried out experimentally with the help of finite element modeling (FEM) and ANSYS software. (Iskhakov et al. 2019) examined the behavior of a two-layer concrete beam experimentally in December 2019. The study focuses on the four-point bending of prestressed full-scale beams. In the tension zone, normal strength concrete was utilized, whereas, in the compression zone, high strength concrete with steel fibers was used. The results were compared to those obtained with non-prestressed beams. The results of the investigation

indicated that there was no de-bonding between the two layers up to the ultimate limit condition, indicating that the two layers interacted properly. Although experimental testing yields real-world findings, full-scale composite beam testing is complex and requires large-scale facilities, as well as being expensive and time-consuming. The FEM, on the other hand, is seen to be a more time and cost-effective technique. FEM might allow us to reliably anticipate the behavior of reinforced concrete beams without the need for experimental confirmation, making it a viable option.

It was found that FE has previously been used to examine multilayered concrete beams in various shapes. Many studies, for example, have been discovered that used FE to examine the behavior of reinforced concrete beams enhanced with fiber reinforced polymers (FRP). FE was used by (Sasmal, Kalidoss, and Srinivas 2012) to study the behavior of reinforced concrete beams reinforced with carbon fiber reinforced polymer (CFRP). The findings were compared to ferrocement-reinforced beams. The results were presented as load-deflection behavior and ultimate load capacity graphs. CFRP strengthening resulted in a significant increase in ultimate load capacity. Other research, such as (Barour and Zergua 2019), (Parandaman and Jayaraman 2014), and (Barour et al. 2019) investigated the capacity of FEA to capture the behavior of reinforced concrete beams enhanced with FRP using FE. Furthermore, FE was previously used to study a two-layer beam made up of concrete and other materials. FE was used by (Anju and Smitha 2016) to investigate the composite effect of a concrete slab and rolled up steel pieces. Four distinct types of shear connections were employed and analyzed in that study. (Katwal, Tao, and Hassan 2018) used FE to construct a FEM to investigate steel-concrete composite

beams. The proposed model can predict load-deformation behavior as well as the connection between shear force and slide. FE was also used to investigate the behavior of timber-concrete beams (Khorsandnia, Valipour, and Crews 2012). Multilayer beams composed of various kinds of concrete were also investigated. The cracking resistance of three layers beams was investigated by (Vu et al. 2019). The lightweight concrete with a strength of 1.15 MPa was used for the middle layer. The exterior layers, on the other hand, were constructed using 21.5 MPa concrete reinforced with glass fibers reinforced polymer bars, as opposed to traditional steel bars. The fracture resistance of glass fibers reinforced polymer bars was found to be higher than that of steel bars.

To the best of the author's knowledge, no one has investigated the flexural behavior of a two-layer reinforced concrete beam using FE. The other stage of the research will use finite element modeling to explore the flexural behavior of completely composite two-layer concrete. The upper concrete layer is there to function as an ice barrier and protect the surface from abrasion damage. There are three benefits to using comparatively greater strength concrete in the compression zone vs lower strength concrete in the tension zone. It protects the beam from abrasion damage by acting as an ice shield, strengthening the beam's bending ability and providing a more cost-effective section.

1.3. Research objectives and significance

Different ways to limit abrasion damage caused by interaction with ice may be used. The first thought that comes to mind is to improve the concrete's ability to resist abrasion damage in such an environment. This can be accomplished by altering its composition or adding various types of additives. This approach was adopted in the current research and hereafter will be called stage 1 (chapters 3, 4, and 5). This stage will provide an experimental analysis that starts with optimization for the coarse to fine aggregate ratio by volume (C/F) and the maximum aggregate size (Am) of the concrete mixture. A quantitative comparison will be provided between the properties of the offshore structural concrete and other concrete types. Followed by investigating the effect of adding hybrid SCMs. The incorporated SCMs will be FA, SF, and MK. The effect of the inclusion of a variety of fiber types with a broad spectrum of mechanical properties will be analyzed; copper coated steel fiber (CCSFs), polypropylene fibers (PPFs), bundled basalt fibers (BBFs), and filament basalt fiber (FBFs). The fibers will be added at 0.1%, 0.3%, and 0.5% by volume. In addition, the research will cover the impact of adding Nano particles such as nano colloidal silica (NCS) and nano titanium dioxide (NTD) on the concrete abrasion resistance as well as an optimization for its incorporation ratio.

However, because the external layer is the layer that is subjected to abrasion, a different technique to limiting abrasion damage may be used. This is accomplished by using an external layer that is highly abrasion-resistant while preserving the concrete as an inside layer. Using an external layer of concrete with higher abrasion resistance and

attaching it to the internal, lower-cost concrete, on the other hand, could be a suitable option. This approach will be also investigated in the current research and will be called hereafter stage 2.

The authors believe that the findings of this study can be used to develop a method for limiting abrasion damage to concrete in a marine environment. It could also catalyze the increased use of relatively new materials in the concrete industry. This can result in a more effective concrete structure, significant maintenance cost savings, and an incentive to increase the building of new offshore structures in harsher environments, which is in high demand.

1.4. Thesis outline

This research proposal consists of seven chapters described as follows:

Chapter 1 describes the research background and motivation, a review of the literature about the areas of concrete abrasion resistance, possible mitigation strategies, and the objectives and the significance of the doctoral dissertation.

Chapter 2 analyzes the sources of variability associated with the abrasion testing that will be used in the first stage. The second chapter is important due to its direct relationship to the first stage results (chapters 3, 4, and 5).

Chapter 3 analyzes the effect of changing the aggregate properties on the properties of the HPSDC. Also, the impact of adding hybrid SCMs (FA, SF, and MK).

Chapter 4 provides an investigation of the impact of adding different types of fibers on the abrasion resistance and mechanical properties of offshore structural concrete.

Chapter 5 investigates the effects of adding various types of Nano materials on the abrasion resistance and mechanical properties of offshore structural concrete.

Chapter 6 investigates the second alternative through which the flexural behavior of two layers composite beams made of two different types of concrete will be investigated.

Chapter 7 presents the summary of the research and drawn conclusions.

1.5. References

"ACI 318-14." 2014. Building Code Requirements for Structural Concrete (ACI 318-14). American Concrete Institute.

Anju, T., and K.K. Smitha. 2016. "Finite Element Analysis of Composite Beam with Shear Connectors." Procedia Technology 24: 179–87. https://doi.org/10.1016/j.protcy.2016.05.025.

Barour, Sabiha, and Abdesselam Zergua. 2019. "Finite Element Modeling of Strengthened Beams Using CFRP." Journal of Building Materials and Structures 6 (2): 77–87.

Barour, Sabiha, Abdesselam Zergua, Farid Bouziadi, and Waleed Abed Jasim. 2019. "Finite Element Analysis of CFRP-Externally Strengthened Reinforced Concrete Beams Subjected to Three-Point Bending." World Journal of Engineering 17 (2): 183–202. https://doi.org/10.1108/WJE-04-2019-0121.

Basalt Fibers LTD. 2013. "Basalt Chopped Fibre- New Brand TURBOBUILD-24- 300 in Concrete Reinforcement Segment." 2013.

Bogas, Jose, and Augusto Gomes. 2014. "Static and Dynamic Modulus of Elasticity of Structural Lightweight and Modified Density Concrete with and without Nanosilica – Characterization and Normalization" IJCE 12 (2): 170–80. http://ijce.iust.ac.ir/article-1-743-en.html.

Borhan, Tumadhir. 2013. "Thermal and Mechanical Properties of Basalt Fibre Reinforced Concrete." Proc. World Acad. Sci., Eng. Technol. 76

Deák, Tamás, and Tibor Czigány. 2009. “Chemical Composition and Mechanical Properties of Basalt and Glass Fibers: A Comparison.” Textile Research Journal 79 (7): 645–51. https://doi.org/10.1177/0040517508095597.

Dias, Dylmar Penteado, and Clelio Thaumaturgo. 2005. “Fracture Toughness of Geopolymeric Concretes Reinforced with Basalt Fibers.” Cement and Concrete Composites 27 (1): 49–54. https://doi.org/10.1016/J.CEMCONCOMP.2004.02.044.

Fernandes, J.F., T. Bittencourt, and P. Helene. 2008. “A Review of the Application of Concrete to Offshore Structures.” ACI Symposium Publication 253. https://doi.org/10.14359/20187.

Fibres Unlimited. 2007. “Test Report of Basalt Fibre Reinforced Concrete, Polypropylene Reinforced Concrete, Polyacrylonitrile Reinforced Concrete.” Technical Data Sheet 31 (0): 11.

Fu, Qiang, Ditao Niu, Jian Zhang, Daguan Huang, Yan Wang, Mengshu Hong, and Lu Zhang. 2018. “Dynamic Compressive Mechanical Behaviour and Modelling of Basalt–Polypropylene Fibre-Reinforced Concrete.” Archives of Civil and Mechanical Engineering 18 (3): 914–27. https://doi.org/https://doi.org/10.1016/j.acme.2018.01.016.

Gautier, Donald L, Kenneth J Bird, Ronald R Charpentier, Arthur Grantz, David W Houseknecht, Timothy R Klett, Thomas E Moore, et al. 2009. “Assessment of Undiscovered Oil and Gas in the Arctic.” Science 324 (5931): 1175 LP – 1179. https://doi.org/10.1126/science.1169467.

Hamed, M. 2018. “Structural Performance of a Proposed Uhp-Frc Shield in Harsh Environment.” Memorial University of Newfoundland.

Hoff, G. C., and R. Elimov. 1995. “Concrete Production for the Hibernia Platform.” In Annual Conference- Canadian Society for Civil Engineering, 693–716.

Iskhakov, I., Y. Ribakov, K. Holschemacher, and T. Mueller. 2014. “Experimental Investigation of Full Scale Two-Layer Reinforced Concrete Beams.” Mechanics of Advanced Materials and Structures 21 (4): 273–83. https://doi.org/10.1080/15376494.2012.680673.

Iskhakov, Iakov, Yuri Ribakov, and Klaus Holschemacher. 2017. “Experimental Investigation of Continuous Two-Layer Reinforced Concrete Beams.” Structural Concrete 18 (1): 205–15. https://doi.org/10.1002/suco.201600027.

Iskhakov, Iakov, Yuri Ribakov, Klaus Holschemacher, and Stefan Kaeseberg. 2019. “Experimental Investigation of Prestressed Two Layer Reinforced Concrete Beams.” Structural Concrete, no. August: 1–12. https://doi.org/10.1002/suco.201900328.

Jiang, Chaohua, Ke Fan, Fei Wu, and Da Chen. 2014. “Experimental Study on the Mechanical Properties and Microstructure of Chopped Basalt Fibre Reinforced Concrete.” Materials & Design 58 (June): 187–93. https://doi.org/10.1016/J.MATDES.2014.01.056.

Katwal, Utsab, Zhong Tao, and Md Kamrul Hassan. 2018. “Finite Element Modelling of Steel-Concrete Composite Beams with Profiled Steel Sheeting.” Journal of

Constructional Steel Research 146: 1–15. https://doi.org/10.1016/j.jcsr.2018.03.011.

Khorsandnia, Nima, Hamid R. Valipour, and Keith Crews. 2012. “Finite Element Modeling of Timber-Concrete Composite Beams under Short-Term Loadings.” ECCOMAS 2012 - European Congress on Computational Methods in Applied Sciences and Engineering, e-Book Full Papers, no. January: 859–67. https://doi.org/10.13140/2.1.2486.1123.

Kılıç, A, C D Atiş, A Teymen, O Karahan, F Özcan, C Bilim, and M Özdemir. 2008. “The Influence of Aggregate Type on the Strength and Abrasion Resistance of High Strength Concrete.” Cement and Concrete Composites 30 (4): 290–96. https://doi.org/https://doi.org/10.1016/j.cemconcomp.2007.05.011.

Lam, Thanh Quang Khai, and Thi My Dung Do. 2019. “Sliding between Layers in 2-Layer Reinforced Concrete Beams and Shell.” International Journal of Engineering and Advanced Technology 8 (5): 1867–71.

Lin, D F, K L Lin, W C Chang, H L Luo, and M Q Cai. 2008. “Improvements of Nano-SiO2 on Sludge/Fly Ash Mortar.” Waste Management 28 (6): 1081–87. https://doi.org/https://doi.org/10.1016/j.wasman.2007.03.023.

Nader, Ghafoori, Najimi Meysam, and Mohammad Aqel. 2014. “Abrasion Resistance of Self-Consolidating Concrete.” Journal of Materials in Civil Engineering 26 (2): 296–303. https://doi.org/10.1061/(ASCE)MT.1943-5533.0000847.

Nazari, Ali. 2011. “The Effects of Curing Medium on Flexural Strength and Water

Permeability of Concrete Incorporating TiO2 Nanoparticles." Materials and Structures/Materiaux et Constructions 44 (May): 773–86. https://doi.org/10.1617/s11527-010-9664-y.

Newhook, J, and D McGinn. 2007. "Ice Abrasion Assessment – Piers of Confederation Bridgeitle." In Proceedings of the Confederation Bridge Engineering Summit.

Nikbin, I M, M H A Beygi, M T Kazemi, J Vaseghi Amiri, E Rahmani, S Rabbanifar, and M Eslami. 2014. "A Comprehensive Investigation into the Effect of Aging and Coarse Aggregate Size and Volume on Mechanical Properties of Self-Compacting Concrete." Materials & Design 59: 199–210. https://doi.org/https://doi.org/10.1016/j.matdes.2014.02.054.

Parandaman, P, and M Jayaraman. 2014. "Finite Element Analysis of Reinforced Concrete Beam Retrofitted with Different Fiber Composites." Middle-East Journal of Scientific Research 22 (7): 948–53. https://doi.org/10.5829/idosi.mejsr.2014.22.07.21979.

Rashad, Alaa M. 2013. "A Preliminary Study on the Effect of Fine Aggregate Replacement with Metakaolin on Strength and Abrasion Resistance of Concrete." Construction and Building Materials 44: 487–95. https://doi.org/https://doi.org/10.1016/j.conbuildmat.2013.03.038.

Saiidi, M., S. Vrontinos, and B. Douglas. 1990. "Model for the Response of Reinforced Concrete Beams Strengthened by Concrete Overlays." ACI Structural Journal 87 (6): 687–95.

Sandvik, M., T. Hovda, and S. Smeplass. 1994. “Modified Normal Density (MND) Concrete for the Troll GBS Platform.” ACI Symposium Publication 149: 81–102. https://doi.org/10.14359/4069.

Sasmal, S., S. Kalidoss, and V. Srinivas. 2012. “Nonlinear Finite Element Analysis of FRP Strengthened Reinforced Concrete Beams.” Journal of The Institution of Engineers (India): Series A 93 (4): 241–49. https://doi.org/10.1007/s40030-013-0028-9.

Shih, Jeng-Ywan, Ta-Peng Chang, and Tien-Chin Hsiao. 2006. “Effect of Nanosilica on Characterization of Portland Cement Composite.” Materials Science and Engineering: A 424 (1): 266–74. https://doi.org/https://doi.org/10.1016/j.msea.2006.03.010.

Sim, Jongsung, Cheolwoo Park, and Do Young Moon. 2005. “Characteristics of Basalt Fiber as a Strengthening Material for Concrete Structures.” Composites Part B: Engineering 36 (6): 504–12. https://doi.org/https://doi.org/10.1016/j.compositesb.2005.02.002.

Sobolev, K., I. Flores, L. M. Torres-Martinez, P. L. Valdez, E. Zarazua, and E. L. Cuellar. 2009. “Engineering of SiO2 Nanoparticles for Optimal Performance in Nano Cement-Based Materials.” Nanotechnology in Construction 3, 139–48. https://doi.org/10.1007/978-3-642-00980-8_18.

Sujjavanich, S, P Suwanvitaya, D Chaysuwan, and G Heness. 2017. “Synergistic Effect of Metakaolin and Fly Ash on Properties of Concrete.” Construction and Building Materials 155: 830–37. https://doi.org/https://doi.org/10.1016/j.conbuildmat.2017.08.072.

Vu, Dinh Tho, Elena Korol, Yuliya Kustikova, and Huy Hoang Nguyen. 2019. “Finite Element Analysis of Three-Layer Concrete Beam with Composite Reinforcement.” E3S Web of Conferences 97 (May). https://doi.org/10.1051/e3sconf/20199702023.

Zhang, Mao-hua, and Hui Li. 2011. “Pore Structure and Chloride Permeability of Concrete Containing Nano-Particles for Pavement.” Construction and Building Materials 25 (2): 608–16. https://doi.org/https://doi.org/10.1016/j.conbuildmat.2010.07.032.

Zhao, Q, J Dong, H Pan, and S Hao. 2010. “Impact Behavior of Basalt Fiber Reinforced Concrete.” Fuhe Cailiao Xuebao/Acta Materiae Compositae Sinica 27 (December): 120–25.

Zhao, Zheng, Jie Kong, and Hong Yang. 2012. “Study on Frost Resistance of Nano SiO2 Cement Concrete.” Applied Mechanics and Materials 198–199 (September): 48–51. https://doi.org/10.4028/www.scientific.net/AMM.198-199.48.

Chapter 2 Evaluating the ASTM C944 rotating cutters method for determining the abrasion resistance of concrete

2.1. Abstract

Abrasion damage is a concern for some types of structures and the need for proper quantification of it is essential. This research is intended to provide an evaluation for ASTM C944 (rotating cutters method) to assess concrete abrasion resistance. The current investigation involves analysis of the interaction between the cutters and the test specimen and the interpretation of the test results. Such details are important so that the test results may be repeatable, reproducible, and always interpreted in the same fashion. Sources that influence the test inaccuracy were studied to quantify its effects on the test results. In the first instance, the characteristics of the resulting abraded area and its effect on the depth measurement strategy were clarified. Then, the evaluation of abrasion depth using different approaches were investigated. In addition, the effect of the concrete tested surface nature (formed, finished, and cut) was examined. The examined points are believed to be the sources of test high variability. A mitigation of this variability was provided by addressing and analyzing them so it can be avoided in future evaluation. The results indicated that by correctly identifying the characteristics of the abraded patterns and by using a suitable measurement approach, less variable average abrasion depth was obtained. In addition, it was noted that using different depth measurement methods could lead to different abrasion depths results. Also, it was found that the tested surface characteristics could highly affect the abrasion test results.

Keywords: Concrete, abrasion, ASTM, depth measurement, surface finish.

2.2. Introduction

Interaction between concrete and moving objects causes removal of concrete particles. The abrasion resistance of concrete is defined as its ability to withstand this mechanical action and tendency to protect its surface. Concrete structures are subjected to abrasion action in different forms and mechanisms. For instance, in pavements, the concrete is affected by the dynamic motion of vehicles (Nader, Meysam, and Aqel 2014). The resulting surface texture depth is due to the continued movement of wheels and depends on the road noise. Similarly, concrete structures in marine environments where ice may form are prone to mechanical wear. The abrasion of the concrete surface caused by the grinding, crushing and sliding of ice is a significant risk to the integrity of the structure. Worn surfaces also increase friction, which increases local and global loads on the structure, and accelerate reinforcement corrosion through loss of cover and crack promotion. In order to limit such damage, effective evaluation of concrete abrasion resistance using standardized testing is required.

ASTM developed many tests that assess the concrete abrasion resistance, each of them is designated for a specific purpose. (“ASTM C418” 2020) is the abrasion resistance testing using sandblasting. It is used to simulate the abrasion damage from waterborne abrasives. While (“ASTM C779” 2019) contains three procedures; procedure A uses revolving disks for evaluating moderate foot traffic and light to medium tire wheeled traffic, procedure B uses dressing wheels to simulate rolling, pounding and the cutting action of studded tires,

procedure C uses ball bearings to simulate repeated dynamic loads. ASTM C1138 evaluates the abrasion resistance of concrete by simulating the abrasive mechanism of water-borne particles on hydraulic structures. The test uses steel grinding balls revolving on the concrete surface submerged underwater.

The common standard for evaluating the concrete abrasion resistance is the ("ASTM C944" 2019), the rotating cutters test. It is primarily used in the quality control of concrete bridges subjected to traffic movement. The aggressive nature of the test enabled it to address abrasion resistance of a wide range of concrete strengths along with mortar (Scott and Safiuddin 2015). The test involves grinding the planar surface of a concrete sample with a rotating tool attached in a drill press. The load, testing duration and number of revolutions per minute are controlled. The abrasive tool is a T bar (see Fig. 2-1), in which the stem is placed in the chuck of the drill press and hardened steel dressing wheels are stacked on the bar making contact with the concrete. The grinding action of the wheels produce concentric circular tracks which together produce a roughened cylindrical depression in the planar concrete surface.

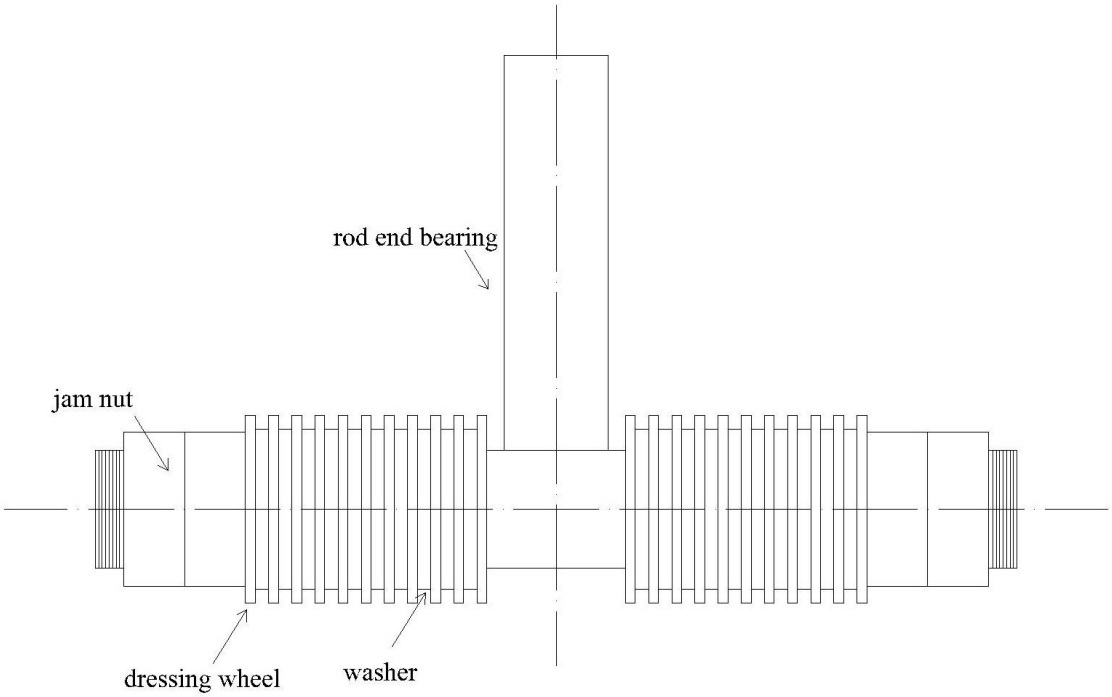

Fig. 2-1 A schematic figure for the ("ASTM C944" 2019) testing tool.

In order to gauge the concrete abrasion resistance, the standard requires that the mass loss, due to abrasion, should be measured to the nearest 0.1 g. Furthermore, the standard also states that the abraded depth should be measured when testing surfaces in situ or if a significant difference in surface density exists. The abrasion depth is measured in accordance with procedure B of ASTM C779 Procedure B, which recommends using a micrometer bridge to measure the average depth to the nearest 0.025 mm. The micrometer bridge is a needle-like tool that can measure the depth at a specific point. The average depth is to be calculated from the measured depths at various points. The standard does not specify the number or locations of the measurement points that should be considered to obtain the average abrasion depth, nor does it explain how to treat the characteristics of the

concentric abraded grooves. Consequently, based on the location and number of measurement points, different average depths of abrasion could be attained. Researchers have independently adopted various techniques to attain the average abrasion depth. (Myers et al. 2012) determined the average abrasion depth as the average of eight measurements. Four measurements within the circumference of the first groove and four measurement points within the perimeter of the last groove. (Naik, Singh, and Hossain 1995) detected the average depth as the average of many measurement points, two points within each groove. Researchers have also adopted different techniques to measure the abrasion depth. For instance, (Pyo, Abate, and Kim 2018) used a digital dial gauge mounted on the drilling press. Whereas, (Horszczaruk 2009) used WMP ECLIPSE CNC 700×1000 ×500 machine that has a piezoelectric contact head ST3 and used HOLOSNT software to analyze the data. While, (Shamsutdinova, Hendriks, and Jacobsen 2017) used a laser scanning method. In which a predefined gridded path, with large number of crossings, were followed by the laser on a step size of 1 mm. The scan results in lines, through which the depth can be measured. That method showed accurate abrasion depth results. But the huge number of paths made it hard to apply.

Although, the attained results may be good enough in terms of repeatability in the same laboratory, they are not reproducible with other laboratories as different strategies are used. That contradicts the purpose of standardized testing methods, which is to provide guidelines for procedures and equipment that will lead to reproducible results between different laboratories. ASTM C944 does not achieve this goal due to its poor reproducibility (Scott and Safiuddin 2015) and large variability in its results (Kevern,

Biddle, and Cao 2015). In order to have an absolute reproducible abrasion depth result, the abraded patterns, in terms of width and depth, should be thoroughly identified and the depth measurement technique adopted should be accurate, robust, and reproducible.

Although concrete surface finishing and surface roughness have a direct effect on the abrasion resistance results of concrete (Jacobsen, Scherer, and Schulson 2015), ("ASTM C944" 2019) specifies testing finished or formed surfaces of the sample. In addition, although it is mentioned in ("ASTM C779" 2019) "procedure A" to operate the abrasion machine for 5 minutes prior to abrasion testing in order to remove surface irregularities, a similar procedure was not mentioned in ("ASTM C944" 2019). If the surface to be tested is the formed surface, this would simulate reality for some structural application such as offshore structures or bridge piers due to ice abrasion or water erosion. In offshore structures or bridge piers, it is usually the formwork adjacent surface is the one that is exposed to abrasion while the finished surface is the one get abraded in other applications such as concrete pavements or slabs on grade. Thus, incomparable results may be obtained according to the selected surface, which also complicates the interpretation of abrasion results from the test.

The investigation provides a detailed quantitative evaluation of the mentioned sources of variability for the evaluation of abrasion resistance of concrete using the ASTM C944 rotating cutters method ("ASTM C944" 2019). Normal strength concrete (NSC) and high-performance concrete (HPC) mixtures were tested. Abraded grooves characteristics were investigated, and different depth measurement methods were adopted and each strategy of

measurement for every method was highlighted with illustration for abrasion depth results difference using each method. In addition, different surfaces (formed, finished, and cut) were tested in order to identify the possible variation according to the characteristics of each surface. This research is intended to provide a better evaluation of concrete abrasion resistance using the rotating cutters approach. That consequently may lead to a more durable and cost-effective concrete structure.

2.3. Concrete mixtures

Table 2-1 shows the materials used for the concrete mixtures. Two mixtures were tested: normal strength concrete and high performance concrete. The mixtures are referred to as specified density concrete. In which, the normal weight coarse aggregate was replaced with 50% by volume with lightweight aggregate (LWA). Table 2-2 presents the composition of the concrete mixtures. Before mixing, the fine aggregate was oven dried at 110 ± 5 C^o for 24 hours to remove the moisture content. The normal weight aggregates were saturated by a specific quantity of water based on the absorption ratio for a reasonable time to reach saturated surface dry (SSD) state. Due to its high absorption, the LWA was kept in a soaked condition for 24 hours and then drained for a period of 6 to 12 hours prior to batching. This is a standard practice in order to achieve a near SSD case and to minimize aggregate moisture content variability (Craig and Wolfe 2012). A similar technique was followed as suggested by Hoff et al. during the construction of the Hibernia platform (Hoff and Elimov 1995). Batches were mixed in a pan mixer. The aggregates, cement, SCMs were added first to the mixer. The mixer was operated for 30 seconds to dry blend these

components. The air entraining admixture (AEA) was added to half the quantity of the batch water and then added to the mixer and mixed for 2 minutes. For HPC mixtures the superplasticizer (SP) was added to the mixer with the other half of the water and mixed for additional 3 minutes. Once the mixing was completed, the batch was tested for slump and air content.

Table 2-1 Materials used for the concrete mixtures.

Cement	general use Portland cement (GU) (ASTM C150 Type I) ("ASTM C150" 2022).
Coarse and fine normal weight aggregate	crushed granite with a specific gravity of 2.6
Lightweight aggregate	expanded slate STALITE lightweight aggregate (ESLWA) with a specific gravity of 1.53 at saturated surface dry state (SSD), absorption of 6% to 9%, and a maximum aggregate size of 12.5 mm.
Superplasticizer	polycarboxylate-based superplasticizer (SP) ("ASTM C494" 2022), ("ASTM C1017" 2013).
Air-entraining agent	An air-entraining agent (AEA) that conforms with ("ASTM C260" 2016).

Table 2-2 Mix proportions of the concrete mixtures.

Mixture designation	Cement (kg/m^3)	Water / binder	LWA (kg/m^3)	NWA (kg/m^3)	F. A. (kg/m^3)	SP (ml/m^3)	AEA (ml/m^3)	Density (kg/m^3)
NSC	300	0.5	315	529	884	_	_	2178
HPC	550	0.3	280	476	595	2650	350	2066

Note: F. A. = Fine Aggregate.

Samples consisted of 100 × 100 × 400 mm prisms and 100 mm diameter × 200 mm height cylinders. The samples were compacted using mechanical vibration table and trowel-finished to obtain smooth surfaces. Twenty-four hours after pouring, the samples

were demolded, labeled, density determined, and placed in a standard curing room, with a temperature of 25 ± 1.5 C^o and 100% relative humidity until required for testing.

2.4. Tests

The tests were carried out at the 28-day. The compressive strength was determined using three identical 100 mm diameter × 200 mm height cylinders from the same batch in accordance with ("ASTM C39" 2021). The abrasion test setup is shown in Fig. 2-2. It was constructed to carefully meet the ("ASTM C944" 2019) standards. The ASTM recommendations covers the loading, number of revolutions per minute (RPM), the duration of testing, the cutters dimensions, and the washers/dressing wheels replacement periods. A standard drill press was modified and used as the abrasion device. The spring that was attached to the spindle was removed. A u-shape extension that can hold the load directly on the spindle was fabricated and installed on the top of the drill press (see Fig. 2-2-a). The purpose of the added part was to maintain a constant load during test time and to minimize any vibrating motion that could affect the abrasion mechanism. The test was performed at a constant speed of 200 RPM (clockwise). The ASTM standard recommends two values of the applied load and two durations of testing. In order to produce an expressing abrasion damage within the constraints set by the ASTM procedure, the test was carried out under a constant load of 19.7 kgs total for six minutes. The rotating cutters were constructed with 20 dressing wheels and 22 washers with an overall diameter of 82.5 mm. The test was performed at the 28-day on the surface of each 100 mm × 100 mm × 100 mm cubes that were cut from different prisms. After the abrasion test was completed, the

surface was cleaned from any remaining debris using compressed air. Then, the abrasion depth was measured.

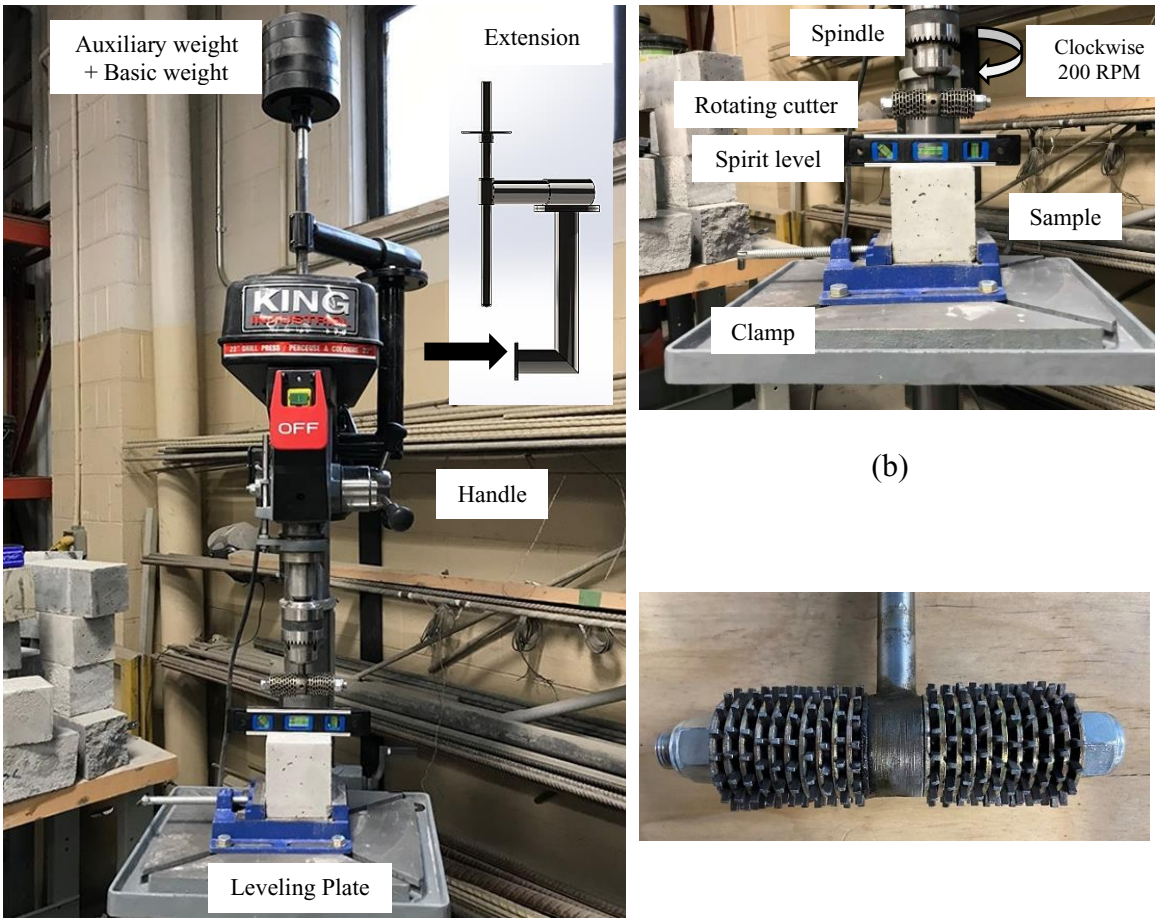

Fig. 2-2 Abrasion resistance test setup: (a) Drill modification, (b) Enlargement of the rotating cutters and sample, and (c) Enlargement of the rotating cutters.

2.5. Depth measurement method

As mentioned earlier, during testing in accordance with ASTM C944 standard, the dressing wheels revolves over the concrete surface producing concentric grooves. In the current study, three depth measurement methods were used to evaluate its ability to provide accurate measurements for the depth of these grooves to determine the average abrasion depth. These methods were as follows.

(1) Micrometer bridge.

(2) Calculating from mass loss: The abrasion depth is calculated from the measured abraded mass loss using Eq. 2-1 and Eq. 2-2.

$$V_t = \frac{M_t}{\rho} \tag{2-1}$$

$$d_{avg.} = \frac{V_t}{A_t} \tag{2-2}$$

where V_t is the total abraded volume, M_t is total abraded mass loss, ρ is the density of the tested concrete, $d_{avg.}$ is the average abrasion depth, and A_t is the total abraded surface area.

(3) Laser scanning approach: The used laser scanner is shown in Fig. 2-3. It is a non-contact FARO Platinum Arm laser scanner. The scanner has an accuracy of 50-µm and a high scan rate of 30 frames/second. It is capable of scanning surfaces without requiring pre-defined paths, which is an easier scanning strategy compared to strategy followed by (Shamsutdinova, Hendriks, and Jacobsen 2017).

Fig. 2-3 Laser scanning arm.

A scan resulted in a large number of data points. The surface data was collected and transferred to a computer. A digital 3-D visual surface was created using Geomagic Control X software. The sample's surface was scanned before the abrasion test was carried out in order to obtain the reference points on the surface. This scan was also used to identify the initial surface roughness of the sample. The initial roughness was calculated using the formula adopted by (Black 2019) as follows:

$$R_a = \frac{1}{n}\sum_{i=1}^{n}|y_i| \tag{2-3}$$

where R_a is the un-abraded surface roughness, n is the number of measurement points, and y_i is the difference between the height at each point and the mean value. The equation defines the surface roughness as the arithmetic average of the absolute values of the roughness profile. Then, the abrasion test was carried out on the surface. After the abrasion test is completed, the surface was re-scanned. Once both surfaces were aligned using the software, the depth of wear was determined for the sample. Figure 2-4 shows the process of determining the depth of wear using scans of a typical sample.

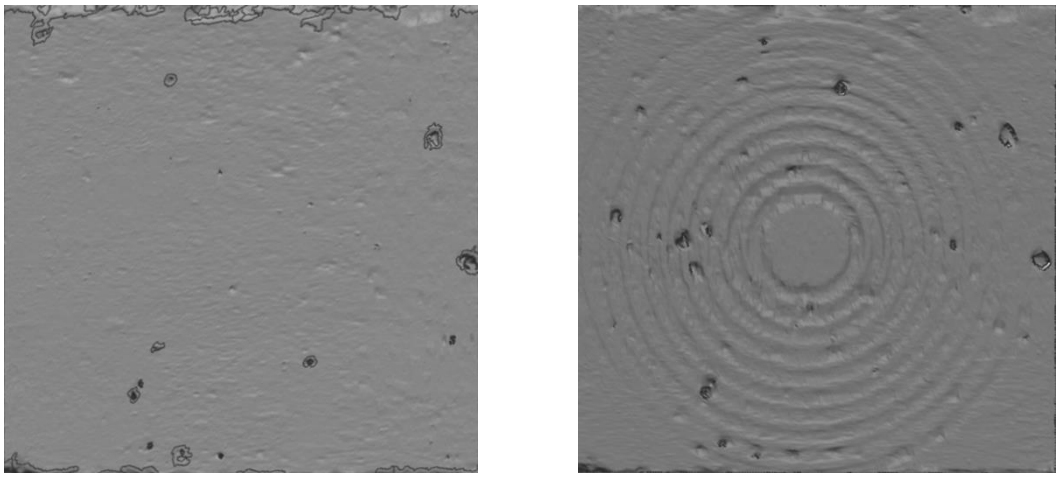

(a) (b)

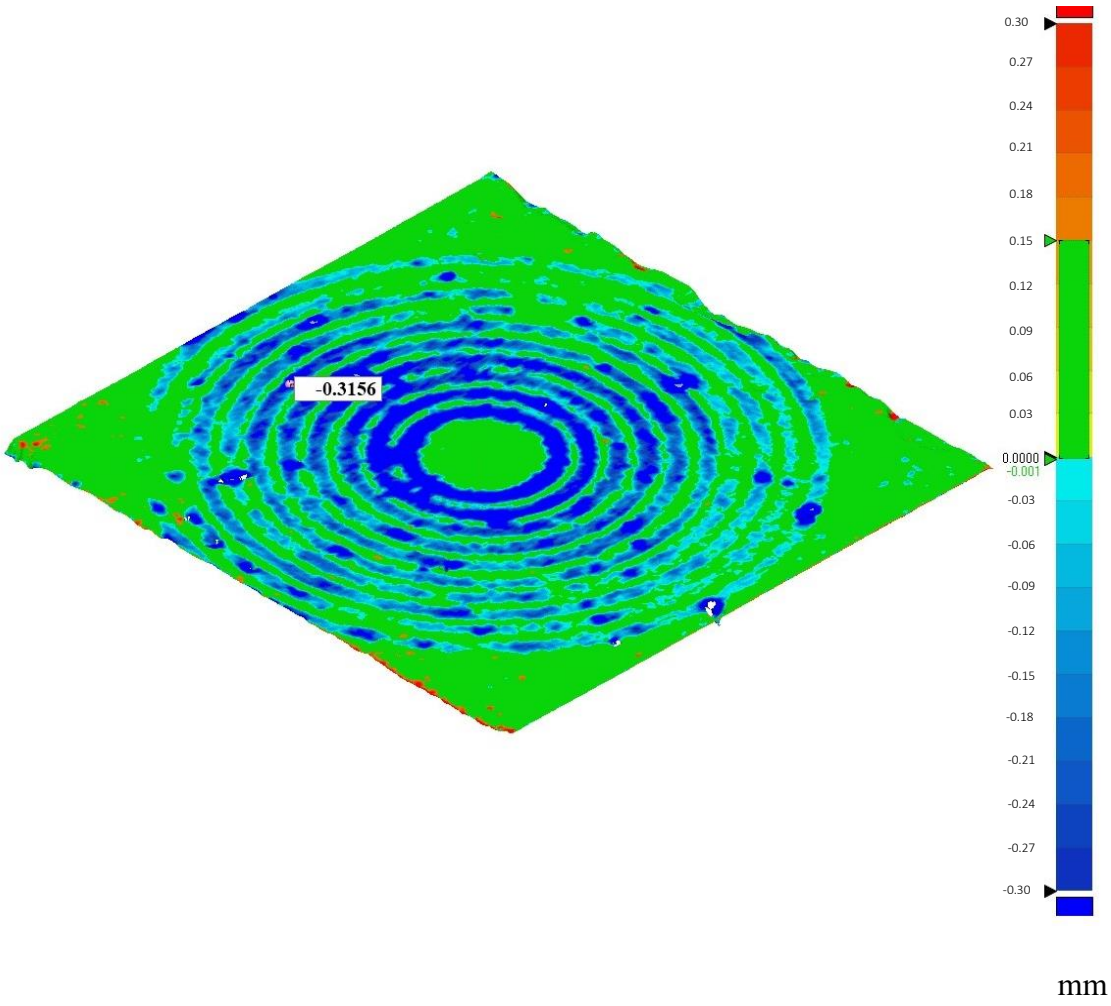

(C)

Figure 2-4 Determining depth of wear process using laser scanning: (a) Initial surface scan, (b) Surface scan after abrasion test, (c) Aligned surfaces and determination of depth of wear.

2.6. Results and discussion

2.6.1. Abraded grooves characteristics

By performing the test on many samples, it was visually sensed that the width and the depth of the abraded grooves are not constant through the abraded sample. That, in turn, may affect the abrasion depth results as each chosen location for the measurement points may have a different depth. Thus, in order to have a meaningful average abrasion depth, the characteristics of the abraded grooves were investigated. For that purpose, the surface data of a laser scanned sample (see Fig. 2-5) was used. A vertical section through the abraded grooves was conducted as can be seen in Fig. 2-5 (a and b). It can be seen that the grooves closer to the centerline of the drill's spindle have higher depths and larger widths. For further validation, the individual points scanned using laser scanning were used. The non-deviated points that represent the patterns between the grooves, were excluded. The coordinates of deviated points were adjusted with respect to the center of the abraded area, which was considered the origin. These points are described by its distance from the origin (r_g), and its deviated depth (d_g). Fig 2-5 (c) represents a relationship between r_g and d_g for each scanned point. This relationship is similar to Fig. 2-5 (b). As Fig. 2-5 (b) is a section over a specific line, but Fig. 2-5 (c) can be considered as a section that collect all measured points along the circumference of the abraded groove. Fig. 2-5 (c) can provide better insight for the characteristics of the abraded grooves. It can be seen from both sections, that a downward trend exists, as the farther the point from the origin, the lower its abrasion depth. That validated the depth variation observation. The phenomena of depth and width

variation could be attributed to the unequal load distribution over each dressing wheel (see Fig. 2-1). The closer wheels to the centerline of the drill's spindle possess higher portion of the load. Therefore, higher depth results at this location. The depth variation can affect the width variation as well. The relationship between the depth and the width is illustrated through the following derivation.

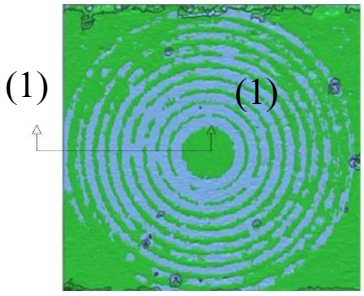

(a)

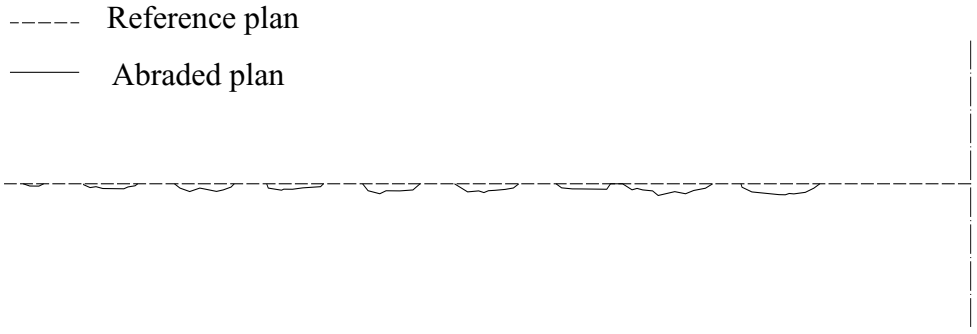

(b)

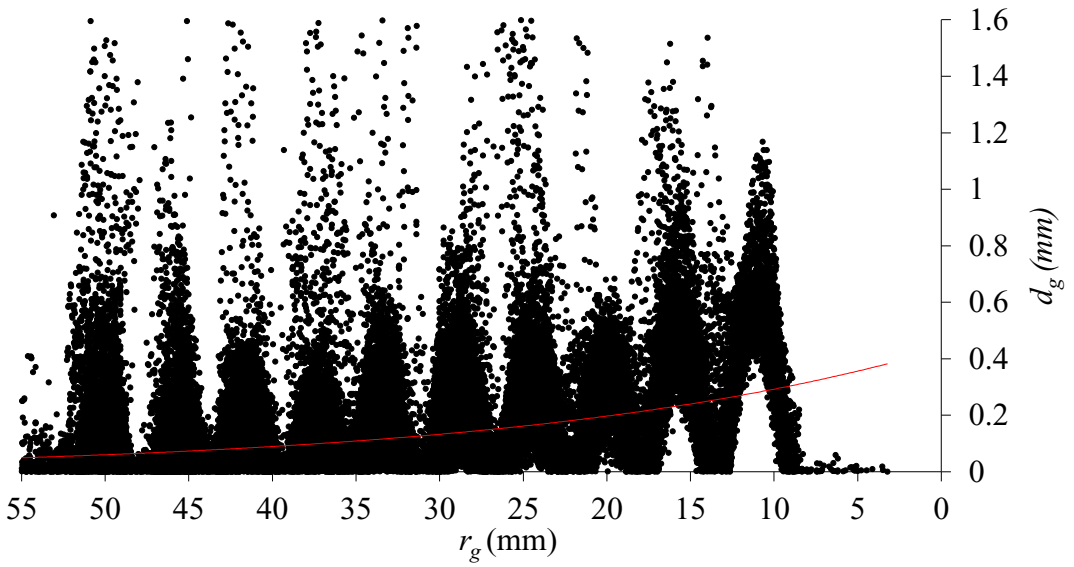

(c)

Fig. 2-5 Laser scanned abraded sample: (a) Abraded sample surface plan, (b) Section 1-1, and (c) r_g and d_g for each scanned point.

As shown in Fig. 2-6 (b)

$$w_g = r_{go} - r_{gi} \tag{2-4}$$

where w_g is the abraded groove width, r_{go} is the outer radius of the groove, and r_{gi} is the inner radius of the abraded groove.

$$r_{go} = \left(\left(r_{gi} + t \right)^2 + (0.5L)^2 \right)^{0.5} \tag{2-5}$$

Where t is the dressing wheel thickness and L is the chord length at a specific depth d_g.

Substituting (Eq. 2-5) in (Eq. 2-4)

$$w_g = \left(\left(r_{gi} + t \right)^2 + (0.5L)^2 \right)^{0.5} - r_{gi} \tag{2-6}$$

As shown in Fig. 2-6 (c)

$$0.5L = (r_w^2 - (r_w - d_g)^2)^{0.5} \tag{2-7}$$

Where L is the chord length, r_w is the dressing wheel radius.

$$L = (8 r_w d_g - 4 {d_g}^2)^{0.5} \tag{2-8}$$

Substituting (Eq. 2-8) in (Eq. 2-6)

$$w_g = ((r_{gi} + t)^2 + 2 r_w d_g - {d_g}^2)^{0.5} - r_{gi} \tag{2-9}$$

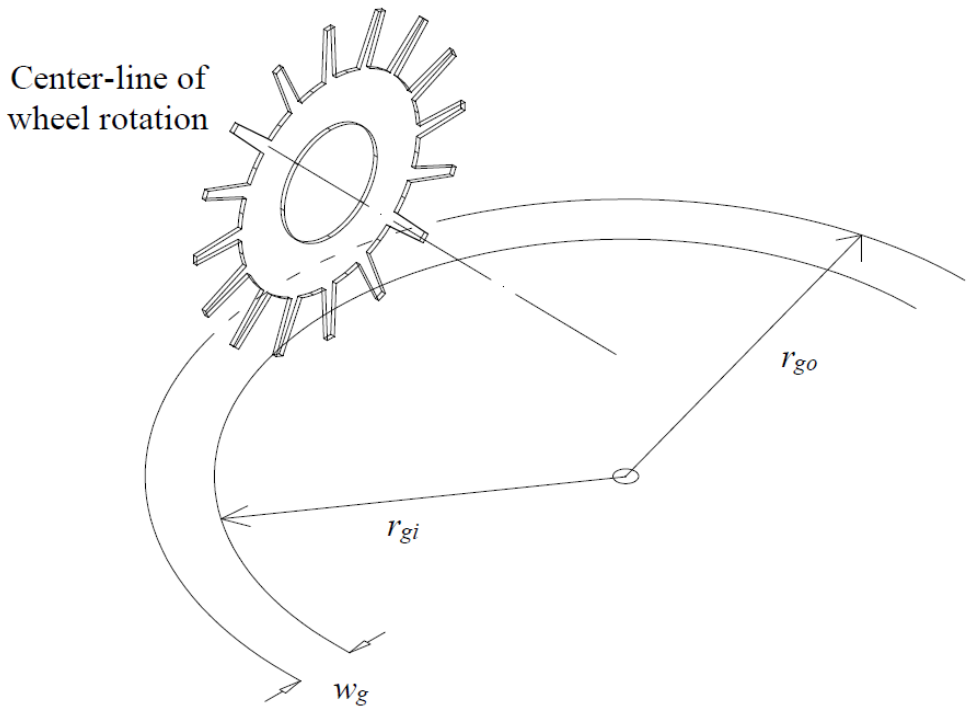

(a)

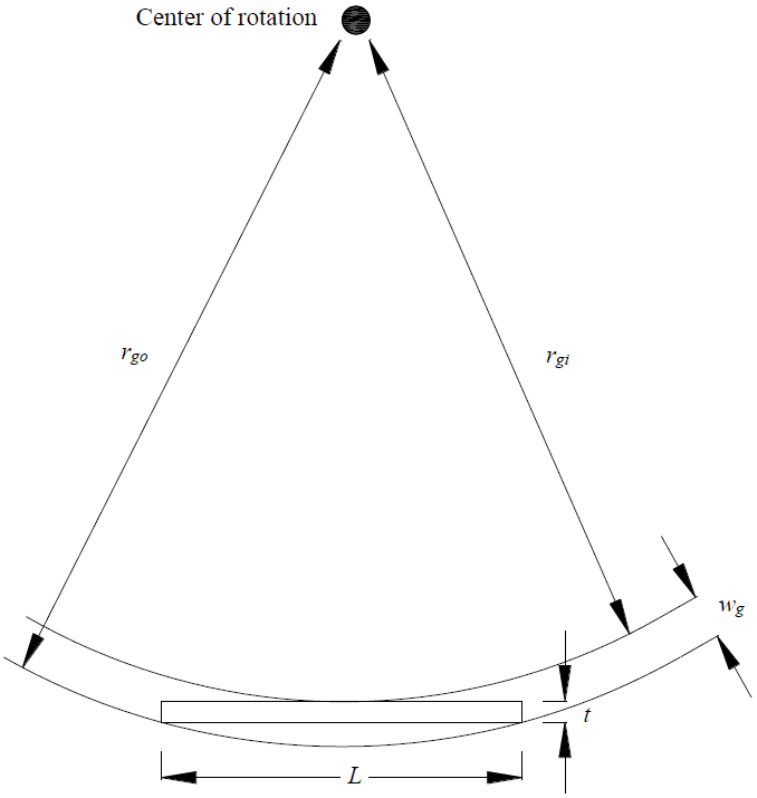

(b)

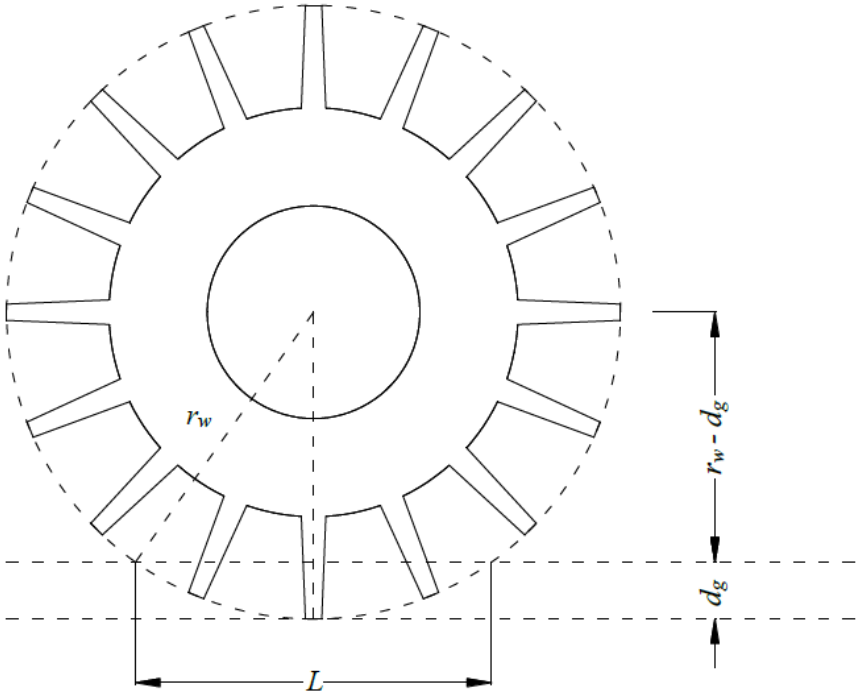

(c)

Fig. 2-6 Notations for a single dressing wheel: (a) Isometric view, (b) Plan view, and (c) Elevation.

From which it can be seen that w_g is inversely proportional to r_{gi} and directly proportional to d_g. That explains the higher widths associated with the higher depths attained at the grooves closer to the centerline of the drill's spindle.

However, it is believed that there are other secondary reasons that contribute to the observed depth and width variation of the abraded grooves. By closely monitoring the motion of each dressing wheel, it was observed that, as the set of dressing wheels rotate around the centerline of the drill's spindle, each dressing wheel undergoes three different

kinds of rotations as illustrated in Fig. 2-7. The first one is the rotation of the dressing wheel around the shaft's horizontal axis (1). The second one is the partial rotation of the dressing wheel around its own vertical axis (2). The third one is the partial rotation of the dressing wheel around its in-plane horizontal axis (3). The first rotation is considered the main source of the abrasion damage. However, it is associated with the drill's RPM. Thus it is of constant rate between all dressing wheels. On the contrary, unlike the first rotation, the rate of the second rotation is not constant between the dressing wheels. Figure 2-8 shows a schematic illustration for the second rotation. The rotation can be described as follows; as the dressing wheel being directed from position 1 to position 2, the dressing wheel makes a partial rotation (Θ) around axis (2). This rotation is similar to a drilling action. That drilling action is another source of abrasion damage for the tested surface and it is associated with the degree of the angle Θ which is directly proportional to the degree of curvature of the followed circular pattern. Each circular pattern has different degree of curvature that is inversely proportional to its radius. That means, each single dressing wheel causes different intensity of abrasion damage (from rotation about axis-2) depending on the radius of the followed pattern. Therefore, the closer the groove to the centerline of the drill's spindle is, the higher the abrasion damage would be. Consequently, higher abrasion depths were developed at the grooves closer to the spindle's centerline.

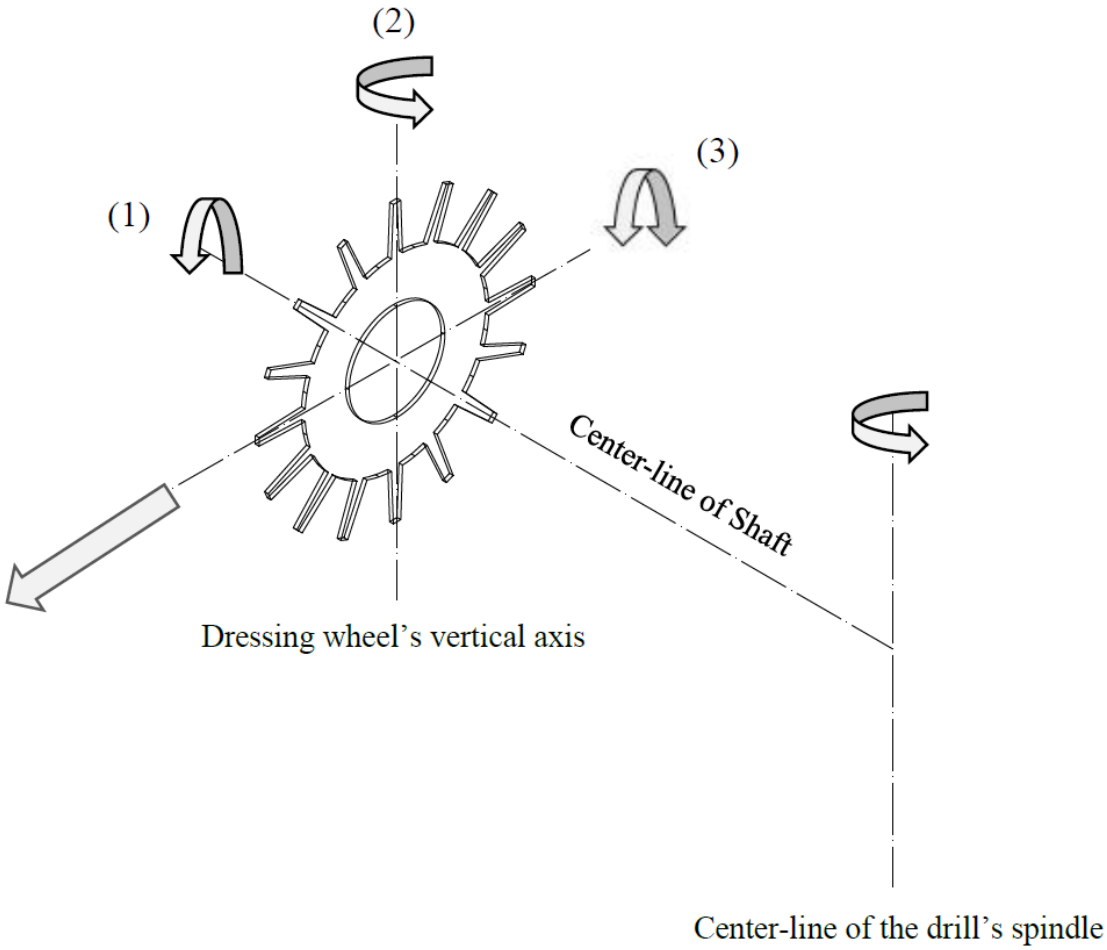

Fig. 2-7 Axes of rotation of a single dressing wheel: (1) shaft's horizontal axis, (2) vertical axis of wheel, and (3) in-plane horizontal axis of wheel.

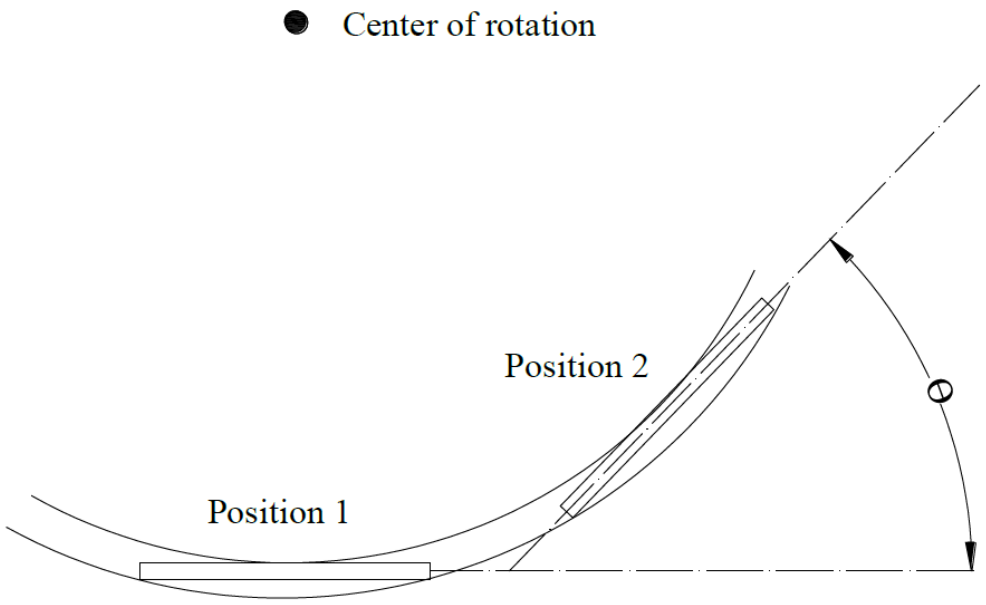

Fig. 2-8 Schematic presentation for the dressing wheel's second rotation.

The second and third rotations originate from existence of a small clearance between the shaft's horizontal axis and the dressing wheel's opening. That small clearance provides the dressing wheel with the ability to partially rotate around axes (2) and (3). These rotations could also lead to widening of the generated abraded grooves and affect the width variation. However, during testing, a centrifugal force is created on the dressing wheels. That force is directly proportional to the distance of the dressing wheel from the centerline of the drill's spindle. The wheels closer to the centerline of the drill's spindle, possesses less centrifugal force. Therefore, more rotation ability exists for the closer wheels compared to further wheels. Consequently, larger grooves widths are created at the grooves closer to the drill's spindle.

Although the illustrated motions contribute to width and/or depth variation of the abraded grooves, their effect is hard to be quantified. Therefore, only the geometrical relationships between the w_g, d_g, and r_g were considered and the relationship is constructed as mentioned in Eq. 2-9.

2.6.1. Depth measurement methods

2.6.1.1. Micrometer bridge

As illustrated earlier, the depth and width are not constant over the abraded area. Thus, when using a micrometer bridge to measure the average abrasion depth, ten measurement points were considered along a diagonal that cuts all the abraded grooves, one point at each groove. Table 2-3 shows the attained average mass loss and the measured average abrasion depth results for the tested mixtures (three samples each) and its compressive strength. It can be seen that, the abrasion depth results measured using a micrometer showed high coefficient of variation values. Such finding highlighted that, even though the selected locations of the measurement points are distributed over the abraded grooves, the results of the abrasion depth using the micrometer bridge were not consistent. This is attributed to the limited abrasion depth that is usually produced at the end of the test, which makes the abrasion depth process hard to be achieved accurately with a micrometer bridge.

Table 2-3 Average abrasion depth for tested concrete mixtures using different measurement methods.

Mixture designation	f_c' (MPa)	Abraded Mass loss (gm)	Abrasion depth (mm) obtained from					
			Micrometer	Coefficient of variation	Laser scanning	Coefficient of variation	Equation 2-14	Coefficient of variation
NSC	35.9	7.65	1.26	38.9%	0.856	7.6%	0.962	7.1%
HPC	73.1	3.87	0.69	78.3%	0.370	8.9%	0.461	9.3%

2.6.1.2.Calculating from mass loss

As mentioned before, the depths and widths of the abraded grooves are not constant over the abraded area. Thus, in order to calculate the abrasion depth using the abraded mass loss, the volume of the abraded grooves had to be identified in terms of width and depth.

$$V_t = \sum(2\pi r_g) d_g w_g \tag{2-10}$$

Substitute w_g from Eq. 2-9

$$V_t = \sum 2\pi r_g d_g ((r_{gi} + t)^2 + 2r_w d_g - {d_g}^2)^{0.5} - r_{gi}) \tag{2-11}$$

As explained, as the distance of the groove from the center-line of the drill's spindle increases, its depth and width decrease. However, its perimeter also increases. From the experimental analysis, as can be seen in Fig. 2-9, it was found that the abraded volume has almost a linear behavior through the distance from the center. So, for simplicity, the volume of the abraded grooves can be considered equal throughout the abraded sample.

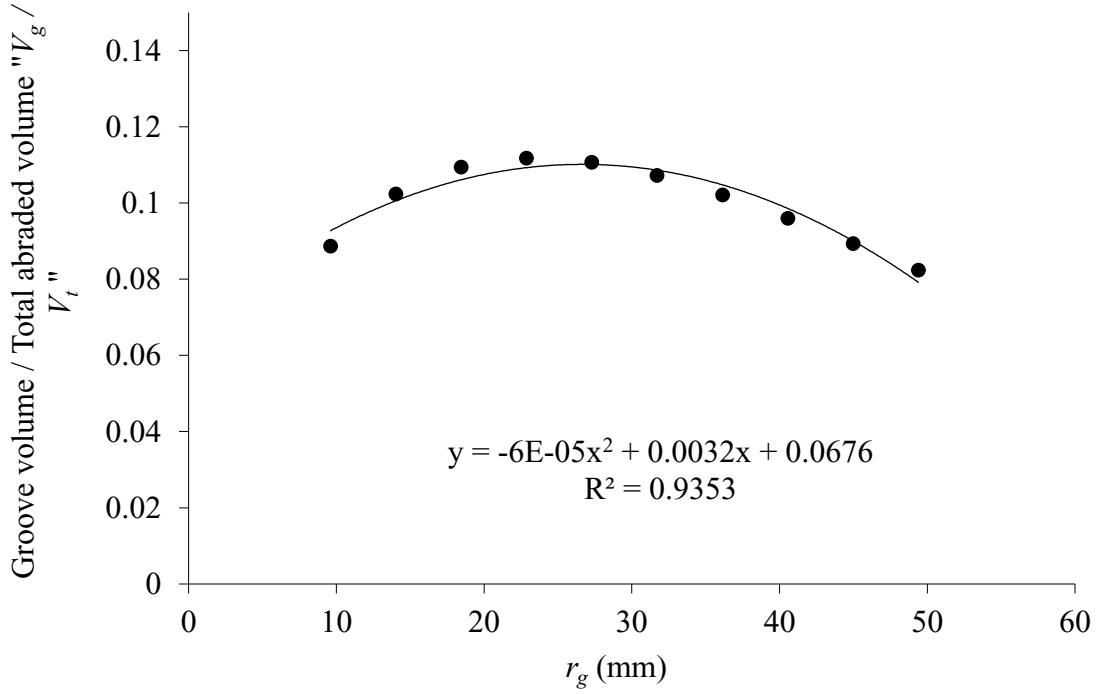

Fig. 2-9 The relationship between the radius of the abraded groove and the ratio of groove abraded volume to the total abraded volume.

$$\frac{V_g}{V_t} = \frac{1}{n} \tag{2-12}$$

where n is the number of grooves

$$V_t = 2\pi r_g d_g n((r_{gi} + t)^2 + 2r_w d_g - {d_g}^2)^{0.5} - r_{gi}) \tag{2-13}$$

Substituting (Eq. 2-13) in (Eq. 2-1)

$$M_t = 2\pi r_g d_g n\rho \times (\,((r_{gi}+t)^2 + 2r_w d_g - {d_g}^2)^{0.5} - r_{gi}) \qquad (2\text{-}14)$$

Equation 2-14 is an original equation that is proposed through this study. It can relate the abraded mass loss M_t to the abrasion depth of each groove d_g, from which an average abrasion depth can be calculated. Table 2-3 shows the results attained for the two tested mixtures (three samples each) using Eq. 2-14. It can be seen, that the coefficient of variation of the attained results was relatively low.

2.6.1.3.Laser scanning approach

As shown in Table 2-3, laser scanning provided low coefficient of variation results for the tested concrete. It can be also noted that the abrasion depths using laser scanning approach were lower than the depths attained using Eq. 2-14. That is attributed to, as explained earlier, that the actual groove width (which is measured using laser scanning) is larger than the width calculated using Eq. 2-14. When calculating the depth from the volume loss, as the width is less than the actual width, higher abrasion depths were attained using Eq. 2-14. However, the laser scanning's high cost, limited its use. Thus, in the current research, hereafter, the average abrasion depth was attained by calculating it from mass loss using the proposed equation (Eq. 2-14) as this equation can provide reliable, accurate abrasion depth measurement at no cost.

2.6.2. Effect of testing different surfaces

As mentioned earlier, three types of surface finishes were examined, namely; surface adjacent to formwork, surface with hand trowel finish, and surface cut using a saw. Table 2-4 shows the average surface roughness from each surface nature as the average of roughness (measured using laser scanning) of three cubic samples for each mixture. The average roughness of the formed surfaces and cut surfaces was nearly equal to zero, while trowel finished surfaces had much higher value of roughness. After the average surface roughness was obtained, the abrasion test was carried out. Table 2-4 and Fig. 2-10 show the abrasion depth results obtained for each surface nature. The tests results revealed that the surface finish has an effect on the abrasion resistance results. Furthermore, although formed surfaces and cut surfaces have a nearly equal surface roughness, formed surfaces had a higher abrasion depth by 46.2% and 76.6% for NSC and HPC, respectively. This could be attributed to that, formed surfaces have a thin layer of paste that is formed during placing and vibrating of concrete. This layer would be the first layer to get abraded during the abrasion process. However, this layer does not fully represent the abrasion resistance of the concrete tested. As the abrasion resistance of concrete is fully evaluated at higher depths passing this layer where the concrete is a more homogenous mixture. These observations are in agreement with the study carried out by (Sonebi and Khayat 2001). The study included testing higher strength concrete ($f_c^{'}$ = 79.8MPa to 91.6MPa) according to procedure c of the ("ASTM C779" 2019).

Table 2-4 Abrasion depth for the tested specimens for different surface finishes.

Mixture designation	Abrasion depth (mm)		
	Formed surface	Trowel finished surface	Cut surface
Average surface roughness	0.009	0.932	0.005
NSC	0.962	1.790	0.658
HPC	0.461	0.758	0.261

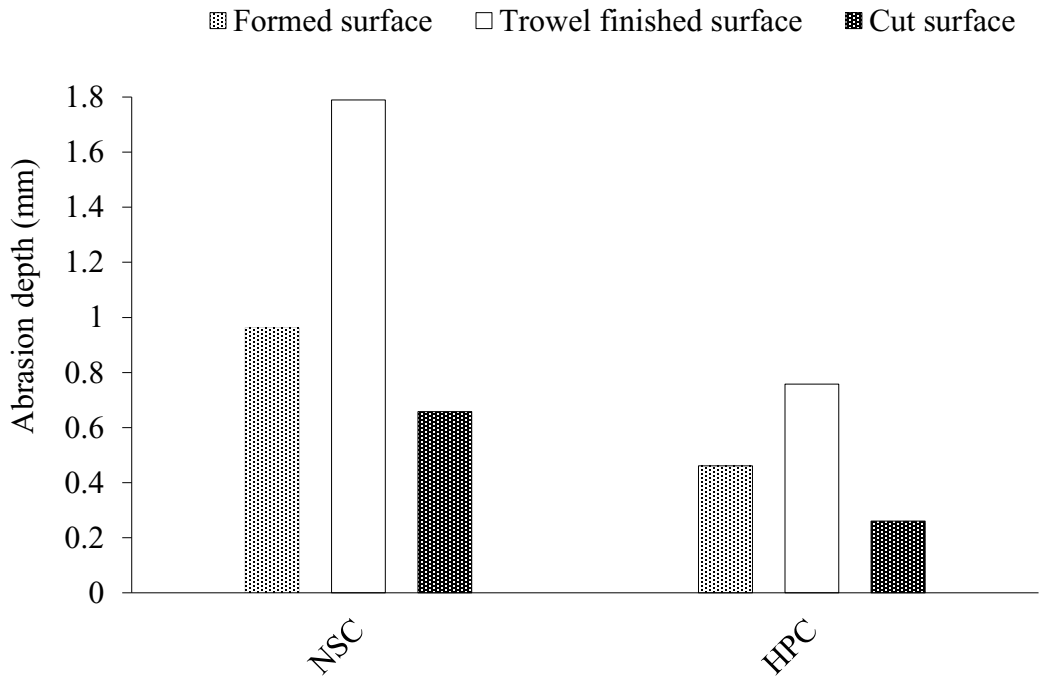

Fig. 2-10 Abrasion depths of formed, trowel finished, and cut surfaces.

On the other hand, trowel finished surfaces had much higher abrasion depths compared to formed surfaces by 86.1% and 64.4% for NSC and HPC, respectively. Also, as can be seen from Fig. 2-11 uniform abrasion depth in the trowel finished surfaces was not achievable. This is mainly due to the high surface roughness of these surfaces. In addition, higher surface roughness that trowel finished surface possesses led to vertical

vibration of the drill during testing, that can be clearly noticed from the vibration of the drill lever, especially at the beginning of the test. This vibration clarified that for high roughness surfaces, the mechanism of concrete abrasion is different compared to smoother surfaces. For high roughness surfaces, the abrasion test process using the cutters is accompanied by impinging the surface that results from the vertical motion that the drill has over the sample. This vertical motion causing an increment of the load applied due to the existence of a dynamic effect. That leads to another form of wear to the trowel finished surface. In addition, usually in smoother surfaces, it is only the vertical load applied that controls the severity of the abrasion process. However, due to high surface irregularities present in the trowel finished surface, the horizontal movement of the wheels also plays a rule in the abrasion process by removing these irregularities, which can occur at any value of the applied load. Furthermore, mixtures tested contains LWA. During placing and vibrating, LWA tends to float on the surface due to its low specific gravity. Which means that the upper finished surface contains higher content of LWA. LWA aggregate used has lower hardness (Los Anglos abrasion value of 25%) compared to the used NWA (Los Anglos abrasion value of 16%). The lower hardness of LWA could be also responsible for the high abrasion depth resulting in trowel finished surfaces, as the concrete abrasion resistance depends mainly on the hardness of the used aggregate (Kılıç et al. 2008).

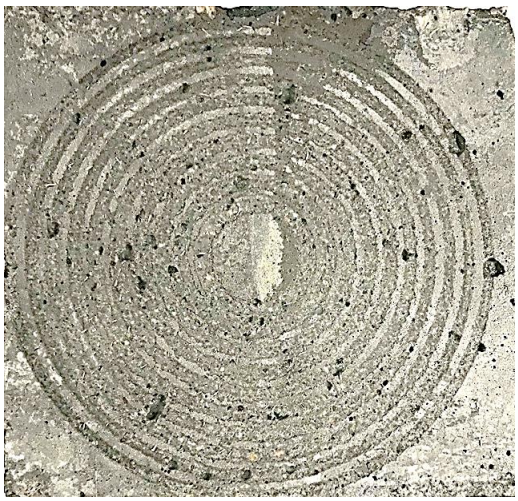

(a)

(b)

(c)

Fig. 2-11 Different tested surfaces nature: (a) Formed surface, (b) Trowel finished surface, and (c) Cut surface.

2.7. Conclusions

This current study provided an evaluation for ("ASTM C944" 2019) (rotating cutters method) to determine abrasion resistance of the concrete. It involved detailed analysis of the interaction between the rotating cutters and the test specimen and the interpretation of the test results. From our analysis it can be concluded that:

1. Due to the rotating cutters testing mechanism, depths and widths of the resulted abrasion grooves were not constant through the abraded area. That have a direct influence on the locations of depth measurement points if to be chosen manually.
2. Using micrometer bridge provided average abrasion depth results with high coefficient of variation.
3. After identifying the abraded pattern of grooves in terms of width and depth, a reliable equation was developed that provided low coefficient of variation average abrasion depth values.
4. Different depth measurement methods can effectively affect depths results, because of accuracy and method of measurement.
5. Testing different surfaces (formed, finished, and cut) leads to different results under same condition of testing, as every surface has its own characteristics of homogeneity and surface roughness. Cut surface had the highest abrasion resistance due to its homogeneity compared to finished surface. While finished surface had the least abrasion resistance due to its high un-abraded surface roughness.

2.8. References

"ASTM C1017." 2013. Standard Specification for Chemical Admixtures for Use in Producing Flowing Concrete.

"ASTM C150." 2022. Standard Specification for Portland Cement. https://doi.org/10.1520/C0150_C0150M-22.

"ASTM C260." 2016. Standard Specification for Air-Entraining Admixtures for Concrete. https://doi.org/10.1520/C0260_C0260M-10AR16.

"ASTM C39." 2021. Standard Test Method for Compressive Strength of Cylindrical Concrete Specimens. https://doi.org/10.1520/C0039_C0039M-21.

"ASTM C418." 2020. Standard Test Method for Abrasion Resistance of Concrete by Sandblasting. https://doi.org/10.1520/C0418-20.

"ASTM C494." 2022. Standard Specification for Chemical Admixtures for Concrete. https://doi.org/10.1520/C0494_C0494M-19E01.

"ASTM C779." 2019. Standard Test Method for Abrasion Resistance of Horizontal Concrete Surfacese. https://doi.org/10.1520/C0779_C0779M-12.

"ASTM C944." 2019. Standard Test Method for Abrasion Resistance of Concrete or Mortar Surfaces by the Rotating-Cutter Method. https://doi.org/10.1520/C0944_C0944M-19.

Black, J Temple. 2019. DeGarmo's Materials and Processes in Manufacturing. Tenth

edition. Hoboken, NJ : Wiley, [2008] ©2008. https://search.library.wisc.edu/catalog/9910066779802121.

Hoff, G. C., and R. Elimov. 1995. “Concrete Production for the Hibernia Platform.” In Annual Conference- Canadian Society for Civil Engineering, 693–716.

Horszczaruk, E K. 2009. “Hydro-Abrasive Erosion of High Performance Fiber-Reinforced Concrete.” Wear 267 (1): 110–15. https://doi.org/https://doi.org/10.1016/j.wear.2008.11.010.

Jacobsen, Stefan, George W Scherer, and Erland M Schulson. 2015. “Concrete–Ice Abrasion Mechanics.” Cement and Concrete Research 73: 79–95. https://doi.org/https://doi.org/10.1016/j.cemconres.2015.01.001.

Kevern, J., D. Biddle, and Q. Cao. 2015. “Effects of Macrosynthetic Fibers on Pervious Concrete Properties.” Journal of Materials in Civil Engineering 27 (9): 6014031. https://doi.org/10.1061/(ASCE)MT.1943-5533.0001213.

Kılıç, A, C D Atiş, A Teymen, O Karahan, F Özcan, C Bilim, and M Özdemir. 2008. “The Influence of Aggregate Type on the Strength and Abrasion Resistance of High Strength Concrete.” Cement and Concrete Composites 30 (4): 290–96. https://doi.org/https://doi.org/10.1016/j.cemconcomp.2007.05.011.

Myers, John, Jeffery Volz, Eric Sells, Krista Porterfield, Trevor Looney, Brian Tucker, and Kyle Holman. 2012. Self-Consolidating Concrete (SCC) for Infrastructure Elements Summary Report.

Nader, Ghafoori, Najimi Meysam, and Mohammad Aqel. 2014. “Abrasion Resistance of Self-Consolidating Concrete.” Journal of Materials in Civil Engineering 26 (2): 296–303. https://doi.org/10.1061/(ASCE)MT.1943-5533.0000847.

Naik, Tarun R., Shiw S Singh, and Mohammad M. Hossain. 1995. “Abrasion Resistance of High-Strength Concrete Made with Class C Fly Ash.” ACI Materials Journal 92 (6). https://doi.org/10.14359/9785.

Pyo, Sukhoon, Selamu Yihune Abate, and Hyeong-Ki Kim. 2018. “Abrasion Resistance of Ultra High Performance Concrete Incorporating Coarser Aggregate.” Construction and Building Materials 165: 11–16. https://doi.org/https://doi.org/10.1016/j.conbuildmat.2018.01.036.

Scott, Benjamin, and Md Safiuddin. 2015. “Abrasion Resistance of Concrete – Design, Construction and Case Study.” Concrete Research Letters 6 (September): 136–48.

Shamsutdinova, Guzel, Max Hendriks, and Stefan Jacobsen. 2017. “Concrete-Ice Abrasion Laboratory Experiments.” Proceedings - International Conference on Port and Ocean Engineering under Arctic Conditions (ISSN 0376-6756) Http://Www.Poac.Com, January.

Sonebi, M, and Kamal Khayat. 2001. “Testing Abrasion Resistance of High-Strength Concrete.” Cement Concrete and Aggregates - CEMENT CONCRETE AGGREGATES 23 (June). https://doi.org/10.1520/CCA10523J.

Craig, Peter and Wolfe, Bill. 2012. “Another Look at the Drying of Lightweight Concrete-A Comparison of Drying Times for Normal weight and Lightweight Floors.” Concrete International: 53–58.

Chapter 3 Abrasion resistance of the high performance specified density concrete for offshore structural application

3.1. Abstract

The high performance specified density concrete (HPSDC) is a type of concrete that is developed by partial replacement of coarse aggregate with lightweight coarse aggregate at a specific percentage. This concrete type is usually used for offshore structural applications. The key objective of the current study is to evaluate and provide an enhancement to the abrasion resistance and the mechanical properties of the HPSDC. The study is comprised of two successive levels. In the first level, the aggregate properties are studied; an optimization for the coarse to fine aggregate ratio by volume (C/F), the maximum aggregate size (A_m), and a quantitative comparison is provided between the properties of the HPSDC compared to the high performance normal weight concrete (HPNWC) and the high performance lightweight aggregate concrete (HPLWAC). In the second level, the effect of adding hybrid supplementary cementitious materials (SCMs) was investigated. The incorporated SCMs were fly ash (FA), silica fume (SF), and metakaolin (MK). The fresh mixtures' workability and percentage of air content were tested. The hardened concrete properties were tested according to seven different ASTM standard tests. The tests results revealed that it is recommended to develop the HPSDC with a C/F aggregate ratio of 1.6 as the abrasion resistance and mechanical properties of the HPSDC showed ultimate performance at this ratio. Changing A_m affected the tensile properties of the HPSDC. However, it affected other tested concrete properties to a lesser

extent. It was also indicated that the HPSDC had lower, yet comparable, mechanical properties and abrasion resistance compared to the HPNWC. However, it had higher mechanical properties and abrasion resistance compared to the HPLWAC. Although usage of FA blended with SF negatively impacted the HPSDC properties at early testing dates, it showed good performance at a later age. On the other hand, the results of the tests revealed that using MK in the SF system showed better performance compared to incorporating FA with SF.

Keywords: High performance specified density concrete, abrasion resistance, mechanical properties, fly ash, silica fume, and metakaolin.

3.2. Introduction

Moving ice sheets interact with offshore concrete structures in harsh environments. That interaction could cause considerable wear which leads to possible damage, higher maintenance cost, and decreased life cycle. An example of a structure in ice-infected water is the 1.3 billion-dollar (CAN) Confederation Bridge in Canada that links Prince Edward Island with the mainland at New Brunswick. Monitoring of the bridge showed some wear damage to the concrete pillars at the water-line due to interaction with the floating ice sheets. Some remediation and restoration work has been proposed and is currently being carried out on its concrete pillars.

Concrete for offshore structures is a special type of concrete. It has to be of high performance to withstand such harsh environmental conditions (“ACI 318-14” 2014). Also, in some cases, it has to be of reduced weight as well. Offshore platforms, for instance,

are constructed onshore and then are towed to their final position. That towing phase requires concrete with specific unit weight. For that reason, the incorporation of lightweight aggregate became an attractive alternative (Fernandes, Bittencourt, and Helene 2008). However, full replacement of concrete coarse aggregate with lightweight aggregate provides concrete with relatively lower mechanical properties and low abrasion resistance. Hence, for offshore structural applications, the replacement of coarse aggregate with lightweight aggregate is preferred to be made partially and the developed concrete is called specified density concrete or modified normal density concrete.

HPSDC has been used widely for offshore structural applications. In 1991, 450,000 tons of concrete, mostly of HPSDC with 50% partial replacement of coarse aggregate by the lightweight aggregate, were used in the construction of the large gravity-based structure, the Hibernia platform (Hoff and Elimov 1995). In addition, it was also used in the construction of the Troll A GBS platform (Sandvik, Hovda, and Smeplass 1994), which was the world largest structure ever moved at that time. The use of HPSDC enabled such a huge structure to be towed in the sea in 1996. Moreover, HPSDC is currently being used in the construction of the new gravity-based structure of West White Rose. However, there is a demand for a more developed HPSDC to be used in harsher environmental regions such as the Arctic. As the Arctic is the holder of 13% of the world's undiscovered oil and 30% of undiscovered gas (Gautier et al. 2009), it is considered a valuable resource in the future of oil and gas. However, one of the reasons that makes exploration there to be limited is the extremely harsh environmental conditions that the concrete is subjected to there.

Despite the huge cost and importance of the HPSDC, very limited research was found on it. (Bogas and Gomes 2014) studied the specified density concrete made with different cement content, different initial wetting conditions, different types and volumes of coarse lightweight aggregate, and the effect of nano-silica addition. They reported a reduction of the modulus of elasticity with the incorporation of LWA. Although one of the main concerns regarding HPSDC in marine environments is its abrasion resistance, it is not yet investigated.

Concrete abrasion resistance is directly related to its composition. It is affected by the type of aggregates (Kılıç et al. 2008), concrete's C/F aggregate ratio, and maximum aggregate size (Nikbin et al. 2014). Also, the incorporation of different types of SCMs can affect the concrete abrasion resistance. (Rashad 2013) studied the effect of incorporating MK on concrete and found an enhancement reached 46.24% in the abrasion resistance, accompanied by higher compressive strength and splitting tensile strength. (Sujjavanich et al. 2017) found an enhancement in the concrete abrasion resistance with the incorporation of MK combined with FA at different blending ratios. (Srivastava 2012) performed a study on the effect of using SF blended with MK on the concrete compressive strength. The study reported that the optimum ratio of SF and MK was found at 6% and 15%, respectively. However, there is no information presently known addressing the HPSDC abrasion resistance compared to other concrete types or the effect of the aggregate composition on it. Also, there are no studies available on the effect of the addition of blended SCMs on HPSDC abrasion resistance.

The limited research and importance of HPSDC highlighted the need for further research investigating its properties. The current investigation starts with optimization of its C/F aggregate ratio and A_m. Followed by a detailed comparison between the HPSDC, HPNWC, and HPLWAC, to quantify its abrasion resistance performance. Also, the impact of adding hybrid SCMs (FA, SF, and MK) on the HPSDC properties was investigated.

Compressive strength, splitting tensile strength (STS), flexural strength (FS), static modulus of elasticity (SME), and dynamic modulus of elasticity (DME) were tested according to ASTM standards. The abrasion resistance was evaluated using the rotating cutters method ("ASTM C944" 2019) and sandblasting ("ASTM C418" 2020)

The authors believe that this study could lead to offshore concrete with developed abrasion resistance and enhanced mechanical properties. Which in turn could lead to a far more cost-effective offshore structure, huge maintenance cost savings, and providing an incentive to extend construction for new offshore structures in harsher environmental regions which is highly demanded.

3.3. Experimental program

3.3.1. Material properties

General use Portland cement (GU) ("ASTM C150" 2022), FA (ASTM C618 Type F) ("ASTM C618" 2022), SF ("ASTM C1240" 2020), and MK (ASTM C618 Class N) were used as binders for the developed mixtures. The chemical analysis and physical properties of the used cement and SCMs are shown in Table 3-1. The lightweight aggregate used was STALITE expanded slate lightweight aggregate (ESLWA) that had a 12.5 mm maximum

aggregate size and specific gravity of 1.53 at saturated surface dry state (SSD). The aggregate had high absorption, due to its porous nature, ranging from 6% to 9%. Table 3-2 shows the ESLWA physical characteristics. The normal weight aggregates (NWA) used, for both coarse and fine aggregate, were crushed granite stones with a specific gravity of 2.6. The normal weight coarse aggregate has 0.6% absorption. Ten millimeters and 20 mm normal weight maximum aggregate sizes were used. Pictures of the ESLWA and coarse normal weight aggregates are shown in Fig. 3-1. The gradation analysis for the aggregates used is presented in Fig. 3-2 with the curves indicating the limits specified by ASTM C33. Polycarboxylate-based superplasticizer (SP) that conforms to ASTM C494 Type A and F, and ASTM C1017 Type I (ASTM: C494/C494M-13 2013), ("ASTM C1017" 2013) was used to achieve the required workability for the developed mixtures. An air-entraining agent (AEA) that confines to ("ASTM C260" 2016) was used to improve the durability of the hardened concrete against freeze and thaw.

Table 3-1 Chemical analysis and physical properties of the used cement and SCMs.

Chemical analysis (%)	Cement	FA	SF	MK
SiO_2	19.64	52	89.1	52
Al_2O_3	5.48	23	0.67	43
Fe_2O_3	2.38	11	0.49	<2.2
CaO	62.44	5	6.12	<0.2
MgO	2.48	-	0.31	<0.1
SO_3	4.32	-	0.16	-
K_2O	-	-	0.49	<0.40
Na_2O	-	-	0.26	<0.05
Cl	-	-	0.04	-
Total alkali	0.97	-	-	-
Free lime	1.03	-	-	-
LOI	2.05	0.21	2.81	0.95
C_3S	52.34	-	-	-
C_2S	16.83	-	-	-
C3A	10.5	-	-	-
C4AF	7.24	-	-	-
Physical properties				
Specific gravity	3.15	2.37	2.20	2.56

Table 3-2 Physical characteristics of ESLWA

Absorption Saturated Surface Dry (ASTM C127)	6% to 9%
Soundness (% Loss) Magnesium Sulfate (ASTM C88)	0 - 0.01%
Sodium Sulfate (ASTM C88)	0 - 0.23%
25 Cycles Freezing and Thawing (AASHTO T 103)	0.22 - 0.80%
Toughness Los Angeles Abrasion (AASHTO T 96)	25 - 28%
Stability Angle of Internal Friction (Loose)	40° - 42°
Angle of Internal Friction (Compacted)	43° - 46°

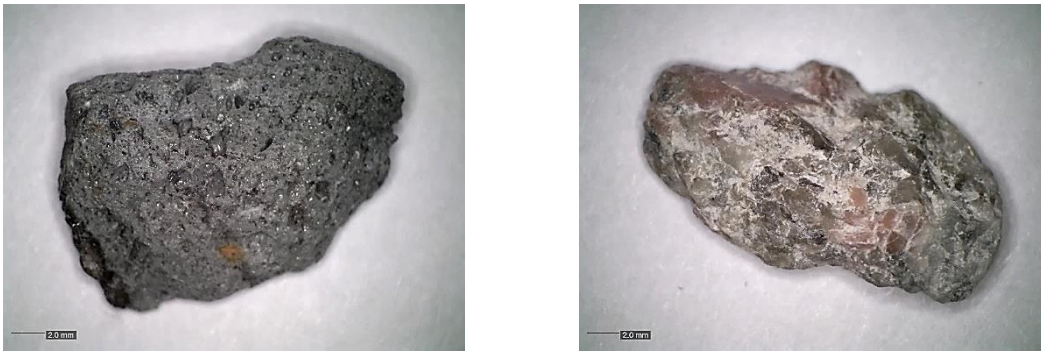

(a) LWA (b) NWA

Fig. 3-1 Coarse aggregates used.

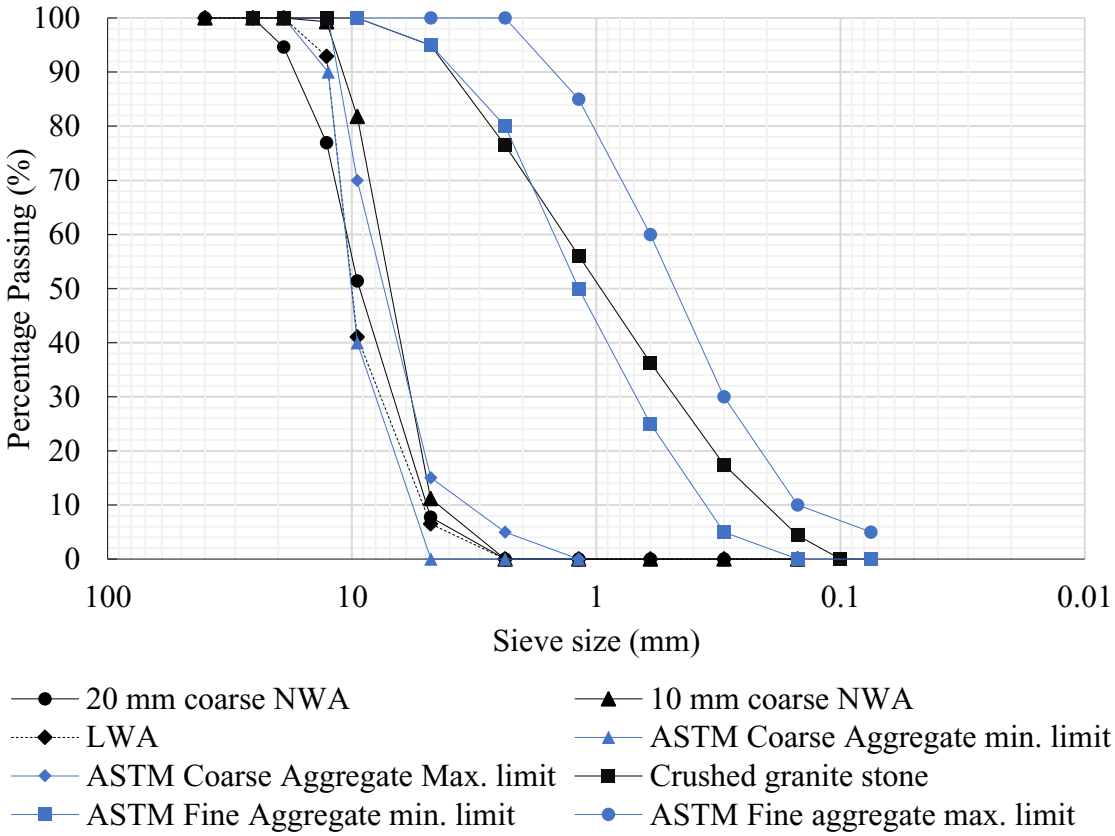

Fig. 3-2 Grading curves for 20 mm coarse NWA, 10 mm coarse NWA, ESLWA, and fine aggregate.

3.3.2. Concrete mixtures development

The small spacing for the reinforcement used in offshore structural elements requires high workability (Fernandes, Bittencourt, and Helene 2008). For that reason, a slump of 180 mm to 220 mm was targeted. Offshore structures are subjected to severe exposure conditions. Thus, air content of 6 - 7.5 % was targeted as recommended by ("ACI 318-14" 2014). Trial mixtures were conducted to optimize the dosage of the SP to achieve the required slump without the risk of segregation. Also, the dosage of the AEA was carefully optimized to achieve the required air content. A total of twenty-six mixtures, 468 cylinders

and 156 prisms, were developed. Cylinders' size was 100 mm × 200 mm, while prisms' size was 100 mm × 100 mm × 400 mm. The mixtures were labeled according to their composition. For example, for level 1, a mixture using a 1.6 C/F aggregate ratio and A_m of 10 mm was labeled as 1.6C/F-10A_m. While for level 2, for instance, a mixture using 10% of FA and 8% of SF was labeled as 10FA-8SF.

Table 3-3 presents the composition of the concrete mixtures. The objective of level 1 was to optimize the C/F aggregate ratio and A_m of the HPSDC and compare. The optimized mixture, 1.6C/F-10A_m, was used to be compared with the HPNWC and the HPLWAC. The same mixture was also used as the control mixture for the second level. In the second level, mixtures 15 to 20 were developed to study the impact of incorporating FA blended with SF. Mixtures 21 to 26 were designed to study the effect of the synergistic action of using MK in the SF system on the properties of the HPSDC mixtures. Fig. 3-3 illustrates the objectives of the two levels and sequencing.

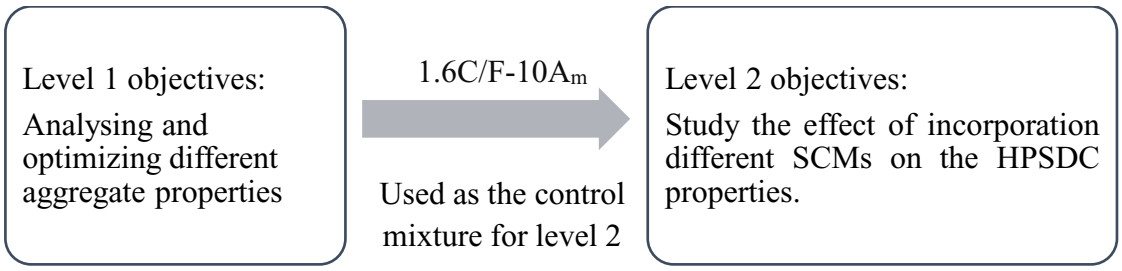

Fig. 3-3 objectives and sequencing of the two levels of the study.

Table 3-3 Composition of the tested mixtures.

Studied parameter	Mixture No.	Mixture designation	C/F	ESLWA / T. C. A	A_m	SP	AEA	SCM			Density
								FA	SF	MK	
			(v_t)	(v_t %)	(mm)	(ml/m^3)	(ml/m^3)	(%)	(%)	(%)	(kg/m^3)
Level 1: Effect of different C/F aggregate ratio, A_m, and type of concrete comparison	1	1C/F-10A_m	1	50%	10	2730	350	_	_	_	2104.1
	2	1.2C/F-10A_m	1.2	50%	10	2730	350	_	_	_	2088.4
	3	1.4C/F-10A_m	1.4	50%	10	2650	350	_	_	_	2076.2
	4	1.6C/F-10A_m	1.6	50%	10	2650	350	_	_	_	2065.9
	5	1.8C/F-10A_m	1.8	50%	10	2500	350	_	_	_	2057.7
	6	2C/F-10A_m	2	50%	10	2450	350	_	_	_	2050.4
	7	1C/F-20A_m	1	50%	20	2600	350	_	_	_	2104.1
	8	1.2C/F-20A_m	1.2	50%	20	2600	350	_	_	_	2088.4
	9	1.4C/F-20A_m	1.4	50%	20	2553	350	_	_	_	2076.2
	10	1.6C/F-20A_m	1.6	50%	20	2553	350	_	_	_	2065.9
	11	1.8C/F-20A_m	1.8	50%	20	2450	350	_	_	_	2057.7
	12	2C/F-20A_m	2	50%	20	2350	350	_	_	_	2050.4
	13	HPNWC	1.6	_	10	2830	350	_	_	_	2256.5
	14	HPLWAC	1.6	100%	10	2480	350	_	_	_	1866.1
Level 2: Effect of FA and SF addition, and MK and SF addition		Control	1.6	50%	10	2650	350	_	_	_	2065.9
	15	5FA-8SF	1.6	50%	10	2900	450	5%	8%	_	2041.1
	16	10FA-8SF	1.6	50%	10	2800	450	10%	8%	_	2034.6
	17	15FA-8SF	1.6	50%	10	2650	450	15%	8%	_	2028.1
	18	20FA-8SF	1.6	50%	10	2650	500	20%	8%	_	2021.5
	19	25FA-8SF	1.6	50%	10	2510	500	25%	8%	_	2015.0
	20	30FA-8SF	1.6	50%	10	2410	600	30%	8%	_	2008.5
	21	5MK-8SF	1.6	50%	10	2970	450	_	8%	5%	2043.1
	22	10MK-8SF	1.6	50%	10	3330	520	_	8%	10%	2038.5
	23	15MK-8SF	1.6	50%	10	3651	600	_	8%	15%	2033.9
	24	20MK-8SF	1.6	50%	10	3810	630	_	8%	20%	2029.4
	25	25MK-8SF	1.6	50%	10	4605	700	_	8%	25%	2024.8
	26	30MK-8SF	1.6	50%	10	5210	800	_	8%	30%	2020.2

Note: All mixtures have 550 kg/m^3 binder content and 0.3 water to binder ratio, T. C. A. = Total Coarse Aggregates.

3.3.3. Procedures

Due to its high absorption ranging from 6 to 9%, the ESLWA was maintained in a soaked condition for 24 hours and then drained for a period of 6 to 12 hours before mixing. This is a standard process to achieve a near SSD case and to reduce aggregate moisture content variability (Craig and Wolfe 2012). A similar technique was suggested by Hoff during the construction of the Hibernia platform (Hoff and Elimov 1995). Before mixing, the fine aggregate was put in the oven and dried at 110 ± 5 C^o for 24 hours to remove the moisture content. The normal weight aggregates were saturated by a specific quantity of water based on the absorption ratio for a reasonable period to achieve a near SSD state. During batching, the aggregates and cement were added first to the mixer. The mixer was operated for 30 seconds to blend these dry components. Then, the AEA added to half the quantity of the batch water was poured into the mixer and mixed for 2 minutes. The SP was added to the other half of the water and mixed for additional 3 minutes. A small portion of water was kept for later usage. The batch was visually assessed to judge its consistency. If the required consistency was not met, an additional amount of SP was added to the remaining portion of water, added to the mixture and mixed for another minute. After visually achieving the required consistency, the batch was tested for slump and air content. The cylinders and prisms were compacted using a mechanical vibrating table and trowel-finished to obtain smooth surfaces. Twenty-four hours after casting the samples, they were demolded, labeled and placed in a curing room, with a temperature of 25 ± 1.5 C^o and 100% relative humidity until the day of testing. All mixtures were poured in 100 L in size.

3.3.4. Testing procedures

3.3.4.1. Fresh and mechanical properties tests

The workability of concrete mixtures and percentage of air content tests were carried out based on ("ASTM C143" 2020) and ("ASTM C231" 2022), respectively. Hardened concrete properties were tested at 14 days and 28 days. Compressive strength according to ("ASTM C39" 2021), STS according to ("ASTM C496" 2017), and static modulus of elasticity according to ("ASTM C469" 2022) were performed, each on three identical cylinders. In addition, three identical prisms were tested to evaluate the FS with third point loading according to ("ASTM C78" 2022). The fundamental longitudinal resonance frequency of three concrete prisms was measured as per ("ASTM C215" 2019) and used to determine the DME.

3.3.4.2. Abrasion resistance tests

The abrasion resistance of the developed concrete mixtures was evaluated using two ASTM standard tests, as follows:

3.3.4.2.1. The rotating-cutters method, as defined by ASTM C944: Fig. 3-4 represents the test setup. It is carefully built to comply with ASTM C944 requirements. The guidelines address the loading, revolutions per minute (RPM), testing duration, cutter dimensions, and replacement intervals for washers and dressing wheels. The abrasion device was created by modifying a conventional drill press. The spindle's spring was detached. On the drill press, a U-shape extension capable of bearing the auxiliary load directly on the spindle was built and fitted. The extension was designed to keep the load constant throughout testing and to reduce any vibrating motion that may interfere with the abrasion mechanism. For

six minutes, the test was carried out at a constant speed of 200 RPM (clockwise) with a constant weight of 19.7 kg in total. This testing set was intended to create expressive abrasion damage within the ASTM procedure's limitations. With an overall diameter of 82.5 mm, the revolving cutters were built with 20 dressing wheels and 22 washers. Dressing wheels and washers were changed every 60 minutes to reduce variance between tested samples caused by spinning cutter erosion. The abrasion test was carried out on three formwork neighboring surfaces of various 100 mm cubes precisely cut from distinct prisms. After the samples were tested, the surface was cleaned using compressed air to remove any residual material. ASTM recommends testing abraded mass loss to determine the abrasion resistance of concrete. When evaluating concrete with substantial differences in density, it is also necessary to measure the abrasion depth instead of the abraded mass loss. In the current study, as there is a comparison between the HPSDC with a normal weight concrete and lightweight aggregate concrete, that has a significant difference in density, abrasion depth will be measured instead of the abraded mass loss. The abrasion depth was calculated using Eq. 2-14 which was developed in chapter 2 with the help of the laser scanning technique as shown in Fig. 3-5, which shows a typical laser-scanned sample.

(a) Drill modification.

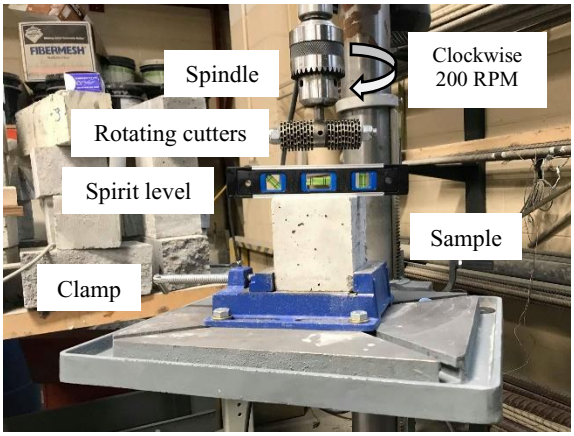

(b) Enlargement of the rotating cutters and the sample.

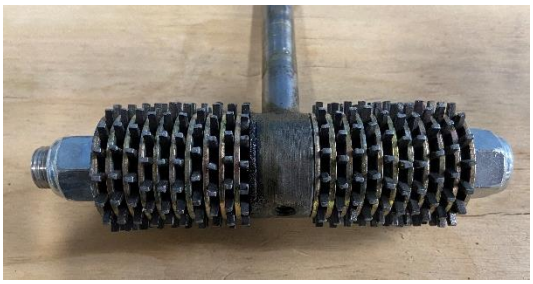

(c) Enlargement of the rotating cutters.

Fig. 3-4 ASTM C944, rotating cutters test.

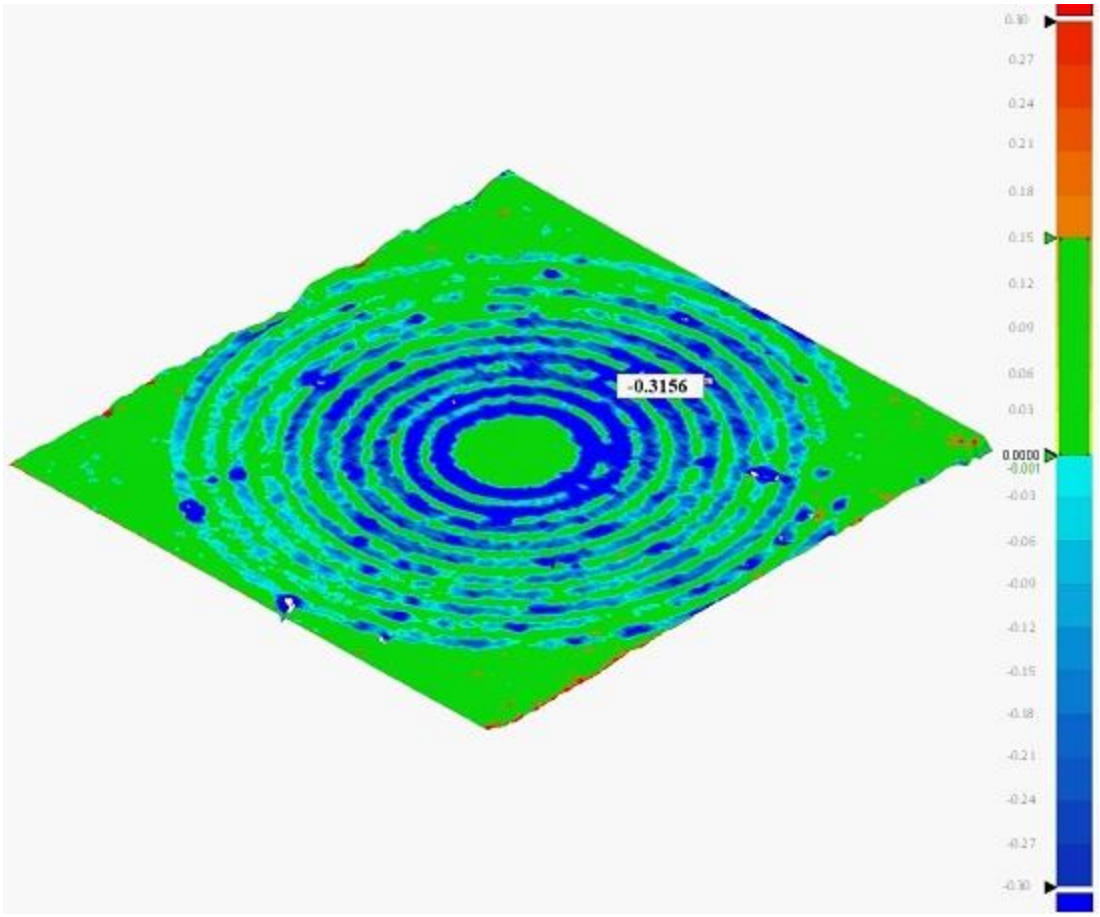

Fig. 3-5 Typical laser scanning of a sample tested using rotating cutters approach.

3.3.4.2.2. ASTM C418, sand blasting test: The test was carried out as per ASTM C418. The test setup (Fig. 3-6) was constructed to carefully meet ASTM C418 recommendations. In that, as the nozzle shape can affect the wear pattern and consequently affect the test results reproducibility, nozzles that follow the ASTM exact dimensions were fabricated as can be seen in Fig. 3-6 (d). The nozzle is 40 mm long with walls of 45^{o} bevel inside at the upper end. A clamp that holds the sample at a fixed normal distance of 75 mm from the nozzle end was used. It has a shield with a 28.7 mm diameter opening. The used abrasive was silica sand that was pre-sieved to pass sieve No. 20 and be retained on sieve No. 30. To maintain consistent results, the silica sand abrasive was never reused in this investigation. The concrete specimens were immersed for 24 hours before testing. The specimen's surface was exposed to the air-driven abrasive sand at a pressure of 59.5 psi for a period of 1 minute. The test was repeated on eight different spots over the sample. ASTM recommends measuring the volume of the abrasion cavity using oil base modeling clay. However, due to the high abrasion resistance of the HPSDC, limited abrasion volumes were usually attained. Thus, the cavity volume was calculated by weighing the sample before and after testing and dividing the mass difference by the concrete density as per Eq. 3-1. The abrasion coefficient was then calculated using Eq. 3-2. The accuracy of this measurement technique was assured by using laser scanning on random samples. A typical laser scanned sample can be seen in Fig. 3-7.

$$V = M / \rho \tag{3-1}$$

Where V is the volume of the abraded cavity, cm^3; M is the abraded mass, gm; and ρ is the concrete density gm / cm^3.

$$A_c = V / A \tag{3-2}$$

Where A_c is the abrasion coefficient, cm^3/cm^2; and A is the abraded surface area.

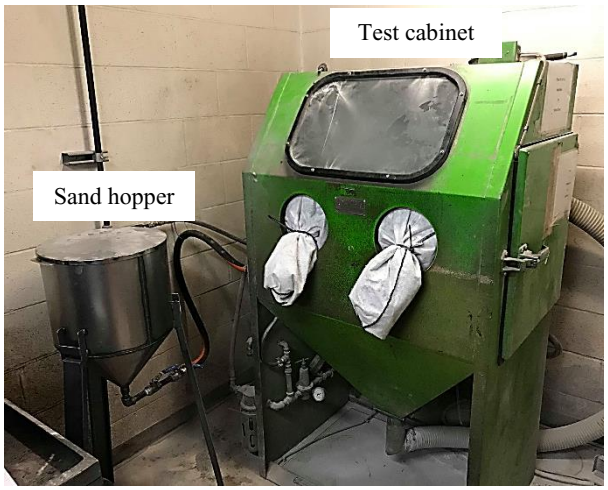

(a) Test cabinet and the sand hopper.

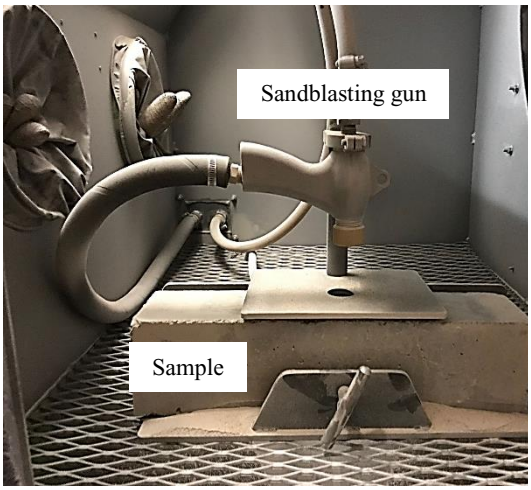

(b) Sandblasting gun

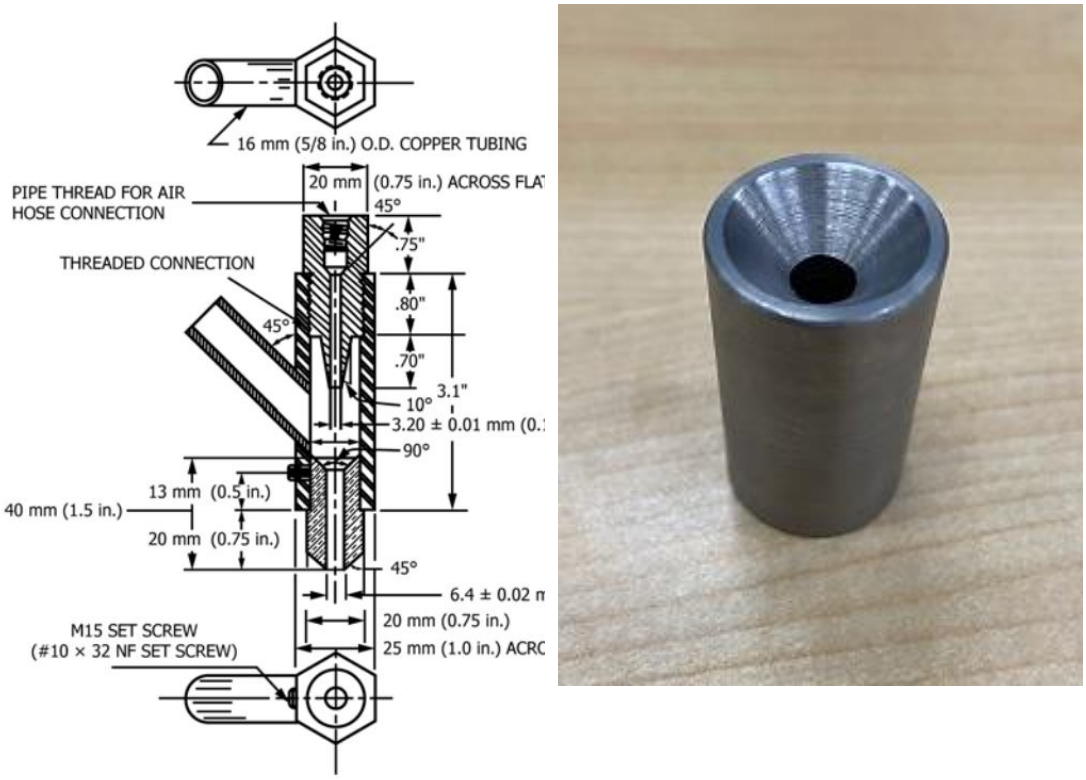

(c) ASTM C418 gun nozzle assembly. (d) Fabricated gun nozzle.

Fig. 3-6 ASTM C418, sandblasting test setup.

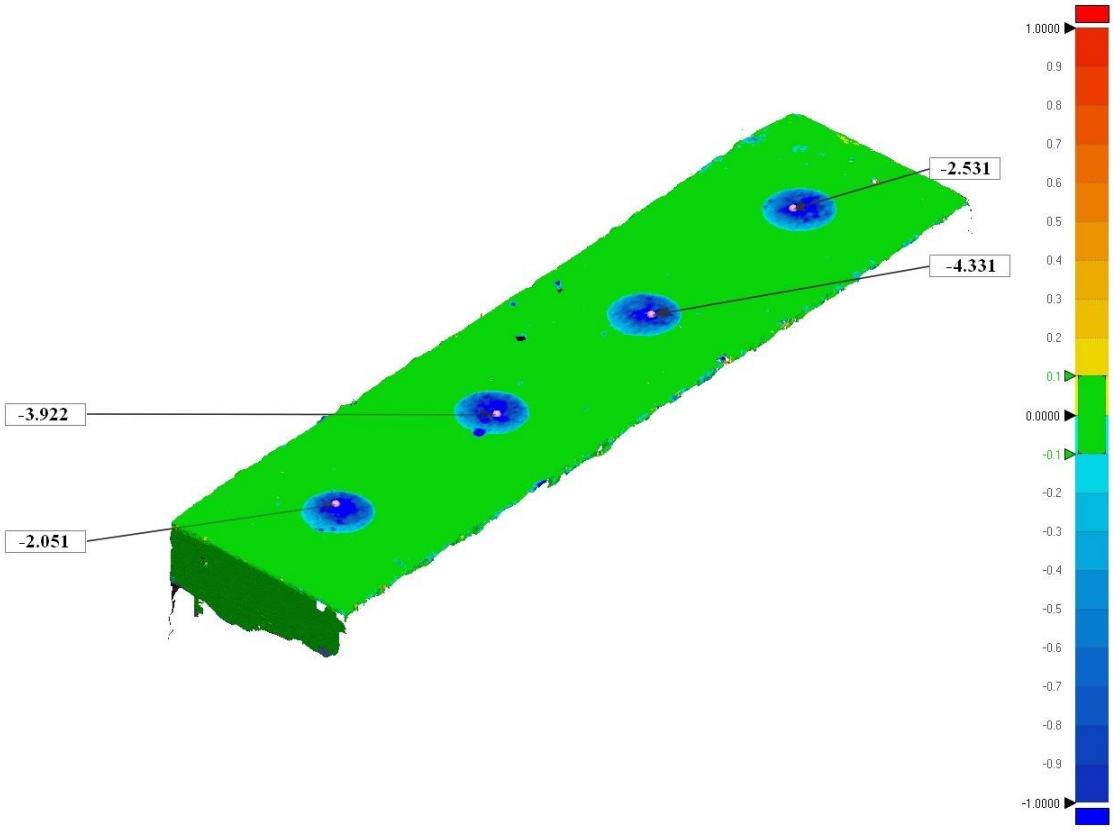

In mm

Fig. 3-7 Typical laser scanning of a sample tested using sandblasting approach.

3.4. Discussion of results

3.4.1. Fresh properties of tested mixtures

3.4.1.1. SP demand

To achieve the targeted slump of 180 mm to 220 mm, the dosages of the SP required were different depending on the mixture composition as shown in Table 3-3. As can be seen from Fig. 3-8, Increasing the C/F aggregate ratio decreased the SP demand. In which by increasing it from 1 to 2, lower dosages of 10.3% and 9.6% were needed to achieve the targeted slump for A_m of 10 mm and A_m of 20 mm, respectively. Similarly, twenty millimeters A_m mixtures showed slightly less SP demand compared to 10 mm A_m mixtures by an average of 4.1%. This is due to the lower surface area that a larger aggregate possesses. That led to less water requirement. In turn, a larger quantity of free water was available in the mixture to provide higher workability. Consequently, a lower SP dosage was needed. But as the A_m of the normal weight aggregate portion only was changed, the effect on the workability was not high.

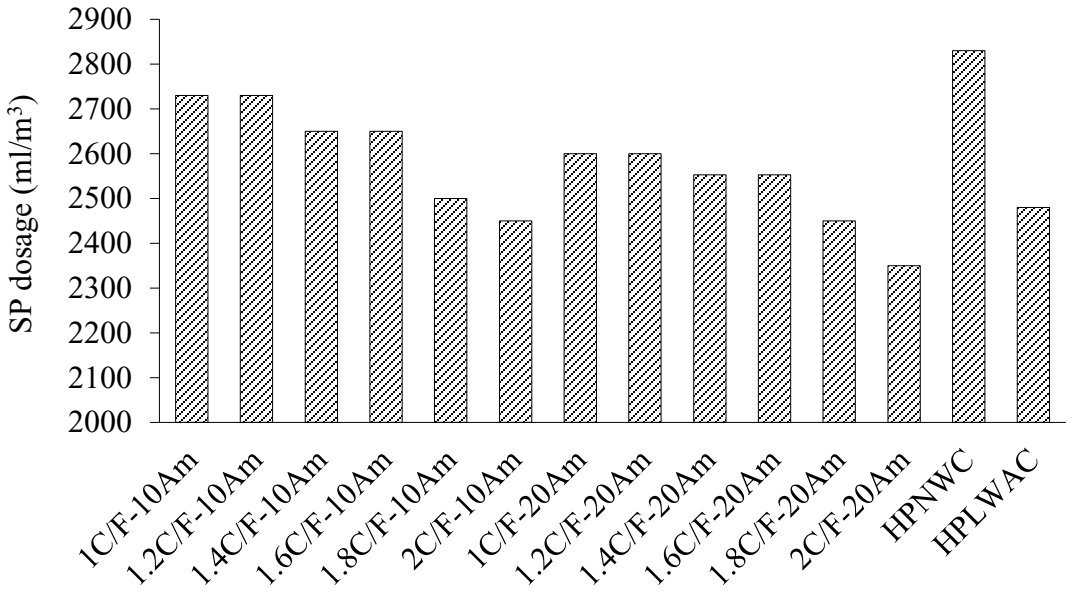

Fig. 3-8 Effect of different C/F aggregate ratio, $A_{m,}$ and different aggregate type on the SP demand of the HPSDC.

As can be seen from Fig. 3-8, compared to the HPSDC mixture, the HPNWC mixture required a slightly higher dosage of SP by 6.8%, while the HPLWAC mixture required a slightly lower dosage of SP of 6.4%. This may be attributed to the larger A_m that the lightweight aggregate possesses compared to the normal weight aggregate. That means a lower total surface area of the lightweight aggregate incorporated mixtures. Consequently, less dosage of SP was needed to achieve the required workability. Also, it is worth mentioning that compared to the HPLWAC, the HPSDC turned out to be a more homogeneous and stable mixture. As can be seen in Fig. 3-9, it was hard to achieve a smooth surface finishing for the HPLWAC mixtures as lightweight aggregates tended to float during the vibrating of the placed mixture.

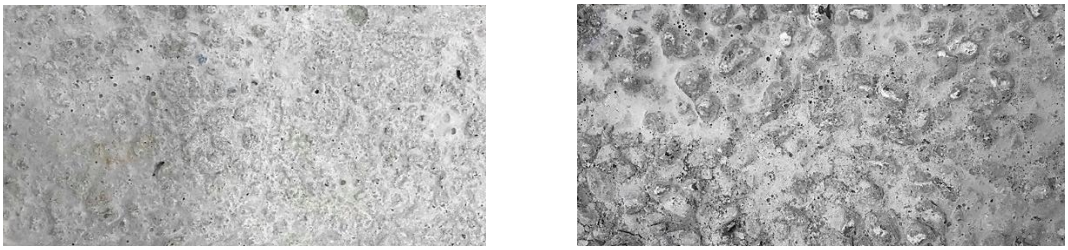

HPSDC HPLWAC

Fig. 3-9 Surface finish of the HPSDC and the HPLWAC.

Incorporating different ratios of FA blended with 8% of SF affected the SP demand. As can be seen in Fig. 3-10, at low ratios of FA usage of 5% and 10%, the SP demand increased by 9.4% and 5.7%, respectively. This is due to the well-documented effect that SF and FA have on concrete workability. In that, SF decreases the workability due to its particles' higher surface area that increases the water requirement. On the contrary, FA enhances the workability of the concrete mixture as it reduces the water demand leaving more free water to achieve higher workability. That appeared more clearly by a further increase in the FA incorporation ratios. For instance, for mixtures that contain 15% and 20% of FA, no additional SP dosages were needed. Furthermore, fewer SP dosages by an average of 5.3% and 9.1% were needed for mixtures with 25% and 30% of FA, respectively. The impact that blending FA with SF has on the mixture workability is in agreement with the results obtained by (Nochaiya, Wongkeo, and Chaipanich 2010).

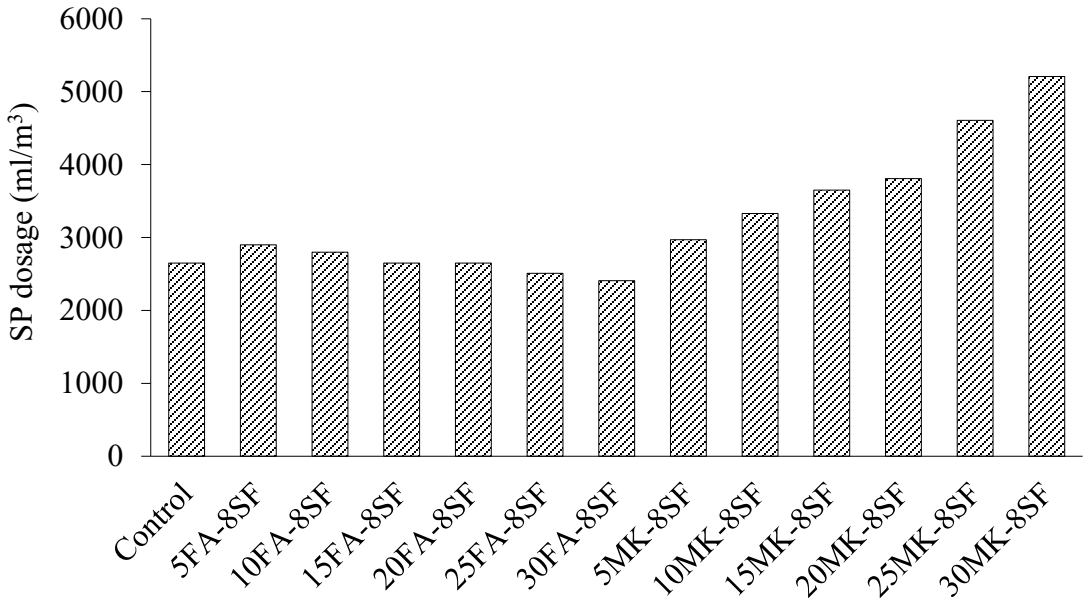

Fig. 3-10 Effect of incorporation of different SCMs on the SP demand of the HPSDC.

To achieve the targeted workability with the addition of different ratios of MK blended with 8% of SF, higher dosages of SP ratios were needed. As can be seen in Fig. 3-10, the SP demand was related to the amount of MK incorporation ratio. In that, SP dosage reached 96.6% higher amount at 30% partial replacement of binder content with MK. This is mainly attributed to the reason explained earlier for SF's impact on concrete workability. Moreover, this effect was marked up by the presence of MK which possesses even higher fineness modules compared to SF. The incorporation of both SCMs led to a decrement in the free water content that is responsible to provide lubrication for the aggregate. Consequently, higher dosages of SP were needed to achieve the required workability.

3.4.1.2. AEA demand

To achieve the recommended air content of 6 – 7.5%, the dosages of the AEA required were different depending on the mixture composition as can be seen in Table 3-3. Changing the C/F aggregate ratio and A_m did not have a noticeable effect on the AEA demand. Also, no effect was observed when comparing the HPSDC to the HPNWC or the HPLWAC. On the contrary, as can be seen in Fig. 3-11, higher dosages of AEA were required to achieve the recommended air content with the incorporation of different SCMs. The higher dosage reached 71.4% with the addition of 30% of fly ash and 8% of silica fume. Furthermore, a remarkably higher dosage reached 128.6% was needed for the similar mixture with MK addition at 30% with silica fume at 8%. This is generally attributed to the known fact that, the carbon content in the SCMs tends to have an interaction with the surfactants used as air-entraining admixtures. Carbon absorbs some of the AEA, leaving less amount to be exploited. As MK has more carbon content, its effect on the air content was more pronounced. So, to compensate for this effect and maintain the required air content, higher dosages of AEA were needed.

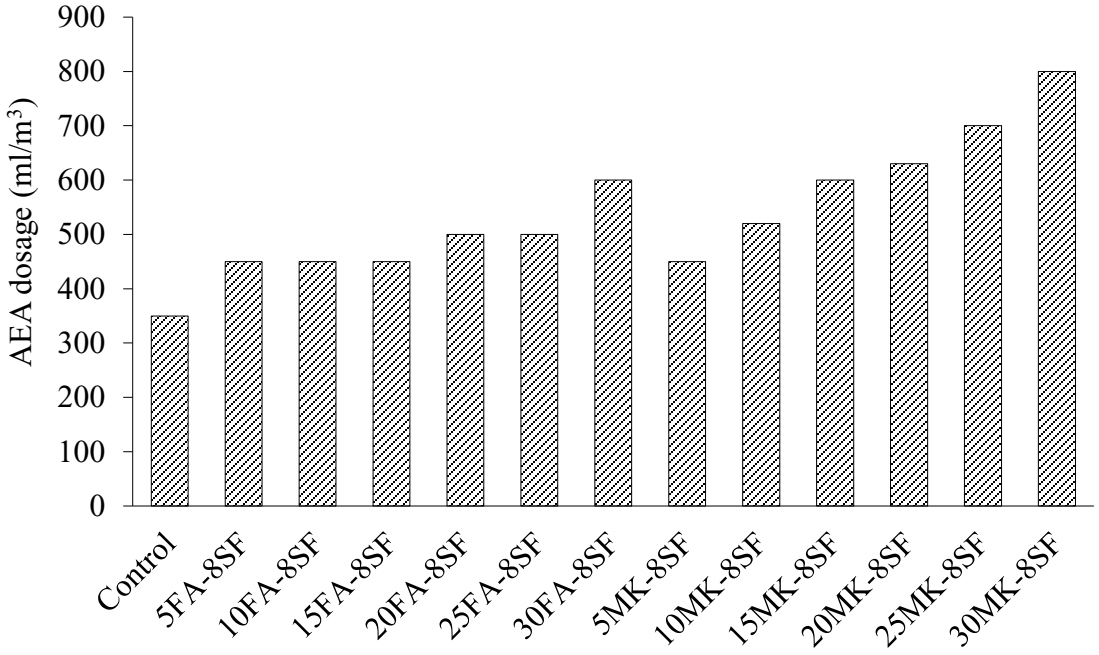

Fig. 3-11 Effect of incorporation of different SCMs on the AEA dosage of the HPSDC.

3.4.2. Hardened properties of tested mixtures

3.4.2.1. Effect of different C/F aggregate ratio and different A_m.

Table 3-4 and Fig. 3-12 show the compressive strength of the tested mixtures developed with different C/F aggregate ratio and different A_m. It can be seen that, increasing the C/F aggregate ratios up to 1.6, increased the HPSDC compressive strength. The highest increase attained was 16.4% and 15.7% at 14- and 28-day, respectively, for 1.6C/F-10A_m compared to 1C/F-10A_m. And by 12.7% and 17.7% at 14- and 28-day, respectively, when comparing 1.6C/F-20A_m with 1C/F-10A_m. This behavior could be attributed to that as the C/F aggregate ratio increases, higher concrete packing was gained. However, further increases in the C/F aggregate ratio of the HPSDC negatively affected its compressive

strength. A decrement of 7.4% and 5.5% at 14- and 28-day, respectively, was noticed when comparing 2C/F-20A_m with 1.6C/F-10A_m. Also, by 5.4% and 5.9% at 14- and 28-day, respectively, when comparing 2C/F-20A_m with 1.6C/F-20A_m. Such a negative effect can be attributed to that the thickness of the interfacial transition zone (ITZ) was increased. As the ITZ is a weak zone with the lowest strength due to a lack of cement presence, an increase in its thickness can lead to less compressive strength. In addition, increasing the C/F aggregate ratio of the HPSDC includes increasing the portion of the LWA in the mixture, which may contribute to the negative impact on the compressive strength. It should be noted that the C/F aggregate ratio that leads to the highest compressive strength is different depending on the composition of the concrete and its composition. (Ruiz 1966) found a similar trend. In that, the compressive strength of the tested concrete increased with the increase in the content of the coarse aggregate, up to a critical volume of aggregate, and then decreased. Similarly, increasing the A_m affects the concrete ITZ and its packing. However, in this study, unlike the difference in the used C/F aggregate ratio, the change in the A_m in the developed mixtures (20 mm compared to 10 mm) was not significant. Also, as only the A_m of the normal weight aggregate portion was changed, not the total quantity of coarse aggregate, the effect of changing A_m on the HPSDC was not pronounced on the HPSDC compressive strength. (Jang and Yun 2018) found a similar behavior. It was concluded that aggregate size does not have a significant effect on the compressive strength of the tested high strength concrete or its modulus of elasticity.

Table 3-4 Mechanical properties results for tested mixtures.

Mixture No.	Mixture designation	Compressive strength (MPa)			STS (MPa)		FS (MPa)		SME (GPa)		DME (GPa)	
		14-day	28-day	91-day	14-day	28-day	14-day	28-day	14-day	28-day	14-day	28-day
1	1C/F-10A_m	61.0	63.2	_	3.29	3.34	6.23	6.52	28.6	30.7	34.2	34.7
2	1.2C/F-10A_m	64.7	67.6	_	3.52	3.56	6.71	7.15	29.0	31.7	36.1	36.8
3	1.4C/F-10A_m	67.0	71.4	_	3.77	3.85	7.25	7.66	30.9	31.8	37.2	38.1
4	1.6C/F-10A_m	71.0	73.1	_	4.06	4.18	7.85	8.10	33.0	34.8	38.2	39.3
5	1.8C/F-10A_m	68.6	71.1	_	3.40	3.41	7.10	7.29	32.3	33.9	37.9	37.4
6	2C/F-10A_m	65.8	69.1	_	3.11	3.14	6.32	6.42	30.6	32.11	36.5	36.8
7	1C/F-20A_m	62.3	63.4	_	3.12	3.13	5.81	5.93	29.3	31.5	33.1	34.1
8	1.2C/F-20A_m	64.9	66.2	_	3.28	3.33	6.33	6.44	29.8	31.9	35.2	36.6
9	1.4C/F-20A_m	68.1	70.9	_	3.50	3.53	6.90	7.20	30.1	31.8	36.1	36.5
10	1.6C/F-20A_m	70.2	74.6	_	3.79	3.80	7.37	7.70	32.90	34.5	38.7	39.1
11	1.8C/F-20A_m	67.5	72.3	_	3.22	3.22	6.73	6.99	31.8	33.2	36.5	36.6
12	2C/F-20A_m	66.4	70.2	_	2.91	2.96	5.93	6.32	31.5	32.1	35.7	36.1
13	HPNWC	78.5	83.2	_	4.90	4.87	8.51	9.20	36.9	40.8	42.8	44.5
14	HPLWAC	64.1	65.2	_	3.32	3.53	7.04	7.01	29.9	32.3	35.7	36.4
	Control	71.0	73.1	76.4	4.06	4.18	7.85	8.10	32.2	34.8	38.2	39.3
15	5FA-8SF	66.2	71.3	81.9	3.37	3.71	7.43	7.69	31.6	35.2	35.6	36.4
16	10FA-8SF	59.2	68.2	78.7	2.91	3.54	7.18	7.66	29.3	33.3	33.3	34.9
17	15FA-8SF	55.9	66.2	75.3	2.79	3.43	7.03	7.57	28.7	32.1	33.2	33.5
18	20FA-8SF	52.3	63.4	73.4	2.62	3.24	6.66	7.20	28.4	30.9	32.1	33.2
19	25FA-8SF	48.7	60.2	68.4	2.41	3.07	6.20	6.78	26.8	29.7	31.1	33.0
20	30FA-8SF	46.0	59.0	66.2	2.37	2.86	6.00	6.50	25.9	29.4	29.5	31.17
21	5MK-8SF	73.1	74.9	_	4.27	4.44	8.11	8.33	34.3	35.8	39.1	40.2
22	10MK-8SF	74.6	75.8	_	4.37	4.48	8.23	8.42	35.0	37.2	39.2	40.4
23	15MK-8SF	76.2	79.0	_	4.50	4.70	8.40	8.71	36.8	38.9	40.5	41.7
24	20MK-8SF	74.7	76.1	_	4.20	4.37	8.10	8.30	34.2	37.1	39.3	39.7
25	25MK-8SF	73.2	75.6	_	4.00	4.10	8.05	8.15	33.1	34.9	38.9	39.0
26	30MK-8SF	72.1	73.2	_	3.92	3.98	7.60	7.72	31.8	34.1	37.3	38.9

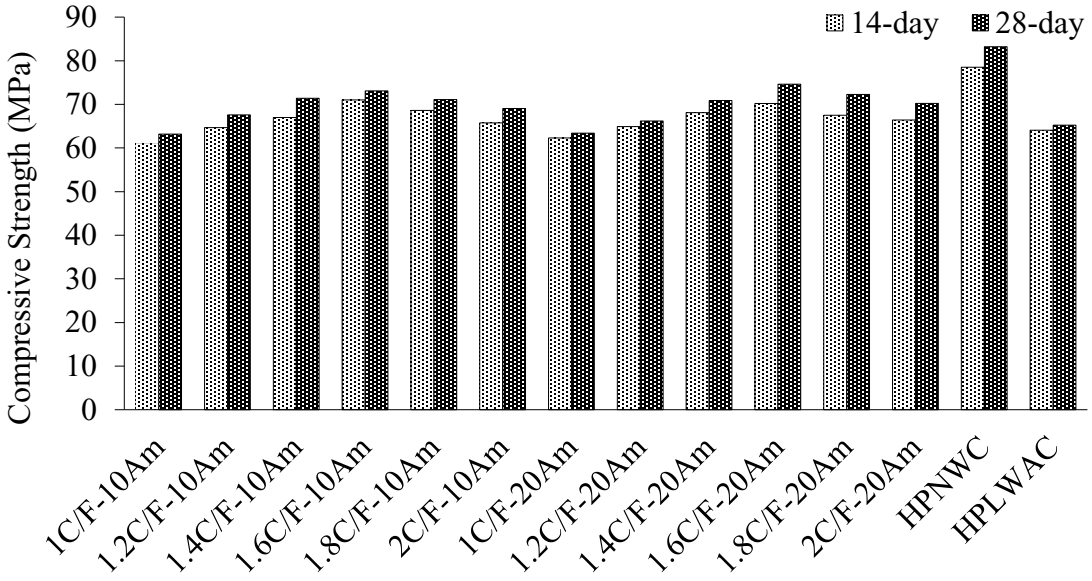

Fig. 3-12 Effect of different C/F aggregate ratio, $A_{m,}$ and different aggregate type on the compressive strength of the HPSDC.

Table 3-4, Fig. 3-13, and Fig 3-14 present the tensile properties (STS and FS) of the tested HPSDC mixtures developed with different C/F aggregate ratios and different A_m. The results indicated that changing the C/F aggregate ratio appeared to have a higher impact on the HPSDC tensile properties than on the compressive strength. By looking at 1.6C/F-10A_m compared to 1C/F-10A_m, it can be observed that the improvements in the STS were 23.5% and 25.2% at 14- and 28-day, respectively. Similarly, by comparing 1.6C/F-20A_m to 1C/F-20A_m, the former had higher STS by 21.4% at both, the 14- and 28-day. From these results, it was indicated that the STS can be affected by adjusting the concrete packing property, by changing the C/F aggregate ratio, more than the compressive strength. Similarly, the FS followed the same trend as the STS. In that, it increased by 26% and 24.3% at the 14- and 28-day, respectively, when comparing 1.6C/F-10A_m to 1C/F-10A_m. Whereas, 1.6C/F-20A_m increased by 26.8% and 29.8% at the 14- and 28-day,

respectively, compared to 1C/F-20A_m. Similar to the compressive strength, the tensile properties decreased at higher C/F aggregate ratio than 1.6. However, the impact was more explicit. For instance, the STS of 2C/F-10A_m was less than 1.6C/F-10A_m by 23.4% and 24.9% at the 14- and 28-day, respectively. While 2C/F-20A_m was less by 23.2% and 22.1% at the 14- and 28-day, respectively, compared to 1.6C/F-20A_m. Likewise, there was a decrement in the FS when increasing the C/F aggregate ratio to 2. For instance, 2C/F-10A_m appeared to have less FS than 1.6C/F-10A_m by 19.5% and 20.7% at the 14- and 28-day, respectively. Also, 2C/F-20A_m had less FS by 19.5% and 17.9% at the 14- and 28-day, respectively, compared to 1.6C/F-20A_m. Such findings revealed that the HPSDC tensile properties (especially STS) are more affected by the ITZ morphology compared to the compressive strength. On the other hand, contrary to the compressive strength, changing the A_m of the HPSDC had a mild, yet noticeable, effect on its tensile properties. For instance, when comparing the 20 A_m mixtures to the 10 A_m incorporated mixtures, the STS decreased by an average of 6.3% and 7% at the 14- and 28-day, respectively. Similarly, the FS decreased by an average of 5.8% and 5.9% at the 14- and 28-day, respectively. This reduction is mainly attributed to the increment of the ITZ when the A_m is changed. That can affect the tensile properties in a higher manner compared to other properties. (Nikbin et al. 2014) studied concrete with a water to cement ratio of 0.38 and found a reduction of 14% in the tensile strength when changing the maximum aggregate size from 9.5 mm to 19 mm. However, in the current study, as mentioned before, only the normal weight A_m portion was changed, not the total quantity of the coarse aggregate, the effect on the tensile properties was not significant.

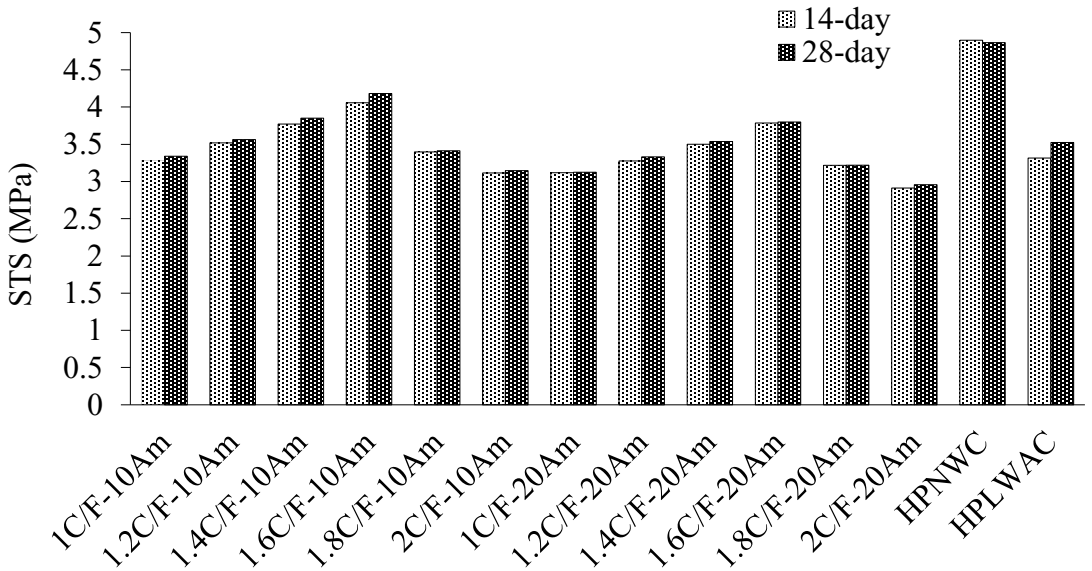

Fig. 3-13 Effect of different C/F aggregate ratio, $A_{m,}$ and different aggregate type on the STS of the HPSDC.

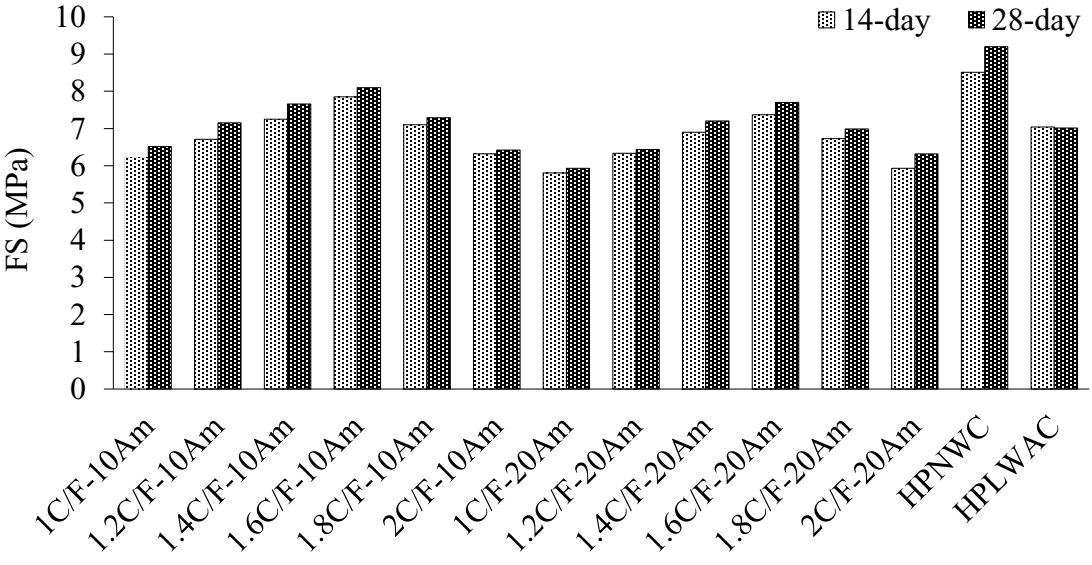

Fig. 3-14 Effect of different C/F aggregate ratio, $A_{m,}$ and different aggregate type on the FS of the HPSDC.

Table 3-4, Fig. 3-15, and Fig 3-16 present the moduli of elasticity of the tested HPSDC mixtures developed with different C/F aggregate ratios and different A_m. The results indicated that changing the C/F aggregate ratio of the HPSDC appeared to have a similar trend as the compressive strength. By looking at 1.6C/F-10A_m compared to 1C/F-10A_m, it can be observed that the 1.6 C/F aggregate ratio mixture had higher SME by 12.4% and 13.4% at 14- and 28-day, respectively. And higher DME by 11.6% and 13.2% at 14- and 28-day, respectively. Meanwhile, when comparing 1.6C/F-20A_m to 1C/F-20A_m, the 1.6 C/F aggregate ratio mixture had higher SME by 12.2% and 9.5% at 14- and 28-day, respectively. And higher DME by 16.9% and 14.7% at 14- and 28-day, respectively. That behavior attributed to that by changing the C/F aggregate ratio, the concrete mixture gained a denser configuration through gaining better packing. That in turn led to a higher stiffness mixture. Similar to other tested properties, the Moduli of elasticity did not show better results at a higher C/F aggregate ratio than 1.6. In that, 2C/F-10A_m appeared to have less SME than 1.6C/F-10A_m by 5.1% and 7.8% at the 14- and 28-day, respectively. And less DME by 4.5% and 6.4% at the 14- and 28-day, respectively. Similarly, 2C/F-20A_m had less SME by 4.4% and 7.1% at the 14- and 28-day, respectively, compared to 1.6C/F-20A_m and less DME by 7.8% and 7.7% at the 14- and 28-day, respectively. As mentioned previously that the mechanical properties of the concrete depends on the ITZ properties. When the C/F aggregate ratio was increased, the ITZ thickness increased. That led to a reduction in the mechanical properties. However, this effect was more pronounced in the STS and FS because they are more affected by the ITZ properties than the compressive strength and moduli of elasticity. On the other hand, similar to the compressive strength, both moduli

of elasticity did not noticeably impact by changing the A_m in the developed mixtures (20 mm compared to 10 mm).

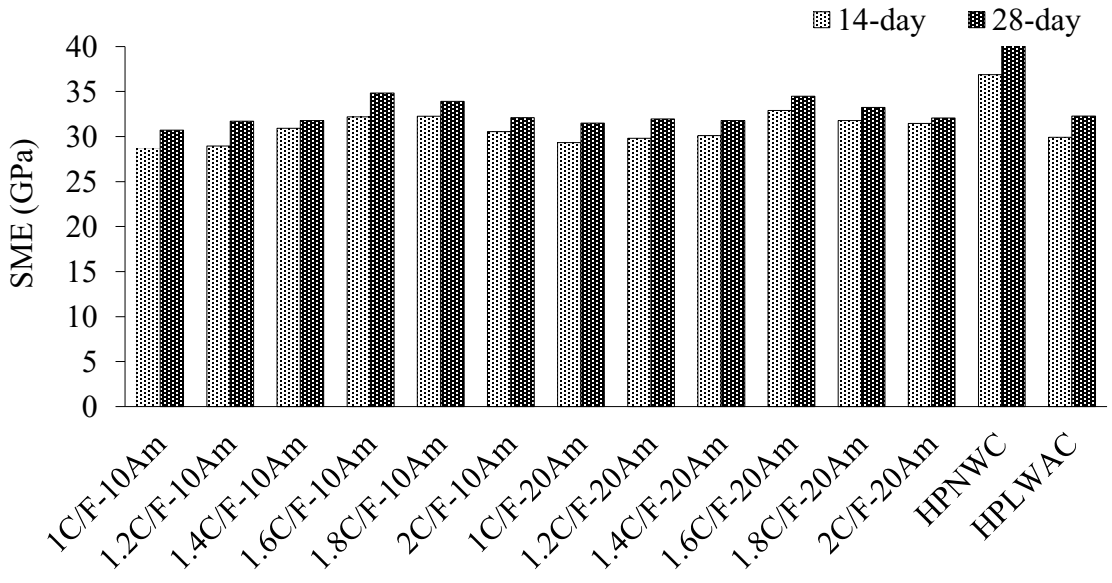

Fig. 3-15 Effect of different C/F aggregate ratio, A_m, and different aggregate type on the SME of the HPSDC.

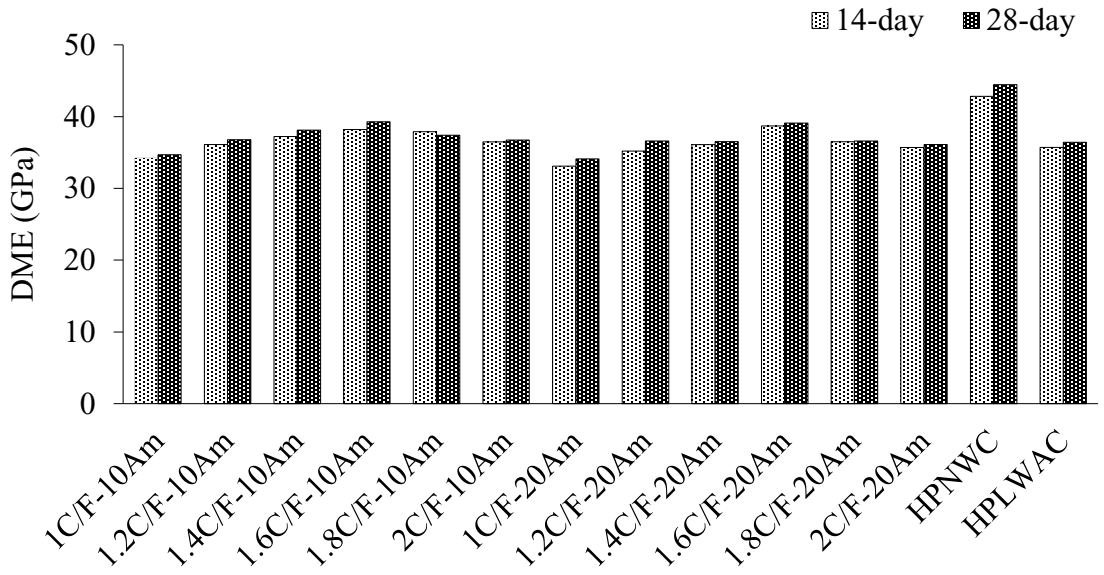

Fig. 3-16 Effect of different C/F aggregate ratio, $A_{m,}$ and different aggregate type on the DME of the HPSDC.

Table 3-5 shows the 14- and 28-day abrasion resistance of the HPSDC developed with different C/F aggregate ratios and different A_m. As mentioned, the abrasion resistance was tested using the rotating cutter method (ASTM C944), expressed as abrasion depth (Fig. 3-17) and sandblasting (ASTM C418) expressed as abrasion coefficient (Fig. 3-18). It can be seen that increasing the C/F aggregate ratio in the HPSDC mixtures from 1 to 1.6 led to enhance its abrasion resistance. For instance, by comparing C/F of 1.6 with C/F of 1, the 14- and 28-day abrasion depth decreased by 14.6% and 13.6%, respectively, for 10 A_m mixtures and by 11.1% and 11.9% at the 14- and 28-day, respectively, for 20 A_m mixtures. That enhancement was assured with the sandblasting test results. As the abrasion coefficient decreased as well by 15.2% at the 28-day, for 10 A_m mixtures. And by 13.4% at the 28-day, for 20 A_m mixtures. That enhancement is mainly due to the better packing

that the C/F of 1.6 provided. Densifying the concrete system makes loss of particles harder to occur. Expectedly, the abrasion resistance was negatively affected at C/F aggregate ratio above 1.6. For instance, when comparing the C/F aggregate ratio of 2 to C/F aggregate ratio of 1.6, a decrement of 23.1% and 21.9% was noticed for 10 A_m mixtures at the 14- and 28-day, respectively and by 17.7% and 21.8% at the 14- and 28-day, respectively, for 20 A_m mixtures. That is due to, as explained earlier, higher C/F aggregate ratios above 1.6 provided higher ITZ thickness that negatively impacted the tested properties. However, it appears that different tests that have different abrading mechanisms could lead to different results as the abrasion coefficient decreased at a higher manner. A decrement of 30.3% and 29.1% for 10 A_m mixtures and 20 A_m mixtures, respectively, at the 28-day was noticed. Such finding root cause is illustrated in Fig. 3-19. The figure demonstrates a cross-section of the concrete specimen to be tested using the rotating cutter (Fig. 3-19a) and using sandblasting (Fig. 3-19b). The concrete consists of three main parts; paste, aggregate, and ITZ. In the rotating cutters test, as the dressing wheels revolve, all the parts are abraded at the same horizontal level. If a part of the mentioned three parts has a higher abrasion resistance than the other parts, it will provide a shield to some extent for the other parts. That means less contribution of the weaker parts to the total attained abrasion resistance. It is believed that the aggregate limited the abrasion damage so, the ITZ had less effect on the final abrasion resistance. On the contrary, in the sandblasting test, all parts were exposed to the air-driven abrasive. That means stronger parts and weaker parts are both tested in an equal manner and that a weaker part could affect the resulted abrasion resistance in a higher manner compared to the rotating cutter test. For that reason, the

increment of the ITZ thickness negatively affected the abrasion resistance of the HPSDC in a larger aspect when testing using sandblasting test than when testing using rotating cutters test. It is worth to mention that, each abrasion test simulates a different abrasion mechanism. The rotating cutter ASTM C944 represent the mechanism of traffic abrading a concrete surface while sandblasting ASTM C418 simulates the waterborne abrasives. However, both don't fully represent the ice-abrasion action. That difference between the two abrasion tests affected the results attained when changing the HPSDC A_m. For instance, as the A_m was increased from 10 mm to 20 mm, no difference in the abrasion resistance was noticed using the rotating cutter test. On the other hand, changing the HPSDC A_m led to a decrement in the abrasion resistance tested using sandblasting. In that, a reduction by an average of 7.9% was attained for 20 mm A_m when compared to 10 mm A_m mixtures at the 28-day.

Table 3-5 Abrasion resistance results for the tested mixtures.

Mixture No.	Mixture designation	Rotating cutters method test (ASTM C944) "Average abrasion depth" (mm)		Sandblasting test (ASTM C418) "Abrasion coefficient" (cm^3/cm^2)
		14-day	28-day	28-day
1	1C/F-10A_m	0.553	0.529	0.365
2	1.2C/F-10A_m	0.521	0.505	0.346
3	1.4C/F-10A_m	0.505	0.481	0.329
4	1.6C/F-10A_m	0.473	0.457	0.310
5	1.8C/F-10A_m	0.523	0.503	0.356
6	2C/F-10A_m	0.582	0.558	0.403
7	1C/F-20A_m	0.537	0.515	0.334
8	1.2C/F-20A_m	0.517	0.501	0.321
9	1.4C/F-20A_m	0.501	0.469	0.293
10	1.6C/F-20A_m	0.477	0.453	0.289
11	1.8C/F-20A_m	0.556	0.541	0.341
12	2C/F-20A_m	0.632	0.622	0.373
13	HPNWC	0.374	0.325	0.237
14	HPLWAC	0.620	0.636	0.393
	Control	0.473	0.461	0.310
15	5FA-8SF	0.509	0.483	0.333
16	10FA-8SF	0.612	0.517	0.357
17	15FA-8SF	0.665	0.523	0.379
18	20FA-8SF	0.705	0.529	0.394
19	25FA-8SF	0.735	0.568	0.411
20	30FA-8SF	0.744	0.580	0.427
21	5MK-8SF	0.458	0.429	0.289
22	10MK-8SF	0.437	0.414	0.246
23	15MK-8SF	0.417	0.405	0.227
24	20MK-8SF	0.445	0.438	0.261
25	25MK-8SF	0.453	0.448	0.278
26	30MK-8SF	0.461	0.447	0.281

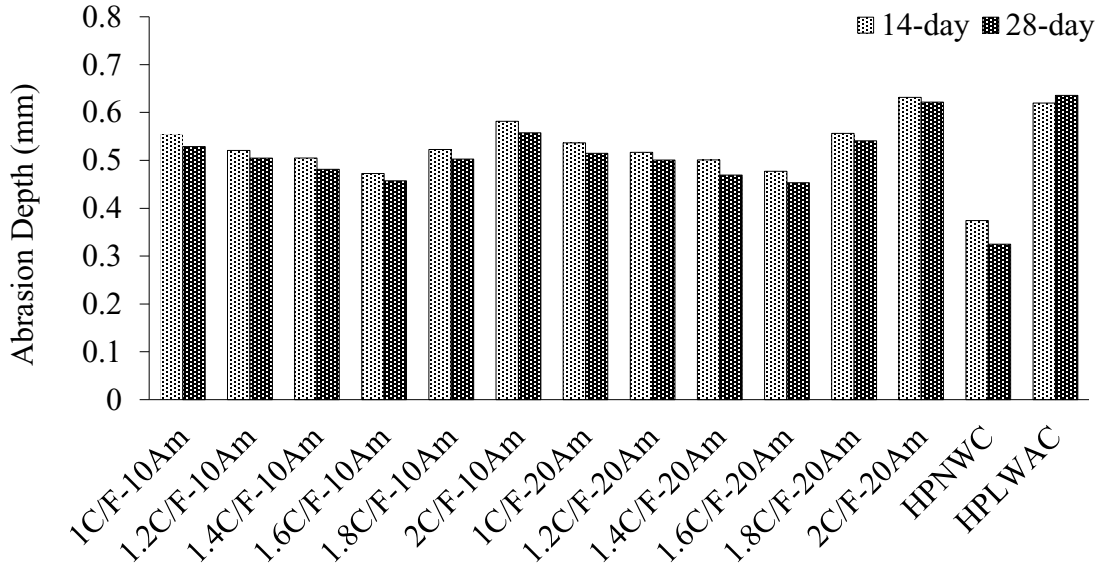

Fig. 3-17 Effect of different C/F aggregate ratio, $A_{m,}$ and different aggregate type on the abrasion resistance of the HPSDC measured using rotating cutters method.

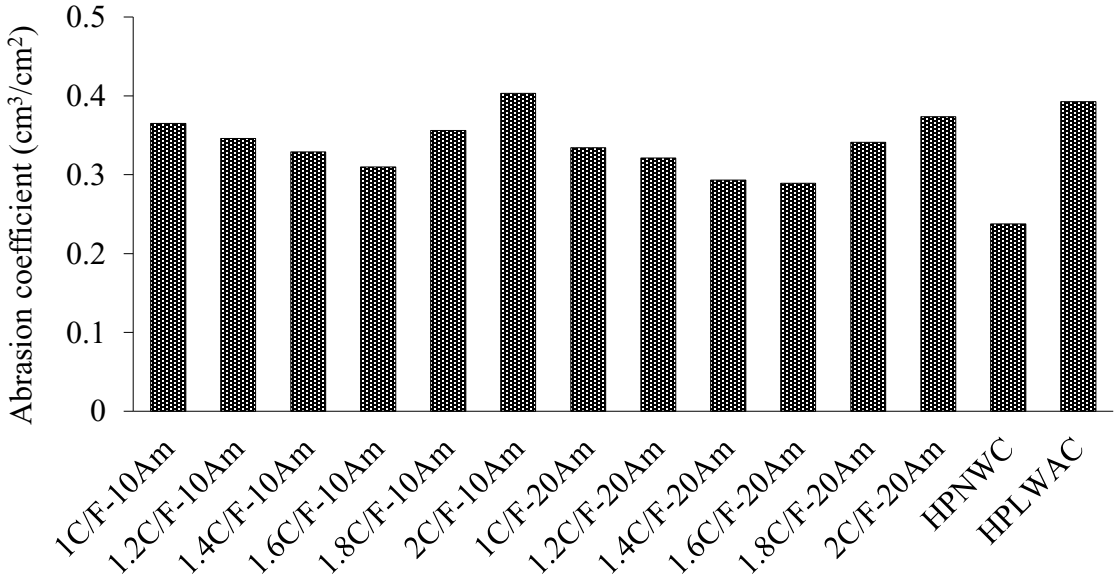

Fig. 3-18 Effect of different C/F aggregate ratio, $A_{m,}$ and different aggregate type on the abrasion resistance of the HPSDC measured using sandblasting method.

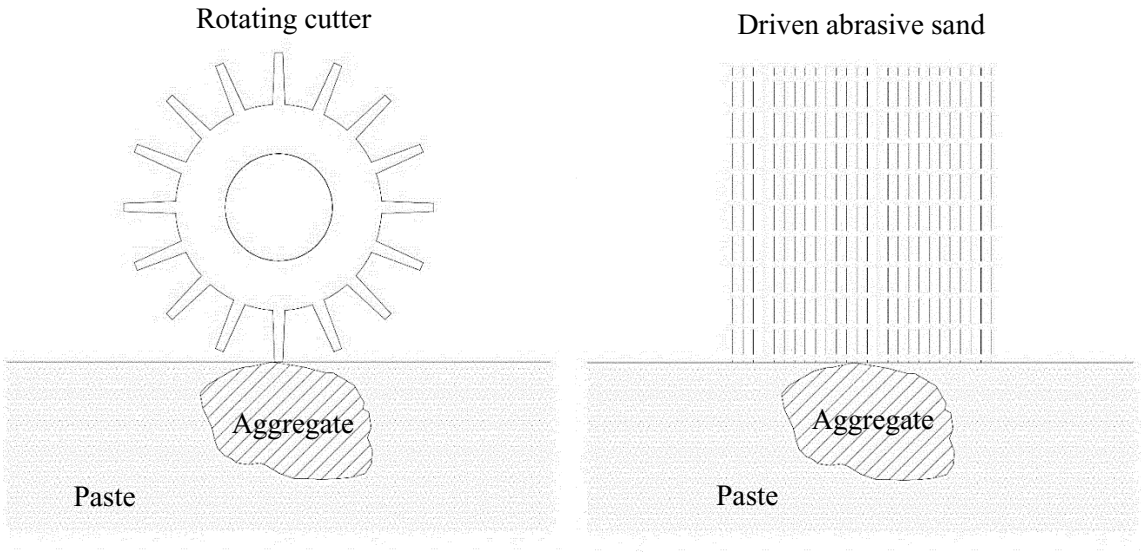

(a) Rotating cutters method (b) sandblasting method.

Fig. 3-19 Schematic figures of the abrasion testing mechanisms.

3.4.2.2. Concrete type comparison

Table 3-4 and Fig. 3-12 show the compressive strength of the tested mixtures. It can be noted that the compressive strength was decayed by increasing ESLWA content in the concrete mixtures. The HPNWC showed higher compressive strength by 10.6% and 13.9% at the 14- and 28-day, respectively. In addition, the HPLWAC showed less compressive strength compared to the HPSDC mixture by 9.8% and 10.8% at the 14- and 28-day, respectively. That is mainly attributed to that in the case of high strength mixtures, where the aggregate is weaker than the surrounding matrix in terms of strength, the mode of failure mainly depends on the aggregate strength. Where the ESLWA has less strength compared to the NWA, that led to less compressive strength with increasing its content in the mixture. This effect of replacement with a different type of aggregate on the compressive strength of concrete is in good agreement with multiple researchers with

similar results. (Wu, Yao, and Zhang 2001) studied the effect of aggregate type on compressive strength using crushed quartzite and marble aggregate and found 10-20% better performance using quartzite.

Table 3-4, Fig. 3-13, and Fig. 3-14 show the tensile properties of the tested mixtures. It can be seen that the aggregate type affected the tensile properties. The HPNWC had higher STS by 20.7% and 16.4% and better FS by 8.4% and 13.6% at 14- and 28-day, respectively, compared to the HPSDC. Also, HPLWAC had less STS by 18.3% and 15.7% and less FS by 10.3% and 13.4% at 14- and 28-day, respectively, compared to the HPSDC. Although it is mentioned in most of the other studies that the aggregate type has no significant impact on the tensile properties (Kozul and Darwin 1997), that was not the case in the current study. However, the current results are in agreement with the results concluded by (Kaplan 1959).

Table 3-4, Fig. 3-15, and Fig. 3-16 show the moduli of elasticity for the tested mixtures. It can be seen that they were also affected by changing the aggregate type. The HPNWC had higher SME by 14.6% and 17.1% and better DME by 12.1% and 13.2% at 14- and 28-day, respectively, compared to the HPSDC. Also, HPLWAC had less SME by 7.1% and 7.3% and less DME by 6.5% and 7.2% at 14- and 28-day, respectively, compared to the HPSDC. This behavior is mainly due to the porous nature of the ESLWA that provides it with less stiffness compared to the NWA. That in turn affects the concrete, causing lower moduli of elasticity with increasing the ESLWA content in the mixture. In addition, it was also noted that, for HPNWC, the difference between the two moduli of elasticity was only 13.9% and 8.3% at 14- and 28-day, respectively. However, the

difference for the HPSDC was 15.7% and 11.3% at 14- and 28-day, respectively and it was 16.2% and 11.4% at 14- and 28-day, respectively, for the HPLWAC. That behavior indicates that the difference between the SME and DME gets lower as the strength increases.

Table 3-5 shows the 14- and 28-day abrasion resistance for different types of concrete mixtures. The abrasion resistance is expressed as the abrasion depth (Fig. 3-17) and abrasion coefficient (Fig. 3-18). By comparing with other properties, it can be seen that concrete abrasion resistance was the most affected concrete property by changing the ESLWA content in the mixtures. That highlighted higher reliance of the concrete abrasion resistance on the aggregate type compared to other properties. The HPNWC had less abrasion depth compared to the HPSDC by 20.8% and 29.6% at 14- and 28-day, respectively. Also, the abrasion coefficient was less by 23.4% at the 28-day. Furthermore, the HPLWAC mixture had a higher abrasion depth of 31.2% and 37.9% at 14- and 28-day, respectively and higher abrasion coefficient by 26.7% at the 28-day. That behavior is mainly associated to the known fact that abrasion resistance of concrete depends mainly on the hardness of used aggregates, so this difference in the concrete abrasion resistance between the three types of concrete is attributed to the lower hardness of ESLWA (Los Anglos abrasion value of 25%) compared to the normal weight aggregate (Los Anglos abrasion value of 16%). This relationship between the concrete abrasion resistance and aggregate's Los Anglos abrasion value was confirmed by (Kılıç et al. 2008). In that study, direct relationship was found between the two values using three different types of concrete abrasion resistance tests.

3.4.2.3. Effect of hybrid addition of SCMs

Table 3-4 and Fig. 3-20 show the compressive strength of the tested mixtures incorporating different SCMs. It can be seen that up to 28 days, FA and SF incorporated mixtures had a less compressive strength compared to the control mixture. A gradual decrement was noticed with increasing the FA content. This decrement reached its peak at the incorporation of 30% of FA and 8% of SF. Less compressive strength by 35.3% and 19.3% at the 14- and 28-day, respectively, was attained. However, it can be noticed that time-dependent enhancement was attained when comparing the 14-day and 28-day results with the control mixture. When testing FA and SF incorporated mixtures for compressive strength at the 91-day, an enhancement of 7.2% when comparing 5% FA and 8% SF incorporated mixture with the control mixture was attained. And an enhancement of 2.9% when comparing the 10% FA and 8% SF incorporated mixture with the control mixture was attained. However, other FA incorporation ratios did not show higher compressive strength compared to the control mixture up to 91-day. This gradual enhancement that mixtures had with respect to time is due to that FA does not play a role and even can lead to a decrease of early strength to some extent, but it provides a gradual enhancement in the concrete performance with time. This time-dependent enhancement was also noticed by (Cai et al. 2016). In that study, 40% usage of fly ash alone as partial cement replacement had less compressive strength by 27.6% at 7-day, 15.7% at 28-day, and ended with 7.1% less compressive strength at 90-day compared to the control mixture. Although blending FA with SF did not significantly improve the HPSDC performance up to 91-day, its usage has advantages as it is a by-product of the coal-burning power industry and considered a

waste that can replace cement and this can lead to overall cost reduction of construction, also its usage has a potential regarding environmental impact. On the other hand, when it is compared to the incorporation of MK blended with SF as SCMs, the MK combination was more effective for providing an enhancement to the HPSDC compressive strength. This enhancement reached its peak at 15% of MK combined with 8% of SF. This combination provided powerful synergistic action that yielded enhanced compressive strength of the HPSDC. It can be noted from Fig. 3-20 that, the compressive strength was enhanced by 7.3% and 8.1% at the 14- and 28-day, respectively, compared to the control mixture. This positive effect that MK combination had on the HPSDC can be attributed to: a) High pozzolanic activity provided additional aluminates to the system through the combined reaction of MK and SF with $Ca(OH)_2$; b) MK and SF have a micro-filler effect that led to improved cement matrix packaging, and thus can lead to pore structure refinement.

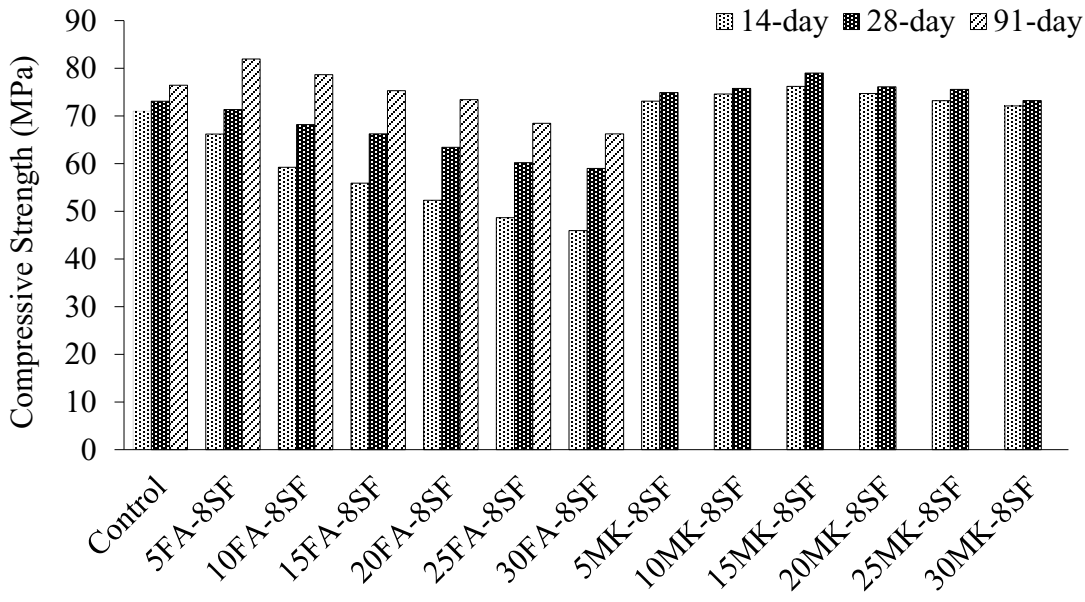

Fig. 3-20 Effect of incorporation of different SCMs on the compressive strength of the HPSDC.

Table 3-4, Fig. 3-21, and Fig. 3-22 show the tensile properties of the tested mixtures incorporating different SCMs. Similar to the compressive strength, up to the 28-day, the FA and SF combination was not effective. In that, the tensile properties of the FA and SF incorporated mixtures were declined compared to the control mixture for up to 28 days. That decrement reached its peak at the incorporation of 30% of FA blended with 8% of SF. In that, at these ratios, STS decreased by 41.6% and 31.5% compared to the control mixture and FS decreased by 23.6% and 19.7%. This decrement is mainly attributed to the fact explained earlier. As the FA pozzolanic reactivity is usually not active at early testing ages. That affected the ITZ morphology between the aggregate and the cement paste. It can be also noted that the STS was more affected by that ITZ weakness. On the other hand, MK

combination positively affected the ITZ yielding enhanced tensile properties. That enhancement reached its peak at the incorporation of 15% of MK blended with 8% of SF. For instance, compared to the control mixture an enhancement in the STS of 10.8% and 12.4% at the 14-day and 28-day, respectively, was attained. Furthermore, the FS increased but also at a less manner compared to the STS. For instance, at these incorporation ratios, the FS increased by 7% and 7.4% at the 14-day and 28-day.

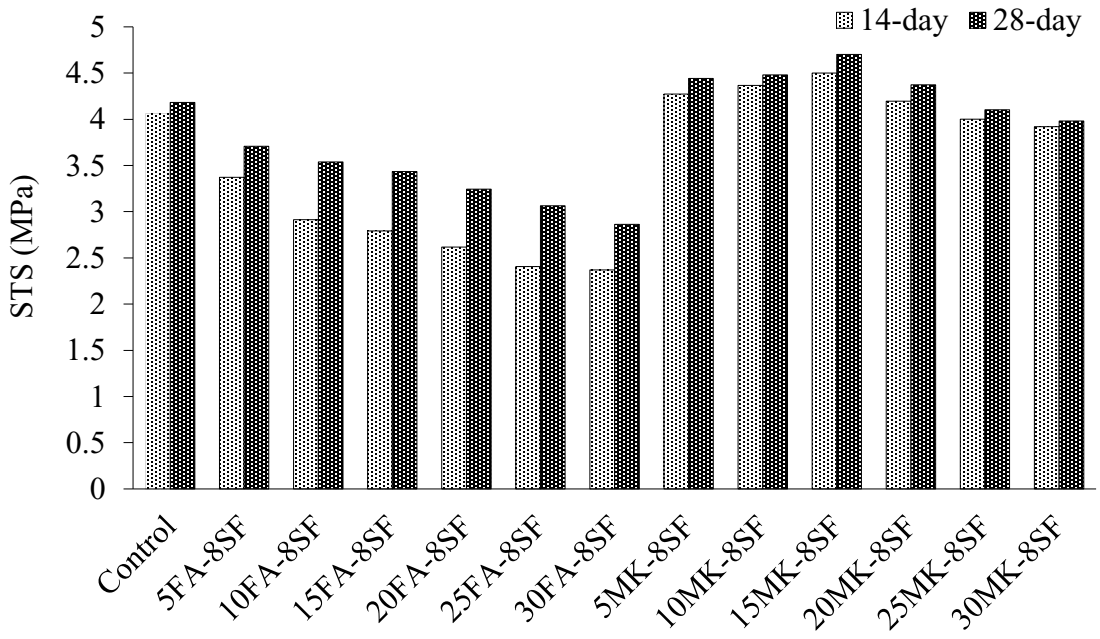

Fig. 3-21 Effect of incorporation of different SCMs on the STS of the HPSDC.

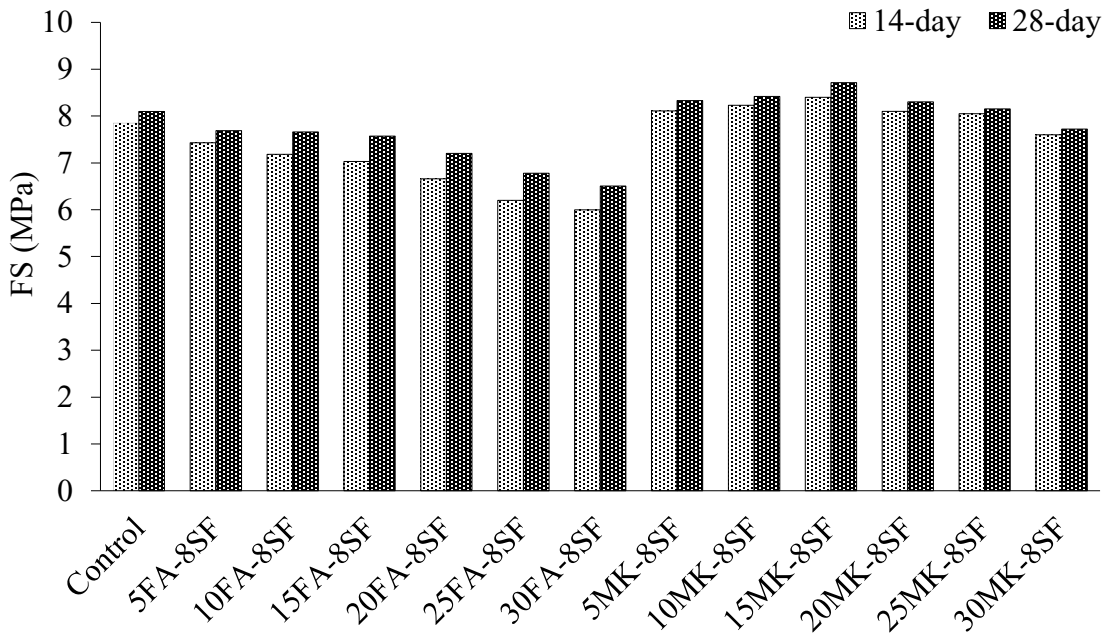

Fig. 3-22 Effect of incorporation of different SCMs on the FS of the HPSDC.

Moreover, the stiffness properties of the tested HPSDC mixtures were affected by the incorporation of the different SCMs. As can be seen from Table 3-4, Fig. 3-23, and Fig. 3-24, similar to other tested properties, incorporation of FA blended with SF had a negative impact on the HPSDC moduli of elasticity up to 28-days. That negative impact was relative to the FA incorporation ratio, as it reached its peak at the incorporation of 30% of FA blended with 8% of SF. At these incorporation ratios, SME dropped by 19.5% and 15.5% compared to the control mixture. Similarly, DME dropped by 22.9% and 20.6%. Also, it can be seen, when comparing the 14-day with 28-day moduli of elasticity, they were also enhanced with respect to time with the addition of FA and SF. On the contrary, incorporating MK at different ratios blended with SF at 8% provided the HPSDC with higher moduli of elasticity. Similar to other tested properties, that enhancement reached its

peak at the incorporation of 15% MK and 8% of SF. That mixture had a higher SME of 14.3% and 11.7% at the 14- and 28-day, respectively, compared to the control mixture. Also, the DME for this mixture was enhanced compared to the control mixture but to a less extent. It increased by 6.1% and 6.3% at the 14- and 28-day, respectively. This behavior is mainly due to the following reasons: a) The MK/SF synergistic action provided the HPSDC's mortar with greater stiffness, b) The matrix-aggregate tensile bond strength was positively altered, c) As reported by (Zhang and Gjørv 1991), that the fine SCMs can penetrate the porous structure of the ESLWA, providing enhanced internal microstructure for the ESLWA. However, other incorporation ratios of MK with SF were not as effective as 15% of MK and 8% of FA.

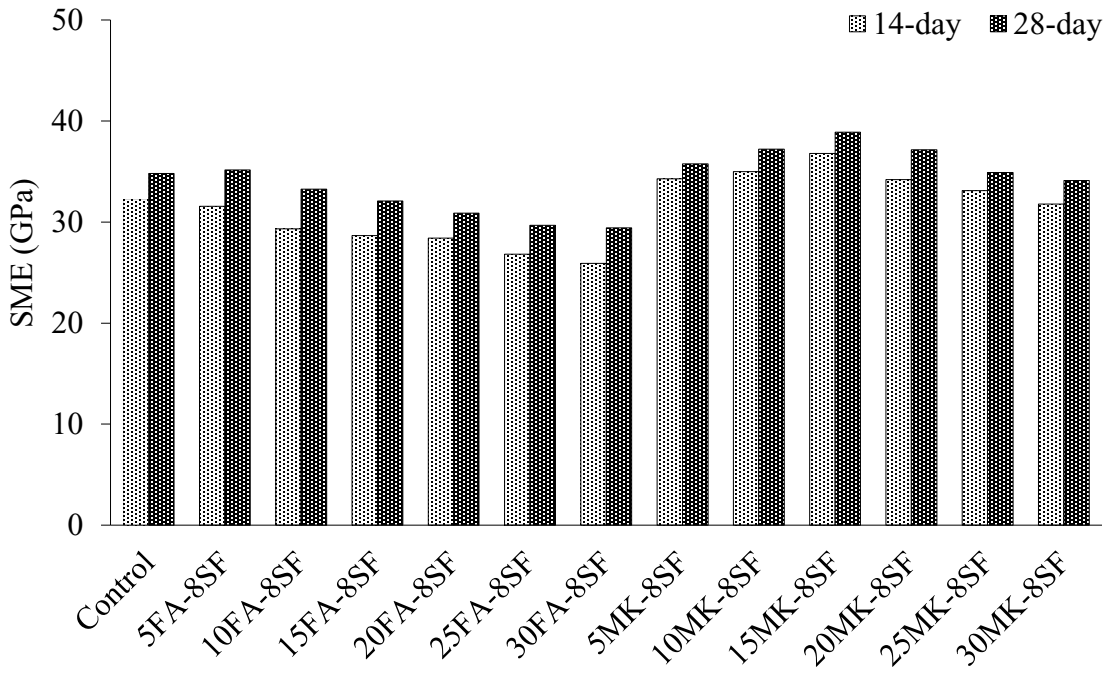

Fig. 3-23 Effect of incorporation of different SCMs on the SME of the HPSDC.

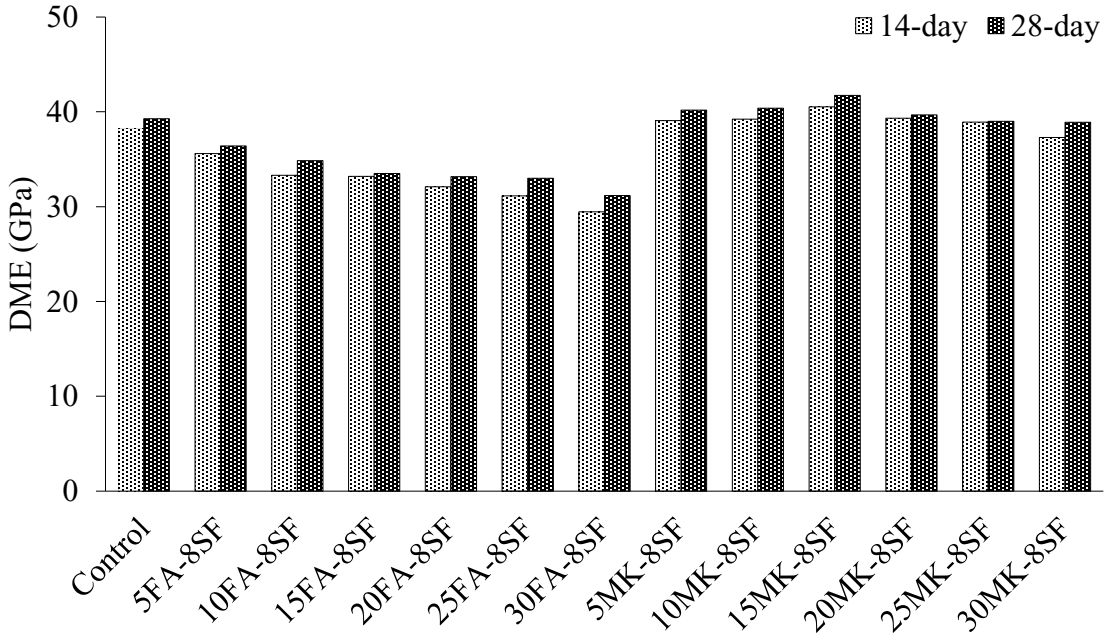

Fig. 3-24 Effect of incorporation of different SCMs on the DME of the HPSDC.

Table 3-5, Fig. 3-25, and Fig. 3-26 show the abrasion resistance of the tested mixtures measured using the two mentioned tests. It can be seen that, compared to other tested properties, the negative impact of incorporation FA blended with SF on the abrasion resistance of the HPSDC was more explicit. For instance, when comparing 30% of FA blended with 8% of SF mixture with the control mixture, an increment in the abrasion depth of 57.6% and 25.8% at the 14- and 28-day, respectively, was attained. That is mainly due to the less hardness of the cement paste those results from the incorporation of the FA combination. However, the impact on the abrasion coefficient was more explicit. For instance, the abrasion coefficient increased, by 37.9% at the 28-day. That difference between the two abrasion tests is due to the reason explained earlier, see Fig. 3-19, as when testing using the rotating cutter method, as the paste is weaker than the used normal weight

aggregate, the normal weight aggregate provides a shield to the other concrete constituents, making the other parts less exposed to the abrasive. However, when testing using the sandblasting method, as the abrasive abrade the surface vertically, all concrete parts are exposed to the abrasive in an equal manner. That leads to more impact on the abrasion coefficient by changing the paste and ITZ properties. Similar to other properties, it can be seen, when comparing the 14-day abrasion resistance with 28-day abrasion resistance, that the abrasion resistance was also enhanced with respect to time with the addition of FA and SF. That is due to, as explained earlier, that FA has a late pozzolanic reactivity that can play a role in providing a gradual enhancement to the concrete performance with respect to time. On the contrary, incorporating MK at different ratios blended with SF at 8% provided the HPSDC with higher abrasion resistance. That enhancement reached its peak at incorporation of 15% MK and 8% of SF. That mixture had less abrasion depth by 11.8% and 12.1% at the 14- and 28-day, respectively, compared to the control mixture. Also, the abrasion coefficient was more affected as the MK combination provided less abrasion coefficient of 26.8% at the 28-day when comparing 15MK-8SF with the control mixture.

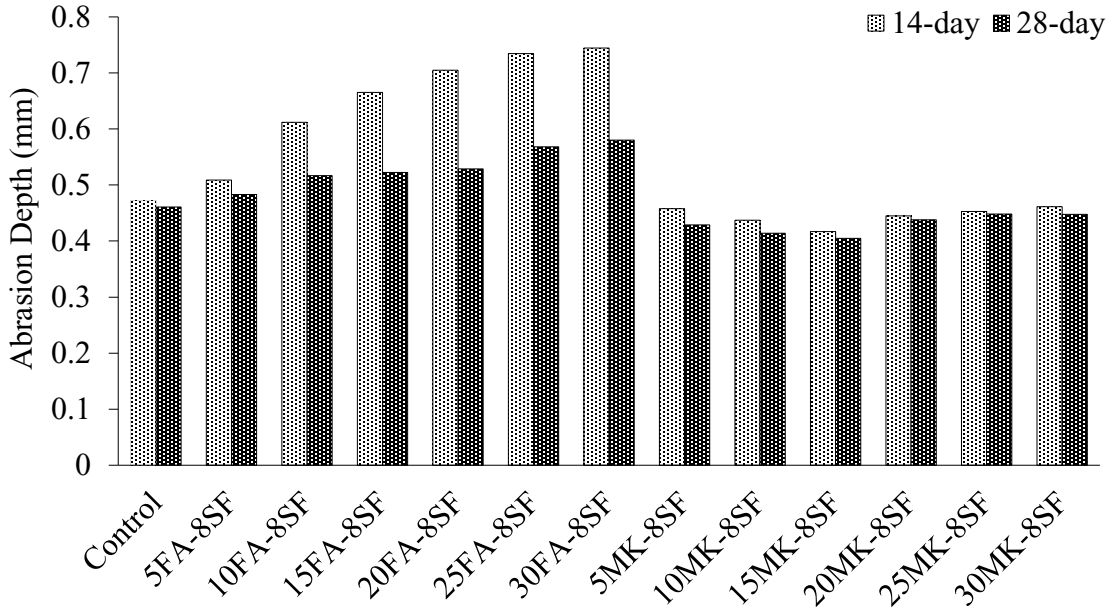

Fig. 3-25 Effect of incorporation of different SCMs on the abrasion resistance of the HPSDC measured using rotating cutters method.

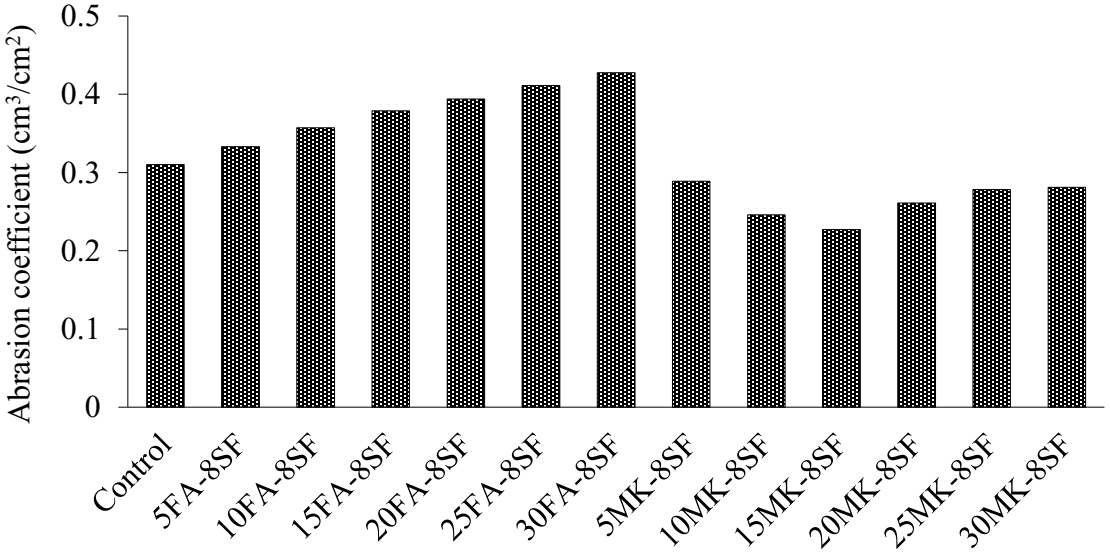

Fig. 3-26 Effect of incorporation of different SCMs on the abrasion resistance of the HPSDC measured using sandblasting method.

3.5. Conclusions

Many parameters were studied to evaluate and enhance the abrasion resistance and mechanical properties of the HPSDC mixture. The parameters studied were different C/F aggregate ratios, different A_m, a comparison between the HPSDC with other types of concrete, the synergistic action of using FA and SF, and the effect of using MK in the SF system. The properties of the fresh mixtures were investigated. The mechanical properties of the developed mixtures were evaluated for compressive strength, STS, FS, SME, and DME. Abrasion resistance was assessed using two tests; the rotating cutters method and sandblasting test. Based on the experimental investigation, the following conclusions were drawn:

1. Increasing the C/F aggregate ratio from 1 to 2 decreased the SP demand by an average of 10.5% while using 20 mm A_m in the HPSDC mixtures required a mild less SP dosage compared to 10 mm A_m. Compared to the HPSDC mixture, the HPNWC mixture required a mild higher dosage, while the HPLWAC mixture required a slightly less dosage. The incorporation of different ratios of FA blended with 8% of SF required higher SP dosages at low FA ratios. However, at higher FA incorporation ratios (more than 10%), the FA impact was more pronounced and fewer SP dosages were needed. On the contrary, remarkably higher SP dosages were needed, reached almost two times with the incorporation of 30% of MK blended with 8% of SF.

2. Changing the C/F aggregate ratio and A_m did not have a remarkable impact on the AEA demand. Similarly, the same AEA dosage was enough for the three types of concrete; HPSDC, HPNWC, and HPLWAC. On the contrary, higher dosages of AEA were required to achieve the recommended air content with the incorporation of different SCMs. Higher dosage reached 71.4% with the addition of 30% of fly ash and 8% of silica fume. And reached 128.6% higher dosage with 30% of MK addition with 8% of SF.
3. C/F aggregate ratio of 1.6 turned out to be the optimum ratio for the HPSDC. As it provided clear enhancement to the HPSDC compressive strength and moduli of elasticity by an average of 15.6% and 13% respectively. Furthermore, the impact was more explicit on its tensile properties. Compared to the C/F aggregate ratio of 1, C/F of 1.6 had higher STS by an average of 22.9% and higher FS by an average of 26.7%. In addition, the abrasion resistance was also clearly enhanced by an average of 12.8% and 14.3% using rotating cutters and sandblasting methods respectively.
4. The results of the tested mixtures indicated that using A_m of 10 mm in the HPSDC provided it with better tensile properties compared to A_m of 20 mm. For instance, the STS was higher by an average of 6.7% while the FS was higher by an average of 5.9%. However, using different A_m did not have a noticeable effect on the compressive strength, moduli of elasticity, or the abrasion resistance using the rotating cutters method. However, 20 mm mixtures showed less abrasion resistance by an average of 7.9% using the sandblasting testing method.

5. Changing the aggregate type affected the mechanical properties of the tested concrete. The HPSDC had less, yet comparable, mechanical properties compared to the HPNWC, while, it had better mechanical properties compared to the HPLWAC. However, when comparing the three different concrete types, the abrasion resistance was more affected compared to the tested mechanical properties. In general, it was noted that the difference in the mechanical properties and abrasion resistance between the three concrete types at 28-day was higher than at 14-day.
6. Incorporating FA blended with SF as partial cement replacement materials in the HPSDC mixtures had a negative impact on the mechanical properties and abrasion resistance of the HPSDC up to the 28-day. However, at low incorporation ratios of 5% and 10% of FA blended with 8% of SF, the compressive strength showed slight enhancement compared to the control mixtures at the 91-day.
7. Synergistic action of MK and SF helped improve the HPSDC properties. The optimum dosage turned out to be 15% of MK and 8% of SF. As, it led to an enhancement in HPSDC compressive strength, STS, FS, SME, and DME by an average of 7.7%, 11.7%, 7.3%, 13%, and 6.2%, respectively. In addition, it led to an enhancement in the HPSDC abrasion resistance by an average of 12% and by an average of 26.8% using the sandblasting testing method. In general, when comparing the MK combination with the FA combination, the MK combination was more effective as SCMs in the HPSDC.

3.6. References

"ACI 318-14." 2014. Building Code Requirements for Structural Concrete (ACI 318-14). American Concrete Institute.

"ASTM C1017." 2013. Standard Specification for Chemical Admixtures for Use in Producing Flowing Concrete.

"ASTM C1240." 2020. Standard Specification for Silica Fume Used in Cementitious Mixtures. https://doi.org/10.1520/C1240-20.

"ASTM C143." 2020. Standard Test Method for Slump of Hydraulic-Cement Concrete. https://doi.org/10.1520/C0143_C0143M-20.

"ASTM C150." 2022. Standard Specification for Portland Cement. https://doi.org/10.1520/C0150_C0150M-22.

"ASTM C215." 2019. Standard Test Method for Fundamental Transverse, Longitudinal, and Torsional Resonant Frequencies of Concrete Specimens. https://doi.org/10.1520/C0215-19.

"ASTM C231." 2022. Standard Test Method for Air Content of Freshly Mixed Concrete by the Pressure Method. 2022. https://doi.org/10.1520/C0231_C0231M-22.

"ASTM C260." 2016. Standard Specification for Air-Entraining Admixtures for Concrete. https://doi.org/10.1520/C0260_C0260M-10AR16.

"ASTM C39." 2021. Standard Test Method for Compressive Strength of Cylindrical Concrete Specimens. https://doi.org/10.1520/C0039_C0039M-21.

"ASTM C418." 2020. Standard Test Method for Abrasion Resistance of Concrete by Sandblasting. https://doi.org/10.1520/C0418-20.

"ASTM C418." 2020. Standard Test Method for Abrasion Resistance of Concrete by Sandblasting. https://doi.org/10.1520/C0418-20.

"ASTM C469." 2022. Standard Test Method for Static Modulus of Elasticity and Poisson's Ratio of Concrete in Compression. https://doi.org/10.1520/C0469_C0469M-22.

"ASTM C494." 2022. Standard Specification for Chemical Admixtures for Concrete. https://doi.org/10.1520/C0494_C0494M-19E01.

"ASTM C496." 2017. Standard Test Method for Splitting Tensile Strength of Cylindrical Concrete Specimens. https://doi.org/10.1520/C0496_C0496M-17.

"ASTM C618." 2022a. Standard Specification for Coal Fly Ash and Raw or Calcined Natural Pozzolan for Use in Concrete. https://doi.org/10.1520/C0618-22.

"ASTM C618." 2022b. Standard Specification for Coal Fly Ash and Raw or Calcined Natural Pozzolan for Use in Concrete. 2022. https://doi.org/10.1520/C0618-22.

"ASTM C78." 2022. Standard Test Method for Flexural Strength of Concrete (Using Simple Beam with Third-Point Loading). https://doi.org/10.1520/C0078_C0078M-22.

"ASTM C944." 2019. Standard Test Method for Abrasion Resistance of Concrete or Mortar Surfaces by the Rotating-Cutter Method. https://doi.org/10.1520/C0944_C0944M-19.

Bogas, Jose, and Augusto Gomes. 2014. "Static and Dynamic Modulus of Elasticity of Structural Lightweight and Modified Density Concrete with and without Nanosilica – Characterization and Normalization" IJCE 12 (2): 170–80. http://ijce.iust.ac.ir/article-1-743-en.html.

Cai, X, Zhen He, S Tang, and Xiaorun Chen. 2016. "Abrasion Erosion Characteristics of Concrete Made with Moderate Heat Portland Cement, Fly Ash and Silica Fume Using Sandblasting Test." Construction and Building Materials 127: 804–14.

Fernandes, J.F., T. Bittencourt, and P. Helene. 2008. "A Review of the Application of Concrete to Offshore Structures." ACI Symposium Publication 253. https://doi.org/10.14359/20187.

Gautier, Donald L, Kenneth J Bird, Ronald R Charpentier, Arthur Grantz, David W Houseknecht, Timothy R Klett, Thomas E Moore, et al. 2009. "Assessment of Undiscovered Oil and Gas in the Arctic." Science 324 (5931): 1175 LP – 1179. https://doi.org/10.1126/science.1169467.

Hoff, G. C., and R. Elimov. 1995. "Concrete Production for the Hibernia Platform." In Annual Conference- Canadian Society for Civil Engineering, 693–716.

Jang, Seok-Joon, and Hyun-Do Yun. 2018. “Combined Effects of Steel Fiber and Coarse Aggregate Size on the Compressive and Flexural Toughness of High-Strength Concrete.” Composite Structures 185: 203–11. https://doi.org/https://doi.org/10.1016/j.compstruct.2017.11.009.

Kaplan, M F. 1959. “Flexural and Compressive Strength of Concrete as Affected by the Properties of Coarse Aggregates.” In .

Kılıç, A, C D Atiş, A Teymen, O Karahan, F Özcan, C Bilim, and M Özdemir. 2008. “The Influence of Aggregate Type on the Strength and Abrasion Resistance of High Strength Concrete.” Cement and Concrete Composites 30 (4): 290–96. https://doi.org/https://doi.org/10.1016/j.cemconcomp.2007.05.011.

Kozul, Rozalija, and D Darwin. 1997. “Effects of Aggregate Type, Size, and Content on Concrete Strength and Fracture Energy.” In .

Nikbin, I M, M H A Beygi, M T Kazemi, J Vaseghi Amiri, E Rahmani, S Rabbanifar, and M Eslami. 2014. “A Comprehensive Investigation into the Effect of Aging and Coarse Aggregate Size and Volume on Mechanical Properties of Self-Compacting Concrete.” Materials & Design 59: 199–210. https://doi.org/https://doi.org/10.1016/j.matdes.2014.02.054.

Nochaiya, Thanongsak, Watcharapong Wongkeo, and Arnon Chaipanich. 2010. “Utilization of Fly Ash with Silica Fume and Properties of Portland Cement–Fly Ash–Silica Fume Concrete.” Fuel 89 (3): 768–74. https://doi.org/https://doi.org/10.1016/j.fuel.2009.10.003.

Rashad, Alaa M. 2013. “A Preliminary Study on the Effect of Fine Aggregate Replacement with Metakaolin on Strength and Abrasion Resistance of Concrete.” Construction and Building Materials 44: 487–95. https://doi.org/https://doi.org/10.1016/j.conbuildmat.2013.03.038.

Ruiz, W M. 1966. Effect of Volume of Aggregate on the Elastic and Inelastic Properties of Concrete. Cornell University, Jan. https://books.google.com.eg/books?id=sOVUAAAAYAAJ.

Sandvik, M., T. Hovda, and S. Smeplass. 1994. “Modified Normal Density (MND) Concrete for the Troll GBS Platform.” ACI Symposium Publication 149: 81–102. https://doi.org/10.14359/4069.

Srivastava, Vikas. 2012. “Effect of Silica Fume and Metakaolin Combination on Concrete.” International Journal of Civil and Structural Engineering 2 (February). https://doi.org/10.6088/ijcser.00202030017.

Sujjavanich, S, P Suwanvitaya, D Chaysuwan, and G Heness. 2017. “Synergistic Effect of Metakaolin and Fly Ash on Properties of Concrete.” Construction and Building Materials 155: 830–37. https://doi.org/https://doi.org/10.1016/j.conbuildmat.2017.08.072.

Craig, Peter and Wolfe, Bill. 2012. “Another Look at the Drying of Lightweight Concrete-A Comparison of Drying Times for Normal weight and Lightweight Floors.” Concrete International: 53–58.

Wu, Ke-Ru, Wu Yao, and Dong Zhang. 2001. “Effect of Coarse Aggregate Type on Mechanical Properties of High-Performance Concrete.” Cement and Concrete Research 31 (October): 1421–25. https://doi.org/10.1016/S0008-8846(01)00588-9.

Zhang, Min-Hong, and Odd Gjørv. 1991. “Mechanical Properties of High-Strength Lightweight Concrete.” Aci Materials Journal 88 (May): 240–47.

Chapter 4 Impact of fibers inclusion on the abrasion resistance of the high performance specified density concrete

4.1. Abstract

The high performance specified density concrete (HPSDC) is a concrete type that is made by substituting normal weight coarse aggregate with lightweight coarse aggregate to a certain extent. It is most commonly used in offshore structural applications. This study was conducted to enhance the HPSDC mechanical properties and abrasion resistance by incorporating of different types of fibers at different ratios. A variety of fibers with a broad spectrum of mechanical properties were used: copper coated steel fiber (CCSFs), polypropylene fibers (PPFs), bundled basalt fibers (BBFs), and filament basalt fiber (FBFs). The fibers were added at 0.1%, 0.3%, and 0.5% by volume. The fresh properties of the reinforced HPSDC were assessed and its mechanical behavior was evaluated through five ASTM standard testing for compressive strength, splitting tensile strength (STS), flexural strength (FS), static modulus of elasticity (SME), and dynamic modulus of elasticity (DME). The HPSDC abrasion resistance was evaluated using two ASTM standard testing; the rotating cutters method ("ASTM C944" 2019) and sandblasting method (ASTM C418) method. The experimental results revealed that the incorporation of CCSFs had the most effective influence on the mechanical properties and abrasion resistance of the HPSDC. CCSFs had an impact on the abrasion resistance of ana average of 24%. PPFs were also able to enhance the compressive strength, STS, and FS (which is the modulus of rupture) of the HPSDC with a limited impact on its abrasion resistance.

Both types of BFs were able to improve the HPSDC tensile properties and abrasion resistance. However, they had a negative impact on its compressive strength.

Keywords: Specified density concrete, offshore, abrasion, fibers.

4.2. Introduction

Concrete has a wide range of applications in the construction industry. However, because concrete is subjected to a variety of loading activities, each application necessitates a concrete with distinct characteristics. Offshore structural concrete, for example, is prone to abrasion by interacting with sliding ice sheets in a hostile environment. This interaction could result in significant wear, which could lead to damage, increased maintenance costs, and a shorter life cycle. The 1.3 billion-dollar (CAN) Confederation Bridge in Canada, which connects Prince Edward Island to the mainland at New Brunswick, is an example of a structure in ice-infested water. This is the world's longest concrete bridge over ice-covered water. Due to interacting with floating ice sheets, monitoring of the bridge revealed some wear damage to the concrete pillars at the water's surface. Work on repair and restoration has previously been suggested and is now underway. This drew attention to the need to design a more abrasion-resistant offshore structural concrete.

Offshore structures require a special type of concrete. To withstand such harsh environmental conditions, it must be of high performance (“ACI 318-14” 2014). In some cases, it must also be lighter in weight. Offshore platforms, for example, are built on land and then towed to their final location. The towing phase necessitates the use of concrete with predetermined unit weight. As a result, using lightweight aggregate as a component

in the concrete mixture became a viable alternative (Fernandes, Bittencourt, and Helene 2008). However, replacing all of the coarse aggregates in concrete with lightweight aggregate results in concrete with reduced mechanical characteristics and abrasion resistance. As a result, for offshore structural applications, it is preferable to partially replace coarse aggregate with lightweight aggregate, and the generated concrete is known as specified density concrete or modified normal density concrete.

For offshore structural applications, the HPSDC has been widely used. In 1991, 450,000 tonnes of concrete, predominantly HPSDC with 50% coarse aggregate replacement by the lightweight aggregate, were used in the construction of the Hibernia platform, a massive gravity-based structure (Hoff and Elimov 1995). It was also utilized in the construction of the Troll A GBS platform (Sandvik, Hovda, and Smeplass 1994), which at the time was the world's largest moving structure. In 1996, HPSDC enabled such a massive structure to be pulled across the sea. Furthermore, HPSDC is currently being employed in the construction of West White Rose's new gravity-based structure. There is, however, a desire for a more advanced HPSDC to be employed in harsher environments, such as the Arctic. The Arctic holds 13% of the world's undiscovered oil and 30% of the world's undiscovered gas (Gautier et al. 2009), making it a valuable resource for the future of oil and gas. However, research is still limited due to the exceptionally hostile environmental conditions that the concrete is subjected to there.

Plain HPSDC, or plain concrete in general, is a brittle material that is characterized by low tensile strength. This is a result of the presence of numerous micro-cracks inside the concrete matrix which begin to rapidly propagate when a load is applied. To overcome

this deficiency continuous reinforcing bars are usually added to the tensile zones. However, concrete cracks are not fully arrested by the usage of these bars solely. For this reason, fibers are added. Although the main purpose of reinforcing concrete with fibers is alternating its tensile behavior, it was found that it affects other concrete properties as well. That brought the authors' attention to study the impact of incorporating different types of fibers in the HPSDC to enhance its mechanical properties and abrasion resistance.

Various types of fibers are used in concrete composites. By analyzing the properties of these fibers and their effect on the concrete, fibers can be broadly classified into two categories. The first category is fibers with high elongation and low elastic modulus such as synthetic fibers (nylon, polypropylene, and polyethylene). This type was found to improve toughness and other concrete properties (Jiang et al. 2014). The other category is fibers characterized by high modulus of elasticity such as steel fiber, carbon fiber, and aramid fiber. That type is proven to be effective in improving the compressive strength, toughness, and stiffness of concrete (Hasan and Dimitris C. 1991). Although the popularity of these mentioned fibers, each has drawbacks. For example, steel fiber is susceptible to corrosion because of chloride penetration and carbonation (Bentur and Mindess 2007). In addition, its incorporation leads to increased dead load and reduced workability. On the other hand, synthetic fibers have a low modulus of elasticity and poor thermal resistance.

The impact of the inclusion of steel fibers and PPFs on the abrasion resistance of the concrete was studied by a handsome of researchers. (Horszczaruk 2009) made a study about the impact of the inclusion of steel fibers and two sizes of PPFs on the abrasion resistance of the high performance concrete. In that study, the abrasion resistance was

evaluated as per ("ASTM C1138" 2019). The results revealed that PPFs had a better performance compared to steel fibers. In addition, it was found that small steel fibers had less impact, while long steel fibers did not affect the concrete abrasion resistance. (Mahdi, Shamkhi, and Abid 2017) reported enhancements to the concrete abrasion resistance that was associated with increasing PPFs content. (Grdic et al. 2012) studied the impact of the incorporation of two types of micro synthetic PPFs in a normal strength concrete and with an addition of 0.1%, a noticeable improvement in the concrete abrasion resistance was reported. The effect of incorporation of PPFs at higher dosages, up to 1.2%, was reported by (Al-mashhadani et al. 2018) using ("ASTM C944" 2019) and an extensive abrasion resistance enhancement was reported.

Recently, BFs have gathered attention as a promising alternative in concrete reinforcing. BFs are inorganic materials that are manufactured from basalt rocks by melting and extrusion. This process is eco-friendly and does not consume much energy which makes BFs relatively cheap (Deák and Czigány 2009). Compared to steel fiber, BFs have much higher tensile strength, less specific gravity, and are immune to corrosion (Fibres Unlimited 2007). In addition, in high alkaline environments, BFs showed good chemical stability that provided it with good adhesion with the surrounding matrix (Basalt Fibers LTD. 2013). These characteristics made BFs an excellent preference for offshore structural application.

Two types of chopped basalt fiber are commercially available. Bundled basalt fiber (BBFs) which is a set of filaments held together during mixing. Whereas filament basalt fibers (FBFs) that disperse into individual filaments during mixing. There is a general

agreement on the optimum dosage of chopped basalt fiber of (0.3-0.5%) by volume and that it can have a detrimental effect at higher dosages (Borhan 2013). However, BFs optimal dosage various significantly with the type of concrete (Ayub, Shafiq, and Nuruddin 2014) and (Dias and Thaumaturgo 2005).

By reviewing the literature, research was found on the usage of continuous basalt fiber as a strengthening material for concrete structures (Sim, Park, and Moon 2005). However, merely limited studies were found on the impact of incorporating chopped basalt fiber on the concrete properties. (Dias and Thaumaturgo 2005) made a study on the relationship between the fiber amount and fracture toughness of basalt fiber incorporated geopolymeric cement concretes mixtures. The basalt fiber incorporated beams showed higher ultimate loads, less sensitivity to cracks, and larger displacement before to failure. (Zhao et al. 2010) investigated the impact strength of concrete reinforced with basalt fiber and found an obvious improvement with the addition of basalt fiber. From other investigations, the incorporation of basalt fiber into concrete has proven to improve its tensile strength (Borhan 2013), and the impact resistance (Fu et al. 2018), with no significant impact on the compressive strength (Jiang et al. 2014).

As can be noticed, the research into reinforcing concrete using BFs has mainly been focused on the fundamental mechanical properties: compressive strength, STS, and FS. Although mechanical properties are the key subject for structure engineering design, abrasion resistance is a crucial concern for offshore structures. Yet, only one study was conducted in the past regarding the effect of basalt fiber on the abrasion resistance of concrete by (Kabay 2014). In that study, it was found that the abrasion resistance was

enhanced with the addition of BFs in normal weight, normal strength concrete, along with improved flexural strength and fracture energy. However, there is no study available on the effect of incorporating different types of basalt fibers on the HPSDC mechanical properties and abrasion resistance.

The key objective of the current study is to evaluate the relative merit of the two types of chopped basalt fibers in enhancing the mechanical behavior and abrasion resistance of the HPSDC. The study provides a detailed comparison of the effect of reinforcing the HPSDC with basalt fiber with respect to the commonly used fibers (steel and synthetic fibers). The steel fibers used were straight and copper coated to eliminate the fiber's corrosive nature. Based on the results, suggestions for the most suitable type of fiber and dosage to be used in the HPSDC will be provided to facilitate the use of fibers in offshore structure concrete. The study aims to enhance the performance of the HPSDC which could help expand the application of the HPSDC. The authors believe that the results obtained from this study will effectively contribute to a more effective offshore structure, huge maintenance cost savings, and provide an incentive to expand construction for new offshore structures in harsher environmental regions which is highly demanded.

4.3. Experimental program

4.3.1. Material properties

General use Portland cement (GU) (ASTM C150 Type I) ("ASTM C150" 2022), MK (ASTM C618 2022) Class N, and SF ("ASTM C1240" 2020) were utilized as binders in the mixes that were created. Table 4-1 shows the chemical analysis and physical properties of the cement and SCMs used. STALITE expanded slate lightweight aggregate (ESLWA) was employed, which had a maximum aggregate size of 12.5 mm and a specific gravity of 1.53 at a saturated surface dry state (SSD). Because of its porous structure, the aggregate exhibited a high absorption rate, ranging from 6% to 9%. The physical properties of the ESLWA can be seen in Table 4-2. Crushed granite stone with a specific gravity of 2.6 was used as the normal weight aggregate for both coarse and fine aggregate. The absorption rate of the normal weight coarse aggregate is 0.6 percent, with a maximum aggregate size of 10 mm. Figure 4-1 shows images of the ESLWA and coarse normal weight aggregates (NWA). Figure 4-2 shows the gradation analysis for the aggregates utilized, with the curves representing the ("ASTM C33" 2018) limitations. Four types of fibers were used: copper coated steel fiber (CCSFs), PPFs, chopped BBFs, and chopped FBFs. Pictures of the used fibers are shown in Fig. 4-3 and their properties are shown in Table 4-3. Polycarboxylate-based superplasticizer (SP) that confines to ("ASTM C494" 2022) Type A and F, and ("ASTM C1017" 2013) Type I was utilized to accomplish the required workability for the developed mixtures. An air-entraining agent (AEA) that confines to ("ASTM C260" 2016) was utilized to increase the hardened concrete's resistance to freeze and thaw.

Table 4-1 Chemical analysis and physical properties of the used cement and SCMs.

Chemical analysis (%)	Cement	SF	MK
SiO_2	19.64	89.1	52
Al_2O_3	5.48	0.67	43
Fe_2O_3	2.38	0.49	<2.2
CaO	62.44	6.12	<0.2
MgO	2.48	0.31	<0.1
SO_3	4.32	0.16	-
K_2O	-	0.49	<0.40
Na_2O	-	0.26	<0.05
Cl	-	0.04	-
Total alkali	0.97	-	-
Free lime	1.03	-	-
LOI	2.05	2.81	0.95
C_3S	52.34	-	-
C_2S	16.83	-	-
C3A	10.5	-	-
C4AF	7.24	-	-
Physical properties			
Specific gravity	3.15	2.20	2.56
Blaine fineness (m^2/kg)	410		

Table 4-2 Physical characteristics of ESLWA.

Absorption Saturated Surface Dry (ASTM C127)	6.0%
Soundness (% Loss) Magnesium Sulfate (ASTM C88)	0 - 0.01%
Sodium Sulfate (ASTM C88)	0 - 0.23%
25 Cycles Freezing and Thawing (AASHTO T 103)	0.22 - 0.80%
Toughness Los Angeles Abrasion (AASHTO T 96)	25 - 28%
Stability Angle of Internal Friction (Loose)	40° - 42°
Angle of Internal Friction (Compacted)	43° - 46°

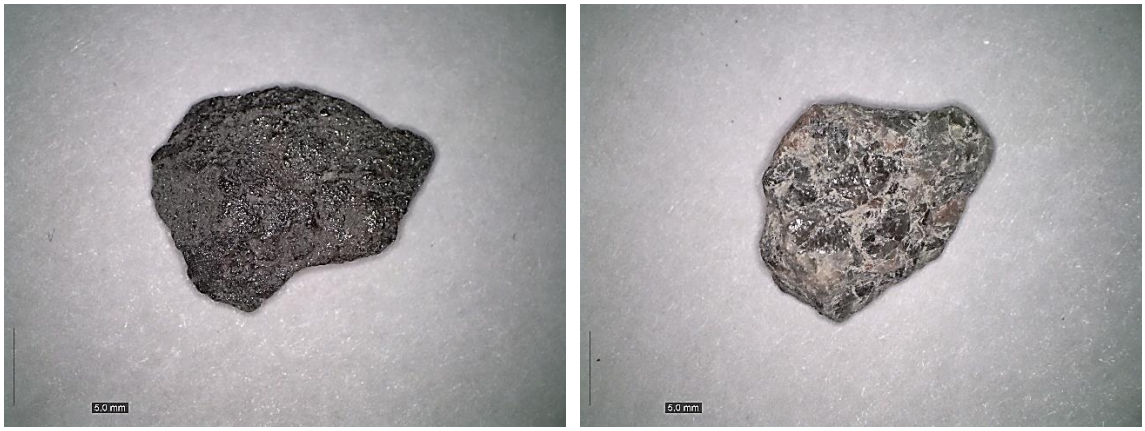

(a) ESLWA (b) NWA

Figure 4-1 Used coarse aggregate.

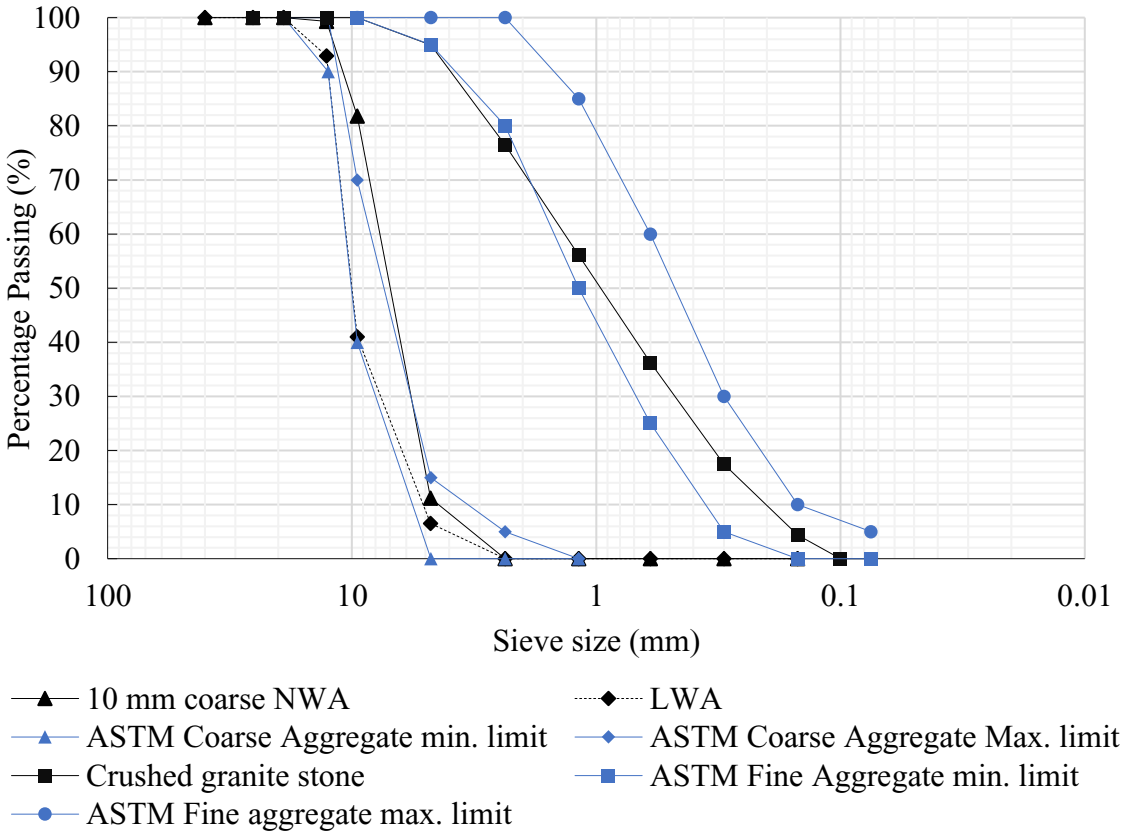

Figure 4-2 Grading curves NWA, ESLWA, and fine aggregate.

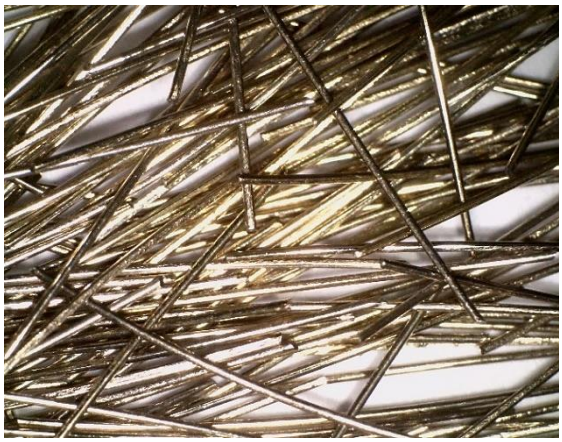

(a) CCSFs

(b) PPFs

(c) BBFs

(d) FBFs

Fig. 4-3 The fibers used

Table 4-3 Properties of fibers used.

Property	CCSFs	PPFs	BBFs	FBFs
Specific Gravity	7.8	0.91	2.67	2.67
Length (mm)	13	12	36	24
Diameter (μm)	200	38	16 (filament diameter)	16 (filament diameter)
Tensile strength (MPa)	1900	300	3000	3000
Elastic modulus (GPa)	203	14.7	86	86
Elongation at break (%)	0.5-3.5	15-25	3.15	3.15

4.3.2. Concrete mixtures development

Because of the close spacing of the reinforcement utilized in offshore structural elements, high workability is required (Fernandes, Bittencourt, and Helene 2008). As a result, a 180 mm to 220 mm slump was targeted. Offshore constructions are exposed to harsh weather conditions. As a result, ("ACI 318-14" 2014) advised a target air content of 6 to 7.5 percent. Trial mixtures were used to determine the best SP dosage for achieving the desired slump without the risk of segregation. Despite the use of superplasticizer, it was found that dosages higher than 0.5% of CCSFs and BBFs led to difficulty to achieve proper consolidation. Thus, a limiting dosage of 0.5% was chosen for this study for all types of fibers. In addition, the AEA dosage was thoroughly adjusted to produce the necessary air content. The four types of fibers were used at three different ratios of 0.1%, 0.3%, and 0.5%. A total of thirteen mixtures, 234 cylinders and 78 prisms, were developed. Cylinders' size were 100 mm × 200 mm, while prisms size was 100 mm × 100 mm × 400 mm. The concrete mixtures' composition is shown in Table 4-4. The mixtures were labeled according to the used fibers' volume and type. For example, a mixture using CCSFs at 0.1% was labeled as 0.1CCSFs. While a mixture using PPFs at 0.3% was labeled as

0.3PPFs. All mixtures were developed with constant ratios of cement replacements with MK and SF at 15% and 8%, as these replacement ratios were found to be optimum through level 2 of the experimental program of the current research (chapter 3).

Table 4-4 Composition of the tested mixtures.

Mixture No.	Mixture designation	Binders content			C/F	ESLWA/ T. C. A.	Fibers		SP	Density
		Cement	MK	SF			Type	volume		
		(kg/m^3)	(kg/m^3)	(kg/m^3)				(%)	(ml/m^3)	(kg/m^3)
1	Control	423.5	82.5	44	1.6	0.5	_	_	3651	2033.9
2	0.1CCSFs	423.5	82.5	44	1.6	0.5	CCSFs	0.1	4375	2039.3
3	0.3CCSFs	423.5	82.5	44	1.6	0.5	CCSFs	0.3	5000	2049.9
4	0.5CCSFs	423.5	82.5	44	1.6	0.5	CCSFs	0.5	5500	2060.6
5	0.1PPFs	423.5	82.5	44	1.6	0.5	PPFs	0.1	4000	2032.6
6	0.3PPFs	423.5	82.5	44	1.6	0.5	PPFs	0.3	4375	2029.8
7	0.5PPFs	423.5	82.5	44	1.6	0.5	PPFs	0.5	4750	2027.1
8	0.1BBFs	423.5	82.5	44	1.6	0.5	BBFs	0.1	4000	2034.3
9	0.3BBFs	423.5	82.5	44	1.6	0.5	BBFs	0.3	4375	2035.1
10	0.5BBFs	423.5	82.5	44	1.6	0.5	BBFs	0.5	4750	2035.9
11	0.1FBFs	423.5	82.5	44	1.6	0.5	FBFs	0.1	4000	2034.3
12	0.3FBFs	423.5	82.5	44	1.6	0.5	FBFs	0.3	4375	2035.1
13	0.5FBFs	423.5	82.5	44	1.6	0.5	FBFs	0.5	4750	2035.9

Note: All mixtures have 550 kg/m^3 binder content and 0.3 water to binder ratio.

4.3.3. Mixing procedures

Because of its high absorption of 6 to 9%, the ESLWA was soaked for 24 hours and then drained for 6 to 12 hours before batching. This is a standard procedure for achieving a near-SSD case and reducing aggregate moisture content variability (Craig and Wolfe 2012). During the construction of the Hibernia platform, a similar strategy was used, as recommended by (Hoff and Elimov 1995). The fine aggregate was oven dried for 24 hours at 110 ± 5 C^o before being mixed. To obtain SSD state, normal weight aggregates

were saturated with a certain amount of water-based on the absorption ratio for a suitable period. The aggregates and cement were added to the mixer initially during batching. To mix these dry components, the mixer was turned on for 30 seconds. Fibers were added while dry mixing. The AEA was then added to half of the batch water and blended for 2 minutes in the mixer. The SP was added to the remaining half of the water and stirred for another 3 minutes. A little amount of water was saved for subsequent use. The batch was visually inspected to determine its consistency. If the needed consistency was not achieved, an additional amount of SP was added to the remaining portion of water, added to the mixer, and stirred for another minute. The batch was tested for slump and air content after visually obtaining the required consistency. The cylinders and prisms were trowel-finished after being compacted with a mechanical vibrating table. The samples were demolded, labeled, and stored in a curing room at a temperature of 25 ± 1.5 C^o and 100 percent relative humidity until the testing day. All of the mixtures were poured into 100 liters volume.

4.3.4. Testing procedures

4.3.4.1. Fresh and mechanical properties tests

The workability of the concrete mixes and the percentage of air content were tested in accordance with ("ASTM C143" 2020) and ("ASTM C231" 2022), respectively. The characteristics of hardened concrete were evaluated after 14 and 28 days. On three similar cylinders, compressive strength according to ("ASTM C39" 2021), STS according to ("ASTM C496" 2017), and SME according to ("ASTM C469" 2022) were measured. Furthermore, three identical prisms were tested to assess the FS with third point loading in

accordance with (“ASTM C78” 2022). The DME was calculated by measuring the fundamental longitudinal resonance frequency of three concrete prisms in accordance with (“ASTM C215” 2019).

4.3.4.2. Abrasion resistance tests

The proposed concrete mixes' abrasion resistance was tested using two ASTM standard tests, which are as follows:

4.3.4.2.1. The rotating-cutters method, ASTM C944: Figure 4-4 depicts the test setup. It is meticulously built to satisfy the ASTM C944 requirements. The guidelines address the loading, number of revolutions per minute (RPM), testing duration, cutter dimensions, and replacement intervals for washers and dressing wheels. As the abrasion device, a conventional drill press was adapted. The spring tied to the spindle was removed. On the drill press, a U-shaped extension capable of bearing the auxiliary load directly on the spindle was built and installed. The extension's function was to keep the load constant during testing and to reduce any vibrating motion that may affect the abrasion mechanism. For six minutes, the test was run at a constant speed of 200 RPM (clockwise) with a constant weight of 19.7 kg total. This testing set was intended to create expressive abrasion damage within the ASTM procedure restrictions. The revolving cutters had an overall diameter of 82.5 mm and were made up of 20 dressing wheels and 22 washers. Dressing wheels and washers were replaced every 60 minutes to reduce variance between tested samples caused by rotating cutter erosion. The abrasion test was carried out on three formwork neighboring surfaces of different 100 mm cubes precisely cut from various prisms. Following the testing of the samples, the surface was cleaned of any residual dirt

with compressed air. ASTM recommends testing the abraded mass loss to determine the abrasion resistance of concrete. When evaluating concrete with a considerable difference in density, it is essential to compare the abrasion depth rather than the abraded mass loss. In level 1 of the experimental investigation (chapter 2), as there was a comparison between the HPSDC with a normal weight concrete and lightweight aggregate concrete, that have a significant difference in density, abrasion depth was measured instead of the abraded mass loss. The current study follows the same approach. The abrasion depth was calculated using Eq. 2-14 which was developed in chapter 2 with the help of the laser scanning technique as shown in Fig. 4-5, which shows a typical laser-scanned sample.

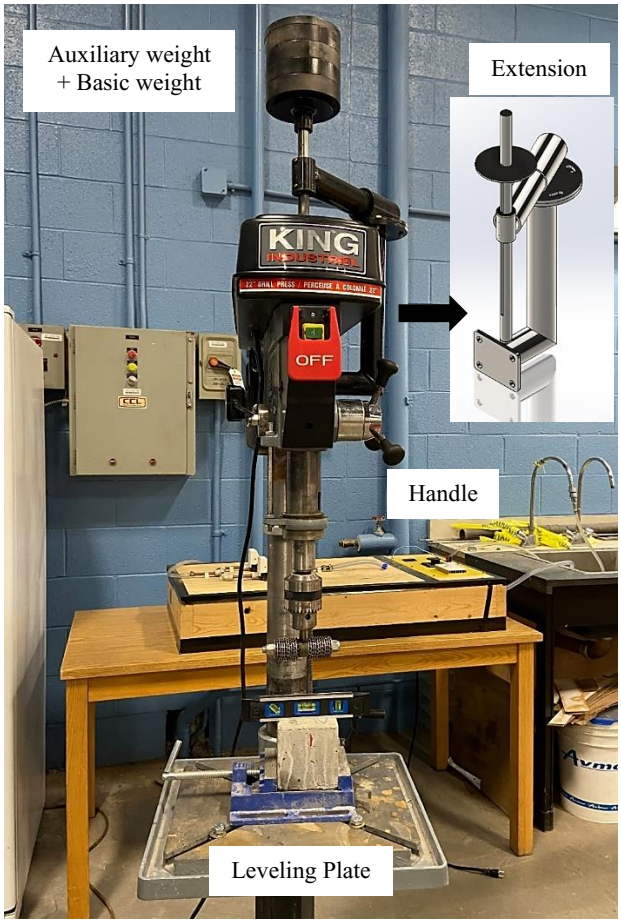

(a) Drill modification.

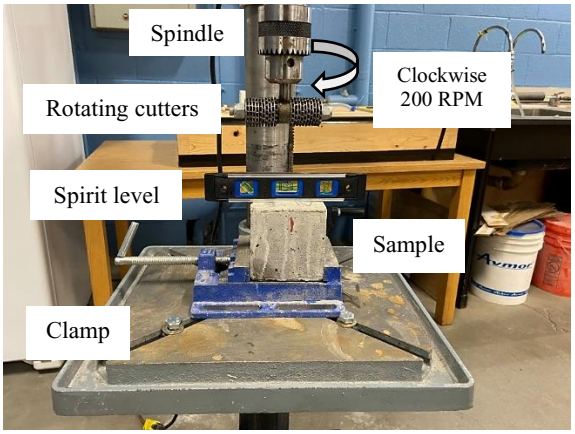

(b) Enlargement of the rotating cutters and the sample.

(c) Enlargement of the rotating cutters.

Fig. 4-4 ASTM C944, rotating cutters test.

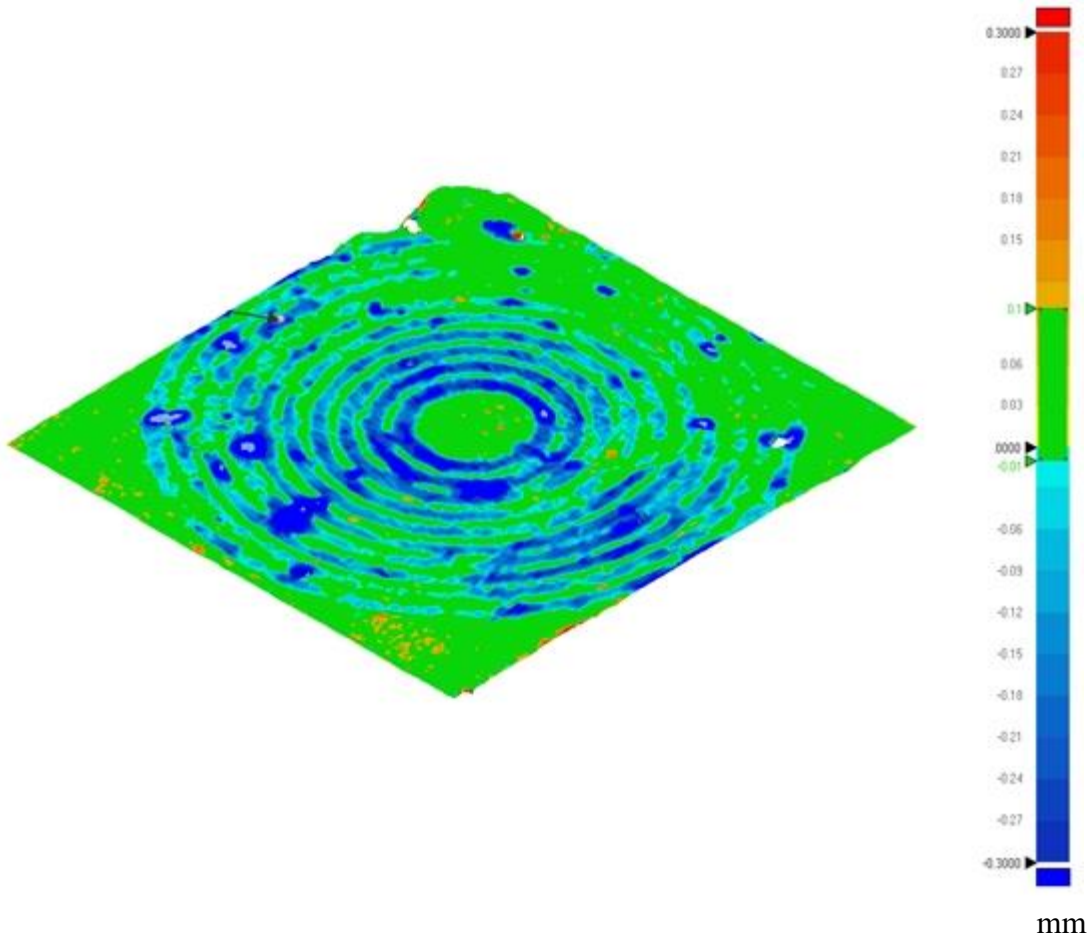

Fig. 4-5 Typical laser scanning of a sample tested using rotating cutters approach.

4.3.4.2.2. ASTM C418, sand blasting test: The test was performed in accordance with ASTM C418. The test arrangement (Fig. 4-6) was meticulously designed to adhere to ASTM C418 guidelines. Because the nozzle shape might impact the wear pattern and therefore the repeatability of the test results, nozzles that adhere to the ASTM precise specifications were created, as shown in Fig. 4-6 (d). The nozzle is 40 mm long and features 45^{o} bevel walls inside at the top end. A clamp was utilized to hold the sample at a set normal distance of 75 mm from the nozzle end. It includes a shield with a 28.7 mm opening. The abrasive employed was silica sand that has been pre-sieved to pass sieve No. 20 but remained on sieve No. 30. The silica sand abrasive was never reused in this research to ensure consistent findings. Before testing, the concrete specimens were submerged for 24 hours. For 1 minute, the specimen's surface was subjected to air-driven abrasive sand at a pressure of 59.5 psi. The test was repeated on eight separate locations across the sample. The volume of the abrasion cavity should be measured using oil-based modelling clay, according to ASTM. However, low abrasion volumes were generally achieved due to the HPSDC's high abrasion resistance. As a result, the cavity volume was estimated using Eq. 4-1 by weighing the sample before and after testing and dividing the mass difference by the concrete density. Eq. 4-2 was then used to determine the abrasion coefficient. Using laser scanning on random samples, the accuracy of this measuring approach was confirmed. Figure 4-7 illustrates a typical laser-scanned sample.

$$V = M / \rho \tag{4-1}$$

Where V is the volume of the abraded cavity, cm^3; M is the abraded mass, gm; and ρ is the concrete density gm / cm^3.

$$A_c = V / A \tag{4-2}$$

Where A_c is the abrasion coefficient, cm^3/cm^2; and A is the abraded surface area

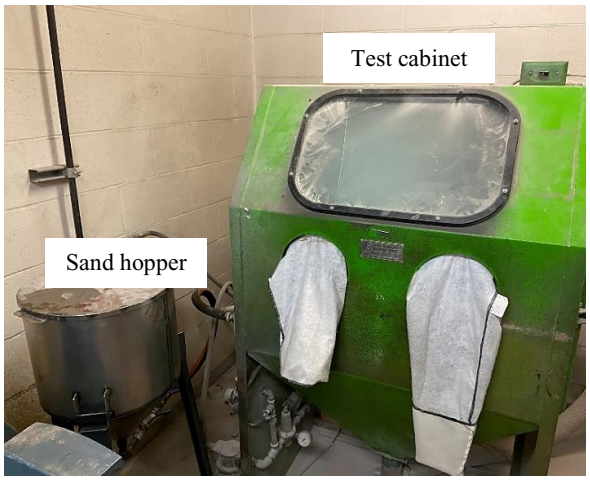

(b) Test cabinet and the sand hopper.

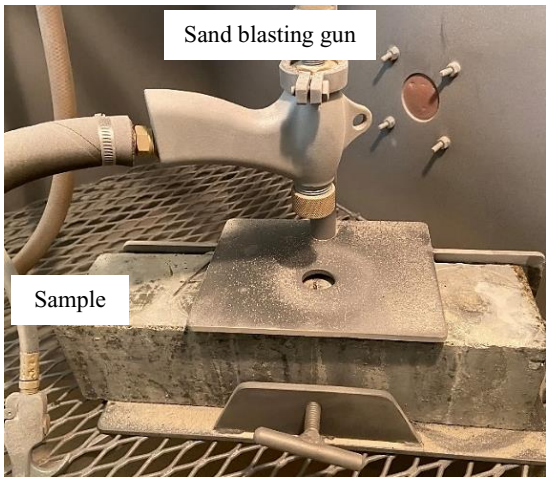

(b) Sand blasting gun

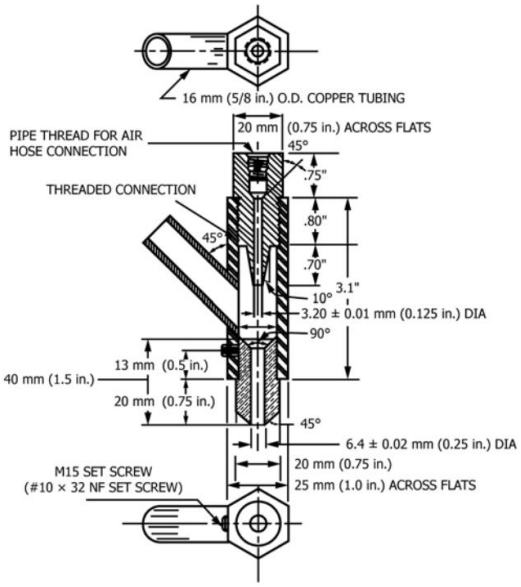

(e) ASTM C418 gun nozzle assembly. (f) Fabricated gun nozzle.

Fig. 4-6 ASTM C418, sand blasting test setup.

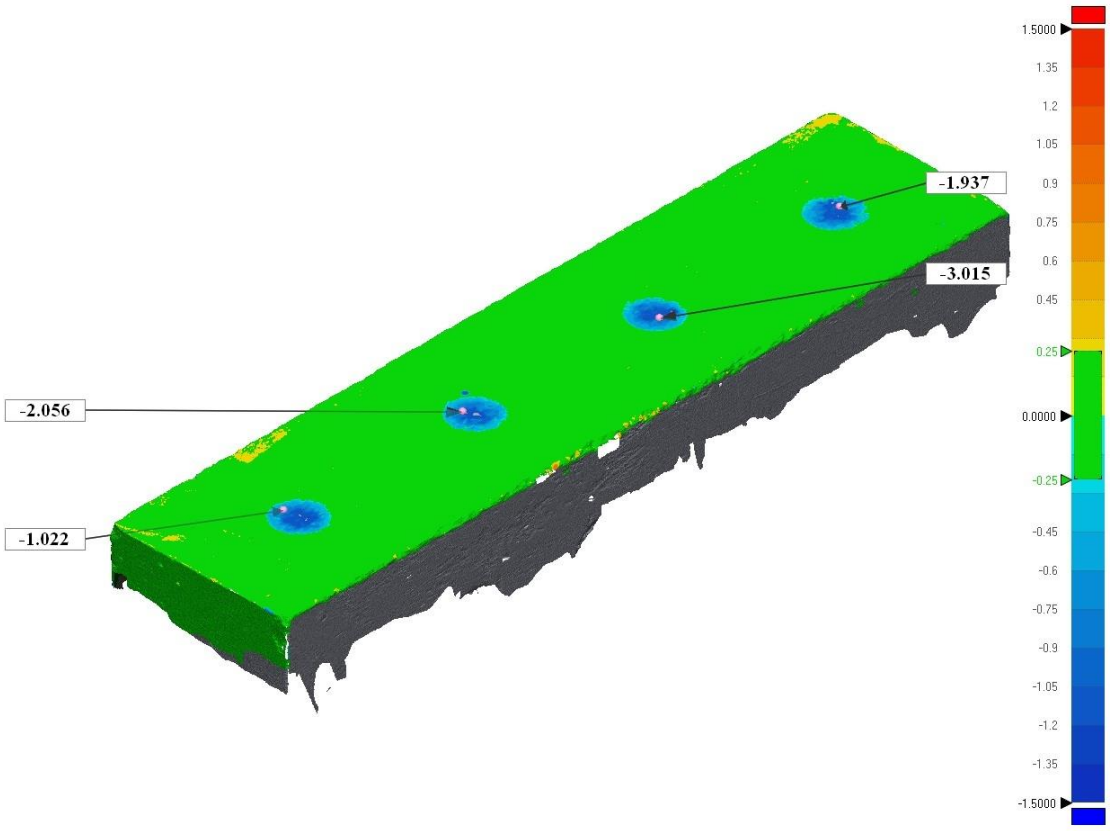

In mm

Figure 4-7 Typical laser scanning of a sample tested using sandblasting approach.

4.4. Results and discussion

4.4.1. Fresh properties

Fig. 4-8 illustrates the fresh concrete mixture with BFs added at the end of mixing. It can be observed that some of the cement particles were still in their powder form. The mixture was rearranged manually to reduce this inhomogeneity as possible. Such a phenomenon implies that BFs have a tendency to prevent the cement powder from engaging with the mixing water. That behavior was also noticed by (Dias and Thaumaturgo 2005).

Fig. 4-8 Fresh mixture incorporating BFs.

In order to achieve the targeted slump of 180 mm to 220 mm, the dosages of the SP were different. Table 4-4 and Fig. 4-9 present the SP demand for the HPSDC made with

different types of fibers at different dosages. The addition of fibers was found to have a negative influence on the HPSDC workability. CCSFs had the highest impact. In that, by the inclusion of 0.5% of CCSFs, the SP dosage used was 50.6% higher than the SP dosage used in the control mixture. While addition of PPFs, BBFs, and FBFs at different ratios was found to have a similar impact on the concrete workability. Thus, the same SP dosages were used for all of them. At a 0.5% addition ratio of these fibers, a 30.1% higher SP dosage was enough to achieve the required workability. On the other hand, the incorporation of fibers did not have a noticeable impact on the HPSDC air content.

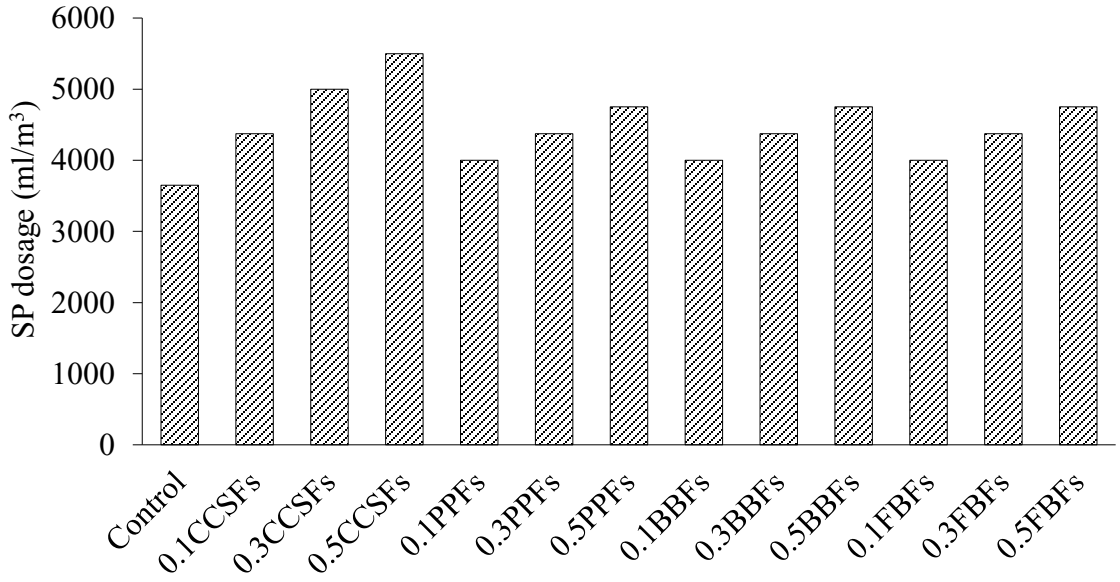

Fig. 4-9 Effect of inclusion of different types of fibers on the SP demand of the HPSDC.

4.4.2. Compressive strength

Table 4-5 and Fig. 4-10 display the 14- and 28-day compressive strength for all the tested mixtures. It can be seen that the incorporation of both CCSFs and PPFs had a positive

effect on the compressive strength of the HPSDC. The compressive strength increased with increasing the content of CCSFs. At 0.5% of CCSFs, compared to the plain concrete mixture, compressive strength reached 16% and 14.6% at the 14-day and 28-day, respectively. Similar to CCSFs, PPFs had a positive effect on the compressive strength. In that, for a 0.1% PPFs incorporation ratio, the HPSDC compressive strength increased by 8% and 6.8%. However, higher PPFs ratios than 0.1% had a similar impact on the compressive strength as the 0.1%. This capability of CCSFs and PPFs to enhance the HPSDC compressive strength is mainly attributed to the bridging action that these fibers provide. In addition, the matrix-aggregate interface may have been improved by the addition of fibers. Which provided the concrete with a higher ability to carry compressive loads. Similar results were stated by (Usman et al. 2020). In that study, the incorporation of steel fibers at 0.5% was able to enhance the compressive strength of the concrete by 9.5%. Similar to the current study, (Jiang et al. 2014) found a similar trend with the incorporation of PPFs. In that study, mixtures showed an increase of 2.41%, 6.13% and 4.32% by the addition of PPFs at 0.05%, 0.1% and 3%, respectively.

Table 4-5 Mechanical properties results for tested mixtures.

Mixture No.	Mixture designation	Compressive strength (MPa)		STS (MPa)		FS (MPa)		SME (GPa)		DME (GPa)	
		14-day	28-day	14-day	28-day	14-day	28-day	14-day	28-day	14-day	28-day
1	Control	76.2	79.0	4.50	4.70	8.40	8.71	36.8	38.9	40.5	41.7
2	0.1CCSFs	80.1	83.2	4.91	5.31	9.42	9.71	36.9	38.7	41.4	43.9
3	0.3CCSFs	84.9	86.4	6.14	6.23	9.93	10.12	39.6	41.1	42.1	44.1
4	0.5CCSFs	88.4	90.5	6.51	6.72	10.20	10.43	39.6	41.1	43.9	45.5
5	0.1PPFs	82.3	84.4	5.15	5.25	8.55	8.99	36.3	39.0	40.9	41.1
6	0.3PPFs	81.2	83.1	5.44	5.99	8.61	9.13	36.9	39.1	39.0	40.7
7	0.5PPFs	80.9	83.0	5.91	6.18	9.25	9.58	37.1	38.7	39.8	41.8
8	0.1BBFs	70.1	72.4	5.30	5.41	8.69	8.95	37.4	39.3	40.1	42.6
9	0.3BBFs	65.6	66.6	5.95	6.13	9.22	9.55	38.2	39.1	39.6	41.9
10	0.5BBFs	60.3	63.4	5.52	5.80	8.49	8.85	39.6	41.6	40.91	40.9
11	0.1FBFs	66.6	69.0	5.05	5.33	8.49	8.83	37.2	39.6	41.3	42.0
12	0.3FBFs	63.5	66.0	5.38	5.75	8.60	8.93	39.5	40.6	41.0	42.0
13	0.5FBFs	58.3	61.3	5.89	6.27	9.16	9.42	40.0	41.1	39.9	42.1

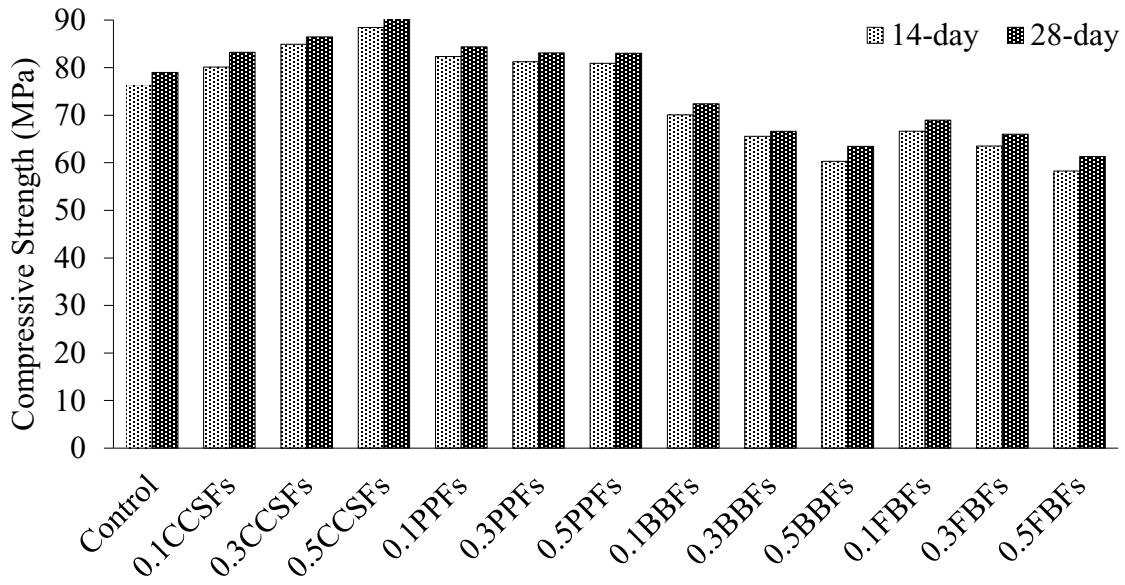

Fig. 4-10 Effect of inclusion of different types of fibers on the compressive strength of the HPSDC.

On the contrary, although BFs possess high tensile strength and higher elastic modulus compared to the surrounding matrix, their incorporation had a negative impact on the HPSDC compressive strength. As can be seen, the reduction was proportional to the BFs volumetric fraction added. By comparing 0.5BBFs mixture to the control mixture, reductions that reached 20.9% and 19.7% at the 14-day and 28-day, respectively, were attained. Similarly, by comparing 0.5FBFs mixture to the control mixture, the reduction attained 23.5% and 22.4% at the 14-day and 28-day, respectively. This behavior is attributed to, as mentioned before, the BFs' tendency to exile the cement powder during mixing. As cement is the main engine for strength enhancement, that action decreased the cement's ability to provide higher compressive strength. It is also believed that the illustrated behavior will impact all the tested properties not only the compressive strength,

which will be discussed later. On the other hand, BFs were also observed to tend to bend and ball during mixing. That could lead to the formation of low strength agglomerations inside the concrete matrix that could also reduce the concrete compressive strength. Similar to the current study, (Dias and Thaumaturgo 2005) reported that the inclusion of 0.5% of BFs led to 3.9% less compressive strength at the 28-day. Also, (Jun and Ye 2010) reported decrements in the compressive strength with increasing the basalt fiber content.

Fig. 4-11 shows the specimens' failure patterns under compression testing. Plain concrete failure was sudden, explosive, and associated with much spalling. However, fibers incorporated mixtures remained their cylindrical appearance after failure. It had little to no spalling which indicates a more ductile failure. That implies the ability of fibers to enhance the ductility performance of the concrete prior to complete failure. However, as can be seen in Fig. 4-11, the two types of BFs were less effective in restraining concrete spalling.

(a) Plain concrete typical specimen

(b) CCSFs incorporated typical specimen

(c) PPFs incorporated typical specimen

(d) BBFs incorporated typical specimen

(e) FBFs incorporated typical specimen

Fig. 4-11 Typical specimens failure patterns under compression testing.

4.4.3. Tensile properties

Table 4-5, Fig. 4-12 and Fig. 4-13 demonstrate the 14- and 28-day STS and FS for all the tested mixtures. In the case of CCSFs and PPFs, the tensile properties enhancements were relative to the number of fibers added. In that, the enhancements reached their peak at a 0.5% inclusion ratio. The addition of CCSFs at 0.5% enhanced the STS by 44.7% and 43% at the 14-day and 28-day, respectively, and increased the FS by 21.4% and 19.7% at the 14-day and 28-day, respectively. That is mainly due to the well-known ability of CCSFs to restrain cracks propagation leading to higher peak load. Incorporation of PPFs at 0.5% enhanced the STS by 31.3% and 31.5% at the 14-day and 28-day, respectively, and increased the FS by 10.1% and 10% at the 14-day and 28-day, respectively. However, due to the lower tensile strength of PPFs compared to CCSFs, CCSFs were able to restrain crack initiation to a higher level and consequently were more effective to enhance the HPSDC tensile properties. Similar results were found by (Song and Hwang 2004). In which, a significant flexural strength increase was detected by the inclusion of steel fiber. (Yurtseven, Yaman, and Tokyay 2006) found an enhancement in the STS of 19.5% by the inclusion of 0.5% of PPFs. While (Sivakumar and Santhanam 2007) reported an increase of 7.6% in the flexural capacity of concrete by adding PPFs at only 0.6 kg/m3.

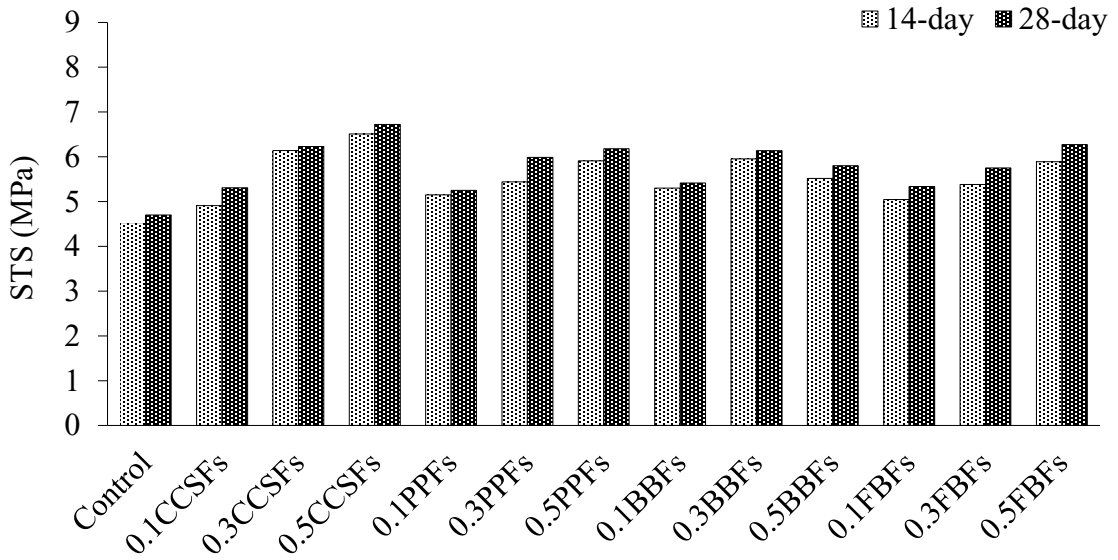

Fig. 4-12 Effect of inclusion of different types of fibers on the STS of the HPSDC.

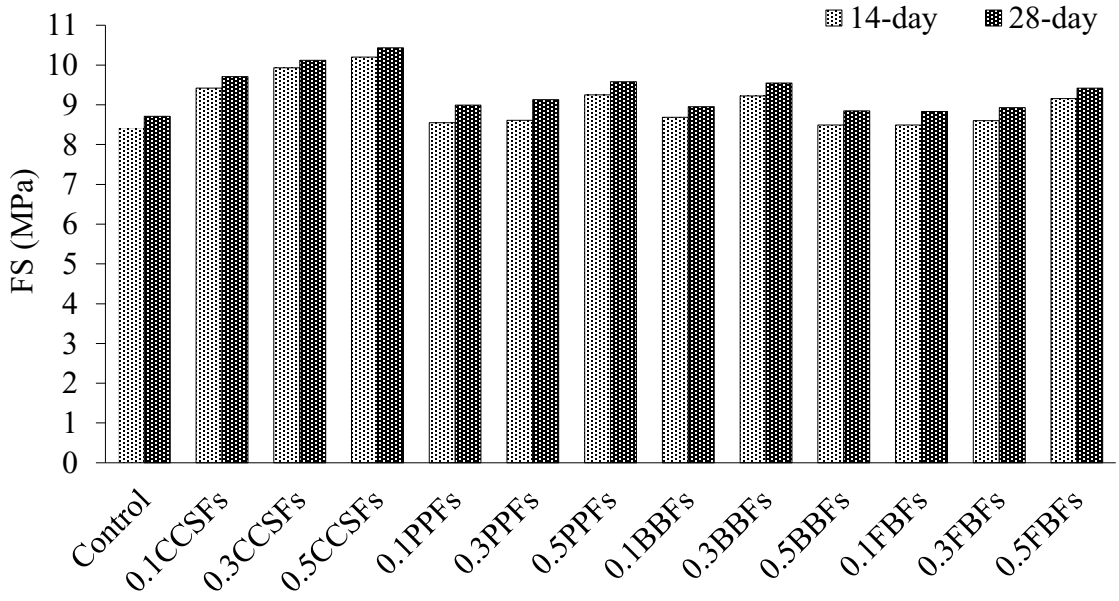

Fig. 4-13 Effect of inclusion of different types of fibers on the FS of the HPSDC.

Similarly, incorporation of BBFs positively affected the HPSDC tensile properties. In that, at 0.3% incorporation ratio, the STS was increased by 32.5% and 30.5% at the 14-day and 28-day, respectively, and the FS was enhanced by 9.8% and 9.6% at the 14-day

and 28-day, respectively. However, 0.5% incorporation ratio of BBFs were less effective compared to 0.3%. Which may be attributed to that, as the developed HPSDC has a high coarse to fine aggregate ratio of 1.6, dispersion of BBFs could not be achieved easily which was harmful for the development of strength. However, such action may be different for other types of concretes and higher incorporation ratios above 0.3% of BBFs may be applicable. (Jun and Ye 2010) found a similar trend. In that, BFs at 0.3% were the optimum ratio with regard to FS and STS. On the other hand, similar to CCSFs and PPFs, 0.5% of FBFs were the most effective ratio. In that 0.5% of FBFs enhanced the STS of the HPSDC by 30.9% and 33.4% at the 14-day and 28-day, respectively, and increased its FS by 9% and 8.1% at the 14-day and 28-day, respectively. These results are in agreement with (Katkhuda and Shatarat 2017). In that study, FBFs were incorporated in concrete made with three types of aggregate. At 0.5% of FBFs, FS was increased by 34%, 27%, and 32.8% for concrete made with natural aggregate, treated recycled concrete aggregate and untreated recycled concrete aggregate, respectively.

It can be seen that 0.5% of PPFs, 0.3% of BBFs, and 0.5% of BBFs had almost similar impacts on the tensile properties of the HPSDC. However, they were only as effective as 0.3% of CCSFs on the STS or 0.3% of CCSFs on the FS. The limited capability of both types of BFs to enhance the HPSDC tensile properties, compared to the CCSFs, may be attributed to the tendency of BFs to bend and ball during mixing as mentioned earlier. That consequently reduced the probability of the existence of fibers oriented in a manner that will restrain cracks. As only the fibers that are parallel (or have a parallel component) to the tensile stress trajectories have a role in controlling the possible cracks.

Fig. 4-14 shows the load-mid span deflection curves for plain concrete and the mixtures with optimum ratios of fibers (0.5% of CCSFs, 0.5% of PPFs, 0.3% of BBFs, and 0.5% of FBFs). It can be seen that, as mentioned before, that the inclusion of fibers increased the load-carrying capacity of the concrete under flexure. Furthermore, in terms of deformability, CCSFs and PPFs specimens failed at higher ultimate deflection. CCSFs and PPFs incorporated specimens at 0.5% exhibited higher ultimate deflections by an average of 18.9% and 19.4%, respectively, compared to the fiber-less specimens at the 28 days. However, as can be seen, both types of BFs provided s slight enhancement to the HPSDC deformability before failure. BBFs and FBFs incorporated specimens at 0.5% exhibited higher ultimate deflections by an average of 6.9% and 4%, respectively, compared to fiber-less specimen at the 28 days. That also means higher toughness (energy absorbing capability) for the fibers incorporated mixtures. On the other hand, it can be seen that, for all types of fibers used, the slope of the stress-strain curve did not change noticeably compared to plain concrete. This would suggest the limited impact of fibers on the concrete modulus of elasticity. However, this will be assured later using the direct tests for the stiffness properties. On the other hand, it can be noticed that none of the incorporated fibers provided enhancement to the post-cracking behavior of the concrete. The specimens showed no ability to carry more load beyond the first crack. This is mainly due to the relatively low volume of fiber added which is below the critical volume of fibers (critical volume is defined by (Beaudoin 1990) as the minimum fiber content required for the concrete to sustain load after fracture).

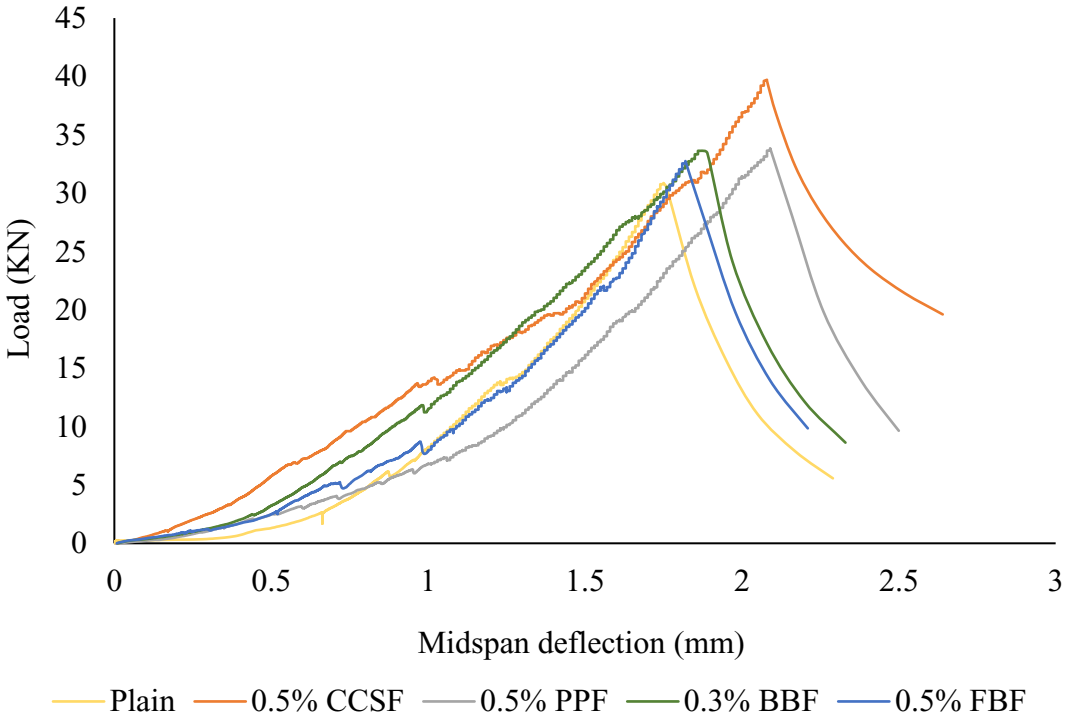

Fig. 4-14 Load-midspan deflection curves for specimens under flexural testing

Fig. 4-15 shows the failure mode of specimens under flexure. Fiber-less concrete reached the ultimate load after which it was broken in a brittle manner. In contrast, CCSFs did not fully split after cracking. CCSFs were noticed across the cracks after failure which implies a pull-out failure, as shown in Fig. 4-15 (b-2). This is an advantage for the CCSFs incorporated concrete because it is gradual and (Ramakrishnan, Tolmare, and Brik 1998). This failure mode is attributed to the higher CCSFs tensile strength compared to their bond strength with the surrounding matrix. On the contrary, PPFs were not observed across the cracks after complete failure. These specimens failed in the same brittle manner as the fiber-less specimens. This may be due to the low tensile strength of the PPFs compared to their fiber-matrix bond. Thus PPFs failure was governed by fibers rupture. Surprisingly,

although the extensive tensile capacity of BFs, the BFs incorporated specimens disintegrated simultaneously with the formation of the first crack under flexure. Both types of BFs, even at the highest dosages, were also not visible across the cracks of the failed cross-section. That indicated fibers rupture failure instead of fibers pull-out failure. Such response was observed by (Branston et al. 2016) as well. In that study, it was found, using a scanning electron microscope, that cement hydration products had penetrated in-between the BFs filaments. Also, the HPSDC used in the current study has a high content of reactive cement replacements (metakaolin and silica fume) that can strengthen the matrix. That in turn could increase the fiber-bond strength. In addition, as mentioned that the BFs tend to bend and deform while mixing, and deformed fibers possess more bond strength with the matrix compared to straight fibers. These actions contributed to enhancing the fiber-matrix bond beyond the BFs tensile strength. Consequently, BFs failure was brittle, sudden, and governed by fiber rupture.

(1) Specimen failure (2) Enlargement of the produced crack

(a) Fiber-less typical specimen

(1) Specimen failure (2) Enlargement of the produced crack

(b) CCSFs incorporated typical specimen

(1) Specimen failure (2) Enlargement of the produced crack

(c) PPFs, BBFs, and FBFs incorporated typical specimen

Fig. 4-15 Typical specimens failure pattern under flexural testing

4.4.4. Stiffness properties

Table 4-5, Fig. 4-16, and Fig. 4-17 demonstrate the stiffness properties (SME and DME) for all the tested mixtures at the 14- and 28-day. The results indicated that the incorporation of CCSFs provided the HPSDC with slightly higher ME. The degree of enhancement was relative to the amount of CCSFs added. By the addition of 0.5% of CCSFs, compared to the fiber-less mixture, the SME increased by 7.7% and 5.7% at the 14-day and 28-day, respectively, and the DME increased by 8.3% and 9% at the 14-day and 28-day, respectively. This is mainly due to the ability of CCSFs to enhance the pre-cracking behavior of the concrete. In that, the relatively high elastic modulus CCSFs (203 GPa) enhanced the modulus of elasticity of the matrix. Also, CCSFs may have provided an interlocking action to the aggregate to some extent, making the propagation of cracks harder to achieve. Which enhanced the overall stiffness of the concrete. (Shallal and Al-Owaisy 2007) found similar results. In that study, by incorporating of 0.5% of steel fibers, only a 6% higher modulus of elasticity was attained.

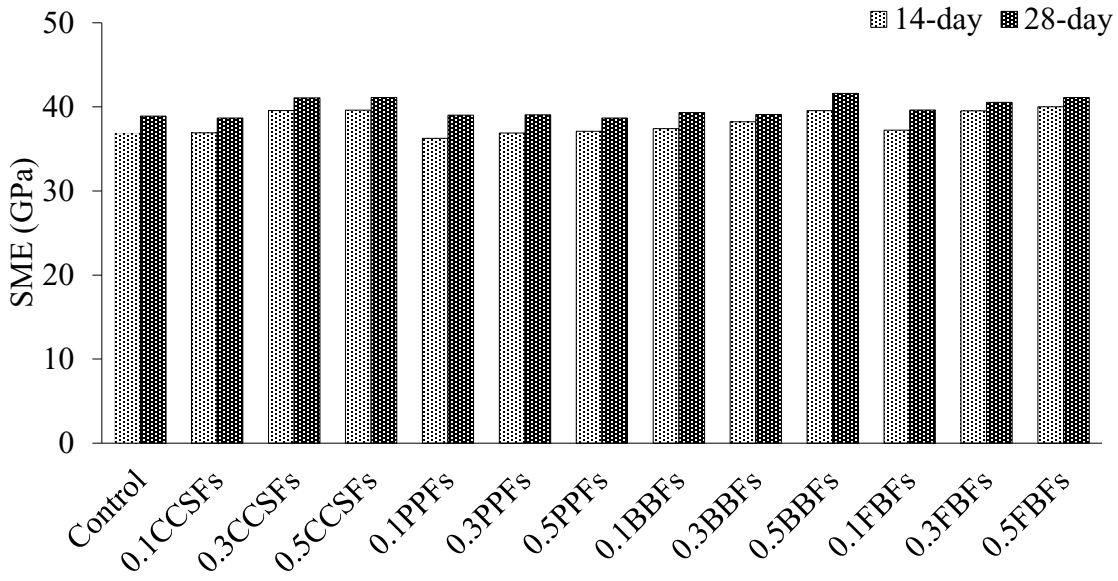

Fig. 4-16 Effect of inclusion of different types of fibers on the SME of the HPSDC.

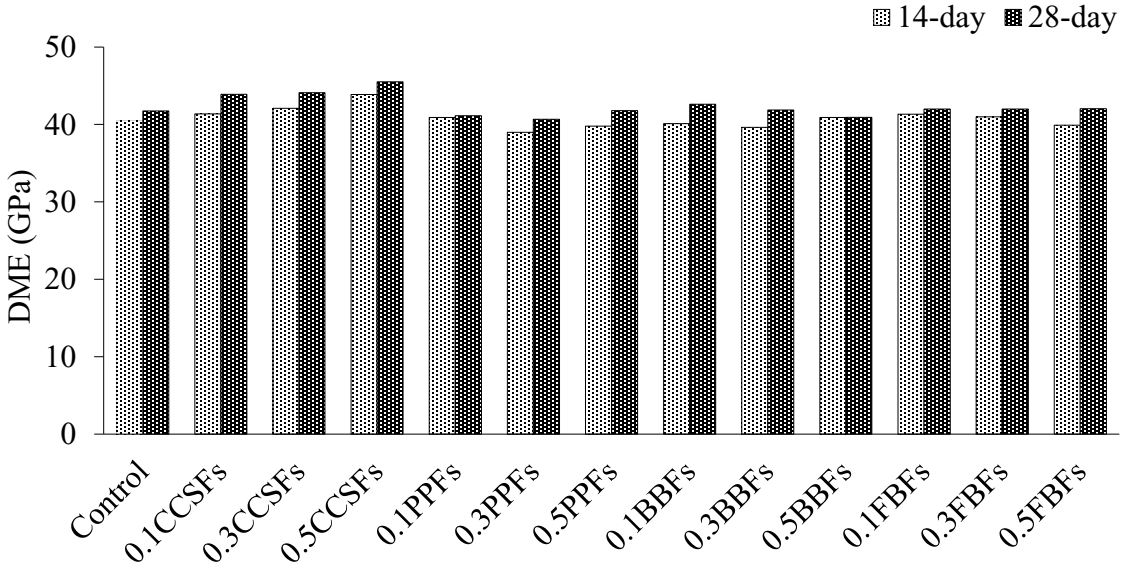

Fig. 4-17 Effect of inclusion of different types of fibers on the DME of the HPSDC.

On the other hand, although the ability of fibers to restrain and delay cracking, PPFs did not have a noticeable impact on the HPSDC elasticity. This is mainly attributed to the low modulus of elasticity (14.7 GPa) of the PPFs. Under compressive loading, PPFs deform with the surrounding matrix. Thus, not offering an increase in the pre-cracking behavior or matrix stiffness.

Similar to CCSFs, incorporation of both types of BFs had a limited positive effect on the stiffness of the HPSDC. Also, the degree of enhancement was relative to the amount of CCSFs added. The SME increased by 7.5% and 7% by addition of 0.5% of BBFs and increased by 8.8% and 5.7% by addition of 0.5% of FBFs. This is due to the ability of BFs, which possess a relatively higher elastic modulus (86 GPa) compared to the surrounding matrix, to enhance the elasticity of the concrete as mentioned earlier. It can be seen that un-similar to the other tested mechanical properties, adding BBFs at 0.5% was more effective than 0.3% on the SME. However, as BFs have less modulus of elasticity compared to the CCSFs, their impact on the HPSDC stiffness was less. In contrast, no noticeable effect was exhibited on the DME of the HPSDC by incorporation of BFs. Such an ambiguous result may require further future inspection.

4.4.5. Abrasion resistance

Table 4-6, Fig. 4-18, and Fig. 4-19 show the abrasion resistance of the tested mixtures measured using the rotating cutters test method and sandblasting test method. It can be seen that the incorporation of 0.1% of CCSFs did not have a noticeable effect on the HPSDC abrasion resistance under both tests. This may be due to the relatively low

aspect ratio of the CCSFs (65) (aspect ratio of fibers, according to (ACI Comite 544.3R 2008), is the ratio of elemental fiber length over its diameter). That limited the existence of elemental fibers within the abraded portion of the sample at this low ratio. As the number of elemental fibers inside the matrix is a function of the fibers' aspect ratio. It can be noticed that, although the incorporation of CCSFs at 0.1% had a noticeable impact on the HPSDC mechanical properties, it did not have a clear effect on its abrasion resistance. This may be attributed to that; the concrete abrasion resistance is a physical property that is affected only by the surface condition. On the contrary, concrete's mechanical properties are bulk properties and are more sensitive to individual composition changes.

Table 4-6 Abrasion resistance results for the tested mixtures.

Mixture No.	Mixture designation	Rotating cutters method test (ASTM C944) "average abrasion depth" (mm)		Sand blasting test (ASTM C418) "abrasion coefficient" (cm^3/cm^2)
		14-day	28-day	28-day
1	Control	0.417	0.405	0.227
2	0.1CCSFs	0.409	0.395	0.226
3	0.3CCSFs	0.421	0.411	0.204
4	0.5CCSFs	0.321	0.304	0.170
5	0.1PPFs	0.411	0.379	0.215
6	0.3PPFs	0.376	0.357	0.206
7	0.5PPFs	0.351	0.342	0.197
8	0.1BBFs	0.367	0.340	0.205
9	0.3BBFs	0.342	0.322	0.185
10	0.5BBFs	0.351	0.357	0.203
11	0.1FBFs	0.371	0.362	0.209
12	0.3FBFs	0.352	0.346	0.198
13	0.5FBFs	0.349	0.331	0.181

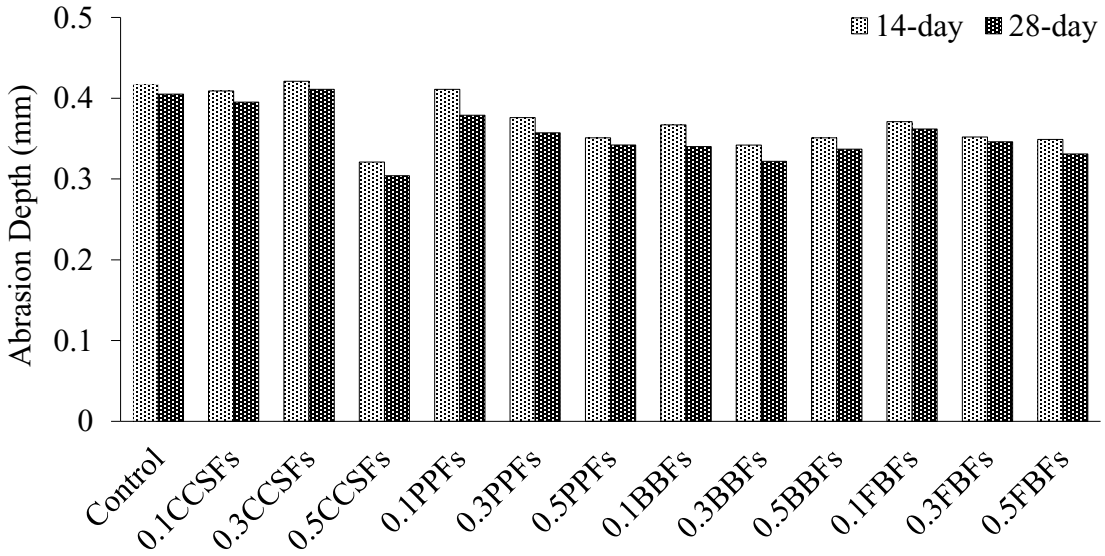

Fig. 4-18 Effect of inclusion of different types of fibers on the abrasion resistance of the HPSDC measured using rotating cutters method.

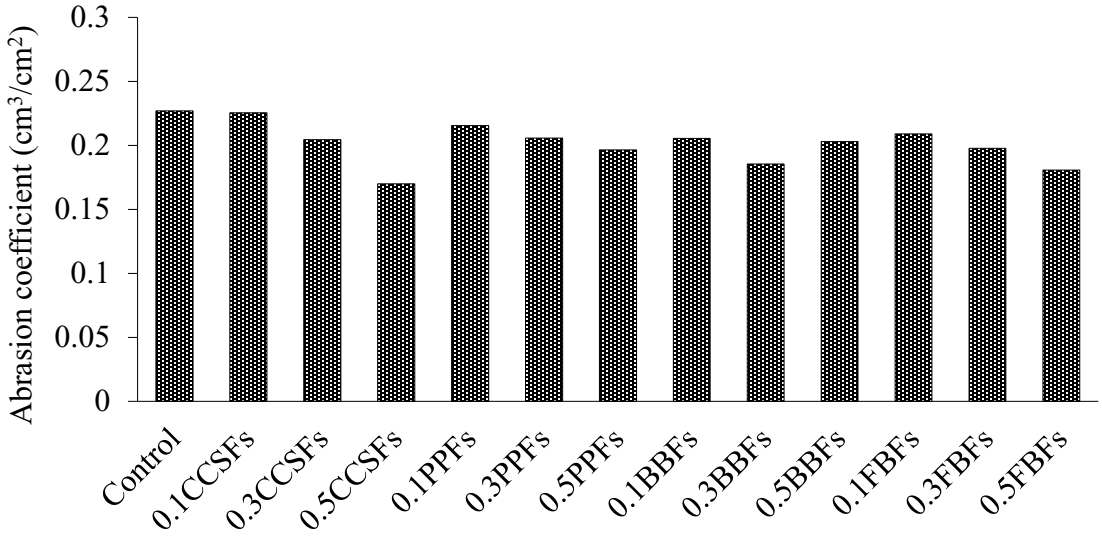

Fig. 4-19 Effect of inclusion of different types of fibers on the abrasion resistance of the HPSDC measured using sandblasting method.

Similarly, incorporation of CCSFs at 0.3% did not have a noticeable effect on the HPSDC abrasion resistance when tested using the rotating cutters method. However, it positively impacted the abrasion resistance tested using the sandblasting method. For instance, the abrasion coefficient decreased by 9.9% at the 28-day. That is mainly due to the presence of some fibers against the abrasive path, that protected the other softer concrete constitutes underneath as abrasion proceeds, as shown in Fig. 4-20. That difference in results between the two abrasion resistance tests is mainly due to the higher penetration depths that the sandblasting test can reach inside the sample compared to the rotating cutters approach. That increased the probability of the presence of CCSFs which could play a role against the abrasion action. Each abrasion test mimics a distinct abrasion mechanism, which is worth mentioning. The revolving cutters method (ASTM C944)

simulates the abrading of a concrete surface by traffic. The sandblasting technique (ASTM C418), on the other hand, replicates aqueous abrasives.

Fig. 4-20 CCSFs specimen tested area sandblasting method.

At 0.5%, CCSFs provided the HPSDC with higher abrasion resistance. The enhancement ratios under the two abrasion tests. The abrasion depth decreased by 23% and 24.9% at the 14-day and 28-day, respectively. While the abrasion coefficient decreased by 25.1% at the 28-day. Although at 0.5% of CCSFs the results were similar under both tests, it is believed that the mechanism through which CCSFs provided the HPSDC with higher abrasion resistance is different according to each test carried out. The abrasive used in the rotating cutters method is steel dressing wheels that have similar hardness compared to the

CCSFs. Thus the abrasion damage may take place in the fibers itself as well as other concrete constitutes under this testing method. In contrast, the sandblasting method's abrasive is silica sand which has less hardness compared to the CCSFs. In turn, wear of CCSFs under sandblasting approach is less possible. In addition, fibers have a different level of ability to affect the concrete abrasion resistance according to their orientation. When testing using the rotating cutters method, both fibers that are presented horizontally, inclined manner or in vertical manner play a role to enhance the abrasion resistance. Horizontal CCSFs could prevent the rotating cutters from penetrating further inside the sample which helped protect the concrete's softer parts underneath. While inclined fibers would create areas at which the rotating cutter would not be able to reach. These areas were noticed also by (Horszczaruk 2009). In that study, these areas were called "shadow zones" and illustrated in Fig. 4-21. Vertically oriented fibers created shadow zones as well. However, after repeated cycles of abrasion, they were bent and acted as inclined fibers then acted as horizontal fibers. On the other hand, regarding sandblasting approach, due to the vertical flow of abrasive impinging the surface, it is believed that only the horizontal fibers or the horizontal component of the CCSFs played a role in the abrasion process, as it protected the other concrete constitutes as mentioned earlier.

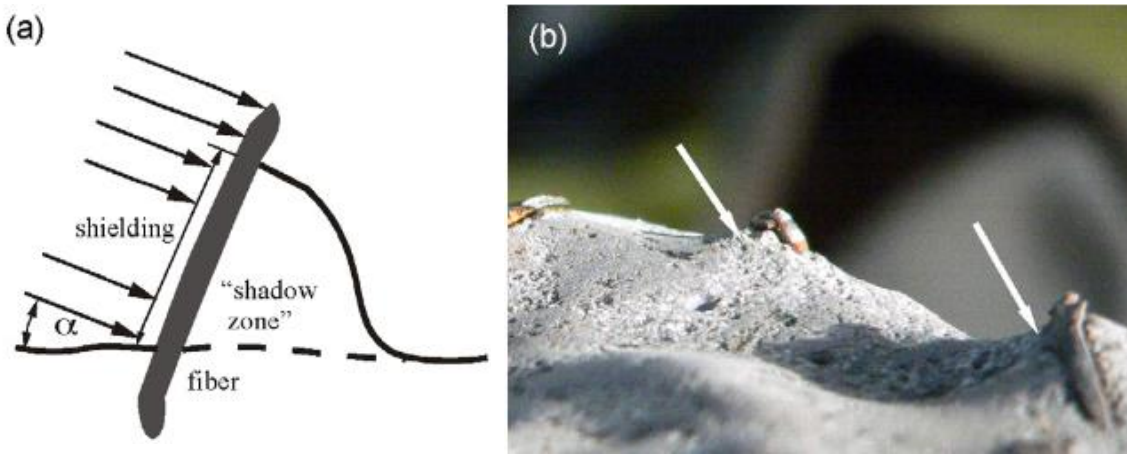

Fig. 4-21 Formed shadow zone in steel fiber reinforced concrete (Horszczaruk 2009): (a) Schematic figure of formed shadow (b) image of the shadow zone formed.

The performance of steel fibers against abrasion damage was assessed by (Horszczaruk 2009) and only marginal effect was reported. On the contrary, (Cheng et al. 2014) found enhancements in the concrete abrasion resistance with the incorporation of steel fibers. The results revealed that, unlike CCSFs, all ratios of PPFs were effective in providing an enhancement to the HPSDC abrasion resistance. This is due to the higher aspect ratio of PPFs (316) compared to CCSFs (65). That provided it with a higher probability to exist within the sample's abraded depth even at low ratios. At 0.5% of PPFs, the abrasion depth reductions, measured using the rotating cutters method, reached 15.8% and 15.6% at the 14-day and 28-day, respectively, compared to the control mixture. That enhancement is attributed to the capability of PPFs filaments to hold the particles over their surface which helps reduce spalling of these particles. However, at 0.5%, CCSFs provided the HPSDC with higher abrasion resistance compared to the PPFs. This is maybe due to the behavior of each type of fiber as the abrasion process took place. In that, CCSFs were

not found to hold the particles across their surface which is maybe due to their low surface area. Instead, it protected the surface in another manner according to their orientation inside the sample as mentioned earlier. The horizontally oriented CCSFs were able to prevent further penetration in the sample to some extent. In contrast, horizontally PPFs which possess less shear strength had limited capability to do the same. Instead, PPFs were found to be fatigued under repeated cycles of shearing stresses from the movement of wheels across the sample's surface. On the other hand, as mentioned before, vertical and inclined CCSFs created shadow zones. On the contrary, PPFs are flabbier (low bending strength) which limited their ability to do a similar behavior.

Under sandblasting test, PPFs at 0.5% were less effective compared to 0.5% of CCSFs. In that, at 0.5% of PPFs, the abrasion coefficient decreased by 13.4% at the 28-day. It is believed that PPFs helped enhance the abrasion resistance of concrete in a way that is different from CCSFs under sandblasting test. In this test, the bonding strength between the matrix and incorporated fibers is tested in a higher manner. The poor bond of CCSFs was primarily evidenced from the broken samples under the FS test and was assured by visually inspecting the CCSFs incorporated samples after abrasion using the sandblasting approach. It was noticed, that the CCSFs elemental fibers were delaminated under the influence of the significant energy of the driven silica sand. Fig. 4-22 shows an elemental CCSF nearly delaminated. Once sufficient surrounding mortar around the elemental fiber was gone, the single fibers were dislodged and blown away. That delamination of a whole fiber due to de-bonding may affect the overall volume loss. However, CCSFs had an advantage over PPFs under this test. This may be due to, as

mentioned earlier, the silica sand that is used as abrasive under sandblasting test method has less hardness compared to the CCSFs, yet higher hardness compared to PPFs. That affected the abrasion resistance. In that, this abrasive can abrade the PPFs themselves, but it was unable to abrade the CCSFs. Eventually, CCSFs were more effective in providing higher abrasion resistance under sandblasting test approach.

Fig. 4-22 Elemental CCSF nearly delaminated under sandblasting abrasion test.

The attained results are in agreement with (Mahdi, Shamkhi, and Abid 2017). In that study a decrement in the abrasion rate was detected with increasing the PPFs content. (Grdic et al. 2012) used two types of micro synthetic PPFs incorporated in normal strength concrete with three different water to cement ratios (0.5-0.7). In that study, by adding PPFs at 0.1%, it was found that the abrasion resistance increased by 7.08% to 14.71%. (Al-

mashhadani et al. 2018) investigated the effect of PPFs addition at a higher dosage of 1.2% in high strength concrete as per ("ASTM C944" 2019) and found a large improvement ranging from 78% to 85.3%.

The results of the rotating cutters test method showed that both types of BFs were able to provide the HPSDC with higher abrasion resistance as well. The optimum incorporation ratio against abrasion of BBFs was 0.3%. While for FBFs, optimum performance was found at 0.5%. In that, 0.3% of BBFs had less abrasion depth by 18% and 20.5% at the 14-day and 28-day, respectively, compared to the control mixture. While 0.5% of FBFs had less abrasion depth by 16.3% and 18.3% at the 14-day and 28-day, respectively, compared to the control mixture.

Under the rotating cutters method, it is believed that BBFs had a similar behavior compared to the CCSFs. They protected according to their orientation inside the sample. However, at 0.5%, CCSFs were more effective. This is maybe due to the higher bending strength and shear strength that the CCSFs possesses compared to the BBFs. On the contrary, FBFs had a behavior that is similar to PPFs. It held the particles over its surface which reduced spalling of these particles easily. However, by comparing FBFs to the PPFs at 0.5%, it can be seen that FBFs were more effective. This is maybe due to the higher shear strength of the FBFs which enabled them to sustain more shear stress under repeated cycles of wearing action. However, FBFs were also found fractured at the end of testing. Also, it can be noticed that BBFs were slightly more effective on the HPSDC abrasion resistance compared to FBFs. That is maybe due to the higher bending and shear strength of the BBFs compared to FBFs.

The results of the sandblasting test method were similar to the rotating cutters test method. Both types of BFs were effective and reached their peak at 0.3% of BBFs and 0.5% of FBFs. 0.3% of BBFs had less abrasion coefficient by 18.3% at the 28-day, compared to the control mixture while 0.5% of FBFs had less abrasion coefficient by 12.9% at the 28-day, compared to the control mixture. It can be seen that both types of BFs had a similar impact on abrasion resistance as CCSFs and PPFs. It also can be seen that, similar to the rotating cutters method, both types of BFs at optimum dosages had a moderate enhancement that was less than the CCSFs but higher than PPFs. That is attributed to the moderate hardness of basalt which is higher than PPFs but less than steel. Yet, BFs hardness is less than the hardness of the abrasive of sandblasting test method (silica sand). Thus, BFs did not provide full protection to the other parts underneath as the CCSFs. On the other hand, it can be noticed that FBFs were slightly more effective compared to BBFs under sandblasting testing approach. This is maybe due to the better dispersion of the FBFs inside the mixture.

In summary, the results revealed that the capability of fibers to provide an enhancement to concrete abrasion resistance depends on the mechanism of the test carried out and the fibers' properties. Each test method is affected by certain fibers properties. The rotating cutters method was found to be more affected by the shear strength and bending strength of the fibers. It is believed that under this kind of test, all fibers' orientations (vertical, inclined, and horizontal) play a role against wear damage. However, under sandblasting test method, it was found that the capability of fibers to provide abrasion resistance enhancements is related to fibers dispersion, bond strength with the surrounding

matrix, and fibers hardness. Under this test, only inclined and horizontally oriented fibers are believed to have an impact on the abrasion resistance of the concrete. In fact, fibers' tensile strength, which is the main fibers' mechanical property, was not found to have a direct impact on the concrete abrasion resistance under both of these tests. For the tested types of fibers, as CCSFs possessed the highest shear strength, bending strength and hardness, they were the most effective type of fibers on the HPSDC abrasion resistance. Even though its relatively low dispersion ability which affected its effectiveness at 0.1% and 0.3%, they were the most effective type at a 0.5% inclusion ratio.

4.5. Conclusions

This study assessed the impact of addition of different types of fibers on the mechanical properties and the abrasion resistance of the HPSDC. Four types of fibers (CCSFs, PPFs, BBFs, and FBFs) at different ratios (0.1%, 0.3%, 0.5%) were added. The mechanical properties were evaluated according to ASTM standards for compressive strength, STS, FS, SME, and DME. The abrasion resistance was evaluated using two different ASTM tests: The rotating cutters method as per C944 and sandblasting method as per C418. Based on the experimental results, the following conclusions were found:

1. Addition of BFs negatively impacted the homogeneity of the fresh mixture. Incorporating different types of fibers required higher SP demand. CCSFs had the highest impact with higher SP demand reaching 50.6% at 0.5% of CCSFs. While the addition of PPFs, BBFs, and FBFs at different ratios was found to have a similar effect on the SP dosages needed.

2. Using CCSFs at different ratios in the HPSDC increased the compressive strength compared to the control mixture. The higher the ratio of the CCSFs, the higher was the compressive strength of the HPSDC. A slight increase in the compressive strength was also detected with the addition of PPFs. On the contrary, for both types of BFs, a noticeable decrease that is relative to the number of fibers added was detected.

3. CCSFs had the ability to enhance the STS and FS of the HPSDC to a high extent. In addition, high deformability of the CCSFs incorporated specimens was detected. Failure of CCSFs incorporated specimens under flexure was governed by fibers pull-out. Also, PPFs were able to enhance the tensile properties of the HPSDC, but to a less extent compared to the CCSFs. In contrast, PPFs did not increase the HPSDC flexural deformability and the specimens' failure was governed by fibers rupture.

4. BBFs were able to enhance the tensile properties of the HPSDC up to 0.3% addition ratio, but due to poor dispersion, 0.5% of BBFs were not effective. Using FBFs had the ability to improve the tensile properties of the HPSDC up to 0.5%. Similar to PPFs, both types of BFs did not enhance the HPSDC flexural deformability and the specimens' failure was governed by fibers rupture.

5. Incorporation of CCSFs, BBFs, and FBFs positively affected the stiffness of the HPSDC to a limited extent. The degree of enhancement was relative to the number of fibers added. In contrast, PPFs did not have a noticeable effect on the HPSDC stiffness properties.

6. Incorporation of 0.1% of CCSFs did not affect the abrasion resistance of the HPSDC measured using the two abrasion test approaches. However, the incorporation of

0.3% of CCSFs decreased the abrasion coefficient measured using the sandblasting method but did not have an impact on the abrasion resistance measured using the rotating cutters method. However, at 0.5% of CCSFs, HPSDC abrasion resistance using the two abrasion testing methods was noticeably improved.

7. PPFs provided the HPSDC with enhanced abrasion resistance and their effectiveness was relative to the dosage of PPFs added. However, by comparing 0.5% of PPFs with 0.5% of CCSFs, PPFs were less effective under both of the abrasion tests carried out.

8. Both types of BFs were positively effective on the HPSDC abrasion resistance. The optimum ratio for BBFs was found to be 0.3%, while optimum performance against abrasion action for FBFs was found at 0.5%. Compared to PPFs, both types of BFs were more effective on the HPSDC abrasion resistance. Under the rotating cutters testing method, BBFs were more effective than

9. FBFs. However, they were less effective than CCSFs. Under sandblasting testing approach, FBFs were more effective than BBFs, yet less effective than CCSFs.

10. In general, CCSFs at 0.5% was found to be the most effective fibers addition to developing HPSDC with improved mechanical properties and abrasion resistance.

4.6. References

"ACI 318-14." 2014. Building Code Requirements for Structural Concrete (ACI 318-14). American Concrete Institute.

ACI Committee 544.3R. 2008. "Guide for Specifying, Proportioning , and Production of Fiber-Reinforced Concrete," 16.

Al-mashhadani, Mukhallad M, Orhan Canpolat, Yurdakul Aygörmez, Mucteba Uysal, and Savaş Erdem. 2018. "Mechanical and Microstructural Characterization of Fiber Reinforced Fly Ash Based Geopolymer Composites." Construction and Building Materials 167: 505–13. https://doi.org/https://doi.org/10.1016/j.conbuildmat.2018.02.061.

"ASTM C1017." 2013. Standard Specification for Chemical Admixtures for Use in Producing Flowing Concrete.

"ASTM C1138." 2019. Standard Test Method for Abrasion Resistance of Concrete (Underwater Method). 2019. https://doi.org/10.1520/C1138M-19.

"ASTM C1240." 2020. Standard Specification for Silica Fume Used in Cementitious Mixtures. https://doi.org/10.1520/C1240-20.

"ASTM C143." 2020. Standard Test Method for Slump of Hydraulic-Cement Concrete. https://doi.org/10.1520/C0143_C0143M-20.

"ASTM C150." 2022. Standard Specification for Portland Cement. https://doi.org/10.1520/C0150_C0150M-22.

"ASTM C215." 2019. Standard Test Method for Fundamental Transverse, Longitudinal, and Torsional Resonant Frequencies of Concrete Specimens. https://doi.org/10.1520/C0215-19.

"ASTM C231." 2022. Standard Test Method for Air Content of Freshly Mixed Concrete by the Pressure Method. 2022. https://doi.org/10.1520/C0231_C0231M-22.

"ASTM C260." 2016. Standard Specification for Air-Entraining Admixtures for Concrete. https://doi.org/10.1520/C0260_C0260M-10AR16.

"ASTM C33." 2018. Standard Specification for Concrete Aggregates. https://doi.org/10.1520/C0033_C0033M-18.

"ASTM C39." 2021. Standard Test Method for Compressive Strength of Cylindrical Concrete Specimens. https://doi.org/10.1520/C0039_C0039M-21.

"ASTM C418." 2020. Standard Test Method for Abrasion Resistance of Concrete by Sandblasting. https://doi.org/10.1520/C0418-20.

"ASTM C469." 2022. Standard Test Method for Static Modulus of Elasticity and Poisson's Ratio of Concrete in Compression. https://doi.org/10.1520/C0469_C0469M-22.

"ASTM C494." 2022. Standard Specification for Chemical Admixtures for Concrete. https://doi.org/10.1520/C0494_C0494M-19E01.

"ASTM C496." 2017. Standard Test Method for Splitting Tensile Strength of Cylindrical Concrete Specimens. https://doi.org/10.1520/C0496_C0496M-17.

ASTM C618. 2022. “ASTM C618.” Standard Specification for Coal Fly Ash and Raw or Calcined Natural Pozzolan for Use. https://doi.org/10.1520/C0618-22.

“ASTM C78.” 2022. Standard Test Method for Flexural Strength of Concrete (Using Simple Beam with Third-Point Loading). https://doi.org/10.1520/C0078_C0078M-22.

“ASTM C944.” 2019. Standard Test Method for Abrasion Resistance of Concrete or Mortar Surfaces by the Rotating-Cutter Method. https://doi.org/10.1520/C0944_C0944M-19.

Ayub, Tehmina, Nasir Shafiq, and M Fadhil Nuruddin. 2014. “Mechanical Properties of High-Performance Concrete Reinforced with Basalt Fibers.” Procedia Engineering 77: 131–39. https://doi.org/https://doi.org/10.1016/j.proeng.2014.07.029.

Basalt Fibers LTD. 2013. “Basalt Chopped Fibre- New Brand TURBOBUILD-24- 300 in Concrete Reinforcement Segment.” 2013.

Beaudoin, J J. 1990. Handbook of Fibre-Reinforced Concrete : Principles, Properties, Developments and Applications. Building Materials Science Series. Park Ridge, N.J. : Noyes Publications: Park Ridge, N.J. : Noyes Publications.

Bentur, Arnon., and Sidney. Mindess. 2007. Fibre Reinforced Cementitious Composites. London; New York: Taylor & Francis.

Borhan, Tumadhir. 2013. “Thermal and Mechanical Properties of Basalt Fibre Reinforced Concrete.” Proc. World Acad. Sci., Eng. Technol. 76 (April).

Branston, John, Sreekanta Das, Sara Y. Kenno, and Craig Taylor. 2016. “Mechanical Behaviour of Basalt Fibre Reinforced Concrete.” Construction and Building Materials 124 (October): 878–86. https://doi.org/10.1016/j.conbuildmat.2016.08.009.

Cheng, T.-C, An Cheng, Ran Huang, and Wei-Ting Lin. 2014. “Abrasion Properties of Steel Fiber Reinforced Silica Fume Concrete According to Los Angeles and Water Abrasion Tests.” Medziagotyra 20 (December): 498–502. https://doi.org/10.5755/j01.ms.20.4.6460.

Deák, Tamás, and Tibor Czigány. 2009. “Chemical Composition and Mechanical Properties of Basalt and Glass Fibers: A Comparison.” Textile Research Journal 79 (7): 645–51. https://doi.org/10.1177/0040517508095597.

Dias, Dylmar Penteado, and Clelio Thaumaturgo. 2005. “Fracture Toughness of Geopolymeric Concretes Reinforced with Basalt Fibers.” Cement and Concrete Composites 27 (1): 49–54. https://doi.org/10.1016/J.CEMCONCOMP.2004.02.044.

Fernandes, J.F., T. Bittencourt, and P. Helene. 2008. “A Review of the Application of Concrete to Offshore Structures.” ACI Symposium Publication 253. https://doi.org/10.14359/20187.

Fibres Unlimited. 2007. “Test Report of Basalt Fibre Reinforced Concrete, Polypropylene Reinforced Concrete, Polyacrylonitrile Reinforced Concrete.” Technical Data Sheet 31 (0): 11.

Fu, Qiang, Ditao Niu, Jian Zhang, Daguan Huang, Yan Wang, Mengshu Hong, and Lu Zhang. 2018. “Dynamic Compressive Mechanical Behaviour and Modelling of Basalt–Polypropylene Fibre-Reinforced Concrete.” Archives of Civil and Mechanical Engineering 18 (3): 914–27. https://doi.org/https://doi.org/10.1016/j.acme.2018.01.016.

Gautier, Donald L, Kenneth J Bird, Ronald R Charpentier, Arthur Grantz, David W Houseknecht, Timothy R Klett, Thomas E Moore, et al. 2009. “Assessment of Undiscovered Oil and Gas in the Arctic.” Science 324 (5931): 1175 LP – 1179. https://doi.org/10.1126/science.1169467.

Grdic, Zoran J, Gordana A Toplicic Curcic, Nenad S Ristic, and Iva M Despotovic. 2012. “Abrasion Resistance of Concrete Micro-Reinforced with Polypropylene Fibers.” Construction and Building Materials 27 (1): 305–12. https://doi.org/https://doi.org/10.1016/j.conbuildmat.2011.07.044.

Hasan, Ahmad, and Lagoudas Dimitris C. 1991. “Effective Elastic Properties of Fiber-Reinforced Concrete with Random Fibers.” Journal of Engineering Mechanics 117 (12): 2931–38. https://doi.org/10.1061/(ASCE)0733-9399(1991)117:12(2931).

Hoff, G. C., and R. Elimov. 1995. “Concrete Production for the Hibernia Platform.” In Annual Conference- Canadian Society for Civil Engineering, 693–716.

Horszczaruk, E K. 2009. “Hydro-Abrasive Erosion of High Performance Fiber-Reinforced Concrete.” Wear 267 (1): 110–15. https://doi.org/https://doi.org/10.1016/j.wear.2008.11.010.

Jiang, Chaohua, Ke Fan, Fei Wu, and Da Chen. 2014a. “Experimental Study on the Mechanical Properties and Microstructure of Chopped Basalt Fibre Reinforced Concrete.” Materials & Design 58: 187–93. https://doi.org/https://doi.org/10.1016/j.matdes.2014.01.056.

Jun, W, and Z Ye. 2010. “Experimental Research on Mechanical and Working Properties of Non-Dipping Chopped Basalt Fiber Reinforced Concrete.” In 2010 3rd International Conference on Information Management, Innovation Management and Industrial Engineering, 4:635–37. https://doi.org/10.1109/ICIII.2010.633.

Kabay, Nihat. 2014. “Abrasion Resistance and Fracture Energy of Concretes with Basalt Fiber.” Construction and Building Materials 50: 95–101. https://doi.org/https://doi.org/10.1016/j.conbuildmat.2013.09.040.

Katkhuda, Hasan, and Nasim Shatarat. 2017. “Improving the Mechanical Properties of Recycled Concrete Aggregate Using Chopped Basalt Fibers and Acid Treatment.” Construction and Building Materials 140: 328–35. https://doi.org/10.1016/j.conbuildmat.2017.02.128.

Mahdi, Noor, Mohammed Shamkhi, and Sallal Abid. 2017. Effect of Polypropylene Fibers on the Abrasion Resistance of Hydraulic Concrete. In 2nd Inetrnational Conference on Civil and Environmental Engineering.

Ramakrishnan, V, Neeraj S. Tolmare, and Vladimir B. Brik. 1998. “Performance Evaluation of 3-D Basalt Fiber Reinforced Concrete & Basalt Rod Reinforced Concrete.”

Report, no. November: 97. http://apps.trb.org/cmsfeed/TRBNetProjectDisplay.asp?ProjectID=2017.

Sandvik, M., T. Hovda, and S. Smeplass. 1994. “Modified Normal Density (MND) Concrete for the Troll GBS Platform.” ACI Symposium Publication 149: 81–102. https://doi.org/10.14359/4069.

Shallal, Muhaned A., and Sallal Rashid Al-Owaisy. 2007. “Strength and Elasticity of Steel Fiber Reinforced Concrete at High Temperatures.” Journal of Engineering and Development 11 (2): 125–33.

Sim, Jongsung, Cheolwoo Park, and Do Young Moon. 2005. “Characteristics of Basalt Fiber as a Strengthening Material for Concrete Structures.” Composites Part B: Engineering 36 (6): 504–12. https://doi.org/https://doi.org/10.1016/j.compositesb.2005.02.002.

Sivakumar, A., and Manu Santhanam. 2007. “Mechanical Properties of High Strength Concrete Reinforced with Metallic and Non-Metallic Fibres.” Cement and Concrete Composites 29 (8): 603–8. https://doi.org/10.1016/j.cemconcomp.2007.03.006.

Song, P. S., and S. Hwang. 2004. “Mechanical Properties of High-Strength Steel Fiber-Reinforced Concrete.” Construction and Building Materials 18 (9): 669–73. https://doi.org/10.1016/j.conbuildmat.2004.04.027.

Usman, Muhammad, Syed Hassan Farooq, Mohammad Umair, and Asad Hanif. 2020. “Axial Compressive Behavior of Confined Steel Fiber Reinforced High Strength

Concrete." Construction and Building Materials 230: 117043. https://doi.org/10.1016/j.conbuildmat.2019.117043.

Craig, Peter and Wolfe, Bill. 2012. "Another Look at the Drying of Lightweight Concrete-A Comparison of Drying Times for Normal weight and Lightweight Floors." Concrete International: 53–58.

Yurtseven, A E, I O Yaman, and M Tokyay. 2006. "MECHANICAL PROPERTIES OF HYBRID FIBER REINFORCED CONCRETE." In Measuring, Monitoring and Modeling Concrete Properties, edited by MARIA S KONSTA-GDOUTOS, 207–14. Dordrecht: Springer Netherlands.

Zhao, Q, J Dong, H Pan, and S Hao. 2010. "Impact Behavior of Basalt Fiber Reinforced Concrete." Fuhe Cailiao Xuebao/Acta Materiae Compositae Sinica 27 (December): 120–25.

Chapter 5 Influence of nano particles addition on the abrasion resistance of the high performance specified density concrete

5.1. Abstract

The high performance specified density concrete (HPSDC) is a type of concrete that is developed by replacing a percentage of the normal weight coarse aggregate with lightweight coarse aggregate. It's most employed in offshore structural applications. This study was conducted to enhance its mechanical properties and abrasion resistance by the incorporation of nano particles (NPs) at different ratios. NPs used were nano colloidal silica (NCS) and nano titanium dioxide (NTD). NCS and NTD were chosen as they are more commercially available compared to other types of NPs. They were added at 0.5%, 1%, 1.5%, 2%, 2.5%, and 3% by mass of cement. The fresh properties of the HPSDC were assessed and its mechanical behavior was evaluated through five ASTM standard testing for compressive strength, static modulus of elasticity (SME), dynamic modulus of elasticity (DME), split-tensile strength (STS), and flexural strength (FS), The HPSDC abrasion resistance was evaluated using two ASTM standard testing; rotating cutters method ("ASTM C944" 2019) and sandblasting method ("ASTM C418" 2020). The experimental results revealed that the incorporation of nano particles positively impacted the HPSDC compressive strength and stiffness properties. Also, it affected its tensile properties to a higher extent compared to the compressive strength and stiffness properties. It was also concluded that, NCS was more effective. Furthermore, the HPSDC abrasion resistance was the most positively affected property by the inclusion of NPs.

Keywords: Concrete, offshore, abrasion, nano particles.

5.2. Introduction

Concrete is widely used in a variety of construction applications. However, because it is subjected to various types of loading actions, each application necessitates concrete with specific requirements. Offshore structural concrete, for instance, is subjected to abrasion action as a result of interacting with moving ice sheets in a marine environment. This contact could result in significant wear, which could lead to damage, increased maintenance costs, and a shorter life cycle. The 1.3 billion-dollar (CAN) Confederation Bridge in Canada, which connects Prince Edward Island to the mainland at New Brunswick, is an example of a construction in an ice-infested sea. This is the world's longest concrete bridge across ice-covered water. Monitoring of the bridge revealed some wear damage to the concrete pillars at the water's edge because of interacting with floating ice sheets. Some remediation and restoration work has already been proposed and is in progress. This drew attention to the need to create an offshore structure concrete with higher abrasion resistance.

A particular form of concrete is used for offshore structures. To resist such harsh environmental conditions, it must be of high performance (“ACI 318-14” 2014). It must also, in some situations, be of a lighter weight. Offshore platforms, for example, are built on land and then dragged to their final destination. That towing phase requires concrete with specific unit weight. For that reason, the incorporation of lightweight aggregate became an attractive alternative (Fernandes, Bittencourt, and Helene 2008). However,

when all of the coarse aggregate in concrete is replaced with lightweight aggregate, the concrete's mechanical properties and abrasion resistance are degraded. So, for offshore structural applications, it is desirable to partially replace coarse aggregate with lightweight aggregate, and the resulting concrete is recognized as specified density concrete or modified normal density concrete.

For offshore structural applications, the HPSDC has been extensively used. The Hibernia platform, a massive gravity-based structure, was constructed in 1991 with 450,000 tonnes of concrete, predominantly HPSDC with a 50% partial replacement of coarse aggregate with lightweight aggregate (Hoff and Elimov 1995). It was also utilized to construct the Troll A GBS platform (Sandvik, Hovda, and Smeplass 1994), which at the time was the world's largest structure ever moved. In 1996, HPSDC allowed such a massive structure to be towed across the sea. HPSDC is also being used to build West White Rose's new gravity-based structure. However, a more advanced HPSDC is needed for use in harsher environments, such as the Arctic. The Arctic possesses 13% of the world's undiscovered oil and 30% of the world's undiscovered gas (Gautier et al. 2009), making it a great resource for oil and gas in the future. However, research is still limited due to the extremely severe environments that the concrete is exposed to there.

Despite the HPSDC's enormous significance, there are only a few studies on it. (Bogas and Gomes 2014) investigated the effect of nano-silica addition on specified density concrete prepared with various cement contents, initial wetting conditions, coarse lightweight aggregate types and volumes. The use of lightweight aggregate resulted in a

decrease in the elastic moduli. Even though abrasion resistance is one of the key concerns of HPSDC in the marine environment, it has yet to be researched.

Recently, the marvel of nanotechnology has drawn considerable attention. Its use and application covered many fields. The incorporation of NPs in concrete is one of these promising fields. NPs are superfine powders, with the size at which the transition between atomic clusters and macroscopic objects occurs. Due to its high surface area, it can affect the concrete properties at the ultrafine level and promote the formation of hydration products. They also act as fillers which leads to densifying the microstructure and reducing the porosity of the concrete. To date, the most used NPs are nano silica, nano titanium dioxide, and nano zirconia.

Nano silica particles are incorporated either as colloidal suspension or as dry powder. Nano colloidal silica (NCS) is considered a new pozzolanic material in the form of ultra-fine silica particles that are collided in water. It was found to be a more effective form compared to dry powder nano silica (Thomas, Jennings, and Chen 2009). On the other hand, nano titanium dioxide (NTD) is an ultra-fine white powder. It is known for its photocatalyst effect that enables it to be a self-cleaning material. Its application is wide from paint, and food coloring to sunscreen. Recently, it has been used in 109 brands in the industry of construction.

Despite that NPs are produced in sizes below 100 nm, when incorporated in concrete mixtures, they have a strong tendency to form agglomerations that were found to be between 1 to 100 mm (Kawashima et al. 2014). These agglomerations reduce the surface area of the nano particles, in turn preventing full exploitation to improve the concrete

performance. Furthermore, these agglomerations are considered weak zones that may negatively impact the concrete properties (Kawashima et al. 2014). Therefore, good dispersion of NPs is vital so that it can achieve its purpose. It was found that regular low shear mixing such as using conventional concrete mixers does not achieve the required dispersion for the particles (Madani et al. 2013). For that reason, researchers adopted various more efficient techniques to effectively disperse nano NPs before using them in the concrete mixture. Such as the use of ultra-sonication, mechanical stirring, higher shear mixing, and adding superplasticizers (Senff et al. 2012; M.-H. Zhang, Islam, and Peethamparan 2012; Haruehansapong, Pulngern, and Chucheepsakul 2014; Gaitero, Campillo, and Guerrero 2008; Jo et al. 2007; Aly et al. 2012; Madani et al. 2013). In addition, the usage of a combination of these methods has been proven to provide a desired state of dispersion (Korayem et al. 2017).

By achieving good dispersion, the impact of nano silica on the concrete mechanical properties was found to be superior. (Zhao, Kong, and Yang 2012) conducted an experiment to study the impact of nano silica addition and found an enhancement in the compressive strength and freeze/thaw resistance of the concrete. In addition, by the inclusion of only 0.25% (by mass of cement) of nano silica, an improvement of 10% in the compressive strength was noted by (Sobolev et al. 2009). Whereas 10% addition remarkably enhanced the concrete compressive strength by 166%. Moreover, as reported by (Shih, Chang, and Hsiao 2006), an addition of 0.6% of nano silica enhanced the compressive strength of cement pastes by around 46% at the 56-day. Furthermore, as reported by (Lin et al. 2008) the effectiveness of incorporation of nano silica on the

compressive strength and flexural strength of the concrete was clear and even more effective than silica fume addition.

Nonetheless, NTD impact on the concrete mechanical properties was thoroughly investigated. (Zhang and Li 2011) incorporated NTD at 1%, 3%, and 5% by mass of cement and reported improvements of 18.03%, 12.76%, and 1.55%, respectively, compared to the control mixture. Whereas, (Nazari 2011) added NTD at 0.5%, 1%, 1.5%, and 2% by mass of cement and found that the compressive strength increased by 36.58%, 48.78%, 56.1% & 65.85%, respectively, with curing in saturated limewater.

The effectiveness of NPs addition on the concrete mechanical properties brought the authors' attention to study its impact on the HPSDC to enhance its abrasion resistance. By reviewing the literature, the effect of NPs addition on the concrete abrasion resistance was rarely investigated. (Li, Zhang, and Ou 2006) conducted a study on the impact of nano silica and NTD on the concrete abrasion resistance. They tested the abrasion resistance as per GB/T16925-1997 (test method for abrasion resistance of concrete and its products, China) which is a ball bearing abrasion testing. The results indicated that both of them were able to positively impact the concrete abrasion resistance. However, adding NTD particles was more pronounced. Whereas, (Riahi and Nazari 2011) studied the effect of the incorporation nano silica and nano CuO particles on the concrete abrasion resistance. It was tested as per ("ASTM C1138" 2019), which is a ball bearing approach as well. It was concluded that nano silica addition had a notable positive impact on the concrete abrasion resistance. In addition, (Gonzalez, Lima, and Tighe 2014) investigated the effect of the incorporation of nano silica on the abrasion resistance of concrete tested as per ("ASTM

C944" 2019) rotating cutters method. The results demonstrated that there was a noticeable decreasing trend in the degree of wear that was related to the amount of nano silica added.

It can be seen that past investigations have been focused on the impact of NPs addition on the concrete main mechanical properties (mainly compressive and flexural strength). However, its impact on other mechanical properties such as STS, SME or DME has remained with unknown influence. Especially when mineral admixtures such as MK, SF, and fibers are incorporated. The presence of these SCMs along with NPs could provide a magnified impact on the concrete performance. Also, with fibers added, the addition of NPs may affect on the fiber-matrix interface which in turn can adjust the fibers' role on the concrete properties to some extent. Especially knowing that, recently, the addition of different SCMs and fibers became highly common and a convenient option for high strength concrete mixtures. Furthermore, there is a lack of data available regarding the effect of NPs addition on the concrete abrasion resistance. Other studies mainly focused on testing the abrasion resistance using one testing approach in each study. It is worth to mention that, each abrasion testing approach simulates a different abrasion mechanisms. The revolving cutters method (ASTM C944), for example, depicts how traffic abrades a concrete surface. The sandblasting method (ASTM C418) is used to imitate waterborne abrasives. Using different testing approaches can enrich our knowledge of the effect of the incorporated materials on the concrete abrasion resistance.

In the work presented hereafter, NCS and NTD were incorporated. An investigation of these additions to the HPSDC properties will be provided. The HPSDC examined has MK and SF incorporated along with copper-coated steel fibers (CCSFs). The current study

will provide more experimental evidence on the impact of NPs addition on the concrete fresh properties, compressive strength, and FS. In addition, it will clarify the effect on the STS, SME, and DME. The study will provide a deeply detailed analysis of the concrete abrasion resistance modified with NPs using two different ASTM testing approaches. The authors believe that the results obtained from this study can be a motivation for more implementation of NPs in the concrete industry. This could lead to a more efficient concrete structure, lower maintenance costs, and a motivation to develop more new offshore buildings in harsher environments, which is in great demand.

5.3. Experimental program

5.3.1. Material properties

The binders that were used for the developed mixtures were general use Portland cement (GU) (Type I) ("ASTM C150" 2022), MK (Class N) (ASTM C618 2022), and SF ("ASTM C1240" 2020). Table 5-1 shows the chemical composition and physical parameters of the cement and SCMs employed. NCS used had 40% solid content with a specific gravity of 1.21. Whereas NTD was an anatase nano powder with TiO_2 purity of 99.9% and an average particles size of 5 nm. Pictures of the used NPs are shown in Fig. 5-1. Expanded slate lightweight aggregate (ESLWA) produced by STALITE, with a maximum aggregate size of 12.5 mm and a specific gravity of 1.53 at saturated surface dry condition, was employed as the lightweight aggregate (SSD). Because of its porous structure, the aggregate exhibited a high absorption rate of 6 to 9%. The physical characteristics of ESLWA are shown in Table 5-2. Crushed granite stone with a specific

gravity of 2.6 was used as the coarse and fine aggregates. The absorption of the normal weight coarse aggregate was 0.6%. It had a maximum aggregate size of 10 mm. Figure 5-2 illustrates images of the ESLWA and coarse normal weight aggregates (NWA). Figure 5-3 shows the gradation analysis for the aggregates utilized, with the curves representing the ("ASTM C33" 2018) limits. CCSFs were incorporated. A Picture of them is shown in Fig. 5-4 and their properties are shown in Table 5-3. Polycarboxylate-based superplasticizer (SP) that confines to ("ASTM C494" 2022) Type A and F, and Type I ("ASTM C1017" 2013) was used to attain the required workability. An air-entraining agent (AEA) that confines to ("ASTM C260" 2016) was used to make hardened concrete more resistant to freeze-thaw cycles.

Table 5-1 Chemical analysis and physical properties of the used cement and SCMs.

Chemical analysis (%)	Cement	FA	SF	MK
SiO_2	19.64	52	89.1	52
Al_2O_3	5.48	23	0.67	43
Fe_2O_3	2.38	11	0.49	<2.2
CaO	62.44	5	6.12	<0.2
MgO	2.48	-	0.31	<0.1
SO_3	4.32	-	0.16	-
K_2O	-	-	0.49	<0.40
Na_2O	-	-	0.26	<0.05
Cl	-	-	0.04	-
Total alkali	0.97	-	-	-
Free lime	1.03	-	-	-
LOI	2.05	0.21	2.81	0.95
C_3S	52.34	-	-	-
C_2S	16.83	-	-	-
C3A	10.5	-	-	-
C4AF	7.24	-	-	-
Physical properties				
Specific gravity	3.15	2.37	2.20	2.56
Blaine fineness (m^2/kg)	410			

Table 5-2 Physical characteristics of ESLWA.

Absorption Saturated Surface Dry (ASTM C127)	6.0%
Soundness (% Loss) Magnesium Sulfate (ASTM C88)	0 - 0.01%
Sodium Sulfate (ASTM C88)	0 - 0.23%
25 Cycles Freezing and Thawing (AASHTO T 103)	0.22 - 0.80%
Toughness Los Angeles Abrasion (AASHTO T 96)	25 - 28%
Stability Angle of Internal Friction (Loose)	40° - 42°
Angle of Internal Friction (Compacted)	43° - 46°

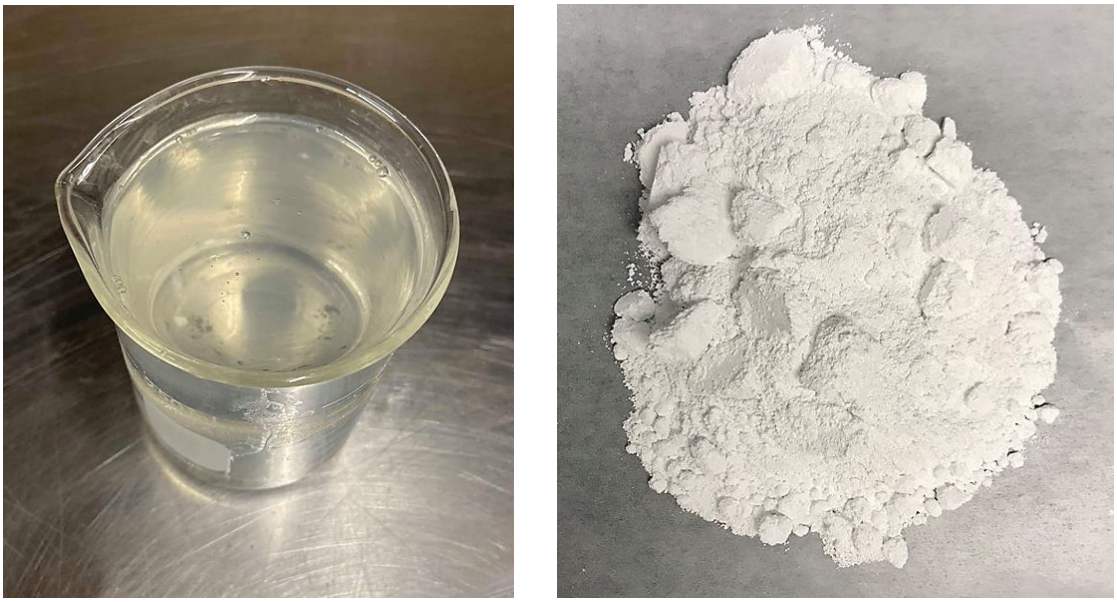

(a) NCS (b) NTD

Fig. 5-1 NPs used.

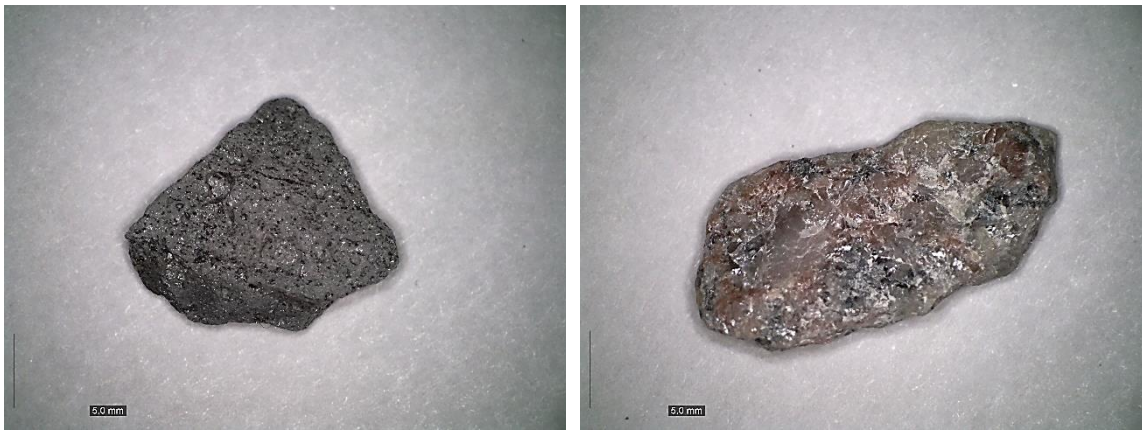

(a) ESLWA (b) NWA

Fig. 5-2 Coarse aggregate used.

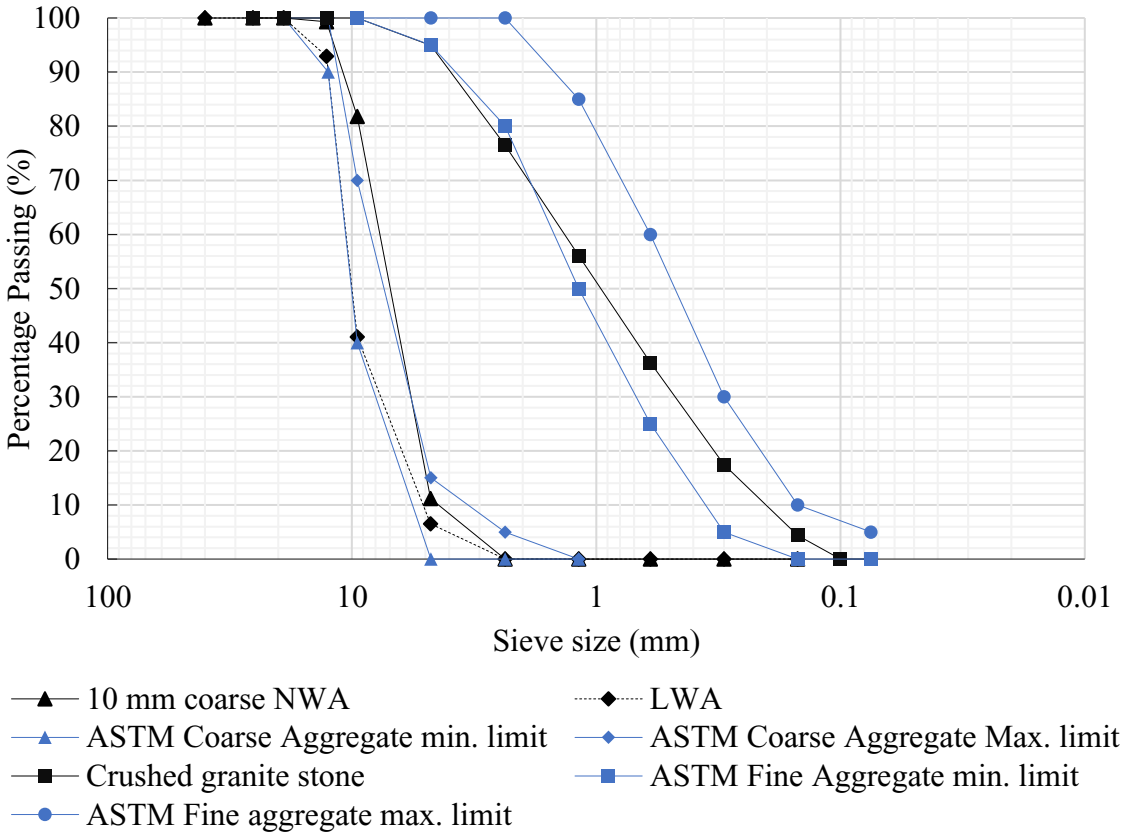

Fig. 5-3 Grading curves for 20 mm coarse NWA, 10 mm coarse NWA, ESLWA, and fine aggregate.

Fig. 5-4 Used CCSFs.

Table 5-3 Properties of fibers used.

Property	CCSFs
Specific Gravity	7.8
Length (mm)	13
Diameter (μm)	200
Tensile strength (MPa)	1900
Elastic modulus (GPa)	203
Elongation at break (%)	0.5-3.5

5.3.2. Concrete mixtures development

Because of the narrow spacing of the reinforcement being used in offshore structural elements, high workability is required (Fernandes, Bittencourt, and Helene 2008). As a result, a 180 mm to 220 mm slump was set as the target. Offshore constructions are exposed to harsh weather. As a result, according to ("ACI 318-14" 2014), air content of 6 to 7.5 percent was desired. Trial mixtures were used to select the optimum SP dosage for achieving the desired slump while avoiding segregation. In addition, the AEA dosage was carefully adjusted to produce the needed air content. The NPs (NCS and NTD) were incorporated at 0%, 0.5%, 1%, 1.5%, 2%, 2.5% and 3%. A total of thirteen mixtures, 234 cylinders and 78 prisms, were developed. Cylinders size were 100 mm × 200 mm, while prisms' size was 100 mm × 100 mm × 400 mm. The composition of the concrete mixtures can be seen in Table 5-4. The mixtures were labeled according to the NPs incorporated in them. For example, a mixture using NCS at 0.5% was labeled as 0.5NCS. While the control mixture refers to the mixture with no NPs added. All mixtures were developed using CCSFs at 0.5% with a constant MK and SF replacement for cement ratios of 15% and 8%, respectively, as these were found to be the optimum ratios through the previous levels of the experimental program of the current research (chapters 3 and 4).

Table 5-4 Composition of the tested mixtures.

Mixture No.	Mixture designation	Binders content				ESLWA/ T. C. A.	NPs Type	NPs solids ratio	SP	AEA	Density
		Cement (kg/m^3)	MK (kg/m^3)	SF (kg/m^3)	C/F			(%)	(ml/m^3)	(ml/m^3)	(kg/m^3)
1	Control	423.5	82.5	44	1.6	0.5	_	_	5500	600	2060.6
2	0.5NCS	420.75	82.5	44	1.6	0.5	NCS	0.5	5500	600	2059.8
3	1NCS	418	82.5	44	1.6	0.5	NCS	1	6000	600	2059.0
4	1.5NCS	415.25	82.5	44	1.6	0.5	NCS	1.5	6000	620	2058.3
5	2NCS	412.5	82.5	44	1.6	0.5	NCS	2	6000	620	2057.5
6	2.5NCS	409.75	82.5	44	1.6	0.5	NCS	2.5	6500	650	2056.7
7	3NCS	407	82.5	44	1.6	0.5	NCS	3	6500	650	2056.0
8	0.5NTD	420.75	82.5	44	1.6	0.5	NTD	0.5	5500	600	2059.8
9	1NTD	418	82.5	44	1.6	0.5	NTD	1	5500	600	2059.0
10	1.5NTD	415.25	82.5	44	1.6	0.5	NTD	1.5	6000	620	2058.3
11	2NTD	412.5	82.5	44	1.6	0.5	NTD	2	6000	620	2057.5
12	2.5NTD	409.75	82.5	44	1.6	0.5	NTD	2.5	6500	650	2056.7
13	3NTD	407	82.5	44	1.6	0.5	NTD	3	6800	650	2056.0

Note: All mixtures have 550 kg/m^3 binder content and 0.3 water to binder ratio.

5.3.3. Mixing procedures

Because of its high absorption rate of 6 to 9%, the ESLWA was soaked for 24 hours and then drained for 6 to 12 hours before batching. To achieve a near SSD case and minimize aggregate moisture content variability, this is a standard practice (Craig and Wolfe 2012). During the construction of the Hibernia platform, a similar technique was being used as suggested by (Hoff and Elimov 1995). To remove moisture from the fine aggregate, it was oven dried for 24 hours at 110 ± 5 C^o before mixing. To reach the SSD state, the normal weight aggregates were saturated with a specific amount of water-based on the absorption ratio for a reasonable amount of time. NTD was dispersed in water first before being added to the concrete mixture. The dispersion was achieved through the

following technique. As shown in Fig. 5-5, the NTD was added to water (with SP added) while applying ultrasonication along with low energy stirring using a magnetic stirrer at the bottom of the container. After dispersing the needed quantity of the NTD for the mixture, it was placed in a larger container where high shear mixing was applied using a regular hand mixer. Whereas the NCS was used directly.

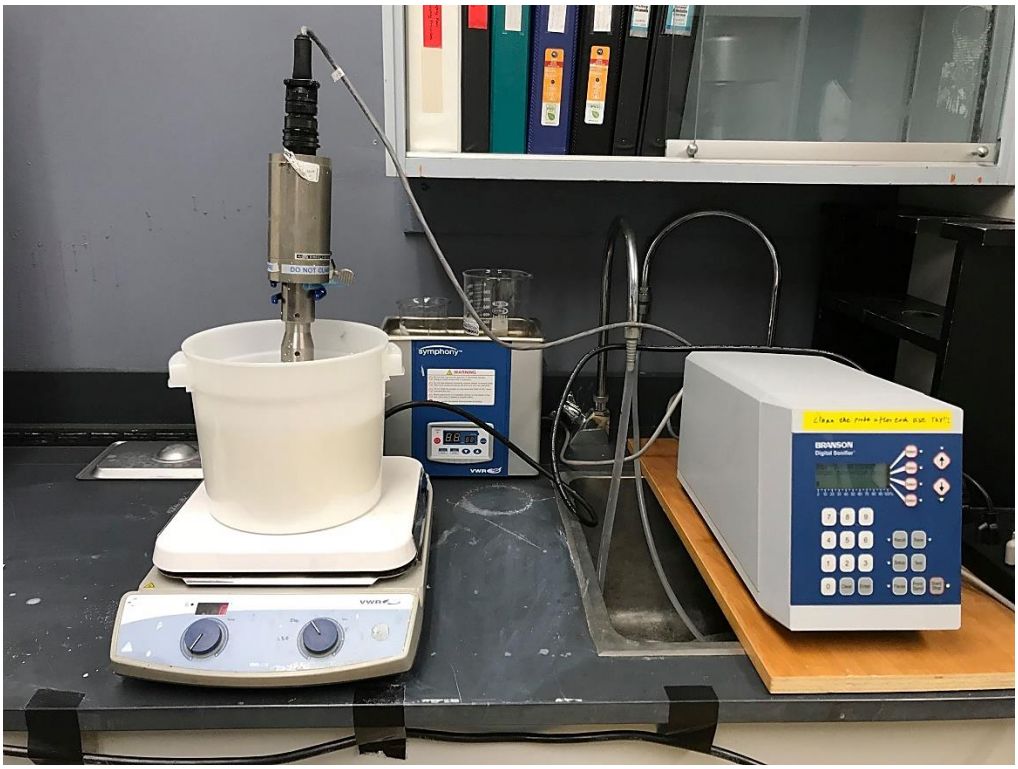

Fig. 5-5 Dispersion of NTD using SP, ultra-sonication, and a magnetic stirrer.

The aggregates and cement were put into the mixer initially during batching. To blend the dry ingredients, the mixer was turned on for 30 seconds. Fibers were added while dry mixing. For the no-NTD-added mixture, the AEA was combined with half the batch water before being placed into the mixer and mixed for 2 minutes. The SP was added to the remaining half of the water and mixed for another 3 minutes. A small amount of water

was conserved for future use. The batch was visually inspected to determine its consistency. If the desired consistency was not attained, an additional amount of SP was added to the remaining portion of water, added to the mixture, and mixed for another minute. After visually reaching the appropriate consistency, the batch was tested for slump and air content. When NCS was used, it was added directly to the mixture at the end of mixing as recommended by the provider. Whereas when NTD was used, water and SP were combined together to achieve the required dispersion as mentioned earlier and then added to the mixture. The cylinders and prisms were compacted and trowel-finished to achieve a flat surface while using a mechanical vibrating table. After 24 hours, the samples were demolded, tagged, and stored in a curing chamber at a temperature of 25 ± 1.5 C^o and 100 percent relative humidity until the testing day. All of the combinations were put into 100 L in size.

5.3.4. Testing procedures

5.3.4.1. Fresh and mechanical properties tests

The workability of the concrete mixes and percentage of air content tests were performed in accordance with ("ASTM C143" 2020) and ("ASTM C231" 2022), respectively. The characteristics of hardened concrete were evaluated after 14 and 28 days. Compressive strength according to ("ASTM C39" 2021), STS according to ("ASTM C496" 2017), and SME according to ("ASTM C469" 2022) were measured on three identical cylinders. In addition, three identical prisms were tested to determine the FS with third point loading according to ("ASTM C78" 2022). The fundamental longitudinal

resonance frequency of three concrete prisms was measured using ("ASTM C215" 2019) and used to calculate the DME.

5.3.4.2. Abrasion resistance tests

The abrasion resistance of the produced concrete mixes was tested using two ASTM standard tests, which are as follows:

5.3.4.2.1. ASTM C944, rotating-cutters method: The test setup is demonstrated in Fig. 5-6. It is precisely built to fulfill ASTM C944 requirements. The guidelines address the loading, the number of revolutions per minute (RPM), the testing duration, the cutter size, and the replacement intervals for washers and dressing wheels. A conventional drill press was adapted and utilized as the abrasion device. The spring that was fastened to the spindle was removed. A U-shaped extension capable of carrying the auxiliary load directly on the spindle was created and put on the drill press. The extension aimed to maintain a steady load during the testing time and to limit any vibrating motion that may impact the abrasion mechanism. For six minutes, the test was performed at a constant speed of 200 RPM (clockwise) with a constant weight of 19.7 kg total. This testing situation was intended to create expressive abrasion damage within the limits of the ASTM method. The revolving cutters had an overall diameter of 82.5 mm and were made using 20 dressing wheels and 22 washers. Dressing wheels and washers were replaced every 60 minutes to reduce variance between tested samples created by rotary cutter erosion. The abrasion test was carried out on three formwork adjacent surfaces of various 100 mm cubes properly cut from different prisms. After evaluating the samples, the surface was cleaned using compressed air to remove any residual material. ASTM recommends evaluating the

abraded mass loss to determine the abrasion resistance of the concrete. When evaluating concrete with considerable density differences, it is necessary to measure the abrasion depth rather than the abraded mass loss. In a previous study, as there was a comparison between the HPSDC with a normal weight concrete and lightweight aggregate concrete, that has a significant difference in density, abrasion depth was measured instead of the abraded mass loss. The current study would follow the same approach. The abrasion depth was calculated using Eq. 2-14 which was developed in chapter 2 with the help of the laser scanning technique as shown in Fig. 5-7, which shows a typical laser-scanned sample.

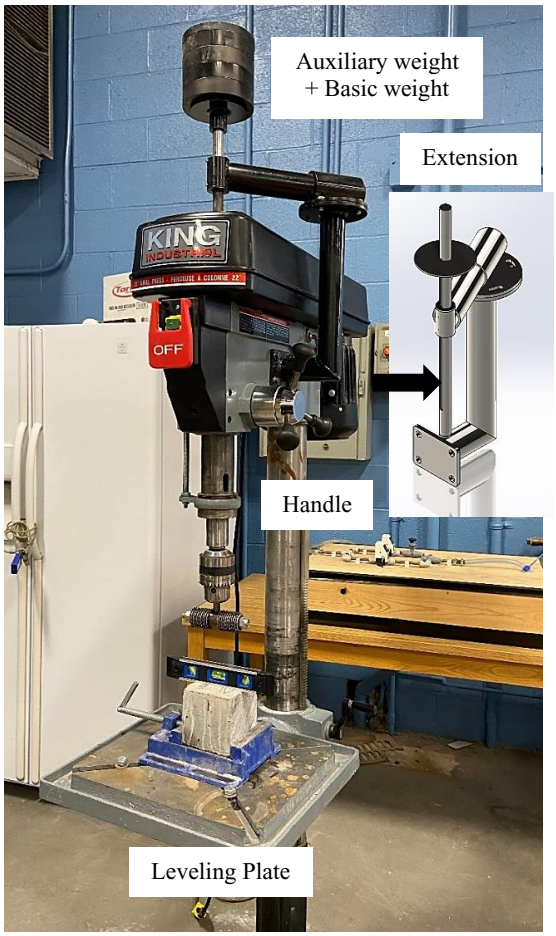

(a) Drill modification.

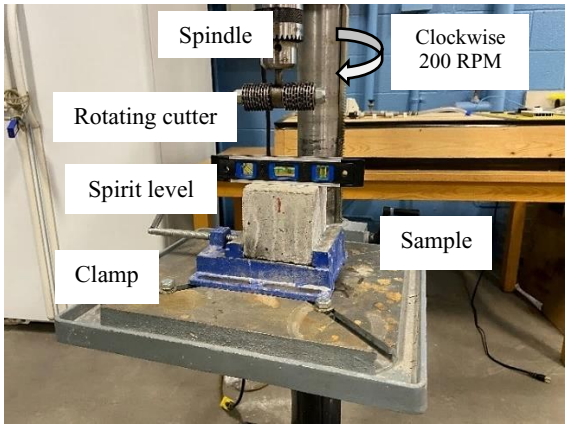

(b) Enlargement of the rotating cutters and the sample.

(c) Enlargement of the rotating cutters.

Fig. 5-6 ASTM C944, rotating cutters test.

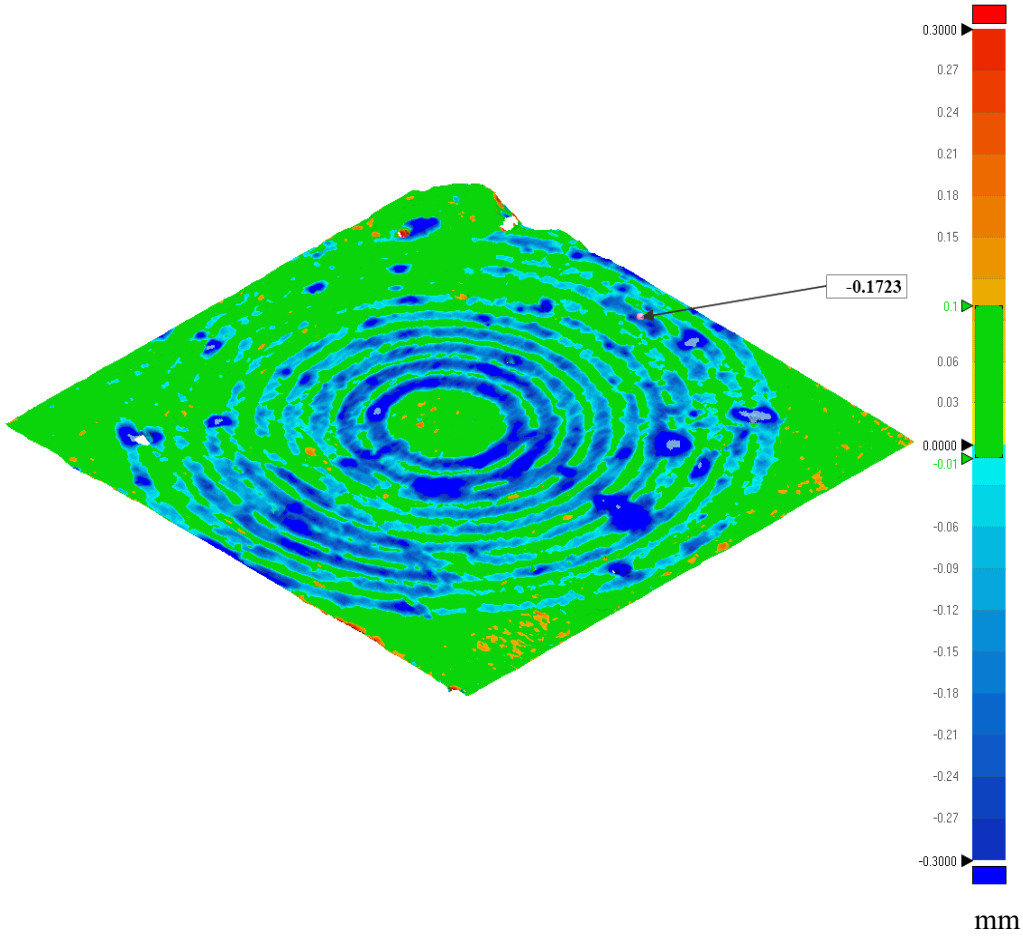

Fig. 5-7 Typical laser scanning of a sample tested using rotating cutters approach.

5.3.4.2.2. ASTM C418, sand blasting test: The test was carried out in accordance with ASTM C418. The test apparatus (Fig. 5-8) was meticulously built to adhere to ASTM C418 guidelines. As the nozzle shape might impact the wear pattern and hence the repeatability of the test results, nozzles that adhere to the ASTM precise specifications were created, as shown in Fig. 5-8. (d). The nozzle is 40 mm long and features 45^{o} bevel walls on the interior at the higher end. A clamp that holds the sample at a set normal distance of 75 mm from the nozzle end was employed. It contains a shield with a 28.7 mm diameter hole. The abrasive employed was silica sand, which had been pre-sieved to pass sieve No. 20 but not

sieve No. 30. The silica sand abrasive was never used again in this research to ensure consistent findings. Prior to testing, the concrete specimens were submerged for 24 hours. For one minute, the specimen's surface was subjected to air-driven abrasive sand at a pressure of 59.5 psi. Over the course of the sample, the test was performed eight times. The volume of the abrasion cavity should be measured with oil-based modeling clay, according to ASTM standards. However, due to the HPSDC's remarkable abrasion resistance, only small abrasion volumes were often achieved. Thus, Eq. 5-1 was used to determine the cavity volume by weighing the sample before and after testing and dividing the mass difference by the concrete density. Eq. 5-2 was then used to determine the abrasion coefficient. Laser scanning on random samples was used to ensure the accuracy of this measuring approach. Figure 5-9 shows a typical laser-scanned sample.

$$V = M / \rho \tag{5-1}$$

Where V is the volume of the abraded cavity, cm^3; M is the abraded mass, gm; and ρ is the concrete density gm / cm^3.

$$A_c = V / A \tag{5-2}$$

Where A_c is the abrasion coefficient, cm^3/cm^2; and A is the abraded surface area.

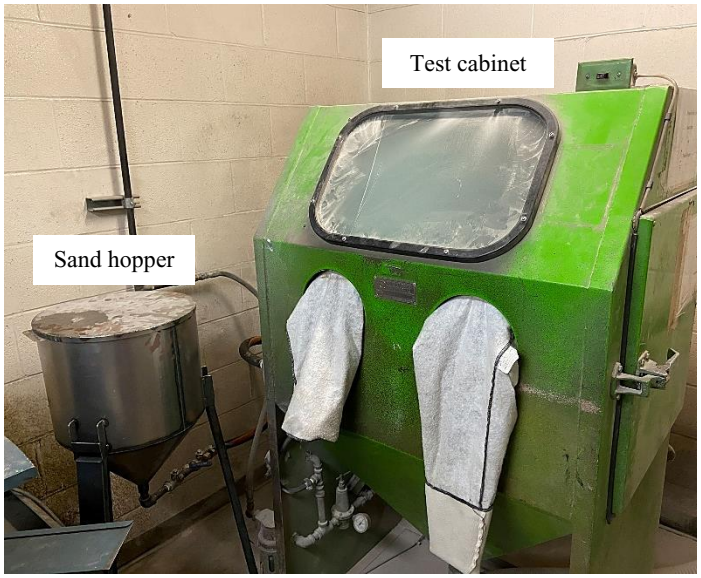

(a) Test cabinet and the sand hopper.

(b) Sand blasting gun

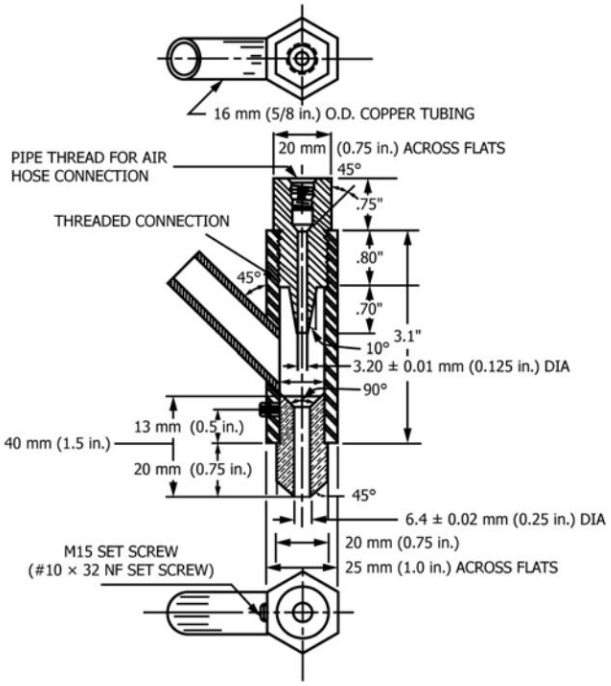

(c) ASTM C418 gun nozzle assembly. (d) Fabricated gun nozzle.

Fig. 5-8 ASTM C418, sand blasting test setup.

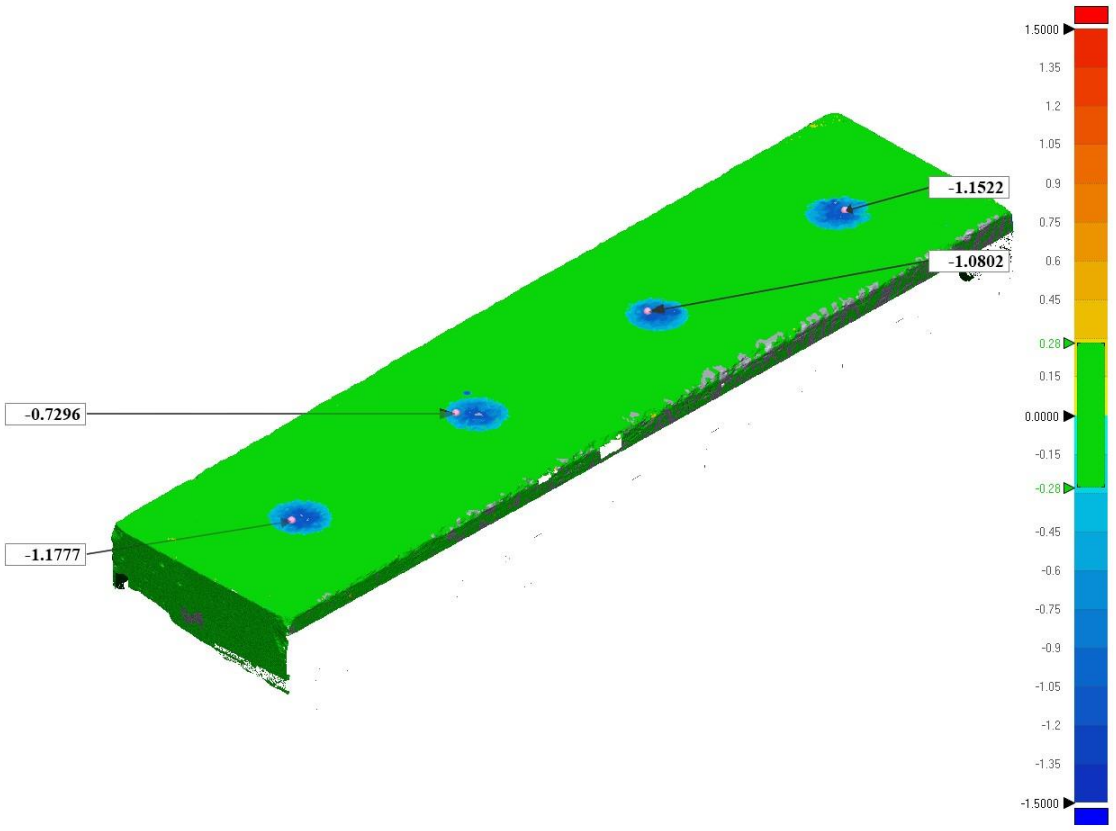

In mm

Figure 5-9 Typical laser scanning of a sample tested using sandblasting approach.

5.4. Results and discussion

5.4.1. Fresh properties

To achieve the targeted slump of 180 mm to 220 mm, the dosages of the SP required were different depending on the mixture composition as shown in Table 5-4. As can be seen from Fig. 5-10, the inclusion of the NPs in the HPSDC mixtures increased the SP demand. Higher SP demand of 18.2% and 23.6% were required at 3% of NCS and 3% of NTD, respectively. This is mainly attributed to the higher surface area of the NPs compared to the replaced cement. That in turn would absorb more water to achieve lubrication. Consequently, leaving less water to be exploited to achieve the required workability.

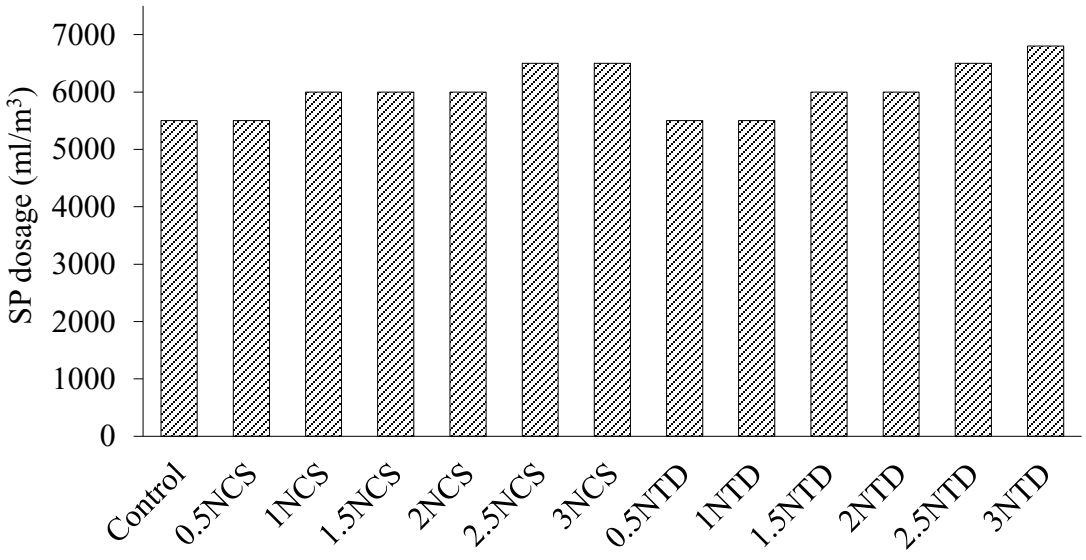

Fig. 5-10 Effect of inclusion of NPs on the SP demand of the HPSDC.

On the other hand, the impact of NPs inclusion on the AEA demand was less pronounced as can be seen in Table 5-4. Higher AEA dosages were needed to achieve the required air content by 8.3% by adding 3% of NCS or 3% of NTD. That may be due to, by

adding NPs, the concrete was more viscous and fewer air voids were formed. That in turn increased the need for AEA dosages.

5.4.2. Compressive strength and stiffness properties

Table 5-5 and Fig. 5-11 display the 14- and 28-day compressive strength for all the tested mixtures. It can be seen that the incorporation of NCS achieved higher compressive strength compared to the control mixture. This increase was a function of the ratio of NCS up to 2%. At this ratio, the HPSDC compressive strength reached 6.9% and 6.2% at the 14-day and 28-day, respectively, higher than the control mixture. This positive impact is due to various reasons; (a) the NCS was able to act as inner fillers to the paste gaps which densified its packing, (b) the increased packing efficiency by adding NPs may have been magnified with the presence of MK and SF which could act as mid-size particles between larger particles size (cement particles) to the nano-sized particles (NCS), (c) NCS can absorb the released C-H and due to its reactivity, it increases the C-S-H content in the paste, which is known as pozzolanic reactivity (d) NCS has the ability to act as nucleation sites for the hydration products, and (e) NCS has the ability to improve the structure of interfacial transition zone between paste and aggregate (Gonzalez, Lima, and Tighe 2014). A similar trend of results was found by (Cheng and Shi 2019). In which, the compressive strength reached its peak by the inclusion of nano silica particles at 2%. It was increased by 16.1% and 10.1% at the 7-day and 28-day, respectively. Similar to the current study, higher ratios were not as effective as 2%. In addition, the study conducted by (Riahi and Nazari 2011) had similar results. In that study, improvements were found by adding nano

silica particles up to 1%. However, higher incorporation ratios were also not as effective as 1%.

Table 5-5 Mechanical properties results for tested mixtures.

Mixture No.	Mixture designation	Compressive strength (MPa)		STS (MPa)		FS (MPa)		SME (GPa)		DME (GPa)	
		14-day	28-day	14-day	28-day	14-day	28-day	14-day	28-day	14-day	28-day
1	Control	88.4	90.5	6.51	6.72	10.20	10.43	39.6	41.1	43.9	45.5
2	0.5NCS	90.1	91.7	6.73	6.94	10.51	10.83	39.9	40.6	44.0	45.7
3	1NCS	90.8	91.6	6.92	7.13	11.23	11.59	40.3	42.0	44.3	46.1
4	1.5NCS	93.1	94.7	7.26	7.55	11.46	11.71	41.1	42.6	44.7	46.5
5	2NCS	94.5	96.2	7.64	7.81	11.61	11.86	41.9	43.1	45.4	47.6
6	2.5NCS	92.9	94.1	7.28	7.46	11.12	11.51	41.2	42.5	43.1	45.3
7	3NCS	92.5	93.2	7.12	7.39	10.69	11.01	40.9	41.6	44.7	45.1
8	0.5NTD	90.1	92.7	6.78	6.91	10.54	10.99	40.6	41.9	44.4	46.1
9	1NTD	92.6	94.9	7.01	7.22	10.92	11.21	41.5	42.9	45.2	46.7
10	1.5NTD	91.4	93.6	6.79	6.93	10.71	11.11	40.2	42.1	44.3	46.0
11	2NTD	89.7	92.2	6.71	6.99	10.15	10.51	40.0	41.9	44.1	45.9
12	2.5NTD	87.9	90.3	6.52	6.73	9.71	10.01	39.1	40.8	43.2	44.8
13	3NTD	85.7	87.1	6.33	6.59	9.83	10.06	38.7	40.4	42.8	44.5

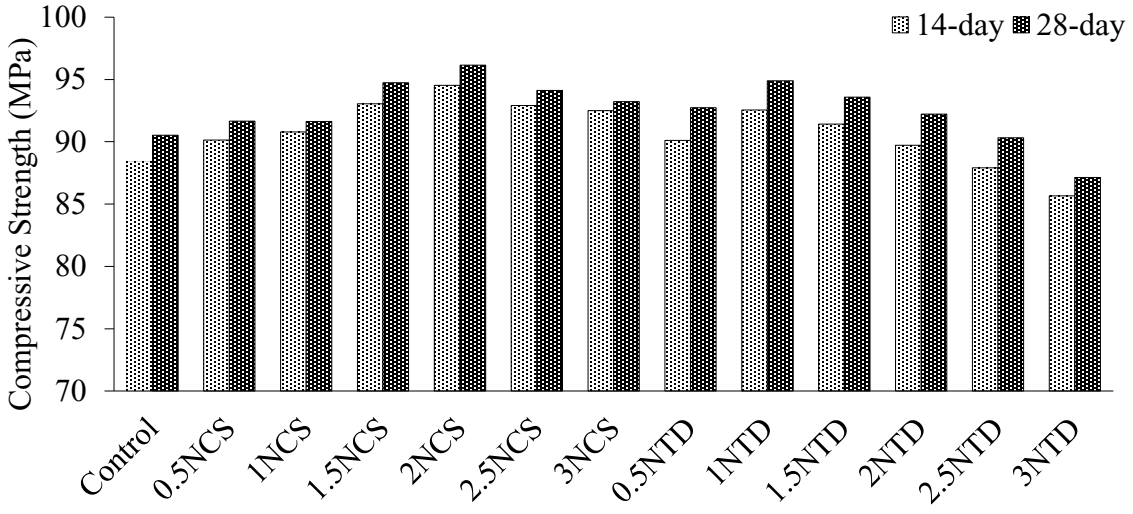

Fig. 5-11 Effect of inclusion of NPs on the compressive strength of the HPSDC.

Table 5-5, Fig. 5-12, and Fig. 5-13 show the 14- and 28-day SME and DME for all the tested mixtures. It can be noticed that, with the addition of NCS, the stiffness property of the HPSDC followed a similar trend compared to the compressive strength. The enhancements reached their peak at a 2% inclusion ratio. At which, the SME increased by 5.8% and 4.9% at the 14-day and 28-day, respectively. Similarly, the DME was enhanced by 3.5% and 4.6% at the 14-day and 28-day, respectively. That is mainly due to the same improvements mentioned earlier. These improvements provided a stiffer cement paste that can show less strain under the applied stress compared to the control mixture.

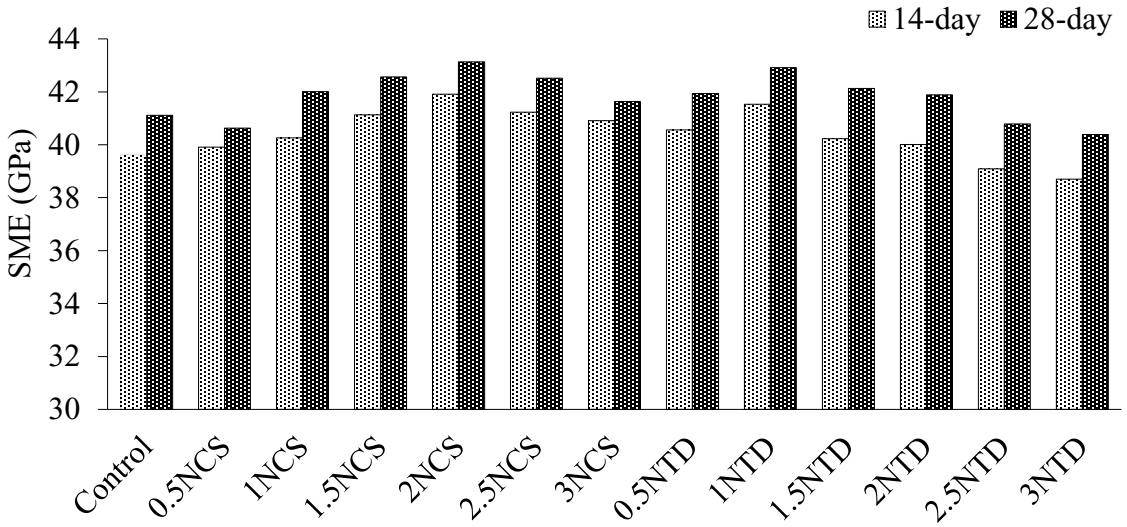

Fig. 5-12 Effect of inclusion of NPs on the STS of the HPSDC.

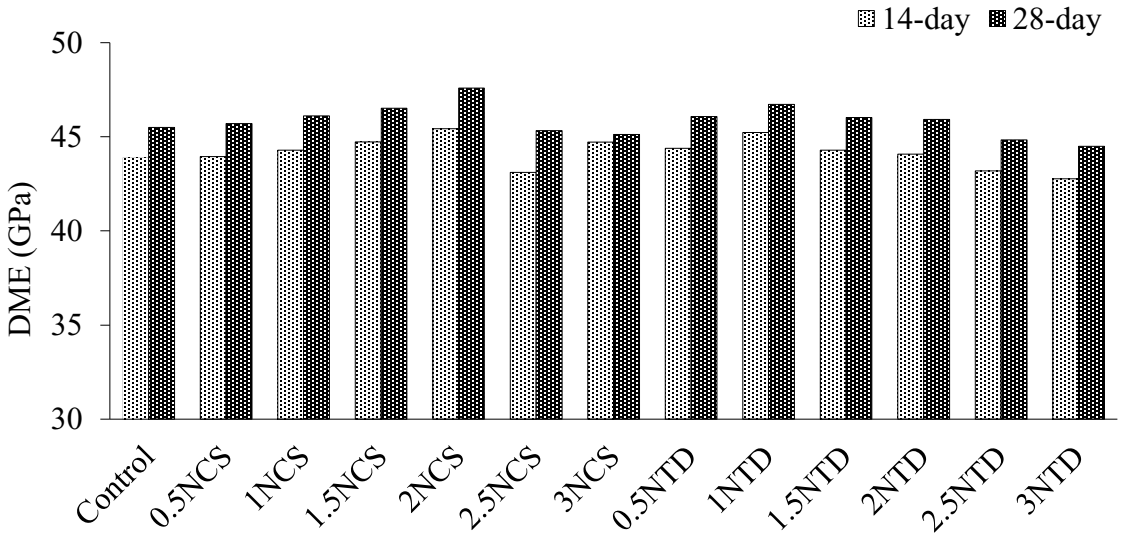

Fig. 5-13 Effect of inclusion of NPs on the DME of the HPSDC.

It can also be noticed that the impact of NCS inclusion on the compressive strength and stiffness properties was more pronounced at the 14- day than the 28- day. That may be due to the known ability of NCS to facilitate a faster reaction for the incorporated SCMs.

However, these differences were not high, as MK and SF are known to have a relatively higher rate of reaction compared to fly ash, for instance.

Incorporation of NTD also positively affected the HPSDC compressive strength, but to a less extent compared to the NCS. These enhancements were optimum at 1% of NTD. In which, the compressive strength reached 4.7% and 4.8% at the 14-day and 28-day, respectively. That behavior is mainly attributed to the ability of NTD particles, similar to NCS, to act as inner fillers, act as nucleation sites, and improve the structure of the interfacial transition zone. However, the less effectiveness of the NTD compared to the NCS may be attributed to the poor pozzolanic reactivity of the NTD. In addition, although trying to effectively disperse NTD particles, it may not have reached the same state of dispersion as the pre-dispersed particles of NCS. These results are in agreement with the investigation carried out by (Li, Zhang, and Ou 2006). In which, the addition of NTD at 1% of cement mass, increased the compressive strength by approximately 18%. Similarly, higher ratios than 1% were not as effective.

Although, the influence of incorporation of NTD on the compressive strength of the HPSDC was not as effective as the NCS addition, its effect on its stiffness was comparable to the NCS. Such contradictory observation may require further future investigation to explain the possible mechanisms that led to that behavior. By adding 1% of NTD, the SME increased by 4.8% and 4.4% at the 14-day and 28-day, respectively. While, the DME was enhanced by 3.1% and 2.7% at the 14-day and 28-day, respectively.

It can be observed that higher ratios of NCS than 2% of NCS or 1% of NTD were not as effective on the HPSDC compressive strength or its stiffness. This behavior may be attributed to the probability that, at higher incorporation ratios, the quantity of incorporated NPs existed in the mixture was higher than the required quantity to fill the voids and densify the concrete matrix which in turn acted as weak zones within the matrix leading to less compressive strength and stiffness.

5.4.3. Tensile properties

Table 5-5, Fig. 5-14 and Fig. 5-15 manifest the 14- and 28-day STS and FS for all the tested mixtures. It can be seen that similar to the compressive strength, the addition of NCS and NTD had a positive impact on the tensile properties of the HPSDC. Also, similar trends of results were attained. The tensile properties reached their peak at 2% and 1% of NCS and NTD, respectively, and decreased at higher addition ratios. By adding 2% of NCS, the STS of the HPSDC increased by 17.4% and 16.2% at the 14-day and 28-day, respectively. While the FS improved by 13.8% and 13.7% at the 14-day and 28-day, respectively, compared to the control mixture. Whereas by the inclusion of 1% of NTD, the STS of the HPSDC increased by 7.7% and 7.4% at the 14-day and 28-day, respectively, and the FS enhanced by 7.1% and 7.5% at the 14-day and 28-day, respectively, compared to the control mixture. This behavior is attributed to, as mentioned earlier, the ability of NPs to enhance the matrix and the matrix-aggregate interface. Furthermore, as explained by (Lan, Li, and Ju 2009), that the NPs dispersed inside the matrix which acts as nucleation sites forms conglomerations around it. Under STS or FS tests, formed cracks can not cross

through these conglomerations easily, which would consume more energy and thus achieve higher strength. Similar results were drawn (Nazari 2011). In that study, NTD was incorporated at 0.5%, 1%, 1.5%, and 2%. FS improvement was noticed that reached its peak at 2% of NTD. Similarly, (Mishra and Tiwari 2018) found improvements in the concrete FS by adding NTD at different ratios.

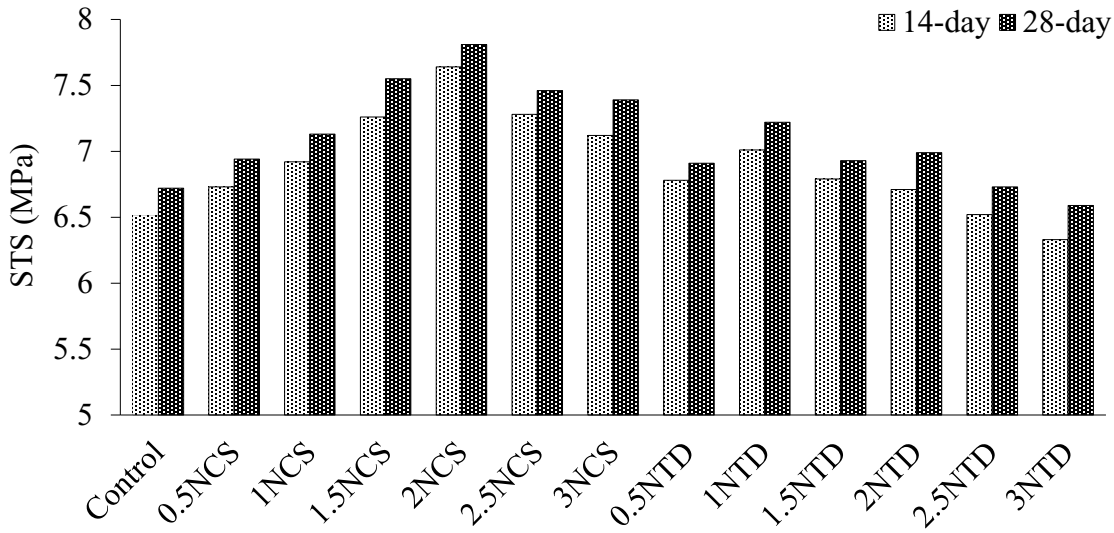

Fig. 5-14 Effect of inclusion of NPs on the STS of the HPSDC.

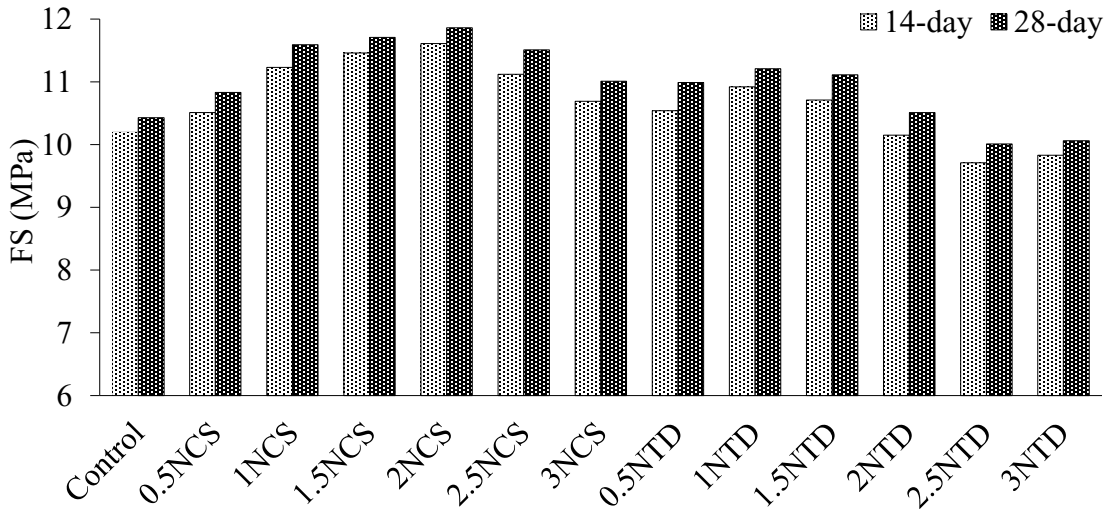

Fig. 5-15 Effect of inclusion of NPs on the FS of the HPSDC.

It is noteworthy that the impact of both NPs on the STS and FS was more pronounced than its effect on the compressive strength and stiffness of the HPSDC. Such an observation may be attributed to the ability of NPs to enhance the fiber-matrix interface which may have increased the fiber-matrix bond. Usually, fibers' properties affect the tensile properties to a higher extent than the compressive strength and the stiffness of the concrete. Though, the failure of the specimens under flexure was still fibers pull-out failure as can be seen in Fig. 5-16 for both control mixture and NPs added mixtures. These observations are the opposite of the results drawn by (Li, Zhang, and Ou 2007). In which, it was concluded that incorporation of NTD with polypropylene fibers reduced the flexural strength of the concrete. That may be due to using different types of fibers which may require further investigation according to different fiber types added.

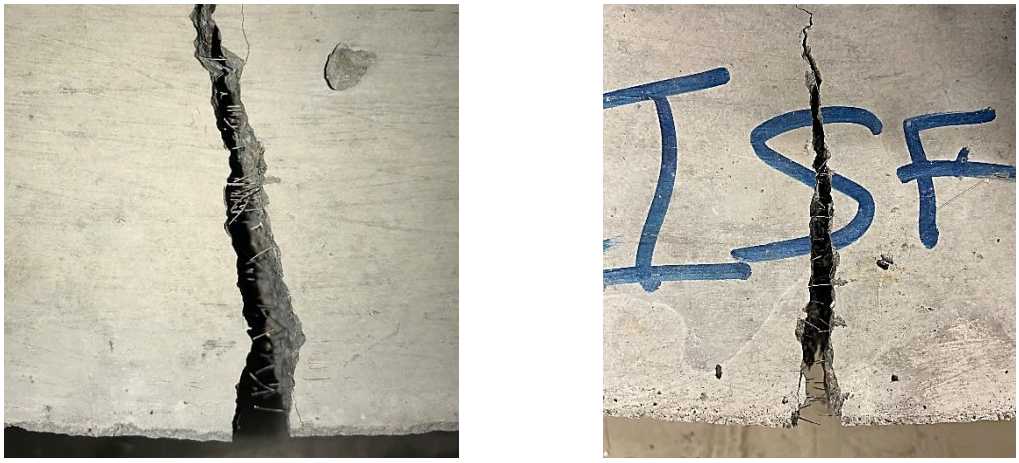

(a) Control mixture typical specimen (b) NPs incorporated typical specimen

Fig. 5-16 Failure pattern of typical specimen under flexural loading.

5.4.4. Abrasion resistance

Table 5-6, Fig. 5-17, and Fig. 5-18 show the abrasion resistance of the tested mixtures measured using rotating cutters and sandblasting testing methods. It can be seen that both incorporated NPs were able to improve the abrasion resistance of the HPSDC. These enhancements reached their peak at 2% of NCS and 2% of NTD. By adding 2% of NCS, the abrasion depth measured using the rotating cutters test method was decreased by 24.9% and 27.6% at the 14-day and 28-day, respectively, compared to the control mixture. Similarly, the abrasion coefficient measured using the sandblasting approach, was less by 32.1% at the 28-day, compared to the control mixture. Whereas, by the inclusion of 2% of NTD, the abrasion depth measured using the rotating cutters test method was decreased by 25.9% and 26.3% at the 14-day and 28-day, respectively, compared to the control mixture. Similarly, the abrasion coefficient measured using the sandblasting approach was less by 33.5% at the 28-day, compared to the control mixture.

Table 5-6 Abrasion resistance results for the tested mixtures.

Mixture No.	Mixture designation	Rotating cutters method test (ASTM C944) "Average abrasion depth" (mm)		Sand blasting test (ASTM C418) "Average abrasion coefficient" (cm^3/cm^2)
		14-day	28-day	28-day
1	Control	0.321	0.304	0.170
2	0.5NCS	0.311	0.291	0.161
3	1NCS	0.291	0.273	0.153
4	1.5NCS	0.264	0.244	0.132
5	2NCS	0.241	0.220	0.115
6	2.5NCS	0.261	0.243	0.127
7	3NCS	0.277	0.255	0.154
8	0.5NTD	0.301	0.281	0.159
9	1NTD	0.281	0.281	0.146
10	1.5NTD	0.261	0.246	0.137
11	2NTD	0.238	0.224	0.113
12	2.5NTD	0.251	0.233	0.122
13	3NTD	0.273	0.251	0.169

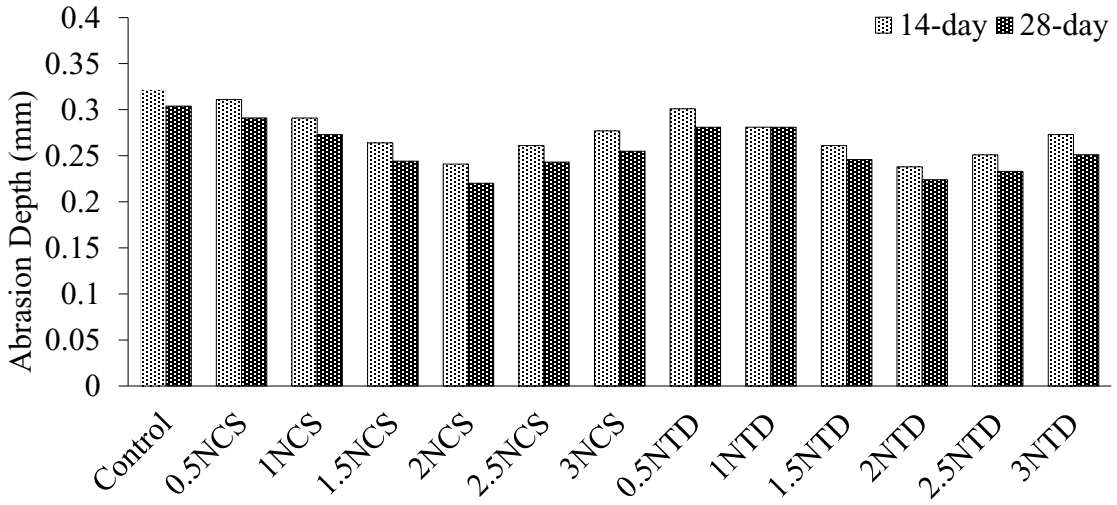

Fig. 5-17 Effect of inclusion of NPs on the abrasion depth (rotating cutters method) of the HPSDC.

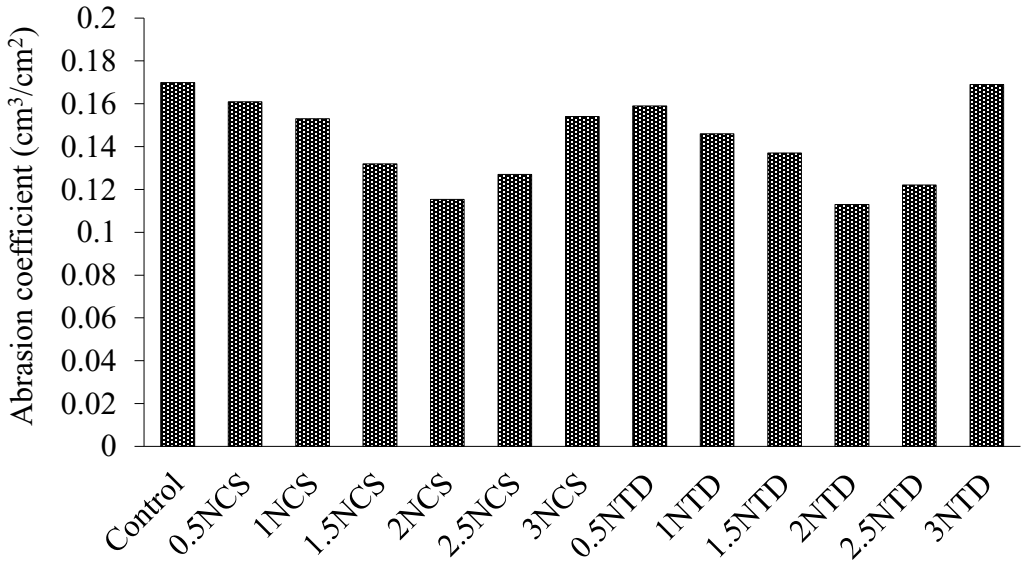

Fig. 5-18 Effect of inclusion of NPs on the abrasion coefficient (Sandblasting method) of the HPSDC.

These improvements are believed to be due to the ability of NPs, through its nucleation effect, to provide a more homogenous matrix. In addition, they are able to create

a more densified matrix through filling the nano sized voids. These effects could provide restriction on the particles movement and increase the energy required to dislocate the particles. That in turn leads to an overall improved concrete abrasion resistance. Furthermore, the NPs, as mentioned earlier, may have provided improvements to the fiber-matrix interface. CCSFs play an important role in the concrete abrasion resistance by providing protection for the other softer parts of the concrete. By enhancing CCSFs' interaction with the surrounding matrix, it may provide an even higher contribution to the concrete abrasion resistance improvements.

Moreover, it can be recognized that, un-similar to the compressive strength, STS, and FS, both NPs (at optimum ratios) had a similar impact on the HPSDC abrasion resistance even though the poor reactivity of the NTD. This may be attributed to the remarkably high hardness of the NTD particles themselves (around 38 GPa). Which provided an additional form of enhancement to the overall concrete abrasion resistance. It can be further noticed that NTD at 1% was the optimum ratio for all the mechanical properties of the HPSDC. However, for its abrasion resistance, the peak performance was attained at 2%. Which implies that, for abrasion resistance, the hardness of the NTD particles has the dominant role over the other effects.

It can be further noticed that the improvements in the concrete abrasion resistance tested under the rotating cutters method were less than the improvement attained under the sandblasting approach. This is mainly attributed to the different abrasion mechanisms that take place under each test (see Fig. 5-19). Because the paste has a lower hardness than the normal weight aggregate used in the rotating cutters technique, the normal weight

aggregate acts as a shield for the other concrete constituents. As a result, the other components are exposed to the abrasive less. When employing the sandblasting process, however, because the abrasive abrades the surface vertically, all concrete components are equally exposed to the abrasive. As a result, the paste and ITZ characteristics have a greater influence on the abrasion coefficient. In addition, as mentioned before, that the NPs may have provided enhancements to the fiber-matrix interface which may have provided a better bond between fibers and the surrounding matrix. In sandblasting approach, the fibers' bond is tested in a higher manner compared to the rotating cutter method. That may have led to a more pronounced impact of adding NPs while testing under sandblasting method.

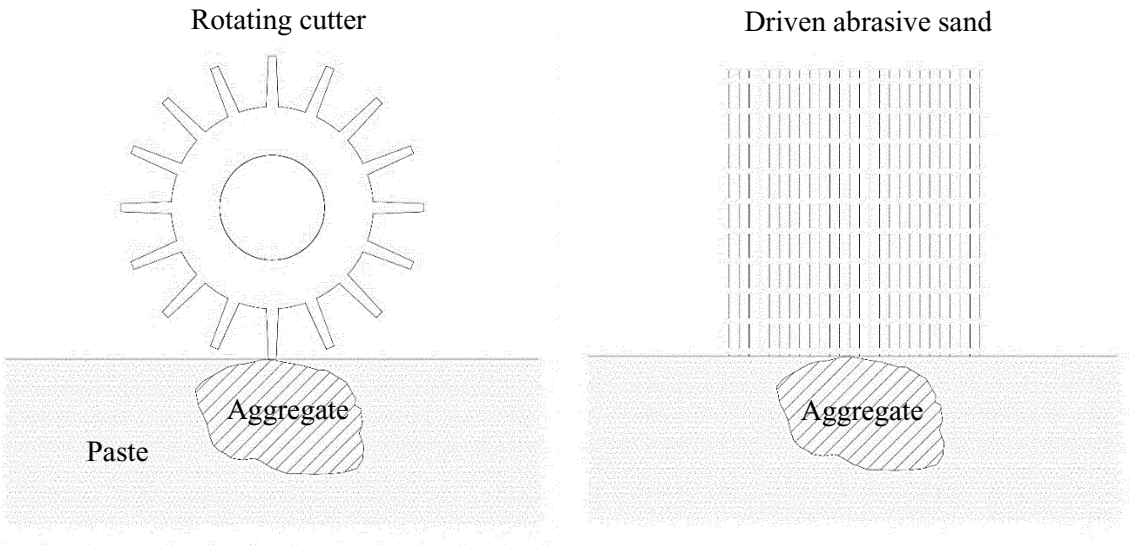

(a) Rotating cutters method (b) sandblasting method.

Fig. 5-19 Schematic figures of the abrasion testing mechanisms.

The impact of NPs addition on the concrete abrasion resistance is in agreement with other studies that used other testing approaches to assess the concrete abrasion resistance. (Ardalan et al. 2017) tested the concrete abrasion resistance using ASTM C1138 and found improvements by adding nano-SiO2 at the 28-day. Whereas, (Li, Zhang, and Ou 2006) conducted the abrasion resistance test according to (test method for abrasion resistance of concrete and its products, China) to assess the impact of adding nano-SiO2 and NTD. Remarkable improvements were found that were similar for both materials. The improvement in the concrete abrasion resistance reached 180.7% for the surface index and 173.3% for the side index. While (Y. Cheng and Shi 2019) tested the concrete abrasion resistance as per (T0567-2005 in Test Methods of Cement and Concrete for Highway Engineering (JTG E30-2005)). It was reported that by adding nano-SiO2, the abrasion rate was decreased 39.1% at the 84-dayEach abrasion test mimics a distinct abrasion mechanism, which is worth noting. The rotating cutters method (ASTM C944) represents the mechanism of traffic abrading a concrete surface. While sandblasting method (ASTM C418) simulates the waterborne abrasives.

5.5. Conclusions

This study assessed the impact of the addition of NPs (NCS and NTD) on the mechanical properties and the abrasion resistance of the HPSDC. NCS and NTD were incorporated at 0%, 0.5%, 1%, 1.5%, 2%, 2.5%, 3%. The mixtures incorporated MK, SF, and CCSFs at 15%, 8%, 0.5%, respectively. The compressive strength, STS, FS, SME, and DME were assessed using ASTM standards. Two ASTM tests were used to determine

abrasion resistance: the rotating cutters method as per ASTM C944 and sandblasting method as per ASTM C418. The following conclusions were reached based on the experimental findings:

1. Addition of NPs increased the SP and AEA demand. The SP demand reached 18.2% and 23.6% at 3% of NCS and 3% of NTD, respectively. While the AEA demand reached 8.3% 3% of NCS or 3% of NTD.

2. Inclusion of NPs enhanced the HPSDC compressive strength. The enhancements reached their peak at 2% of NCS and 1% of NTD. At 2% NCS, the compressive strength reached 6.6% on average, compared to the control mixture. While with 1% of NTD, it reached 4.7% on average, compared to the control mixture.

3. Using NCS and NTD had a similar impact on the HPSDC stiffness. The SME increased by 4.9% on average. While the DME improved by 3.5% on average compared to the control mixture.

4. Compared to the compressive strength and stiffness properties, adding NCS and NTD in the HPSDC had a higher impact on its tensile properties. The STS and FS reached their peak at 2% of NCS with 16.8% and 13.8%, respectively, on average, higher than the control mixture. While with adding 1% of NTD, the STS and FS increased by 7.6% and 7.3%, respectively, on average, higher than the control mixture.

5. Abrasion resistance of the HPSDC was the most positively impacted property by the addition of NPs. An improvement of 26.3%, on average, in the abrasion depth (rotating

cutters approach), and 32.1% in the abrasion coefficient (sandblasting approach) were detected by adding NCS at 2%. Whereas by adding 2% of NTD, improvements of 26.1%, on average, in the abrasion depth (rotating cutters approach), and 33.5% in the abrasion coefficient (sandblasting approach) were found.

5.6. References

"ACI 318-14." 2014. Building Code Requirements for Structural Concrete (ACI 318-14). American Concrete Institute.

Aly, M, M S J Hashmi, A G Olabi, M Messeiry, E F Abadir, and A I Hussain. 2012. "Effect of Colloidal Nano-Silica on the Mechanical and Physical Behaviour of Waste-Glass Cement Mortar." Materials & Design 33: 127–35. https://doi.org/https://doi.org/10.1016/j.matdes.2011.07.008.

Ardalan, R. Bani, N. Jamshidi, H. Arabameri, A. Joshaghani, M. Mehrinejad, and P. Sharafi. 2017. "Enhancing the Permeability and Abrasion Resistance of Concrete Using Colloidal Nano-SiO2 Oxide and Spraying Nanosilicon Practices." Construction and Building Materials 146: 128–35. https://doi.org/10.1016/j.conbuildmat.2017.04.078.

"ASTM C1017." 2013. Standard Specification for Chemical Admixtures for Use in Producing Flowing Concrete.

"ASTM C1138." 2019. Standard Test Method for Abrasion Resistance of Concrete (Underwater Method). 2019. https://doi.org/10.1520/C1138M-19.

"ASTM C1240." 2020. Standard Specification for Silica Fume Used in Cementitious Mixtures. https://doi.org/10.1520/C1240-20.

"ASTM C143." 2020. Standard Test Method for Slump of Hydraulic-Cement Concrete. https://doi.org/10.1520/C0143_C0143M-20.

"ASTM C150." 2022. Standard Specification for Portland Cement. https://doi.org/10.1520/C0150_C0150M-22.

"ASTM C215." 2019. Standard Test Method for Fundamental Transverse, Longitudinal, and Torsional Resonant Frequencies of Concrete Specimens. https://doi.org/10.1520/C0215-19.

"ASTM C231." 2022. Standard Test Method for Air Content of Freshly Mixed Concrete by the Pressure Method. 2022. https://doi.org/10.1520/C0231_C0231M-22.

"ASTM C260." 2016. Standard Specification for Air-Entraining Admixtures for Concrete. https://doi.org/10.1520/C0260_C0260M-10AR16.

"ASTM C33." 2018. Standard Specification for Concrete Aggregates. https://doi.org/10.1520/C0033_C0033M-18.

"ASTM C39." 2021. Standard Test Method for Compressive Strength of Cylindrical Concrete Specimens. https://doi.org/10.1520/C0039_C0039M-21.

"ASTM C418." 2020. Standard Test Method for Abrasion Resistance of Concrete by Sandblasting. https://doi.org/10.1520/C0418-20.

"ASTM C469." 2022. Standard Test Method for Static Modulus of Elasticity and Poisson's Ratio of Concrete in Compression. https://doi.org/10.1520/C0469_C0469M-22.

"ASTM C494." 2022. Standard Specification for Chemical Admixtures for Concrete. https://doi.org/10.1520/C0494_C0494M-19E01.

"ASTM C496." 2017. Standard Test Method for Splitting Tensile Strength of Cylindrical Concrete Specimens. https://doi.org/10.1520/C0496_C0496M-17.

ASTM C618. 2022. "ASTM C618." Standard Specification for Coal Fly Ash and Raw or Calcined Natural Pozzolan for Use. https://doi.org/10.1520/C0618-22.

"ASTM C78." 2022. Standard Test Method for Flexural Strength of Concrete (Using Simple Beam with Third-Point Loading). https://doi.org/10.1520/C0078_C0078M-22.

"ASTM C944." 2019. Standard Test Method for Abrasion Resistance of Concrete or Mortar Surfaces by the Rotating-Cutter Method. https://doi.org/10.1520/C0944_C0944M-19.

Bogas, Jose, and Augusto Gomes. 2014. "Static and Dynamic Modulus of Elasticity of Structural Lightweight and Modified Density Concrete with and without Nanosilica – Characterization and Normalization" IJCE 12 (2): 170–80. http://ijce.iust.ac.ir/article-1-743-en.html.

Cheng, Youkun, and Zhenwu Shi. 2019. "Experimental Study on Nano-SiO 2 Improving Concrete Durability of Bridge Deck Pavement in Cold Regions." Advances in Civil Engineering 2019. https://doi.org/10.1155/2019/5284913.

Fernandes, J.F., T. Bittencourt, and P. Helene. 2008. "A Review of the Application of Concrete to Offshore Structures." ACI Symposium Publication 253. https://doi.org/10.14359/20187.

Gaitero, J J, I Campillo, and A Guerrero. 2008. “Reduction of the Calcium Leaching Rate of Cement Paste by Addition of Silica Nanoparticles.” Cement and Concrete Research 38 (8): 1112–18. https://doi.org/https://doi.org/10.1016/j.cemconres.2008.03.021.

Gautier, Donald L, Kenneth J Bird, Ronald R Charpentier, Arthur Grantz, David W Houseknecht, Timothy R Klett, Thomas E Moore, et al. 2009. “Assessment of Undiscovered Oil and Gas in the Arctic.” Science 324 (5931): 1175 LP – 1179. https://doi.org/10.1126/science.1169467.

Gonzalez, Marcelo, Arthur De Oliveira Lima, and Susan L. Tighe. 2014. “Nanoconcrete for Rigid Pavements: Abrasion Response and Impact on Friction.” Transportation Research Record 2441: 28–37. https://doi.org/10.3141/2441-05.

Haruehansapong, Sattawat, Tawich Pulngern, and Somchai Chucheepsakul. 2014. “Effect of the Particle Size of Nanosilica on the Compressive Strength and the Optimum Replacement Content of Cement Mortar Containing Nano-SiO2.” Construction and Building Materials 50: 471–77. https://doi.org/https://doi.org/10.1016/j.conbuildmat.2013.10.002.

Hoff, G. C., and R. Elimov. 1995. “Concrete Production for the Hibernia Platform.” In Annual Conference- Canadian Society for Civil Engineering, 693–716.

Jo, Byung-Wan, Chang-Hyun Kim, Ghi-ho Tae, and Jong-Bin Park. 2007. “Characteristics of Cement Mortar with Nano-SiO2 Particles.” Construction and Building Materials 21 (6): 1351–55. https://doi.org/https://doi.org/10.1016/j.conbuildmat.2005.12.020.

Kawashima, Shiho, Jung-Woo Ted Seo, David Corr, Mark C Hersam, and Surendra P Shah. 2014. “Dispersion of CaCO3 Nanoparticles by Sonication and Surfactant Treatment for Application in Fly Ash–Cement Systems.” Materials and Structures 47 (6): 1011–23. https://doi.org/10.1617/s11527-013-0110-9.

Korayem, A. H., N. Tourani, M. Zakertabrizi, A. M. Sabziparvar, and W. H. Duan. 2017. “A Review of Dispersion of Nanoparticles in Cementitious Matrices: Nanoparticle Geometry Perspective.” Construction and Building Materials 153: 346–57. https://doi.org/10.1016/j.conbuildmat.2017.06.164.

Lan, C, H Li, and Y Ju. 2009. “Ductility of High Strength Concrete Containing Nano-Particles.” In Proc.SPIE. Vol. 7493.

Li, Hui, Mao-hua Zhang, and Jin-ping Ou. 2006. “Abrasion Resistance of Concrete Containing Nano-Particles for Pavement.” Wear 260 (11): 1262–66. https://doi.org/https://doi.org/10.1016/j.wear.2005.08.006.

Li, Hui, Mao-hua Zhang, and Jin-ping Ou. 2007. “Flexural Fatigue Performance of Concrete Containing Nano-Particles for Pavement.” International Journal of Fatigue - INT J FATIGUE 29 (July): 1292–1301. https://doi.org/10.1016/j.ijfatigue.2006.10.004.

Lin, D F, K L Lin, W C Chang, H L Luo, and M Q Cai. 2008. “Improvements of Nano-SiO2 on Sludge/Fly Ash Mortar.” Waste Management 28 (6): 1081–87. https://doi.org/https://doi.org/10.1016/j.wasman.2007.03.023.

Madani, Hesam, Alireza Bagheri, Tayebeh Parhizkar, Amirmaziar Raisghasemi, and Aliakbar Ramezanianpoor. 2013. “The Aggregation Status of Nanosilicas and Silica Fume, Used in Cementitious Mixtures.” Sustainable Construction Materials and Technologies 2013-Augus.

Mishra, Archana, and Shivanshu Tiwari. 2018. “Effect on Flexural Strength of Concrete by Addition of Nano Titanium Dioxide and Nano Calcium Carbonate.” International Journal of Science and Research (IJSR) 7 (3): 1184–86. https://doi.org/10.21275/ART2018841.

Nazari, Ali. 2011. “The Effects of Curing Medium on Flexural Strength and Water Permeability of Concrete Incorporating TiO2 Nanoparticles.” Materials and Structures/Materiaux et Constructions 44 (May): 773–86. https://doi.org/10.1617/s11527-010-9664-y.

Riahi, Shadi, and Ali Nazari. 2011. “Compressive Strength and Abrasion Resistance of Concrete Containing SiO2 and CuO Nanoparticles in Different Curing Media.” Science China Technological Sciences 54 (9): 2349–57. https://doi.org/10.1007/s11431-011-4463-4.

Sandvik, M., T. Hovda, and S. Smeplass. 1994. “Modified Normal Density (MND) Concrete for the Troll GBS Platform.” ACI Symposium Publication 149: 81–102. https://doi.org/10.14359/4069.

Senff, L, D Hotza, S Lucas, V M Ferreira, and J A Labrincha. 2012. “Effect of Nano-SiO2 and Nano-TiO2 Addition on the Rheological Behavior and the Hardened Properties of

Cement Mortars." Materials Science and Engineering: A 532: 354–61. https://doi.org/https://doi.org/10.1016/j.msea.2011.10.102.

Shih, Jeng-Ywan, Ta-Peng Chang, and Tien-Chin Hsiao. 2006. "Effect of Nanosilica on Characterization of Portland Cement Composite." Materials Science and Engineering: A 424 (1): 266–74. https://doi.org/https://doi.org/10.1016/j.msea.2006.03.010.

Sobolev, K., I. Flores, L. M. Torres-Martinez, P. L. Valdez, E. Zarazua, and E. L. Cuellar. 2009. "Engineering of SiO2 Nanoparticles for Optimal Performance in Nano Cement-Based Materials." Nanotechnology in Construction 3, 139–48. https://doi.org/10.1007/978-3-642-00980-8_18.

Thomas, Jeffrey J, Hamlin M Jennings, and Jeffrey J Chen. 2009. "Influence of Nucleation Seeding on the Hydration Mechanisms of Tricalcium Silicate and Cement." The Journal of Physical Chemistry C 113 (11): 4327–34. https://doi.org/10.1021/jp809811w.

Craig, Peter and Wolfe, Bill. 2012. "Another Look at the Drying of Lightweight Concrete-A Comparison of Drying Times for Normal weight and Lightweight Floors." Concrete International: 53–58.

Zhang, Mao-hua, and Hui Li. 2011. "Pore Structure and Chloride Permeability of Concrete Containing Nano-Particles for Pavement." Construction and Building Materials 25 (2): 608–16. https://doi.org/https://doi.org/10.1016/j.conbuildmat.2010.07.032.

Zhang, Min-Hong, Jahidul Islam, and Sulapha Peethamparan. 2012. "Use of Nano-Silica to Increase Early Strength and Reduce Setting Time of Concretes with High Volumes of

Slag." Cement and Concrete Composites 34 (5): 650–62. https://doi.org/https://doi.org/10.1016/j.cemconcomp.2012.02.005.

Zhao, Zheng, Jie Kong, and Hong Yang. 2012. "Study on Frost Resistance of Nano SiO2 Cement Concrete." Applied Mechanics and Materials 198–199 (September): 48–51. https://doi.org/10.4028/www.scientific.net/AMM.198-199.48.

Chapter 6 Finite element analysis for the flexural behavior of two layers concrete beam

6.1. Abstract

In this paper, a finite element model (FEM) was developed to investigate the flexural behavior of two layers composite beams made of two different types of concrete. The upper concrete layer is added to act as an ice shield against abrasion damage. FEM was carried out using Abaqus software using nonlinear static analysis. The FEM is based on the theoretical context of the concrete damaged plasticity (CDP) model. The validity of the proposed FEM was established by comparing the FEM results with experimental test results. The proposed FEM predictions showed good agreement with the experimental results, in particular, crack pattern, load-deflection response, and beam's ultimate bending capacity. Finally, a parametric study that explored the effect of changing the concrete type and beam's thickness on the flexural behavior of the beam. The results revealed that changing the beam's thickness or the addition of another concrete layer has an effect on the beams' ultimate bending capacity. Changing the concrete type also had an impact on the beam's bending capacity.

Keywords: Finite element; Abaqus; Concrete damaged plasticity; Load-deflection response.

6.2. Introduction

The usage of concrete is wide and covers many construction applications. However, each application requires concrete with specific requirements as it is subjected to different types of loading actions. For example, in a harsh environment, offshore structural concrete is subjected to abrasion action that is a result of interacting with moving ice sheets. This contact might result in major wear, which could result in damage, increased maintenance costs, and a shortened life cycle. The 1.3 billion-dollar (CAN) Confederation Bridge in Canada, which connects Prince Edward Island to the mainland in New Brunswick, is an example of a construction in an ice-infested sea. This is the world's longest concrete bridge over ice-covered water. Due to interacting with floating ice sheets, monitoring of the bridge detected minor wear damage to the concrete pillars at the water's edge. Work on cleanup and restoration has previously been planned and is currently underway.

Limiting abrasion damage due to interacting with ice may have different approaches. The first approach that may come to mind is to enhance the ability of the concrete, used in such an environment, to resist such abrasion damage. This can be done by optimizing the concrete composition or incorporating different types of additives. Through a previous phase of the current research, this method was proposed and covered. However, the cost of such a technique may set a limitation on its applicability. On the other hand, as the external layer is the layer that is subjected to the abrasion process, another approach to limit abrasion damage may be implemented. Which is by using a high abrasion-resistant external layer while keeping the concrete as an internal layer. Such a technique was applied at the

Confederation Bridge by adding steel shields around the concrete piers. However, the steel shields got corroded and were separated from some piers. On the contrary, using an external layer of concrete that has relatively higher abrasion resistance, attached to the internal lower cost concrete, maybe a good alternative. That technique will be the focus of the current investigation. The main issue that needs to be achieved in such a technique is to provide full attachment of the external layer to the internal layer. This can be said from a structural point of view, to achieve a composite section.

A composite section is a section of two or more layers acting together. Concrete composite sections are usually used in the rehabilitation and strengthening of old elements. The major concern about a composite section is the horizontal shear transfer between its layers. The horizontal shear stresses are transferred through shear friction, cohesion between the two layers, and dowel action provided using reinforcement at the interface. The behavior of a composite section has two boundaries. The maximum benefit occurs when there is absolutely no slippage between the layers (fully composite action). Achieving composite action results in a system that is stronger than the sum of the section's parts. On the contrary, if a slip occurs, the section's parts will act as two separate beams above each other resulting in less load-carrying capacity.

By reviewing the literature, various studies were found that investigated the behavior of two layers reinforced concrete beams experimentally. In 1990, (Saiidi, Vrontinos, and Douglas 1990) experimentally investigated the behavior of reinforced concrete beam that is strengthened with a concrete layer in the compression and tension zones. (Iskhakov et

al. 2014) conducted an experimental study for two layers beams with high strength concrete layer above a normal strength concrete layer. (Iskhakov, Ribakov, and Holschemacher 2017) studied the behavior of two spans composite beams with high strength concrete in the compression zone. (Hamed 2018) proposed using ultra-high-performance concrete (UHPC) as a top layer for composite beams, while using high performance fiber reinforced concrete as the bottom layer. That study was originally performed for the use of UHPC as an ice shield against abrasion damage. UHPC is an advanced type of concrete. It has high cement content, no coarse aggregate, low water to binder ratio. It is characterized by high compressive strength (above 150 MPa), high durability and superior abrasion resistance. These characteristics make it attractive for being implemented as an ice shield for offshore structures. Through that study, the effect of changing the top layer thickness, type of shear connector, and spacing between shear connectors were examined. Experimental results of that study will be used in the current investigation to verify the proposed FE model. Further details about that study can be found in the next sections. (Lam and Do 2019) investigated the suitable position (upper layer or lower layer) of the fiber reinforced concrete layer with respect to the normal strength concrete layer so that the sliding between them is minimal while loading. That investigation was carried out experimentally and using FEM with ANSYS software. (Iskhakov et al. 2019) experimentally investigated the behavior of the two layers concrete beam. The study focused on testing prestressed full-scale beams under four points bending. Normal strength concrete was used at the tension zone while high strength concrete incorporating steel fibers was used at the compression zone. Results were compared with non-prestressed beams. Results of that study showed no de-bonding

between the two layers up to the ultimate limit state which demonstrated proper interaction between the two layers. Although experimental testing results in real-life response, testing full-scale composite beams is sophisticated and requires large-scale facilities and it is also considered to be costly and time-consuming. On the other hand, the FEM is considered to be a more time and cost-effective tool. FEM could enable us to confidently predict reinforced concrete beams' behavior without experimental proof which makes it a viable alternative.

It was found that multilayered concrete beams in various forms were previously investigated using FE. For instance, many studies were found that investigated the behavior of reinforced concrete beams strengthened with fiber reinforced polymers (FRP) using FE. (Sasmal, Kalidoss, and Srinivas 2012) investigated the behavior of reinforced concrete beams strengthened with carbon fiber reinforced polymer (CFRP) using FE. The results were compared to beams reinforced with ferrocement. The data was reported in the form of load-deflection behavior and ultimate load capacity. Remarkable enhancement was found in the ultimate load capacity using CFRP strengthening. Other studies were also conducted to investigate the ability of FEA to capture the behavior of reinforced concrete beams strengthened with FRP using FE such as (Barour and Zergua 2019), (Parandaman and Jayaraman 2014), and (Barour et al. 2019). In addition, two layers beams that consist of concrete and other materials were previously investigated using FE. (Anju and Smitha 2016) studied the composite action of a concrete slab and rolled up steel sections using FE. In that study, four different types of shear connectors were used and evaluated. (Katwal, Tao, and Hassan 2018) developed a FEM to study steel-concrete composite beams using

FE. The model developed can predict load-deformation behavior and the shear force-slip relationship. Also, the behavior of timber-concrete beams was studied using FE (Khorsandnia, Valipour, and Crews 2012) and (Khorsandnia, Valipour, and Crews 2014). Furthermore, multilayers beams made of different types of concrete were explored. (Vu et al. 2019) carried out a study investigating the cracking resistance of three layers beams. The middle layer was made from lightweight concrete with a strength of 1.15 MPa. While the external layers were made using 21.5 MPa concrete reinforced with glass fiber reinforced polymer bars and compared to using conventional steel bars. It was found that the cracking resistance was enhanced using glass fiber reinforced polymer bars compared to using steel bars. However, to the best of the authors' knowledge, the flexural behavior of two layers reinforced concrete beam using FE is not yet investigated.

The current study investigates the flexural behavior of fully composite two layers concrete beams using FEM. The upper concrete layer is added to act as an ice shield against abrasion damage. Using relatively higher strength concrete in the compression zone, compared to the lower strength concrete in the tension zone, has three advantages: It acts as an ice shield against abrasion damage, it strengthens the beam's bending capacity, and it provides a more cost-effective section. Numerical simulations were carried out using commercial software Abaqus standard 6.14. Abaqus software was used as it is a powerful engineering simulation program. It is based on the finite element method that can simulate linear and nonlinear analyzes. Modeling of concrete material was carried out using CDP model available in Abaqus software. The CDP model assumes isotropic material's behavior. It considers two failure mechanisms: compressive crushing and tensile cracking.

The FEM results are presented in terms of the crack patterns, load versus deflection behavior, beams uncracked stiffness, yield load, yield deflection, cracked stiffness, and ultimate load capacity. As mentioned earlier, the FE results were validated using the experimental data obtained in (Hamed 2018). Finally, a parametric analysis was conducted to explore the impact of different variables on the load deflection behavior of the composite beams. The main objective of the numerical study is to provide a practical solution for the abrasion damage problem. Results of the current study could provide a recommendation of the two layer composite section to be implemented for offshore structures.

6.3. Concrete properties

The properties of three different types of concrete mixtures were used; normal strength concrete (NSC), high performance concrete (HPC), and UHPC. NSC and HPC mixtures were developed, and their properties were tested through an earlier stage of the current investigation. Both NSC and HPC were made of specified density concrete. Specified density concrete type of concrete is made with partial replacement of normal weight coarse aggregate with lightweight aggregate to make it suitable for offshore structural applications. Table 6-1 presents the composition of the developed NSC and HPC mixtures.

Table 6-1 Composition of the developed NSC and HPC mixtures.

Concrete type	Binder content (Kg/m^3)	Coarse to fine aggregate ratio	Fibers type and volumetric ratio
NSC	300	1.2	_
HPC-63	550	1	_
HPC-86	550	1.6	CCSFs at 0.3%

Where CCSFs= copper coated steel fibers

Mechanical properties of the developed mixtures were tested; compressive strength according to ("ASTM C39" 2021), splitting tensile strength according to ("ASTM C496" 2017), and modulus of elasticity according to ("ASTM C469" 2022) were performed, each on three identical cylinders. Tested concrete mechanical properties are shown in Table 6-2.

Table 6-2 Tested concrete mechanical properties.

Concrete type	Compressive strength (MPa)	Modulus of elasticity (GPa)	Splitting tensile strength (MPa)
NSC	33.3	25.8	3.1
HPC-63	63.2	30.7	3.3
HPC-86	86.4	41.2	6.2
*UHPC	167.4	58.2	14.5

*The mechanical properties of the UHPC was used as tested by (Hamed 2018).

6.4. Tested specimens' properties.

Various flexural specimens, composite and non-composite, were cast and tested by (Hamed 2018). The experimental testing results of four beams were used for the verification of the proposed FE model. In Hamed's investigation, non-composite beams consisting of HPC mixture which had the same properties as the previously mentioned HPC-86 mixture were tested. While composite beams had UHPC mixture as the top layer and HPC or NSC mixture as the bottom layer. All specimens were 300 mm in width and 1950 mm in length with variable overall thickness depending on the top layer thickness. These beams had a total thickness of 230 mm and 255 mm and were reinforced with four 15 mm bar at the bottom and two 10 mm bars at the top. 10M two-legged stirrups at 200 mm were used as shear reinforcement for the two non-composite beams. For composite beams, the top layer was of UHPC with two different thicknesses (50 mm and 75 mm). This layer had a reinforcement of 10M mesh in the middle. T-headed studs shear connectors were used to achieve composite action for the beams. The beams were tested experimentally using four-point loading where the load was applied using MTS hydraulic actuator. Linear variable differential transducers (LVDTs) were used to measure the deflection of all the specimens while testing. The spacing between the two loading points was 130 mm. Whereas, the supports were 75 mm away from the specimen face on both sides leaving an 1800 span. Geometrical and reinforcement details of the typical composite and non-composite specimens are shown in Fig. 6-1.

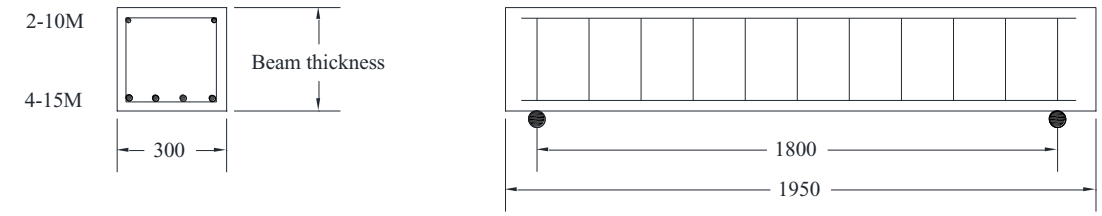

(a)

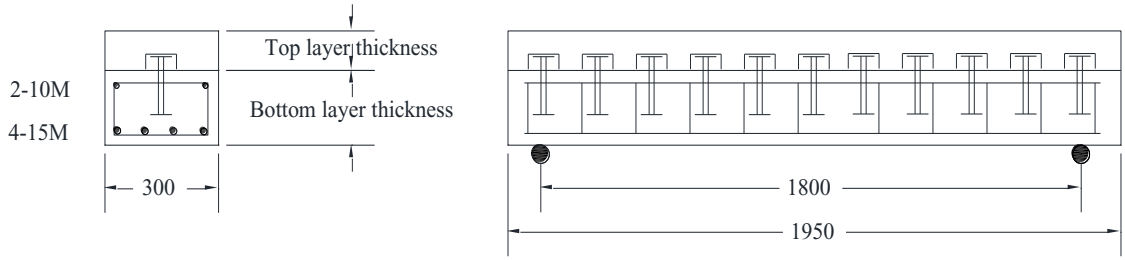

(b)

Fig. 6-1 Details of typical beams tested by (Hamed 2018) in mm (a) non-composite beam and (b) composite beam.

6.5. Finite element modeling

6.5.1. General methodology

Numerical simulations of the two layers reinforced concrete beam was carried out using commercial software Abaqus standard 6.14. Modeling of specimens, the concrete material models, boundary conditions, and geometrical and material parameters will be discussed in detail in the following sections. Concrete material was modeled using C3D8R elements. These reduced integration elements with hourglass control were used to control shear locking. Reinforcement was modeled using T3D3 elements. The concrete damaged plasticity model available in Abaqus was used for the numerical simulations.

6.5.2. Modeling of layers interface

Surface-to-surface interactions were adopted to model the contact between the two concrete layers. For normal interaction between the two layers, hard contact with no penetration was defined. As mentioned earlier, shear stresses are transferred through shear friction, cohesion between the two layers, and dowel action provided using reinforcement at the interface. Shear studs were modeled as solid elements. In the tangential direction, penalty friction with a 0.15 friction coefficient was assumed. The contact in the tangential direction is defined in Abaqus is based on the Coulomb friction model. The fundamental idea behind the Coulomb friction model is to link the contact pressure between the contacting bodies to the maximum permissible frictional (shear) stress across an interface. Prior to starting to slide relative to one another, two contacting surfaces can carry shear forces across their interface up to a certain magnitude.

6.5.3. FE Model's geometry, boundary conditions, and loading

Due to symmetry, only half the beam was modeled to reduce computational time. Figure 6-2 shows the applied displacement and boundary conditions.

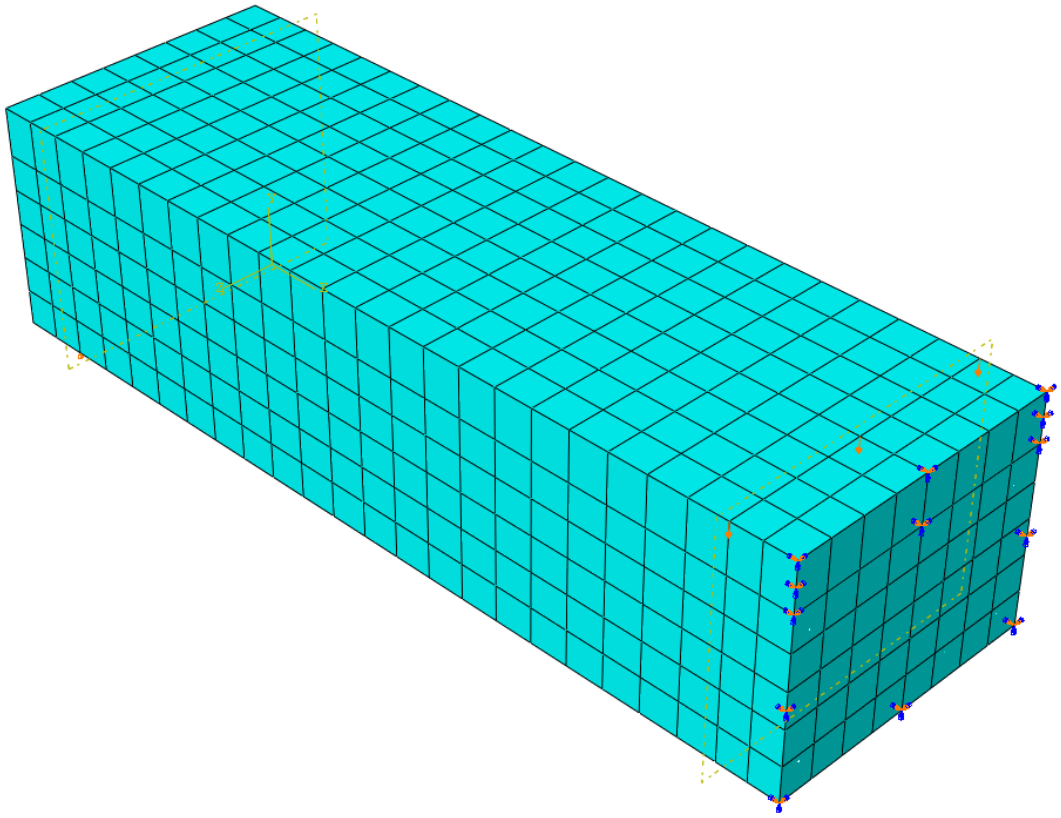

Figure 6-2 Applied displacement and boundary conditions of a typical composite two layers specimen.

The boundary conditions were applied along the lines of supports and loadings and the symmetry surface. The supports were modeled as roller supports where translation in y and z directions were constrained. An induced displacement was applied on the top of the beam to achieve displacement-controlled testing. Embedded region constraint was used to define the bonding of reinforcing bars with the surrounding concrete as shown in Fig. 6-3.

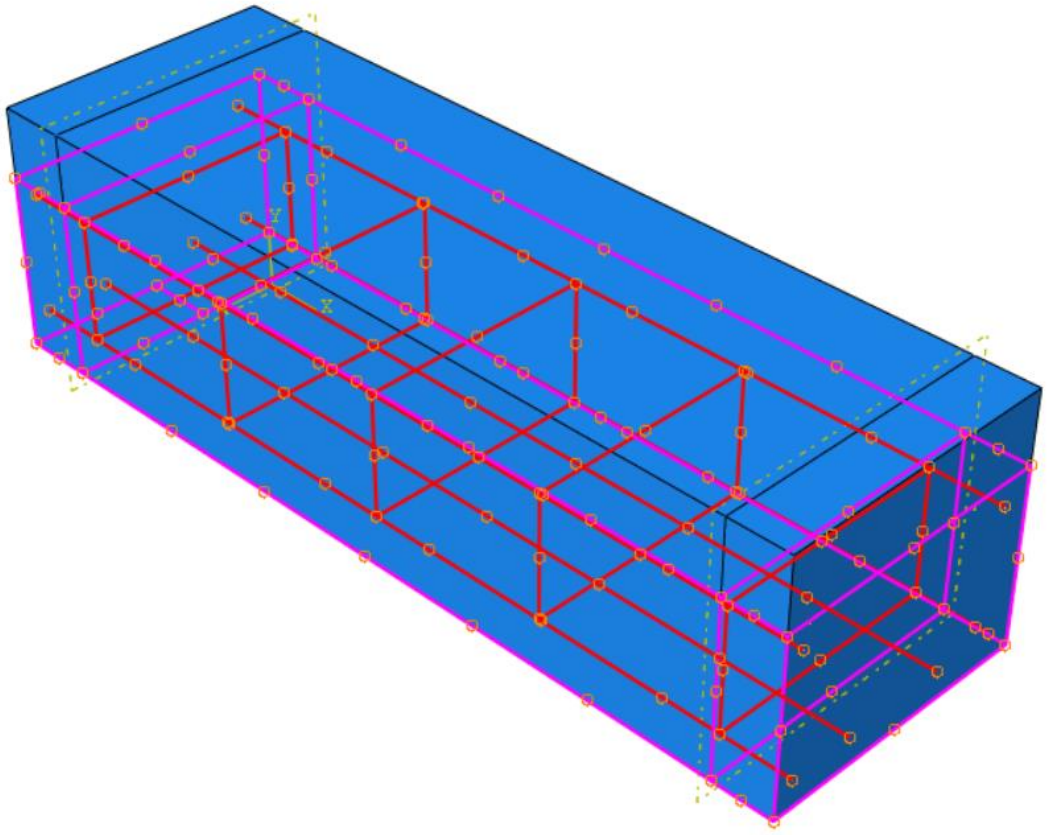

Fig. 6-3 Interaction between reinforcement and surrounding concrete.

Under compressive stresses, due to the formation of microcracks, concrete behavior is divided into two parts. The first part was assumed to be linear elastic up to the proportionality limit. The proportionality limit was assumed to be 0.4 f_c', as per ("CSA-A23.3-14" 2014), where f_c' is the compressive strength of a standard size concrete cylinder. The elastic behavior of the concrete in compression was defined using Poisson's ratio of 0.2 and the modulus of elasticity mentioned in Table 6-1. CDP model was adopted for the current study.

6.5.3. Concrete Damaged Plasticity (CDP) Model

The model is based on the classical theory of plasticity and can define compression and tension degradation and treat them separately. CDP model is widely accepted for modeling the nonlinear behavior of reinforced concrete (Piscesa, Attard, and Samani 2017). The required information in the CDP model is in terms of inelastic strain which is the total strain minus the elastic strain. Abaqus automatically converts the values of the entered inelastic strains to plastic strains using damage parameters in compression (d_c) and in tension (d_t). The values of d_c and d_t were calculated based on the following equation.

$$d_c = 1 - (f_c / f_c^{'}) \tag{6-1}$$

$$d_t = 1 - (\sigma_t / \sigma_{t0}) \tag{6-2}$$

Where f_c is the attained compressive stress at a specific time, $f_c^{'}$ is the concrete compressive strength, σ_t is the attained tensile stress at a specific time, and σ_{t0} is the tensile strength.

The CDP model in Abaqus consists of plastic behavior, compressive behavior, and tensile behavior of concrete. These behaviors are discussed in the following sections.

6.5.4.1. Plastic Behavior of concrete

The parameters required to define the plasticity model are as follows: dilation angle, eccentricity, fb0/fc0, K, and viscosity parameter. Dilation angle is the ratio between the material's volume change to its shear strain. Through investigating the literature, it was found that for concrete, the typical value of dilation angle used was found to be 30^o to 40^o. The value of the dilation angle used for concrete in the current study was 35^o. The eccentricity was assumed to be 0.1, which is the default value used in Abaqus. In the CDP model, the value fb0/fc0 represents the strength of the material under biaxial stress to its strength under uniaxial stress. (Hussein 1998) studied the biaxial compressive response of high-strength concrete with compressive strength of up to 100 MPa. It was concluded that the value of fb0/fc0 is from around 1.1 to 1.2. While (Papanikolaou and Kappos 2007) proposed Eq. 6-3 based on large statistical data analysis.

$$\frac{f_{b0}}{f_{c0}} = 1.5(f_c^{'})^{-0.075} \tag{6-3}$$

Where $f_c^{'}$ is the concrete compressive strength.

Eq. 6-3 also results in fb0/fc0 in the same range of 1.1 to 1.2. Thus, in the current investigation, the Abaqus default value of 1.16 was utilized. Whereas the shape factor of the yielding surface in the deviatoric plane (K) was assumed as 0.667. While the viscosity parameter was taken as 0.0005.

6.5.4.2. Compressive and tensile behavior of concrete

It is not always possible to clearly identify the behavior of concrete under compression experimentally. There are numerous models proposed to define the compressive stress strain curve mathematically. The model proposed by (Collins and Mitchell 1997) was adopted in the current study due to its ability to well represent concrete of different strengths. This model is represented by Eq. (6-4).

$$\frac{f_c}{f_c^{'}} = \frac{n\left(\frac{\varepsilon_c}{\varepsilon_0}\right)}{n-1+\left(\frac{\varepsilon_c}{\varepsilon_0}\right)^{nk}} \tag{6-4}$$

where,

ε_0 = concrete strain at $f_c^{'}$

n = curve fitting factor = $0.8 + f_c^{'}/17$

k = stress post peak decay factor, taken as 1.0 for $\varepsilon_c/\varepsilon_0 < 1$ and as $0.67 + f_c^{'}/62$ for $\varepsilon_c/\varepsilon_0 > 1$

On the other hand, to simulate the tensile behavior of the concrete, the stress-strain relationship proposed by (Nayal and Rasheed 2006), which was modified by (Wahalathantri et al. 2011) was adopted. This relationship is shown in Fig. 6-4.

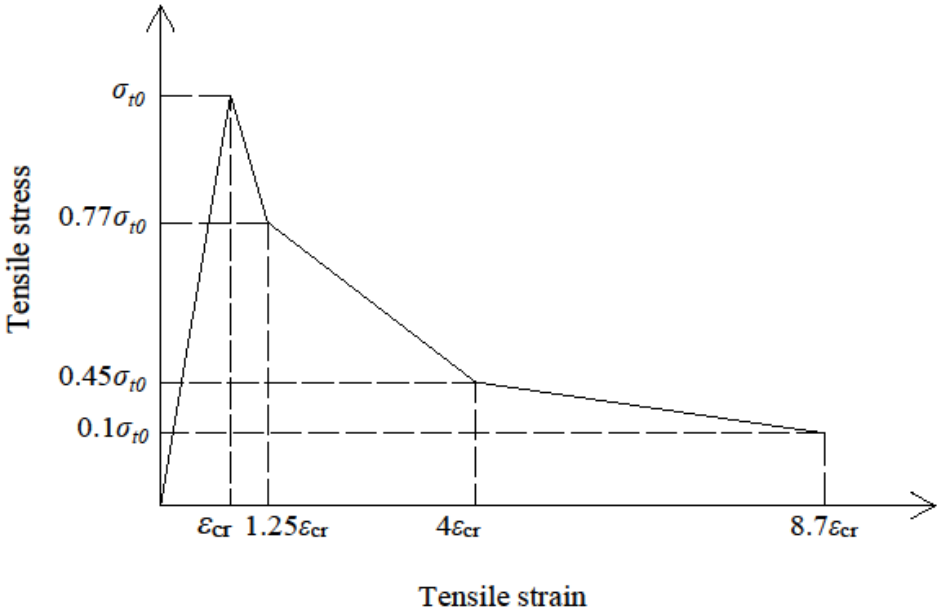

Fig. 6-4 Tension stiffening model proposed by Nayal and Rasheed (Nayal and Rasheed 2006).

The ultimate tensile strength was taken as the value obtained from the splitting tensile test. The mentioned models representing the compressive and tensile behaviors of concrete were adopted for the three types of concrete mixtures NSC, HPC, and UHPC.

6.5.4. Modelling of reinforcement

Truss elements for the reinforcement (RFT) were utilized. The RFT stress-strain behavior was modeled as trilinear elastic-plastic. In the elastic region, modulus of elasticity of 200 GPa, Poisson's ratio of 0.3, and yield stress of 400 MPa were used. In the plastic region, the tangent modulus was assumed to be one-tenth of the elastic modulus. This assumption was also adopted by (Alam 2010) and provided acceptable results for the beam's overall flexural behavior. The behavior was assumed to be perfectly plastic after

reaching the ultimate strength. The behavior of steel reinforcement was assumed to be identical in tension and compression. The RFT was modeled as an embedded region inside the concrete. A perfect bond between the RFT and the surrounding concrete was assumed.

6.6. Results and discussion

6.6.1. Effect of element size

A mesh convergence study was performed to study the dependency of the results on the mesh size in the same manner carried out by (Alam 2010). Five mesh sizes (30 mm, 40 mm, 50 mm, 60 mm, and 70 mm) were used. Mesh size that is less than 30 mm was not analyzed, as according to (Bažant and Oh 1983), element size should be larger than three times the maximum aggregate size which is 10 mm in the current study. Figure 6-5 displays a FEM deformed typical beam specimen at the end of loading. Figure 6-6 shows FE analysis load deflection behavior with different element sizes and the experimental results of a typical specimen.

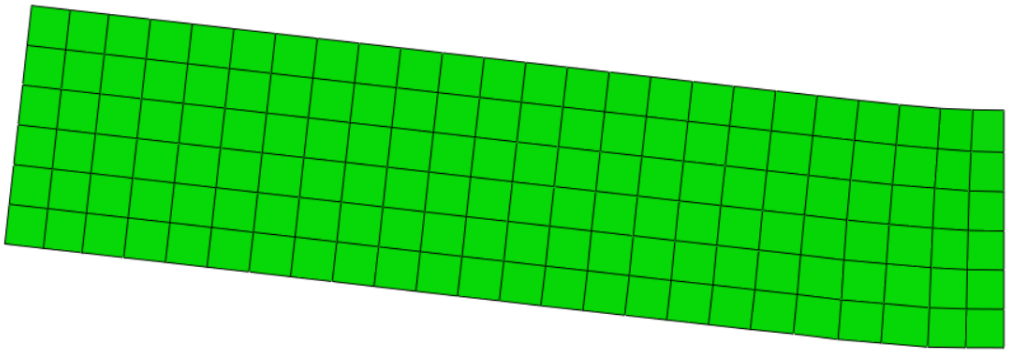

Figure 6-5 FEM deformed typical beam specimen at the end of loading

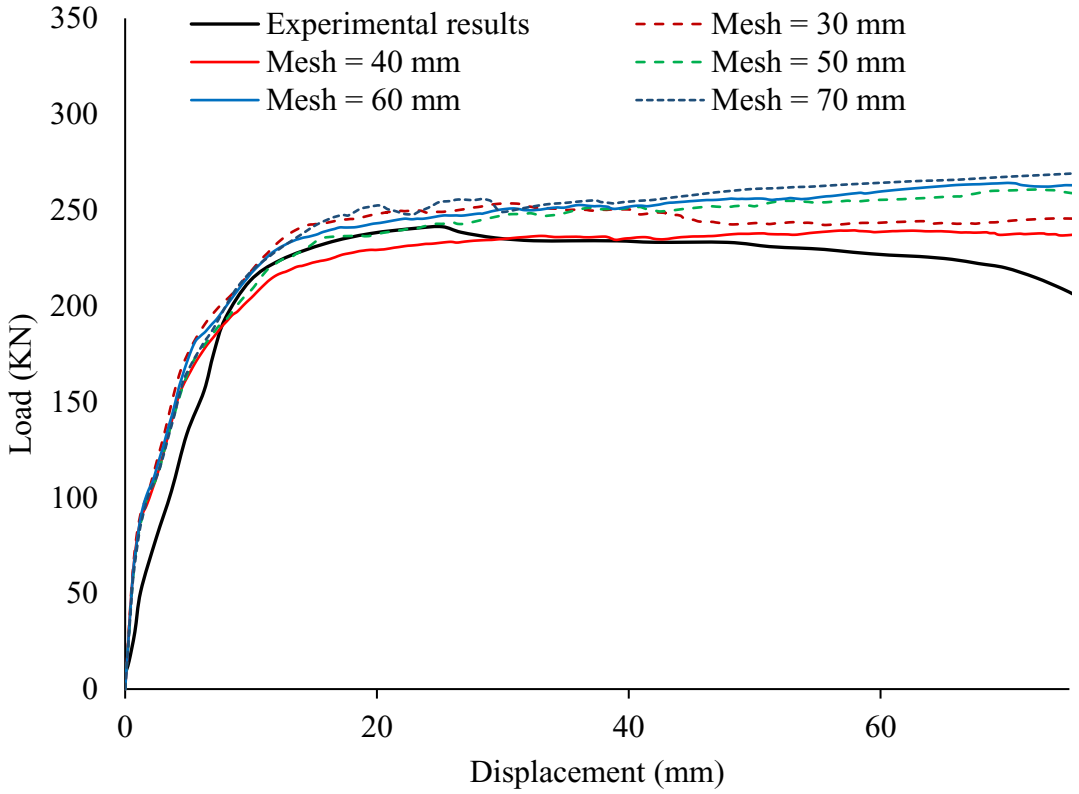

Figure 6-6 Typical specimen's load-deflection behavior for the different mesh sizes

It can be seen that the different mesh sizes analyzed showed a similar trend. However, it can be seen that the 40 mm mesh size was able to capture the experimental

behavior more than the other sizes, especially for the post-peak behavior. Thus, a 40 mm mesh size was chosen for the current FE model.

6.6.2. Model verification

6.6.2.1. Crack pattern

Figure 6-7 shows a typical crack pattern attained from the experiment and the principal stresses of the FE model for a typically tested specimen.

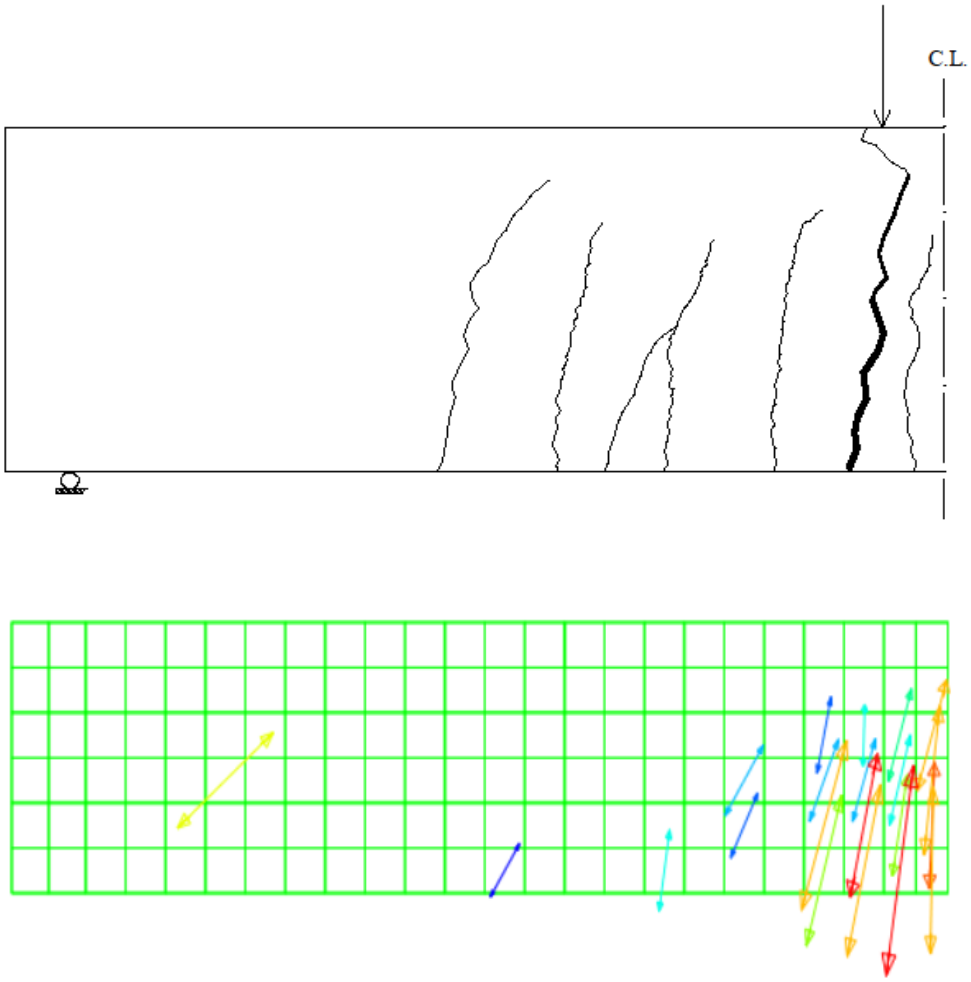

Figure 6-7 Comparison between the experimental crack patterns and stress tensors directions obtained from FEM.

It can be assumed that the direction of the minimum stress tensors represents the direction of the possible cracks. In the FE model, the minimum shear stress tensors direction was almost vertical at midspan (flexural cracks), which also was the case in the experimental observations. While inclined cracks (flexural-shear cracks) appear with going further from the beam's centerline. It started vertical at the bottom fibers, then with going

upwards, it rotated due to the gradual increase in the shear stress values. A fair match was attained between the experimental crack pattern and FE minimum stress tensors direction.

6.6.2.2. Load deflection behavior

To verify the present FE model's capability of simulating the flexural behavior of the composite and non-composite beams, the results were compared with the experimental results. Four different specimens were used for FEM verification. Table 6-3 shows the properties of the specimens.

Table 6-3 properties of the specimens used for FEM verification.

#	**Top layer concrete type**	**Bottom layer concrete type**	**Beam thickness**	**Top layer thickness**	**Bottom layer thickness**
1	HPC-86		230	_	_
2	HPC-86		255	_	_
3	HPC-86	UHPC-167	230	50	180
4	HPC-86	UHPC-167	255	75	180

Figures 6-8, 6-9, 6-10, and 6-11 show comparisons between FEM predictions and experimental results for the load deflection behavior of two non-composite beams and two composite beams.

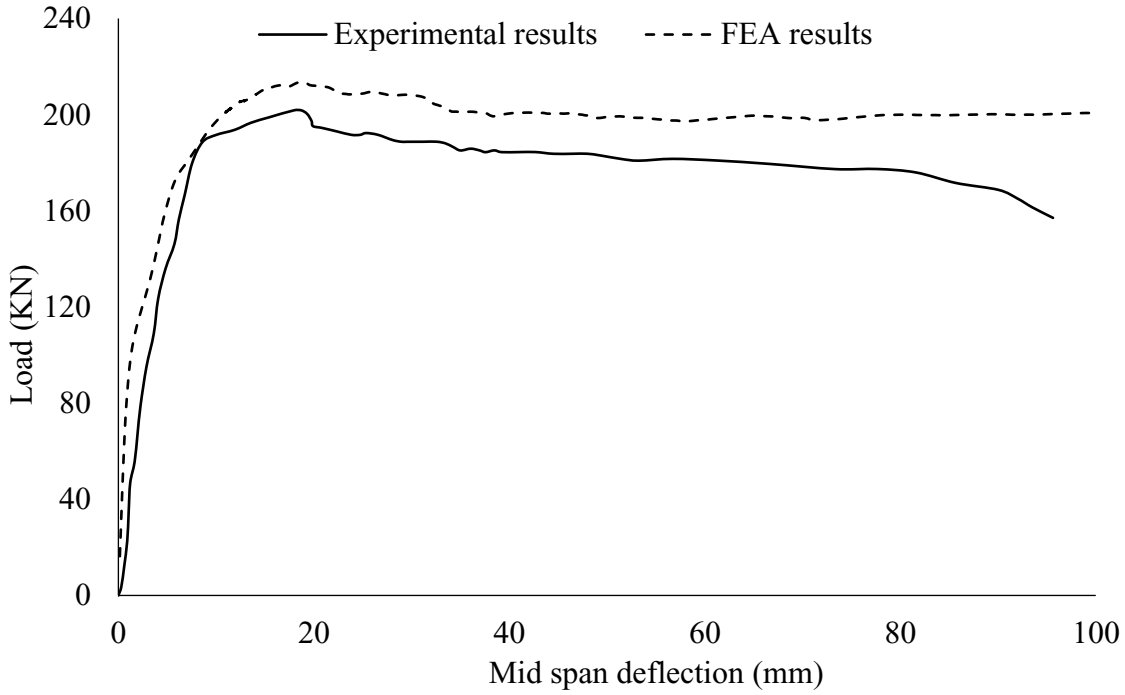

Figure 6-8 Comparison of load-deflection behavior between experimental results and FEM results for beam #1

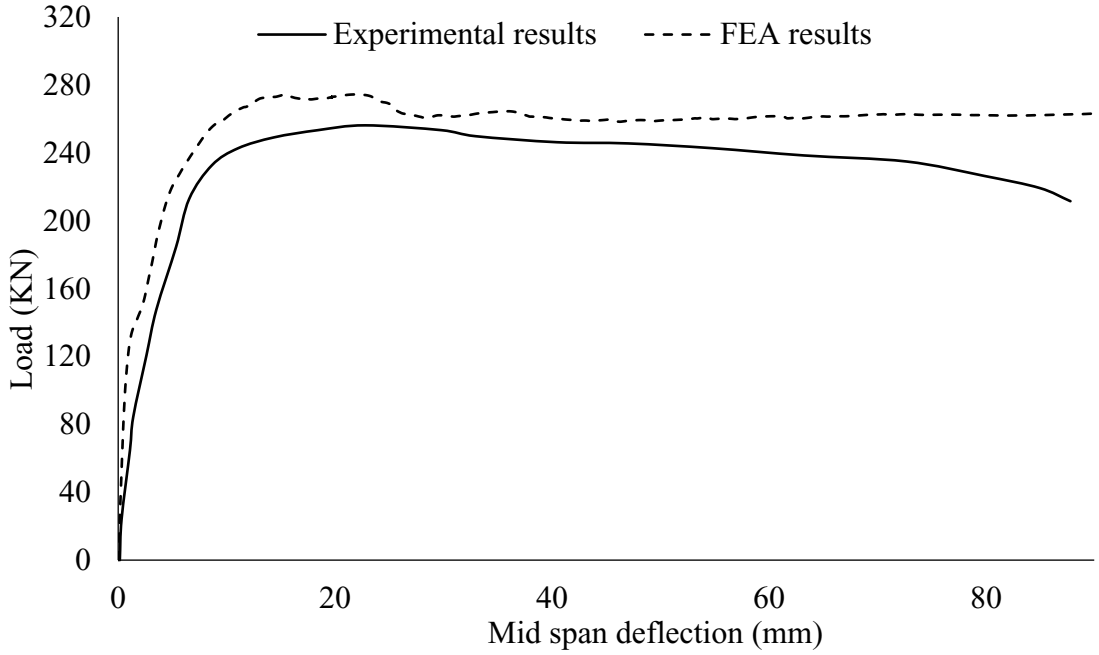

Figure 6-9 Comparison of load-deflection behavior between experimental results and FEM results for beam #2

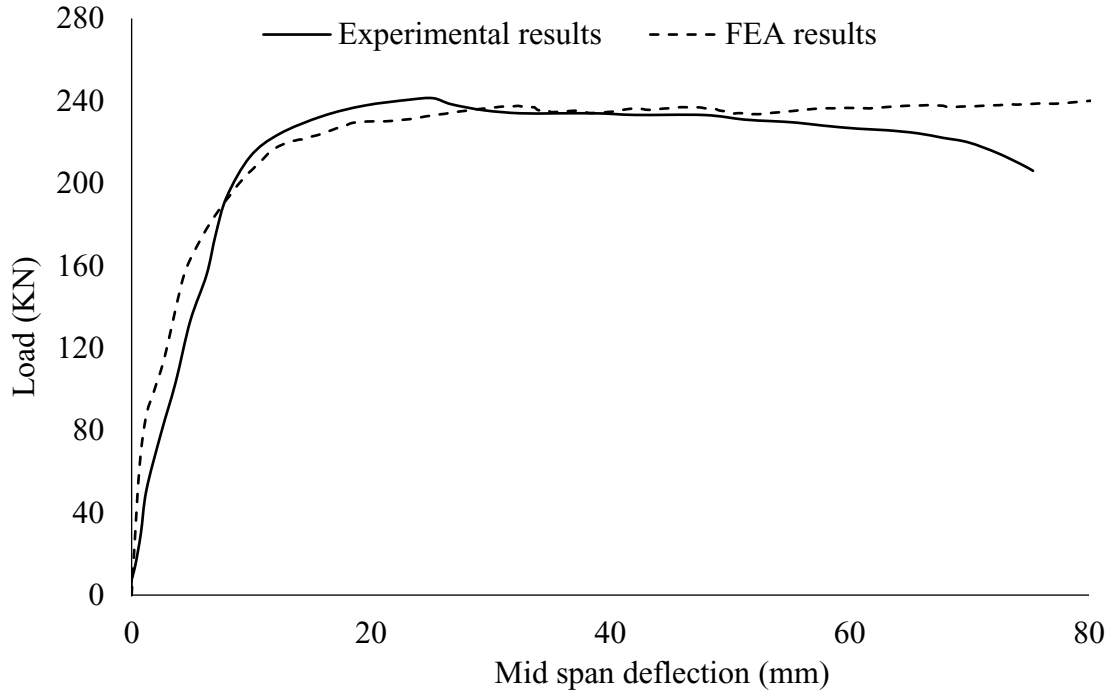

Figure 6-10 Comparison of load-deflection behavior between experimental results and FEM results for beam #3

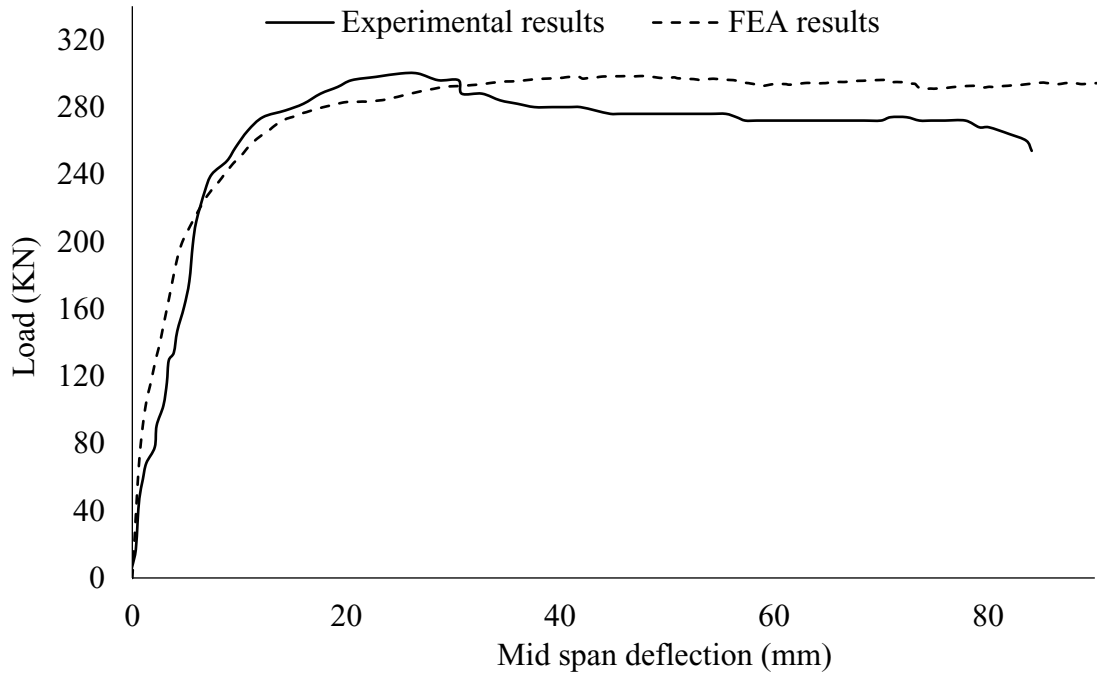

Figure 6-11 Comparison of load-deflection behavior between experimental results and FEM results for beam #4

It can be seen that the overall load-deflection behaviors for the four specimens were quite reasonable. Both experimental and FEM curves responses were linear up to the first crack. In the uncracked-elastic region, the predicted stiffnesses were overestimated. This may be due to the impact of some assumptions that are adopted that are related to the concrete's tensile and compressive properties, steel properties, and boundary conditions. It also may be related to the uncertainties involved in the experimental testing such as material deficiencies or geometrical variations. However, in the cracked-elastic region, the stiffnesses were similar. The FEM predicted the yield point with fair accuracy. Whereas it predicted the ultimate load capacity for the specimens with an average difference of 4.9% compared to the experimental values. The close agreement in the results of the FE model

compared to the experimental results indicates an acceptable prediction accuracy of the FE model.

6.6.3. Parametric analysis

Based on the shown accuracy of the developed FEM, this section of the study presents a parametric analysis to study the effect of different variables. The proposed FEM has been used to simulate 18 different beams. The data was analyzed to investigate the effects of the layer's concrete type and beam's thickness on the behavior under bending. Table 6-4 demonstrates the properties of the tested beams. The specimens were designated according to their concrete type's compressive strength at the top layer and bottom layer and the specimen's thickness. For example, a specimen that has NSC-33 at the bottom and HPC-63 at the top with an overall thickness of 230 mm was designated as 33/63-230. Each specimen's results will be briefly described in terms of the parameter adjusted in the next sections.

Table 6-4 properties of the tested beams.

Group number	#	**Bottom layer concrete type**	**Top layer concrete type**	**Beam thickness**	**Bottom layer thickness**	**Top layer thickness**	**Specimen designation**
	1	NSC-33		230	_	_	33-230
	2	NSC-33	HPC-63	230	180	50	33/63-230
	3	NSC-33	HPC-86	230	180	50	33/86-230
	4	NSC-33	UHPC-167	230	180	50	33/167-230
Group 1	5	HPC-63		230	_	_	63-230
	6	HPC-63	HPC-86	230	180	50	63/86-230
	7	HPC-63	UHPC-167	230	180	50	63/167-230
	8	HPC-86		230	_	_	86-230
	9	HPC-86	UHPC-167	230	180	50	86/167-230
	10	NSC-33		255	_	_	33-255
	11	NSC-33	HPC-63	255	180	75	33/63-255
	12	NSC-33	HPC-86	255	180	75	33/86-255
	13	NSC-33	UHPC-167	255	180	75	33/167-255
Group 2	14	HPC-63		255	_	_	63-255
	15	HPC-63	HPC-86	255	180	75	63/86-255
	16	HPC-63	UHPC-167	255	180	75	63/167-255
	17	HPC-86		255	_	_	86-255
	18	HPC-86	UHPC-167	255	180	75	86/167-255

- Figure 6-12 shows the load-deflection behavior for all the examined beams.

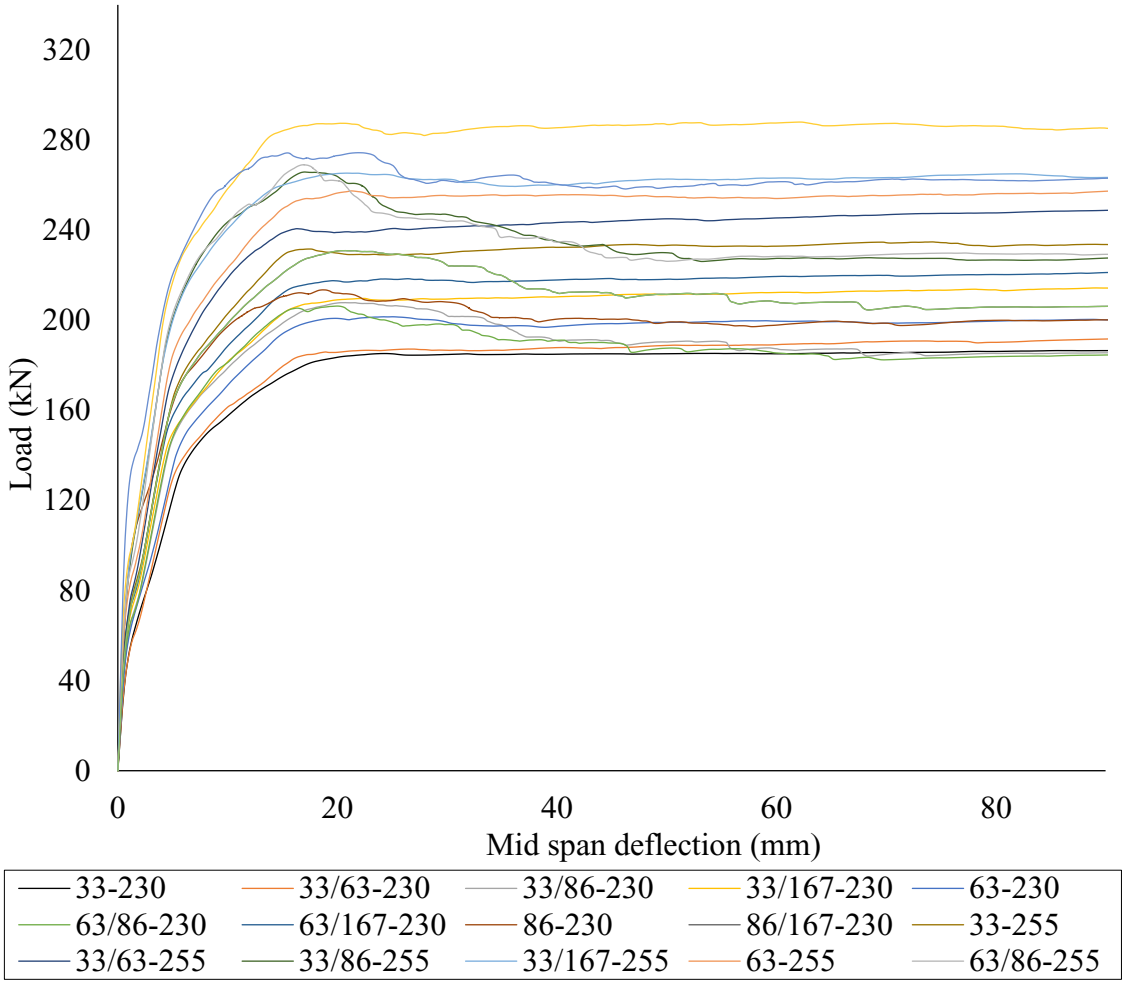

Figure 6-12 Load-deflection behavior for the examined beams.

It can be seen that the overall behavior of the beams was similar. As mentioned earlier, as the load is increased, the beam developed multiple cracks. All the tested specimens showed a similar overall cracking pattern under loading as discussed earlier. After the cracks are developed, the behavior of the load-deflection curve changed to reach a yielding of main reinforcement bars. After which, the specimens continue to sustain the load and undergo plastic deformation until it reaches complete failure. Figure 6-13 shows a bar chart for the moment capacity in kN. m for each specimen.

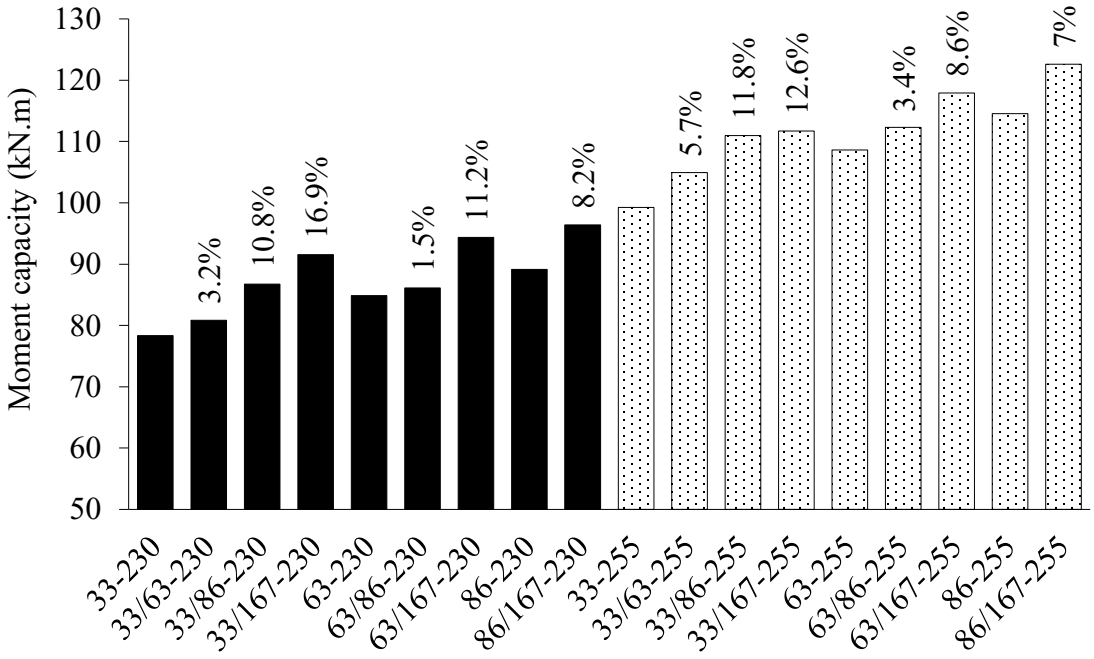

Figure 6-13 Moment capacity for each specimen.

It can be seen that 255 mm specimens had a higher moment capacity of 27.3 % on average compared to 230 mm specimens. This is mainly due to increasing the top layer thickness which led to an increase in the moment capacity of these specimens. It can be also noticed that, for non-composite specimens, using a higher compressive strength concrete provided a beam with marginal higher moment capacity. In that, HPC-63 beams had a higher moment capacity by 8.9% on average compared to NSC specimens. While HPC-86 beams had a higher moment capacity of 14.6% on average compared to NSC specimens. That is due to using a higher compressive strength concrete increased the ability of concrete to sustain more load before reaching complete failure. For composite specimens, changing the concrete type at the top layer had an influence on the flexural capacity of the tested beams. Each composite specimen was compared to its non-composite

reference beam that has the same bottom layer and the same thickness. The percentages of increase in the flexural capacity are shown in Figure 6-13. This increase is mainly due to replacing lower strength concrete with higher strength concrete. When full attachment is achieved between the two layers, the flexural capacity increases. The attained values for the beam's flexural capacity were compared to the theoretical values using the equation as per ("CSA-A23.3-14" 2014). Table 6-5 Lists the attained flexural capacity using FEA and the theoretical value using the code equation.

Table 6-5 Comparison of nominal moments.

#	**Specimen designation**	FEA (kN. m)	CSA A23.3-14 (kN. m)
1	33-230	78.3	55.1
2	33/63-230	80.9	58
3	33/86-230	86.8	58.8
4	33/167-230	91.6	60.1
5	63-230	84.8	58
6	63/86-230	86.1	58.8
7	63/167-230	94.3	60.1
8	86-230	89.1	58.8
9	86/167-230	96.4	60.1
10	33-255	99.3	63.1
11	33/63-255	104.9	66
12	33/86-255	111.0	66.9
13	33/167-255	111.7	68.1
14	63-255	108.6	66
15	63/86-255	112.3	66.9
16	63/167-255	117.9	68.1
17	86-255	114.5	66.9
18	86/167-255	122.6	68.1

It was found that the attained values using FEA were higher, or in other words, the values using the code equations were conservative.

6.7. Conclusions

A 3D FEM has been developed in this study to investigate the flexural behavior of composite and non-composite beams. The FEM was validated and used to predict the behavior of the beams with different variables. Based on the previous analysis, the following conclusions could be drawn:

1. Abaqus's CDP model was able to capture the behavior of the used concrete types (NSC, HPC and UHPC). Also, the used models for concrete's compressive and tension stiffening behaviors were suitable for simulating the behavior of the two concrete types.
2. The presented FE model is capable of predicting the actual flexural behavior of the composite and non-composite beams satisfactorily.
3. Adding another layer of concrete or changing the beam's overall thickness or changing the concrete type had an influence on the beam's ultimate flexural capacity. However, it had no clear impact on the load-deflection behavior.
4. The theoretical values using CSA A23.3-14 for predicting the beam's ultimate moment capacity were found to be conservative compared to the attained results using the current FE model.

6.8. References

Alam, Md. Shah. 2010. “Influence of Different Parameters on Shear Strength of FRP Reinforced Concrete Beams without Web Reinforcement.”

Anju, T., and K.K. Smitha. 2016. “Finite Element Analysis of Composite Beam with Shear Connectors.” Procedia Technology 24: 179–87. https://doi.org/10.1016/j.protcy.2016.05.025.

“ASTM C39.” 2021. Standard Test Method for Compressive Strength of Cylindrical Concrete Specimens. https://doi.org/10.1520/C0039_C0039M-21.

“ASTM C469.” 2022. Standard Test Method for Static Modulus of Elasticity and Poisson’s Ratio of Concrete in Compression. https://doi.org/10.1520/C0469_C0469M-22.

“ASTM C496.” 2017. Standard Test Method for Splitting Tensile Strength of Cylindrical Concrete Specimens. https://doi.org/10.1520/C0496_C0496M-17.

Barour, Sabiha, and Abdesselam Zergua. 2019. “Finite Element Modeling of Strengthened Beams Using CFRP.” Journal of Building Materials and Structures 6 (2): 77–87.

Barour, Sabiha, Abdesselam Zergua, Farid Bouziadi, and Waleed Abed Jasim. 2019. “Finite Element Analysis of CFRP-Externally Strengthened Reinforced Concrete Beams Subjected to Three-Point Bending.” World Journal of Engineering 17 (2): 183–202. https://doi.org/10.1108/WJE-04-2019-0121.

Bažant, Zdeněk P., and B. H. Oh. 1983. “Crack Band Theory for Fracture of Concrete.” Matériaux et Constructions 16 (3): 155–77. https://doi.org/10.1007/BF02486267.

Collins, M P, and D Mitchell. 1997. Prestressed Concrete Structures. Response Publications.

"CSA-A23.3-14." 2014. Design of Concrete Structures : CAN/CSA-A23.3-14 : A National Standard of Canada. Canadian Standard Association. 2014.

Hamed, M. 2018. "Structural Performance of a Proposed Uhp-Frc Shield in Harsh Environment." Memorial University of Newfoundland.

Hussein, Amgad. 1998. "Behaviour of High-Strength Concrete under Biaxial Loading Conditions." Memorial university of Newfoundland.

Iskhakov, I., Y. Ribakov, K. Holschemacher, and T. Mueller. 2014. "Experimental Investigation of Full Scale Two-Layer Reinforced Concrete Beams." Mechanics of Advanced Materials and Structures 21 (4): 273–83. https://doi.org/10.1080/15376494.2012.680673.

Iskhakov, Iakov, Yuri Ribakov, and Klaus Holschemacher. 2017. "Experimental Investigation of Continuous Two-Layer Reinforced Concrete Beams." Structural Concrete 18 (1): 205–15. https://doi.org/10.1002/suco.201600027.

Iskhakov, Iakov, Yuri Ribakov, Klaus Holschemacher, and Stefan Kaeseberg. 2019. "Experimental Investigation of Prestressed Two Layer Reinforced Concrete Beams." Structural Concrete, no. August: 1–12. https://doi.org/10.1002/suco.201900328.

Katwal, Utsab, Zhong Tao, and Md Kamrul Hassan. 2018. “Finite Element Modelling of Steel-Concrete Composite Beams with Profiled Steel Sheeting.” Journal of Constructional Steel Research 146: 1–15. https://doi.org/10.1016/j.jcsr.2018.03.011.

Khorsandnia, Nima, Hamid Valipour, and Keith Crews. 2014. “Structural Response of Timber-Concrete Composite Beams Predicted by Finite Element Models and Manual Calculations.” Advances in Structural Engineering 17 (11): 1601–21. https://doi.org/10.1260/1369-4332.17.11.1601.

Khorsandnia, Nima, Hamid R. Valipour, and Keith Crews. 2012. “Finite Element Modeling of Timber-Concrete Composite Beams under Short-Term Loadings.” ECCOMAS 2012 - European Congress on Computational Methods in Applied Sciences and Engineering, e-Book Full Papers, no. January: 859–67. https://doi.org/10.13140/2.1.2486.1123.

Lam, Thanh Quang Khai, and Thi My Dung Do. 2019. “Sliding between Layers in 2-Layer Reinforced Concrete Beams and Shell.” International Journal of Engineering and Advanced Technology 8 (5): 1867–71.

Nayal, Rim, and Hayder A. Rasheed. 2006. “Tension Stiffening Model for Concrete Beams Reinforced with Steel and FRP Bars.” Journal of Materials in Civil Engineering 18 (6): 831–41. https://doi.org/10.1061/(asce)0899-1561(2006)18:6(831).

Papanikolaou, Vassilis K., and Andreas J. Kappos. 2007. “Confinement-Sensitive Plasticity Constitutive Model for Concrete in Triaxial Compression.” International Journal of Solids and Structures 44 (21): 7021–48. https://doi.org/10.1016/j.ijsolstr.2007.03.022.

Parandaman, P, and M Jayaraman. 2014. “Finite Element Analysis of Reinforced Concrete Beam Retrofitted with Different Fiber Composites.” Middle-East Journal of Scientific Research 22 (7): 948–53. https://doi.org/10.5829/idosi.mejsr.2014.22.07.21979.

Piscesa, Bambang, Mario M. Attard, and Ali K. Samani. 2017. “Three-Dimensional Finite Element Analysis of Circular Reinforced Concrete Column Confined with FRP Using Plasticity Model.” Procedia Engineering 171: 847–56. https://doi.org/10.1016/j.proeng.2017.01.377.

Saiidi, M., S. Vrontinos, and B. Douglas. 1990. “Model for the Response of Reinforced Concrete Beams Strengthened by Concrete Overlays.” ACI Structural Journal 87 (6): 687–95.

Sasmal, S., S. Kalidoss, and V. Srinivas. 2012. “Nonlinear Finite Element Analysis of FRP Strengthened Reinforced Concrete Beams.” Journal of The Institution of Engineers (India): Series A 93 (4): 241–49. https://doi.org/10.1007/s40030-013-0028-9.

Vu, Dinh Tho, Elena Korol, Yuliya Kustikova, and Huy Hoang Nguyen. 2019. “Finite Element Analysis of Three-Layer Concrete Beam with Composite Reinforcement.” E3S Web of Conferences 97 (May). https://doi.org/10.1051/e3sconf/20199702023.

Wahalathantri, B L, D P Thambiratnam, T H T Chan, and S Fawzia. 2011. “A Material Model for Flexural Crack Simulation in Reinforced Concrete Elements Using ABAQUS.” First International Conference on Engineering, Design and Developing the Built ENvironment for Sustainable Wellbeing, no. April: 260–64.

Chapter 7 Summary and conclusions

The following summarized conclusions can be drawn from the dissertation:

- The current research started with an evaluation of the ASTM C944 (rotating cutters technique) for determining the concrete's abrasion resistance. It entailed a thorough examination of the interaction between the spinning cutters and the test specimen, as well as the interpretation of the data.
- The depths and widths of the resulting abrasion grooves were not consistent across the abraded region due to the rotating cutters testing mechanism. If depth measurement points are chosen manually, this has a direct impact on their location.
- The average abrasion depth was obtained using a micrometer bridge with a large coefficient of variation.
- After determining the abraded groove pattern in terms of width and depth, a valid equation was created that produced average abrasion depth values with a low coefficient of variation.
- Because of the precision and manner of measurement, different depth measuring methods can have a significant impact on depth results.
- Because every surface has its unique features of homogeneity and surface roughness, evaluating different surfaces (formed, finished, and cut) yields varied results under the same testing conditions. Due to its uniformity, the cut surface exhibited the maximum abrasion resistance when compared to the completed surface. Due to its significant un-abraded surface roughness, the finished surface had the least abrasion resistance.

- Many parameters were studied to evaluate and enhance the abrasion resistance and mechanical properties of the HPSDC mixture. The parameters studied were different C/F aggregate ratio, different A_m, a comparison between the HPSDC with other types of concrete, the synergistic action of using FA and SF, and the effect of using MK in the SF system. The research also assessed the impact of the addition of different types of fibers on the mechanical properties and the abrasion resistance of the HPSDC. Four types of fibers (CCSFs, PPFs, BBFs, and FBFs) at different ratios (0.1%, 0.3%, 0.5%) were added. In addition, the research assessed the impact of the addition of NPs (NCS and NTD) on the mechanical properties and the abrasion resistance of the HPSDC. NCS and NTD were incorporated at 0%, 0.5%, 1%, 1.5%, 2%, 2.5%, 3%. The mixtures incorporated MK, SF, and CCSFs at 15%, 8%, 0.5%, respectively. The fresh mixtures' properties were investigated. The mechanical properties of the developed mixtures were evaluated for compressive strength, STS, FS, SME, and DME. Abrasion resistance was assessed using two tests; the rotating cutters method and sandblasting test.
- Increasing the C/F aggregate ratio from 1 to 2 reduced SP demand by 10.5% on average. When compared to 10 mm Am, employing 20 mm Am in HPSDC combinations required somewhat less SP dose. The HPNWC mixture required slightly more dose than the HPSDC mixture, whereas the HPLWAC mixture required slightly less dosage. At low FA ratios, including various ratios of FA mixed with 8% SF necessitated larger SP doses. The FA effect was more evident at greater FA incorporation ratios (more than 10%), and smaller SP doses were required. On the

contrary, significantly larger SP doses were required, which were nearly doubled with the addition of 30% MK mixed with 8% SF.

- Changing the C/F aggregate ratio and A_m had no noticeable impact on the AEA demand. The same amount of AEA was used for all three types of concrete: HPSDC, HPNWC, and HPLWAC. Incorporation of various SCMs, on the other hand, necessitated larger AEA doses to reach the required air content. With the addition of 30% fly ash and 8% silica fume, the dose was increased to 71.4%. And with 30% MK and 8% SF, a 128.6% greater dose was required.
- For the HPSDC, a C/F aggregate ratio of 1.6 was found to be optimal. Because it increased the HPSDC compressive strength and modulus of elasticity by an average of 15.6% and 13%, respectively. Furthermore, the influence on its tensile characteristics was more obvious. When compared to a C/F aggregate ratio of 1, the C/F of 1.6 had a greater STS of 22.9% and a higher FS of 26.7%. Furthermore, utilizing rotating cutters and sandblasting techniques, abrasion resistance was improved by an average of 12.8% and 14.3%, respectively.
- In comparison to Am of 20 mm, the findings of the tested mixes revealed that utilizing Am of 10 mm in the HPSDC provided it with higher tensile properties. In that, the STS was up 6.7% on average, while the FS was up 5.9% on average. Employing rotating cutters, however, using various A_m had no discernible influence on compressive strength, moduli of elasticity, or abrasion resistance. Using the sandblasting testing method, however, 20 mm mixes revealed a 7.9% reduction in the abrasion resistance.

- The mechanical properties of the tested concrete were affected by changing the aggregate type. In this regard, the HPSDC had less, but comparable, mechanical characteristics to the HPNWC, whereas the HPLWAC had greater mechanical properties. When comparing the three different concrete kinds, however, the abrasion resistance was more influenced than the mechanical characteristics that were evaluated. The difference in mechanical characteristics and abrasion resistance between the three concrete kinds was larger after 28 days than at 14 days, in general.
- Up to the 28-day, including FA mixed with SF as partial cement replacement materials in HPSDC mixes had a detrimental influence on the mechanical characteristics and abrasion resistance of the HPSDC. However, at the 91-day, low incorporation ratios of 5% and 10% FA blended with 8% SF exhibited a modest increase in compressive strength when compared to the control mixes.
- The HPSDC characteristics were improved thanks to the synergistic effect of MK and SF. The best combination of MK and SF was found to be 15% MK and 8% SF. As a result, HPSDC compressive strength, STS, FS, SME, and DME all improved by an average of 7.7%, 11.7%, 7.3%, 13%, and 6.2%, respectively. Furthermore, utilizing the sandblasting testing method, increased HPSDC abrasion resistance by an average of 12% and by an average of 26.8%. In general, when evaluating the MK and FA combinations as SCMs in the HPSDC, the MK combination was more successful.
- Using different types of fibers necessitated a greater SP demand. CCSF had the greatest impact, with a 50.6% increase in SP demand in 0.5% of CCSFs. PPFs, BBFs, and FBFs in various ratios were shown to have a comparable effect on the SP doses required.

- In comparison to the control mixture, using CCSFs at varied ratios in the HPSDC improved compressive strength. The compressive strength of the HPSDC increased as the CCSFs ratio increased. The inclusion of PPFs also resulted in a small improvement in compressive strength. On the contrary, for both types of BFs, a significant reduction was seen that was proportional to the number of fibers added.
- CCSFs could significantly improve the HPSDC's STS and FS. Furthermore, the CCSFs included specimens that were shown to have high deformability. Fiber pull-out was the determining factor in the failure of CCSFs integrated specimens under flexure. In addition, PPFs were able to improve the tensile characteristics of the HPSDC, but to a lesser amount than CCSFs. PPFs, on the other hand, had no effect on HPSDC flexural deformability, and the failure of the specimens was determined by fibers rupture.
- BBFs were able to improve the tensile characteristics of the HPSDC up to a 0.3% addition ratio, however, 0.5% of BBFs were ineffective due to inadequate dispersion. Using FBFs, which were able to increase the HPSDC's tensile characteristics by 0.5%. Both forms of BFs, like PPFs, did not improve HPSDC flexural deformability, and specimen failure was driven by fibers rupture.
- The incorporation of CCSFs, BBFs, and FBFs had a modest beneficial effect on the stiffness of the HPSDC. The number of fibers added affected on the degree of amplification. PPFs, on the other hand, had no apparent influence on the HPSDC stiffness characteristics.
- The inclusion of 0.1% CCSFs had no effect on the HPSDC's abrasion resistance as evaluated by the two abrasion test techniques. Incorporation of 0.3% CCSFs, on the

other hand, reduced the abrasion coefficient assessed by sandblasting but had no effect on the abrasion resistance evaluated by rotating cutters. HPSDC abrasion resistance was considerably enhanced by utilizing the two abrasion testing techniques at 0.5% of CCSFs.

- PPFs improved the HPSDC's abrasion resistance, and their efficiency was proportional to the amount of PPFs used. However, when 0.5% of PPFs were compared to 0.5% of CCSFs, PPFs were shown to be less effective in both abrasion tests.
- The HPSDC abrasion resistance was improved by both types of BFs. BBFs had the best ratio at 0.3%, while FBFs had the best performance against abrasion action at 0.5%. Both types of BFs outperformed PPFs in terms of abrasion resistance in the HPSDC. BBFs were more effective than FBFs when using rotating cutters as a test method. CCSFs, on the other hand, were more effective. FBFs were more effective than BBFs, but not as successful as CCSFs, in sandblasting testing.
- CCSFs were shown to be the most effective fibers addition on generating HPSDC with increased mechanical characteristics and abrasion resistance at a concentration of 0.5%.
- The addition of NPs boosted the demand for SP and AEA. At 3% of NCS and 3% of NTD, respectively, the SP demand reached 18.2% and 23.6%, respectively. While the AEA demand reached 8.3%, accounting for 3% of NCS and 3% of NTD.
- The addition of NPs improved the compressive strength of the HPSDC. At 2% of NCS and 1% of NTD, the enhancements were at their peak. When compared to the control mixture, the compressive strength reached 6.6% on average at 2% NCS. In comparison to the control mixture, it reached 4.7% on average with 1% NTD.

- The HPSDC stiffness was affected similarly by NCS and NTD. The average rise in the SME was 4.9%. In comparison to the control mixture, the DME increased by 3.5% on average.
- Adding NCS and NTD to the HPSDC had a greater influence on its tensile characteristics than it did on its compressive strength and stiffness properties. The STS and FS achieved their peak at 2% NCS, with 16.8% and 13.8%, respectively, greater than the control combination on average. While adding 1% NTD raised the STS and FS by 7.6% and 7.3%, respectively, on average, greater than the control mixture.
- The inclusion of NPs had the most positive effect on the HPSDC's abrasion resistance. Adding NCS at 2% resulted in an average improvement of 26.3% in abrasion depth (rotating cutters technique) and 32.1% in abrasion coefficient (sandblasting approach). By adding 2% NTD, the abrasion depth was improved by 26.1% on average (rotating cutters approach) and the abrasion coefficient was improved by 33.5% (sandblasting technique).
- In addition, the research provided another alternative to the abrasion damage issue. The study used a three-dimensional finite element model to explore the flexural behavior of composite and non-composite beams. The FEM was verified and used to anticipate how the beams would behave under various conditions.
- The CDP model in Abaqus was able to represent the behavior of the concrete types used (NSC, HPC and UHPC). In addition, the models for compressive and tension stiffening behaviors in concrete were adequate for modeling the behavior of the two concrete kinds.

- The proposed FE model is capable of accurately predicting the flexural behavior of composite and non-composite beams.
- Adding another layer of concrete or altering the total thickness of the beam had an impact on the ultimate flexural capacity of the beam. It had no real effect on load-deflection behavior. The bending capacity of the beam was also affected by changing the concrete type.
- When compared to the obtained findings using the present FE model, the theoretical values utilizing CSA A23.3-14 for estimating the beam's ultimate moment capacity were determined to be conservative.

References

"ACI 318-14." 2014. Building Code Requirements for Structural Concrete (ACI 318-14). American Concrete Institute.

ACI Comite 544.3R. 2008. "Guide for Specifying , Proportioning , and Production of Fiber-Reinforced Concrete," 16.

Al-mashhadani, Mukhallad M, Orhan Canpolat, Yurdakul Aygörmez, Mucteba Uysal, and Savaş Erdem. 2018. "Mechanical and Microstructural Characterization of Fiber Reinforced Fly Ash Based Geopolymer Composites." *Construction and Building Materials* 167: 505–13. https://doi.org/https://doi.org/10.1016/j.conbuildmat.2018.02.061.

Alam, Md. Shah. 2010. "Influence of Different Parameters on Shear Strength of FRP Reinforced Concrete Beams without Web Reinforcement."

Aly, M, M S J Hashmi, A G Olabi, M Messeiry, E F Abadir, and A I Hussain. 2012. "Effect of Colloidal Nano-Silica on the Mechanical and Physical Behaviour of Waste-Glass Cement Mortar." *Materials & Design* 33: 127–35. https://doi.org/https://doi.org/10.1016/j.matdes.2011.07.008.

Anju, T., and K.K. Smitha. 2016. "Finite Element Analysis of Composite Beam with Shear Connectors." *Procedia Technology* 24: 179–87. https://doi.org/10.1016/j.protcy.2016.05.025.

Ardalan, R. Bani, N. Jamshidi, H. Arabameri, A. Joshaghani, M. Mehrinejad, and P.

Sharafi. 2017. “Enhancing the Permeability and Abrasion Resistance of Concrete Using Colloidal Nano-SiO2 Oxide and Spraying Nanosilicon Practices.” *Construction and Building Materials* 146: 128–35. https://doi.org/10.1016/j.conbuildmat.2017.04.078.

“ASTM C1017.” 2013. *Standard Specification for Chemical Admixtures for Use in Producing Flowing Concrete*.

“ASTM C1138.” 2019. Standard Test Method for Abrasion Resistance of Concrete (Underwater Method). 2019. https://doi.org/10.1520/C1138M-19.

“ASTM C1240.” 2020. *Standard Specification for Silica Fume Used in Cementitious Mixtures*. https://doi.org/10.1520/C1240-20.

“ASTM C143.” 2020. *Standard Test Method for Slump of Hydraulic-Cement Concrete*. https://doi.org/10.1520/C0143_C0143M-20.

“ASTM C150.” 2022. *Standard Specification for Portland Cement*. https://doi.org/10.1520/C0150_C0150M-22.

“ASTM C215.” 2019. *Standard Test Method for Fundamental Transverse, Longitudinal, and Torsional Resonant Frequencies of Concrete Specimens*. https://doi.org/10.1520/C0215-19.

“ASTM C231.” 2022. Standard Test Method for Air Content of Freshly Mixed Concrete by the Pressure Method. 2022. https://doi.org/10.1520/C0231_C0231M-22.

“ASTM C260.” 2016. *Standard Specification for Air-Entraining Admixtures for*

Concrete. https://doi.org/10.1520/C0260_C0260M-10AR16.

"ASTM C33." 2018. *Standard Specification for Concrete Aggregates*. https://doi.org/10.1520/C0033_C0033M-18.

"ASTM C39." 2021. *Standard Test Method for Compressive Strength of Cylindrical Concrete Specimens*. https://doi.org/10.1520/C0039_C0039M-21.

"ASTM C418." 2020. *Standard Test Method for Abrasion Resistance of Concrete by Sandblasting*. https://doi.org/10.1520/C0418-20.

"ASTM C469." 2022. *Standard Test Method for Static Modulus of Elasticity and Poisson's Ratio of Concrete in Compression*. https://doi.org/10.1520/C0469_C0469M-22.

"ASTM C494." 2022. *Standard Specification for Chemical Admixtures for Concrete*. https://doi.org/10.1520/C0494_C0494M-19E01.

"ASTM C496." 2017. *Standard Test Method for Splitting Tensile Strength of Cylindrical Concrete Specimens*. https://doi.org/10.1520/C0496_C0496M-17.

ASTM C618. 2022. "ASTM C618." *Standard Specification for Coal Fly Ash and Raw or Calcined Natural Pozzolan for Use*. https://doi.org/10.1520/C0618-22.

"ASTM C618." 2022. *Standard Specification for Coal Fly Ash and Raw or Calcined Natural Pozzolan for Use in Concrete*. https://doi.org/10.1520/C0618-22.

"ASTM C779." 2019. *Standard Test Method for Abrasion Resistance of Horizontal Concrete Surfacese*. https://doi.org/10.1520/C0779_C0779M-12.

"ASTM C78." 2022. *Standard Test Method for Flexural Strength of Concrete (Using Simple Beam with Third-Point Loading)*. https://doi.org/10.1520/C0078_C0078M-22.

"ASTM C944." 2019. *Standard Test Method for Abrasion Resistance of Concrete or Mortar Surfaces by the Rotating-Cutter Method*. https://doi.org/10.1520/C0944_C0944M-19.

Ayub, Tehmina, Nasir Shafiq, and M Fadhil Nuruddin. 2014. "Mechanical Properties of High-Performance Concrete Reinforced with Basalt Fibers." *Procedia Engineering* 77: 131–39. https://doi.org/https://doi.org/10.1016/j.proeng.2014.07.029.

Barour, Sabiha, and Abdesselam Zergua. 2019. "Finite Element Modeling of Strengthened Beams Using CFRP." *Journal of Building Materials and Structures* 6 (2): 77–87.

Barour, Sabiha, Abdesselam Zergua, Farid Bouziadi, and Waleed Abed Jasim. 2019. "Finite Element Analysis of CFRP-Externally Strengthened Reinforced Concrete Beams Subjected to Three-Point Bending." *World Journal of Engineering* 17 (2): 183–202. https://doi.org/10.1108/WJE-04-2019-0121.

Basalt Fibers LTD. 2013. "Basalt Chopped Fibre- New Brand TURBOBUILD-24- 300 in Concrete Reinforcement Segment." 2013.

Bažant, Zdeněk P., and B. H. Oh. 1983. "Crack Band Theory for Fracture of Concrete." *Matériaux et Constructions* 16 (3): 155–77. https://doi.org/10.1007/BF02486267.

Beaudoin, J J. 1990. *Handbook of Fibre-Reinforced Concrete : Principles, Properties, Developments and Applications*. *Building Materials Science Series*. Park Ridge, N.J. : Noyes Publications: Park Ridge, N.J. : Noyes Publications.

Bentur, Arnon., and Sidney. Mindess. 2007. *Fibre Reinforced Cementitious Composites*. London; New York: Taylor & Francis.

Black, J Temple. 2019. *DeGarmo's Materials and Processes in Manufacturing*. Tenth edition. Hoboken, NJ : Wiley, [2008] ©2008. https://search.library.wisc.edu/catalog/9910066779802121.

Bogas, Jose, and Augusto Gomes. 2014. "Static and Dynamic Modulus of Elasticity of Structural Lightweight and Modified Density Concrete with and without Nanosilica – Characterization and Normalization" *IJCE* 12 (2): 170–80. http://ijce.iust.ac.ir/article-1-743-en.html.

Borhan, Tumadhir. 2013. "Thermal and Mechanical Properties of Basalt Fibre Reinforced Concrete." *Proc. World Acad. Sci., Eng. Technol.* 76 (April).

Branston, John, Sreekanta Das, Sara Y. Kenno, and Craig Taylor. 2016. "Mechanical Behaviour of Basalt Fibre Reinforced Concrete." *Construction and Building Materials* 124 (October): 878–86. https://doi.org/10.1016/j.conbuildmat.2016.08.009.

Cai, X, Zhen He, S Tang, and Xiaorun Chen. 2016. "Abrasion Erosion Characteristics of Concrete Made with Moderate Heat Portland Cement, Fly Ash and Silica Fume

Using Sandblasting Test." *Construction and Building Materials* 127: 804–14.

Cheng, T.-C, An Cheng, Ran Huang, and Wei-Ting Lin. 2014. "Abrasion Properties of Steel Fiber Reinforced Silica Fume Concrete According to Los Angeles and Water Abrasion Tests." *Medziagotyra* 20 (December): 498–502. https://doi.org/10.5755/j01.ms.20.4.6460.

Cheng, Youkun, and Zhenwu Shi. 2019. "Experimental Study on Nano-SiO 2 Improving Concrete Durability of Bridge Deck Pavement in Cold Regions." *Advances in Civil Engineering* 2019. https://doi.org/10.1155/2019/5284913.

Collins, M P, and D Mitchell. 1997. *Prestressed Concrete Structures*. Response Publications.

"CSA-A23.3-14." 2014. Design of Concrete Structures : CAN/CSA-A23.3-14 : A National Standard of Canada. Canadian Standard Association. 2014.

Deák, Tamás, and Tibor Czigány. 2009. "Chemical Composition and Mechanical Properties of Basalt and Glass Fibers: A Comparison." *Textile Research Journal* 79 (7): 645–51. https://doi.org/10.1177/0040517508095597.

Dias, Dylmar Penteado, and Clelio Thaumaturgo. 2005. "Fracture Toughness of Geopolymeric Concretes Reinforced with Basalt Fibers." *Cement and Concrete Composites* 27 (1): 49–54. https://doi.org/10.1016/J.CEMCONCOMP.2004.02.044.

Fernandes, J.F., T. Bittencourt, and P. Helene. 2008. "A Review of the Application of Concrete to Offshore Structures." *ACI Symposium Publication* 253.

https://doi.org/10.14359/20187.

Fibres Unlimited. 2007. “Test Report of Basalt Fibre Reinforced Concrete, Polypropylene Reinforced Concrete, Polyacrylonitrile Reinforced Concrete.” *Technical Data Sheet* 31 (0): 11.

Fu, Qiang, Ditao Niu, Jian Zhang, Daguan Huang, Yan Wang, Mengshu Hong, and Lu Zhang. 2018. “Dynamic Compressive Mechanical Behaviour and Modelling of Basalt–Polypropylene Fibre-Reinforced Concrete.” *Archives of Civil and Mechanical Engineering* 18 (3): 914–27. https://doi.org/https://doi.org/10.1016/j.acme.2018.01.016.

Gaitero, J J, I Campillo, and A Guerrero. 2008. “Reduction of the Calcium Leaching Rate of Cement Paste by Addition of Silica Nanoparticles.” *Cement and Concrete Research* 38 (8): 1112–18. https://doi.org/https://doi.org/10.1016/j.cemconres.2008.03.021.

Gautier, Donald L, Kenneth J Bird, Ronald R Charpentier, Arthur Grantz, David W Houseknecht, Timothy R Klett, Thomas E Moore, et al. 2009. “Assessment of Undiscovered Oil and Gas in the Arctic.” *Science* 324 (5931): 1175 LP – 1179. https://doi.org/10.1126/science.1169467.

Gonzalez, Marcelo, Arthur De Oliveira Lima, and Susan L. Tighe. 2014. “Nanoconcrete for Rigid Pavements: Abrasion Response and Impact on Friction.” *Transportation Research Record* 2441: 28–37. https://doi.org/10.3141/2441-05.

Grdic, Zoran J, Gordana A Toplicic Curcic, Nenad S Ristic, and Iva M Despotovic. 2012. "Abrasion Resistance of Concrete Micro-Reinforced with Polypropylene Fibers." *Construction and Building Materials* 27 (1): 305–12. https://doi.org/https://doi.org/10.1016/j.conbuildmat.2011.07.044.

Hamed, M. 2018. "Structural Performance of a Proposed Uhp-Frc Shield in Harsh Environment." Memorial University of Newfoundland.

Haruehansapong, Sattawat, Tawich Pulngern, and Somchai Chucheepsakul. 2014. "Effect of the Particle Size of Nanosilica on the Compressive Strength and the Optimum Replacement Content of Cement Mortar Containing Nano-SiO2." *Construction and Building Materials* 50: 471–77. https://doi.org/https://doi.org/10.1016/j.conbuildmat.2013.10.002.

Hasan, Ahmad, and Lagoudas Dimitris C. 1991. "Effective Elastic Properties of Fiber-Reinforced Concrete with Random Fibers." *Journal of Engineering Mechanics* 117 (12): 2931–38. https://doi.org/10.1061/(ASCE)0733-9399(1991)117:12(2931).

Hoff, G. C., and R. Elimov. 1995. "Concrete Production for the Hibernia Platform." In Annual Conference- Canadian Society for Civil Engineering, 693–716.

Horszczaruk, E K. 2009. "Hydro-Abrasive Erosion of High Performance Fiber-Reinforced Concrete." *Wear* 267 (1): 110–15. https://doi.org/https://doi.org/10.1016/j.wear.2008.11.010.

Hussein, Amgad. 1998. "Behaviour of High-Strength Concrete under Biaxial Loading

Conditions." Memorial university of Newfoundland.

Iskhakov, I., Y. Ribakov, K. Holschemacher, and T. Mueller. 2014. "Experimental Investigation of Full Scale Two-Layer Reinforced Concrete Beams." *Mechanics of Advanced Materials and Structures* 21 (4): 273–83. https://doi.org/10.1080/15376494.2012.680673.

Iskhakov, Iakov, Yuri Ribakov, and Klaus Holschemacher. 2017. "Experimental Investigation of Continuous Two-Layer Reinforced Concrete Beams." *Structural Concrete* 18 (1): 205–15. https://doi.org/10.1002/suco.201600027.

Iskhakov, Iakov, Yuri Ribakov, Klaus Holschemacher, and Stefan Kaeseberg. 2019. "Experimental Investigation of Prestressed Two Layer Reinforced Concrete Beams." *Structural Concrete*, no. August: 1–12. https://doi.org/10.1002/suco.201900328.

Jacobsen, Stefan, George W Scherer, and Erland M Schulson. 2015. "Concrete–Ice Abrasion Mechanics." *Cement and Concrete Research* 73: 79–95. https://doi.org/https://doi.org/10.1016/j.cemconres.2015.01.001.

Jang, Seok-Joon, and Hyun-Do Yun. 2018. "Combined Effects of Steel Fiber and Coarse Aggregate Size on the Compressive and Flexural Toughness of High-Strength Concrete." *Composite Structures* 185: 203–11. https://doi.org/https://doi.org/10.1016/j.compstruct.2017.11.009.

Jiang, Chaohua, Ke Fan, Fei Wu, and Da Chen. 2014a. "Experimental Study on the

Mechanical Properties and Microstructure of Chopped Basalt Fibre Reinforced Concrete." *Materials & Design* 58: 187–93. https://doi.org/https://doi.org/10.1016/j.matdes.2014.01.056.

Jo, Byung-Wan, Chang-Hyun Kim, Ghi-ho Tae, and Jong-Bin Park. 2007. "Characteristics of Cement Mortar with Nano-SiO2 Particles." *Construction and Building Materials* 21 (6): 1351–55. https://doi.org/https://doi.org/10.1016/j.conbuildmat.2005.12.020.

Jun, W, and Z Ye. 2010. "Experimental Research on Mechanical and Working Properties of Non-Dipping Chopped Basalt Fiber Reinforced Concrete." In *2010 3rd International Conference on Information Management, Innovation Management and Industrial Engineering*, 4:635–37. https://doi.org/10.1109/ICIII.2010.633.

Kabay, Nihat. 2014. "Abrasion Resistance and Fracture Energy of Concretes with Basalt Fiber." *Construction and Building Materials* 50: 95–101. https://doi.org/https://doi.org/10.1016/j.conbuildmat.2013.09.040.

Kaplan, M F. 1959. "Flexural and Compressive Strength of Concrete as Affected by the Properties of Coarse Aggregates." In .

Katkhuda, Hasan, and Nasim Shatarat. 2017. "Improving the Mechanical Properties of Recycled Concrete Aggregate Using Chopped Basalt Fibers and Acid Treatment." *Construction and Building Materials* 140: 328–35. https://doi.org/10.1016/j.conbuildmat.2017.02.128.

Katwal, Utsab, Zhong Tao, and Md Kamrul Hassan. 2018. “Finite Element Modelling of Steel-Concrete Composite Beams with Profiled Steel Sheeting.” *Journal of Constructional Steel Research* 146: 1–15. https://doi.org/10.1016/j.jcsr.2018.03.011.

Kawashima, Shiho, Jung-Woo Ted Seo, David Corr, Mark C Hersam, and Surendra P Shah. 2014. “Dispersion of CaCO3 Nanoparticles by Sonication and Surfactant Treatment for Application in Fly Ash–Cement Systems.” *Materials and Structures* 47 (6): 1011–23. https://doi.org/10.1617/s11527-013-0110-9.

Kevern, J., D. Biddle, and Q. Cao. 2015. “Effects of Macrosynthetic Fibers on Pervious Concrete Properties.” *Journal of Materials in Civil Engineering* 27 (9): 6014031. https://doi.org/10.1061/(ASCE)MT.1943-5533.0001213.

Khorsandnia, Nima, Hamid Valipour, and Keith Crews. 2014. “Structural Response of Timber-Concrete Composite Beams Predicted by Finite Element Models and Manual Calculations.” *Advances in Structural Engineering* 17 (11): 1601–21. https://doi.org/10.1260/1369-4332.17.11.1601.

Khorsandnia, Nima, Hamid R. Valipour, and Keith Crews. 2012. “Finite Element Modeling of Timber-Concrete Composite Beams under Short-Term Loadings.” *ECCOMAS 2012 - European Congress on Computational Methods in Applied Sciences and Engineering, e-Book Full Papers*, no. January: 859–67. https://doi.org/10.13140/2.1.2486.1123.

Kılıç, A, C D Atiş, A Teymen, O Karahan, F Özcan, C Bilim, and M Özdemir. 2008. “The Influence of Aggregate Type on the Strength and Abrasion Resistance of High

Strength Concrete." *Cement and Concrete Composites* 30 (4): 290–96. https://doi.org/https://doi.org/10.1016/j.cemconcomp.2007.05.011.

Korayem, A. H., N. Tourani, M. Zakertabrizi, A. M. Sabziparvar, and W. H. Duan. 2017. "A Review of Dispersion of Nanoparticles in Cementitious Matrices: Nanoparticle Geometry Perspective." *Construction and Building Materials* 153: 346–57. https://doi.org/10.1016/j.conbuildmat.2017.06.164.

Kozul, Rozalija, and D Darwin. 1997. "Effects of Aggregate Type, Size, and Content on Concrete Strength and Fracture Energy." In .

Lam, Thanh Quang Khai, and Thi My Dung Do. 2019. "Sliding between Layers in 2-Layer Reinforced Concrete Beams and Shell." *International Journal of Engineering and Advanced Technology* 8 (5): 1867–71.

Lan, C, H Li, and Y Ju. 2009. "Ductility of High Strength Concrete Containing Nano-Particles." In *Proc.SPIE*. Vol. 7493.

Li, Hui, Mao-hua Zhang, and Jin-ping Ou. 2006. "Abrasion Resistance of Concrete Containing Nano-Particles for Pavement." *Wear* 260 (11): 1262–66. https://doi.org/https://doi.org/10.1016/j.wear.2005.08.006.

Li, Hui, Mao-hua Zhang, and Jin-ping Ou. 2007. "Flexural Fatigue Performance of Concrete Containing Nano-Particles for Pavement." *International Journal of Fatigue - INT J FATIGUE* 29 (July): 1292–1301. https://doi.org/10.1016/j.ijfatigue.2006.10.004.

Lin, D F, K L Lin, W C Chang, H L Luo, and M Q Cai. 2008. “Improvements of Nano-SiO2 on Sludge/Fly Ash Mortar.” *Waste Management* 28 (6): 1081–87. https://doi.org/https://doi.org/10.1016/j.wasman.2007.03.023.

Madani, Hesam, Alireza Bagheri, Tayebeh Parhizkar, Amirmaziar Raisghasemi, and Aliakbar Ramezanianpoor. 2013. “The Aggregation Status of Nanosilicas and Silica Fume, Used in Cementitious Mixtures.” *Sustainable Construction Materials and Technologies* 2013-Augus.

Mahdi, Noor, Mohammed Shamkhi, and Sallal Abid. 2017. *Effect of Polypropylene Fibers on the Abrasion Resistance of Hydraulic Concrete*. In 2nd Inetrnational Conference on Civil and Environmental Engineering.

Mishra, Archana, and Shivanshu Tiwari. 2018. “Effect on Flexural Strength of Concrete by Addition of Nano Titanium Dioxide and Nano Calcium Carbonate.” *International Journal of Science and Research (IJSR)* 7 (3): 1184–86. https://doi.org/10.21275/ART2018841.

Myers, John, Jeffery Volz, Eric Sells, Krista Porterfield, Trevor Looney, Brian Tucker, and Kyle Holman. 2012. *Self-Consolidating Concrete (SCC) for Infrastructure Elements Summary Report*.

Nader, Ghafoori, Najimi Meysam, and Mohammad Aqel. 2014. “Abrasion Resistance of Self-Consolidating Concrete.” *Journal of Materials in Civil Engineering* 26 (2): 296–303. https://doi.org/10.1061/(ASCE)MT.1943-5533.0000847.

Naik, Tarun R., Shiw S Singh, and Mohammad M. Hossain. 1995. "Abrasion Resistance of High-Strength Concrete Made with Class C Fly Ash." *ACI Materials Journal* 92 (6). https://doi.org/10.14359/9785.

Nayal, Rim, and Hayder A. Rasheed. 2006. "Tension Stiffening Model for Concrete Beams Reinforced with Steel and FRP Bars." *Journal of Materials in Civil Engineering* 18 (6): 831–41. https://doi.org/10.1061/(asce)0899-1561(2006)18:6(831).

Nazari, Ali. 2011. "The Effects of Curing Medium on Flexural Strength and Water Permeability of Concrete Incorporating TiO2 Nanoparticles." *Materials and Structures/Materiaux et Constructions* 44 (May): 773–86. https://doi.org/10.1617/s11527-010-9664-y.

Newhook, J, and D McGinn. 2007. "Ice Abrasion Assessment – Piers of Confederation Bridgeitle." In *Proceedings of the Confederation Bridge Engineering Summit*.

Nikbin, I M, M H A Beygi, M T Kazemi, J Vaseghi Amiri, E Rahmani, S Rabbanifar, and M Eslami. 2014. "A Comprehensive Investigation into the Effect of Aging and Coarse Aggregate Size and Volume on Mechanical Properties of Self-Compacting Concrete." *Materials & Design* 59: 199–210. https://doi.org/https://doi.org/10.1016/j.matdes.2014.02.054.

Nochaiya, Thanongsak, Watcharapong Wongkeo, and Arnon Chaipanich. 2010. "Utilization of Fly Ash with Silica Fume and Properties of Portland Cement–Fly Ash–Silica Fume Concrete." *Fuel* 89 (3): 768–74.

https://doi.org/https://doi.org/10.1016/j.fuel.2009.10.003.

Papanikolaou, Vassilis K., and Andreas J. Kappos. 2007. "Confinement-Sensitive Plasticity Constitutive Model for Concrete in Triaxial Compression." *International Journal of Solids and Structures* 44 (21): 7021–48. https://doi.org/10.1016/j.ijsolstr.2007.03.022.

Parandaman, P, and M Jayaraman. 2014. "Finite Element Analysis of Reinforced Concrete Beam Retrofitted with Different Fiber Composites." *Middle-East Journal of Scientific Research* 22 (7): 948–53. https://doi.org/10.5829/idosi.mejsr.2014.22.07.21979.

Piscesa, Bambang, Mario M. Attard, and Ali K. Samani. 2017. "Three-Dimensional Finite Element Analysis of Circular Reinforced Concrete Column Confined with FRP Using Plasticity Model." *Procedia Engineering* 171: 847–56. https://doi.org/10.1016/j.proeng.2017.01.377.

Pyo, Sukhoon, Selamu Yihune Abate, and Hyeong-Ki Kim. 2018. "Abrasion Resistance of Ultra High Performance Concrete Incorporating Coarser Aggregate." *Construction and Building Materials* 165: 11–16. https://doi.org/https://doi.org/10.1016/j.conbuildmat.2018.01.036.

Ramakrishnan, V, Neeraj S. Tolmare, and Vladimir B. Brik. 1998. "Performance Evaluation of 3-D Basalt Fiber Reinforced Concrete & Basalt Rod Reinforced Concrete." *Report*, no. November: 97. http://apps.trb.org/cmsfeed/TRBNetProjectDisplay.asp?ProjectID=2017.

Rashad, Alaa M. 2013. “A Preliminary Study on the Effect of Fine Aggregate Replacement with Metakaolin on Strength and Abrasion Resistance of Concrete.” *Construction and Building Materials* 44: 487–95. https://doi.org/https://doi.org/10.1016/j.conbuildmat.2013.03.038.

Riahi, Shadi, and Ali Nazari. 2011. “Compressive Strength and Abrasion Resistance of Concrete Containing SiO2 and CuO Nanoparticles in Different Curing Media.” *Science China Technological Sciences* 54 (9): 2349–57. https://doi.org/10.1007/s11431-011-4463-4.

Ruiz, W M. 1966. *Effect of Volume of Aggregate on the Elastic and Inelastic Properties of Concrete*. Cornell University, Jan. https://books.google.com.eg/books?id=sOVUAAAAYAAJ.

Saiidi, M., S. Vrontinos, and B. Douglas. 1990. “Model for the Response of Reinforced Concrete Beams Strengthened by Concrete Overlays.” *ACI Structural Journal* 87 (6): 687–95.

Sandvik, M., T. Hovda, and S. Smeplass. 1994. “Modified Normal Density (MND) Concrete for the Troll GBS Platform.” *ACI Symposium Publication* 149: 81–102. https://doi.org/10.14359/4069.

Sasmal, S., S. Kalidoss, and V. Srinivas. 2012. “Nonlinear Finite Element Analysis of FRP Strengthened Reinforced Concrete Beams.” *Journal of The Institution of Engineers (India): Series A* 93 (4): 241–49. https://doi.org/10.1007/s40030-013-0028-9.

Scott, Benjamin, and Md Safiuddin. 2015. “Abrasion Resistance of Concrete – Design, Construction and Case Study.” *Concrete Research Letters* 6 (September): 136–48.

Senff, L, D Hotza, S Lucas, V M Ferreira, and J A Labrincha. 2012. “Effect of Nano-SiO2 and Nano-TiO2 Addition on the Rheological Behavior and the Hardened Properties of Cement Mortars.” *Materials Science and Engineering: A* 532: 354–61. https://doi.org/https://doi.org/10.1016/j.msea.2011.10.102.

Shallal, Muhaned A., and Sallal Rashid Al-Owaisy. 2007. “Strength and Elasticity of Steel Fiber Reinforced Concrete at High Temperatures.” *Journal of Engineering and Development* 11 (2): 125–33.

Shamsutdinova, Guzel, Max Hendriks, and Stefan Jacobsen. 2017. “Concrete-Ice Abrasion Laboratory Experiments.” *Proceedings - International Conference on Port and Ocean Engineering under Arctic Conditions (ISSN 0376-6756) Http://Www.Poac.Com*, January.

Shih, Jeng-Ywan, Ta-Peng Chang, and Tien-Chin Hsiao. 2006. “Effect of Nanosilica on Characterization of Portland Cement Composite.” *Materials Science and Engineering: A* 424 (1): 266–74. https://doi.org/https://doi.org/10.1016/j.msea.2006.03.010.

Sim, Jongsung, Cheolwoo Park, and Do Young Moon. 2005. “Characteristics of Basalt Fiber as a Strengthening Material for Concrete Structures.” *Composites Part B: Engineering* 36 (6): 504–12. https://doi.org/https://doi.org/10.1016/j.compositesb.2005.02.002.

Sivakumar, A., and Manu Santhanam. 2007. “Mechanical Properties of High Strength Concrete Reinforced with Metallic and Non-Metallic Fibres.” *Cement and Concrete Composites* 29 (8): 603–8. https://doi.org/10.1016/j.cemconcomp.2007.03.006.

Sobolev, K., I. Flores, L. M. Torres-Martinez, P. L. Valdez, E. Zarazua, and E. L. Cuellar. 2009. “Engineering of SiO2 Nanoparticles for Optimal Performance in Nano Cement-Based Materials.” *Nanotechnology in Construction 3*, 139–48. https://doi.org/10.1007/978-3-642-00980-8_18.

Sonebi, M, and Kamal Khayat. 2001. “Testing Abrasion Resistance of High-Strength Concrete.” *Cement Concrete and Aggregates - CEMENT CONCRETE AGGREGATES* 23 (June). https://doi.org/10.1520/CCA10523J.

Song, P. S., and S. Hwang. 2004. “Mechanical Properties of High-Strength Steel Fiber-Reinforced Concrete.” *Construction and Building Materials* 18 (9): 669–73. https://doi.org/10.1016/j.conbuildmat.2004.04.027.

Srivastava, Vikas. 2012. “Effect of Silica Fume and Metakaolin Combination on Concrete.” *International Journal of Civil and Structural Engineering* 2 (February). https://doi.org/10.6088/ijcser.00202030017.

Sujjavanich, S, P Suwanvitaya, D Chaysuwan, and G Heness. 2017. “Synergistic Effect of Metakaolin and Fly Ash on Properties of Concrete.” *Construction and Building Materials* 155: 830–37. https://doi.org/https://doi.org/10.1016/j.conbuildmat.2017.08.072.

Thomas, Jeffrey J, Hamlin M Jennings, and Jeffrey J Chen. 2009. "Influence of Nucleation Seeding on the Hydration Mechanisms of Tricalcium Silicate and Cement." *The Journal of Physical Chemistry C* 113 (11): 4327–34. https://doi.org/10.1021/jp809811w.

Usman, Muhammad, Syed Hassan Farooq, Mohammad Umair, and Asad Hanif. 2020. "Axial Compressive Behavior of Confined Steel Fiber Reinforced High Strength Concrete." *Construction and Building Materials* 230: 117043. https://doi.org/10.1016/j.conbuildmat.2019.117043.

Vu, Dinh Tho, Elena Korol, Yuliya Kustikova, and Huy Hoang Nguyen. 2019. "Finite Element Analysis of Three-Layer Concrete Beam with Composite Reinforcement." *E3S Web of Conferences* 97 (May). https://doi.org/10.1051/e3sconf/20199702023.

Wahalathantri, B L, D P Thambiratnam, T H T Chan, and S Fawzia. 2011. "A Material Model for Flexural Crack Simulation in Reinforced Concrete Elements Using ABAQUS." *First International Conference on Engineering, Design and Developing the Built ENvironment for Sustainable Wellbeing*, no. April: 260–64.

Craig, Peter and Wolfe, Bill. 2012. "Another Look at the Drying of Lightweight Concrete-A Comparison of Drying Times for Normal weight and Lightweight Floors." Concrete International: 53–58.

Wu, Ke-Ru, Wu Yao, and Dong Zhang. 2001. "Effect of Coarse Aggregate Type on Mechanical Properties of High-Performance Concrete." *Cement and Concrete Research* 31 (October): 1421–25. https://doi.org/10.1016/S0008-8846(01)00588-9.

Yurtseven, A E, I O Yaman, and M Tokyay. 2006. “MECHANICAL PROPERTIES OF HYBRID FIBER REINFORCED CONCRETE.” In *Measuring, Monitoring and Modeling Concrete Properties*, edited by MARIA S KONSTA-GDOUTOS, 207–14. Dordrecht: Springer Netherlands.

Zhang, Mao-hua, and Hui Li. 2011. “Pore Structure and Chloride Permeability of Concrete Containing Nano-Particles for Pavement.” *Construction and Building Materials* 25 (2): 608–16. https://doi.org/https://doi.org/10.1016/j.conbuildmat.2010.07.032.

Zhang, Min-Hong, and Odd Gjørv. 1991. “Mechanical Properties of High-Strength Lightweight Concrete.” *Aci Materials Journal* 88 (May): 240–47.

Zhang, Min-Hong, Jahidul Islam, and Sulapha Peethamparan. 2012. “Use of Nano-Silica to Increase Early Strength and Reduce Setting Time of Concretes with High Volumes of Slag.” *Cement and Concrete Composites* 34 (5): 650–62. https://doi.org/https://doi.org/10.1016/j.cemconcomp.2012.02.005.

Zhao, Q, J Dong, H Pan, and S Hao. 2010. “Impact Behavior of Basalt Fiber Reinforced Concrete.” *Fuhe Cailiao Xuebao/Acta Materiae Compositae Sinica* 27 (December): 120–25.

Zhao, Zheng, Jie Kong, and Hong Yang. 2012. “Study on Frost Resistance of Nano SiO2 Cement Concrete.” *Applied Mechanics and Materials* 198–199 (September): 48–51. https://doi.org/10.4028/www.scientific.net/AMM.198-199.48.